THE UNIVERSITY
of EDINBURGH

The roles of the transcription factor Pax6 in regulating embryonic development of the prethalamus

Tian Tian MScR

A thesis submitted for the degree of Doctor of Philosophy
at the University of Edinburgh

2019

Declaration

I declare that this thesis was composed by myself, that the work contained herein is my own except the following:

(1) All the results in Chapter 5 (except for Figure 5.7) were obtained by Chrysoula Giasafaki when she was a MScR student under my supervision in the lab. The same results were included in Chrysoula Giasafaki's thesis submitted for the degree of MSc by Research in Biomedical Sciences (Life Sciences)

(2) Data analysis for mixed-effect model in Chapter 3 and Chapter 4, and Bioinformatic analysis (hierarchical clustering, principal component (PC) analysis, RefSeq annotation) in Chapter 6 were performed by Zrinko Kozić.

This work has not been submitted for any other degree or processional qualification except as specified.

Parts of this work have been published in:
Quintana-Urzainqui, I., Kozić, Z., Mitra, S., **Tian, T**., Manuel, M., Mason, J. O., & Price, D. J. (2018). Tissue-Specific Actions of Pax6 on Proliferation and Differentiation Balance in Developing Forebrain Are Foxg1 Dependent. iScience, 10, 171-191.

Signed…… Date……

Acknowledgement

I would like to express my sincere gratitude to all the people who have supported me throughout the past five years of my life in Edinburgh.

Firstly, I'm exceptionally grateful to my supervisors, Prof David Price, Dr Idoia Quintana-Urzainqui, Dr Thomas Pratt and my thesis committee chair Dr John Mason. Without their guidance and support, I would not have made it this far. I have learned so much from each of them, not only how to do research but also how to be good supervisors if I have my own students one day. I am exceptionally lucky to have them as my mentors, role models and friends.

Secondly, I'd like to thank all my dearest friends in the Hugh Robson Building. Idoia, Duan, Stella, Zrinko, Kai, Sarah, Farhana, Michela, Rosie, Soham, Johnothan, Kerstin and Thomas, Mike and Martine, Theo, Calvin, Sandy, Alazne, Jorge, and Javi. It has been amazing to work alongside all these wonderful people, and I will always be grateful to their support and encouragement.

Thirdly, I'd like to thank all the people who have provided me with technical support whenever I needed, especially Dr Anisha Kubasik-Thayil, Dr Rolly Wiegand, Dr Crispin Jordan, Dr Danai Katsanevaki and Dr Adam Jackson.

Fourthly, I also want to thank the staffs in the Biological Teaching Organisation and the Biomedical Teaching Organisation. I have found such great passion when I teach, and I'm really grateful to them for providing me with such opportunities. I would like to thank Dr Nadia Tuzi especially, for guiding me through many of my favourite teaching moments, and all the valuable experiences she shared with me.

Lastly, for Giannis and my parents. I want to thank Giannis for his support, company, patience, encouragement and the inspirations he brings to me every single day. And I want to thank my parents for always believing in me and being there for me. They are my role models in life, who taught me to be kind, honest, brave, curious, empathetic, perseverant and always passionate about life. I feel exceptionally lucky and I am always grateful to be their daughter.

Abstract

The transcription factor Pax6 is a pleiotropic player during neural development. In the central nervous system, Pax6 is mostly expressed by neural progenitors, where its functions have been most extensively studied. However, in the anterior diencephalon, the prethalamus, Pax6 is expressed in both neural progenitors and post-mitotic neurons. This distinctive expression pattern of Pax6 makes the prethalamus a unique place in which to explore the functions of Pax6 and its mechanisms of action during development.

I have found that in post-mitotic prethalamic neurons, Pax6 seems to regulate the process of neuronal morphogenesis. Gene ontology analysis on the RNAseq data, which showed significant transcriptional changes of genes in the prethalamus when Pax6 is lost, revealed that genes involved in neuritogenesis, establishment of neuronal polarity, axon elongation and axon initial segment (AIS) were significantly differentially expressed. To further explore this, I performed dissociated cell cultures of the prethalamus at embryonic day 13.5. Various aspects of neuronal morphogenesis were analysed in these primary neurons cultured for 1-9 days in vitro (DIV). I found that Pax6-null prethalamic neurons constantly displayed fewer neurites and a disturbed rate of neurite elongation. Additionally, I discovered that the AISs of these neurons were located further away from the soma. The AIS is where the neurons generate action potentials, and its location and molecular composition can determine the amplitudes and firing frequencies of the neurons. I found that the components of the AISs seemed to have been altered as increased amount of voltage-gated sodium channels and AnkyrinG was found in the AISs of the Pax6-null prethalamic neurons. AnkyrinG is a cytoskeletal protein known to be the master regulator of AIS formation. Therefore, my analysis suggested that the Pax6-null prethalamic neurons might display different electrophysiological properties. Indeed, whole-cell patch clamping on dissociated prethalamic neurons showed that the Pax6-null neurons required a much lower amplitude of current stimuli to initiate an action potential. In the adult brain, derivative neurons of the prethalamus are organized into nuclei,

which innervate with the thalamus in a reciprocal manner and can modulate the activities of the thalamus. The thalamus is the relay station where all sensory inputs (except olfactory) are received, processed and further projected to the cortex. Consequently, the loss of Pax6 in the embryonic prethalamus might impact the functionality of entire nervous system.

Additionally, I have also found that Pax6 removal from the prethalamus significantly deregulates the activity of various genes involved in canonical and non-canonical Wnt-signaling pathways. My data indicate that in the prethalamic ventricular zone, where neural progenitors reside, Pax6 seems to suppress the expression of various canonical Wnt-signalling pathway effectors by promoting the expression of antagonists of Wnt-signaling pathways, such as Sfrp2 and Dkk3.

By utilising the RNAseq data and comparing the transcriptome profiles of the thalamus and prethalamus, I found that in the absence of Pax6, the prethalamus develops a thalamus-like expression profile of the voltage-gated ion channels and AIS component genes. During embryonic development, the thalamus and prethalamus reside adjacent to each other, and receive the same amounts of morphogens. However, the thalamus and prethalamus give rise to neurons with completely different morphologies and functions. Pax6 is expressed simultaneously by the thalamus and prethalamus. However, in the thalamus, Pax6 is only expressed in the progenitors, whereas in the prethalamus, Pax6 is expressed by both the progenitors and post-mitotic cells. My results thus indicated that such differential expression of Pax6 helps to explain the inter-regional diverse development of the thalamus and prethalamus.

My study revealed novel and distinct functions of Pax6 in the developing prethalamus of the mouse embryos- suppressing the activity of canonical Wnt signalling pathway in the progenitor cells and regulating neuronal morphogenesis and functionality in a cell autonomous manner in the post-

mitotic cells. Additionally, Pax6's expression in the prethalamus also influences the prethalamic electrophysiological identities from the neighbouring thalamus, thus contributing to the differential development of these two tissues. My findings hence provide new insight into the temporal and spatial regulation governed by master regulators such as Pax6 during brain development.

Lay abstract

My PhD project focuses on investigating how a single gene, Pax6, controls the way neurons are formed in an area of the brain called the prethalamus in mouse embryos.

Pax6 is important because it controls the activities of hundreds of other genes. Therefore, errors in this gene can have catastrophic cascading effects. For example, in human patients, mutations of both copies of the Pax6 gene are lethal, whereas mutations in only one copy of the Pax6 gene can cause eye defects, structural brain defects and intellectual disabilities.

In the developing central nervous system, Pax6 is very active in the newborn cells, where it controls the process of cell division and proliferation. As the newborn cells mature and become neurons, most of them lose their Pax6 activities. However, in certain areas of the brain, such as the prethalamus, a structure situated deep in the brain and essential for modulating perception, Pax6 continues to be active in the mature neurons, and we have no clue of what Pax6's functions are in these cells.

I started my PhD by asking whether Pax6 continues to function in the mature neurons of the prethalamus and what those functions might be. I have found that in the prethalamus, Pax6 seems to control an important cell-cell signalling pathway (Wnt signalling) in the newborn cells. However, in mature neurons, it seems to regulate how they develop their shapes. As a neuron matures, it changes its original shape and sends out protrusions called axons and dendrites to connect with other neurons, thus forming a neural network. I have developed a culture system to observe this process as the neurons of the prethalamus mature. I found that disabling Pax6's activities in these neurons results in a decrease in the number of dendrites and a disturbance in the rate at which these neurons send out their protrusions.

The above results indicate that the shapes of the prethalamus neurons change when Pax6 is lost. Next, I want to find out if the behaviours of these neurons also change when Pax6 is mutated. Interestingly, losing Pax6 seems to affect an important structure called the axon initial segment (AIS). The AIS is where the neurons generate electrical impulses and it is crucial for how they transmit information. My preliminary data showed that without Pax6, these neurons are hyperactive as they generate more electrical activity under the same amount of stimulation. In the adult brain, prethalamic neurons connect with and fine-tune the activities of other brain regions. Therefore, changes in how active these neurons are could potentially affect the cognitive function of the whole nervous system.

Given Pax6's known function to control the expression of hundreds of other genes, to have a better understanding of the global effect of Pax6's loss on development of the prethalamus, I analysed all the active genes in the prethalamus by big data processing. I found that when I eliminate Pax6, the prethalamus loses the activity of some of its signature genes but activates other genes that are typically active in a nearby brain region- the thalamus. This effect was particularly strong for genes that are involved in the AIS, and other genes that also function to determine how the neurons would generate their electrical impulses. These results indicated that Pax6 not only functions to control how these neurons develop their shapes and behaviours, but it is also essential for the distinctive development of the prethalamus itself.

As most studies on Pax6 focus on its functions in the newborn cells, my results revealed new roles of this important gene in the maturing neurons of the developing nervous system. Additionally, these findings show how the same gene can have different functions at different developmental stages of a cell in the embryonic brain, providing interesting insights into the mechanisms of genetic regulation underlying the process of embryonic development.

CONTENTS

Chapter 1 Introduction

Chapter 2 Materials and Methods

Chapter 4 The roles of Pax6 in regulating the establishment and maintenance of neuronal polarity during the development of the prethalamic neurons

Chapter 5 Pax6 inhibits the activities of Wnt signalling pathways in the prethalamus

List of figures

List of tables

Abbreviations

ABPs	Actin binding proteins
AIS	Axon initial segment
AP	Anterior-posterior
APC	Adenomatous Polyposis coli
CNS	Central nervous system
Ctrl	Control group
DIV	Days in vitro
Dkk3	Dickkopf-3
DV	Dorsal-ventral
GABA	*gamma*-Aminobutyric acid
GAPs	GTPase activating proteins
GEFs	Guanine nucleotide exchange factors
GFP	Green fluorescent protein
GO	Gene ontology
Hom	homozygous mutant group
LFC	Log2 fold changes
MAP	Microtubule-associated proteins
P1, P2, P3	Prosomere 1, 2, 3
PC	Principal component
PCP	Planar cell polarty
PCR	Polymerase chain reaction
PSPB	Pallial-subpallial boundary
RGCs	Retinal ganglionic cells
RMP	Resting membrane potential
Sfrp2	Secreted Frizzled-related protein 2
Shh	Sonic hedgehog
TCA	Thalamocortical axon
Tcf/Lef	T-cell factor/Lymphoid enhancer factor
TRN	Thalamic reticular nucleus
VZ	Ventricular zone
ZLI	Zona limitans intrathalamica

Chapter 1

Introduction

1.1 Genetic control of the development of the diencephalon

1.1.1 Introduction

The diencephalon is the caudal-most component of the forebrain (1). It is a twinned bulb-shaped structure that forms at the top of the brainstem on either side of the third ventricle (2).

The diencephalon consists of three major alar domains- the prethalamus, the thalamus and the pretectum (3). As development proceeds, the neurons within the diencephalon are further organised into nuclei along the anterior-posterior (AP) and dorsal-ventral (DV) axes of the neural tube (4–6). The thalamic nuclei serve as morphological and functional units that filter all afferent sensory information (except olfactory) and connect reciprocally with the overlying cerebral cortex in the adult brain (2). Therefore, the thalamus is often described as the "the gateway to consciousness" (7). The nuclei derived from the prethalamus receive input from the cortex, the basal telencephalon and connect reciprocally with the thalamic nuclei and function to modulate the activities of the latter (8). The telencephalon and diencephalon are thus the embryonic anlage of higher cognition and information integration centres (5). Malformations or damage to the diencephalon has been shown to result in cognitive disorders such as schizophrenia, amnesia, Alzheimer's disease, dementia, etc. (9). Therefore, a fully developed diencephalon with correct patterning is an essential prerequisite to a healthy brain, and it is of great importance for us to understand the genetic regulations that take place during diencephalic development.

1.1.2 The prosomeric model and the subdivisions of the embryonic diencephalon

During mouse embryonic development, neurulation occurs at about E8.5 as the neural plate folds at its dorsal midline to form the neural tube (10) (Figure

1.1A). As development proceeds, the anterior neural tube enlarges, giving rise to the prosencephalon (forebrain vesicle), the mesencephalon (midbrain vesicle) and the rhombencephalon (hindbrain vesicle) (Figure 1.1B) (1,3,8,11).

Based on a wide-ranging analysis of histological landmarks and gene expression patterns in the forebrain, Bergquist (1932) first theorised the prosomeric model, which was later revised by Puelles, Rubenstein et al (12–14). The prosomeric model proposed that the prosencephalon can be divided into 6 transverse segments along its anteroposterior (AP) axis and 4 longitudinal domains along its dorsoventral (DV) axis (13,14). The six transverse segments are termed Prosomeres 1-6 from posterior to anterior, whereas the four longitudinal subdivisions are the floor plate, basal plate, alar plate and roof plate from ventral to dorsal (13,14). Anteriorly, prosomeres 4-6 (P4-P6) give rise to the secondary prosencephalon, whereas prosomeres 1-3 (P1-P3) will give rise to the diencephalon that is situated posteriorly (Figure 1.1C) (3,14). The secondary prosencephalon later develops into hypothalamus and telencephalon, whereas the telencephalon further gives rise to the cerebral cortex, basal ganglion and hippocampus (Figure 1.1D-E) (3,5,8,14). In mouse, morphological segmentation of the diencephalon starts at E9.5. At about E10-11, the diencephalic prosomeres P1-P3 are morphologically distinct (15). In their roof and alar plates, P1 gives rise to the pretectum that resides anteriorly adjacent to the midbrain. P2 differentiates into thalamus and epithalamus, whereas P3 develops into the prethalamus and eminentia thalamus that is situated posteriorly to the telencephalon (Figure 1.1D-E) (3,8,14). Figure 1.1F is the schematic representation of the coronal view of the neural tube, which shows the anatomy of the diencephalon and the telencephalon at the indicated level of sectioning (16).

The prosomeric model has proved useful as it provides a topographical framework for studies on forebrain development (17). Additionally, it has been tested by numerous studies examining gene expression during neural development in various species, and widely supported due to its corroborated

capacity to attribute morphological meanings to these gene expression patterns (14). However, the expression domains of various forebrain markers were found to be highly dynamic spatially and temporally, and did not confine to the putative segments especially at early developmental stages before the appearance of morphological boundaries (17,18). Additionally, recent fate mapping experiments revealed that cells were able to cross the proposed boundaries of P1/P2, P2/P3 and the boundary between the prethalamus (P3) and the secondary prosencephalon, raising the question of whether these areas can be considered as true compartments or segments (17,19) . Finally, several boundaries, especially those postulated in the hypothalamus and telencephalon, were ambiguous (5). These concerns resulted in a revision of the prosomeric model that no longer includes the secondary prosencephalon as a prosomeric structure (5,14). Nonetheless, the prosomeric model still provides a comprehensible framework to interpret forebrain, especially diencephalon, development, which is why I used it to introduce early development of the prethalamus and the thalamus.

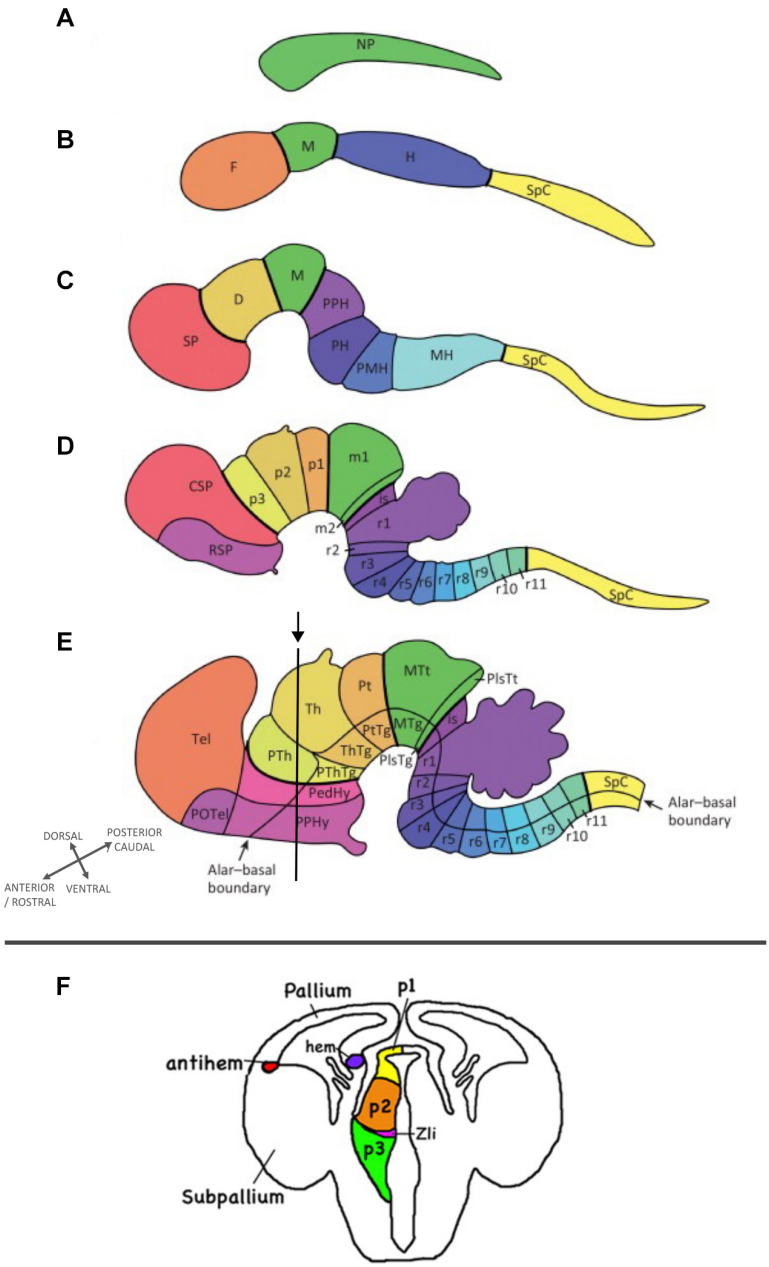

Figure 1.1 Schematic representation of early development of the diencephalon. (A-E) Schematic representation of the sagittal view of early development of the central nervous system. **(A)** After neurulation, the neural primordium (NP) is a hollow tube with no subdivisons. **(B)** The anterior part of the neural tube expands, giving rise to the prosencephalon (forebrain vesicle, F), the mesencephalon (midbrain vesicle, M) and the rhombencephalon (hindbrain vesicle, H). **(C)** The forebrain vesicle further develops, giving rise to the secondary prosencephalon (SP) anteriorly and the diencephalon (D) posteriorly. **(D-E)** SP further give rise to the telencephalon, which further develops into the cerebral cortex, basal ganglion and hippocampus, whereas the three prosomeres (P1-P3) of diencephalon further differentiate into the pretectum, thalamus and epithalamus, and prethalamus respectively. The cross made with two perpendicular double arrows indicates the orientation of the developing neural tube in (A)-(E). Figure adapted from reference (3). **(F)** Coronal view of the developing neural tube sectioned at the level pointed by an arrow in (E). The dorsal (pallium) and ventral (subpallium) telencephalon are divided by the cortical hem (purple) and pallium/subpallium boundary (antihem, red). The diencephalon contains p1, p2 and p3 from dorsal to ventral. In between p2 and p3 resides the secondary organiser zona limitans intrathalamica (ZLI). Figure adapted from reference (16).

1.1.3 Prepatterning of the diencephalic area and the formation of the zona limitans intrathalamica (ZLI)

In the process of neural patterning (or regionalisation), morphogens induce neural patterning by providing positional information through controlling the expressions of transcription factors in the neural progenitor cells. By binding to the regulatory elements on DNA and altering the expression of specific genes, transcription factors can initiate cascades of various signalling pathways in these neural progenitor cells. As a result, the progenitor cells undergo a sequence of finely regulated events of proliferation, cell fate specification, migration and eventually acquire their specific neuronal shape and position within a fully developed brain (1,11,20). During neural development, morphogens are released by groups of cells called organisers (11). While the primary organisers are responsible for releasing the first batches of morphogens, the secondary organisers carry on this job further in development, fine-detailing structures in the forebrain, midbrain and the hindbrain (8,11).

Secondary organisers (or local organisers) are small groups of cells that direct development of the surrounding tissues by secretion of signalling molecules while at the same time serve as segment boundaries that prevent mixing of cells with their neighbours. Loss of secondary organisers leads to loss of the surrounding structures. Additionally, ectopic induction of cell fates of the secondary organisers and ectopic provision of principle signal molecules of the secondary organisers can both result in the ectopic appearance of respective surrounding structures (1,20,21). The effectiveness of the secondary organisers in directing development depends on the timing of their presence, the efficiency of the signal molecules' spread and also the competence of the target cells to respond to a particular combination of signal molecules (2,21).

During development of the diencephalon, secondary organisers play critical roles in the execution of this AP, DV patterning. One of the most important secondary organisers for diencephalic AP patterning is the zona limitans

intrathalamica (ZLI), which is a narrow strip of cells separating the thalamus and prethalamus (Figure 1.2B) (2,8,11). The ZLI forms at about E9-10 in mouse embryos (22). It appears as a wedge-shaped lineage-restricted compartment with sonic hedgehog (Shh) expression that initiates ventrally from the basal plate and extends dorsally through the alar plate to the roof plate (Figure 1.2A-B) (11,23).

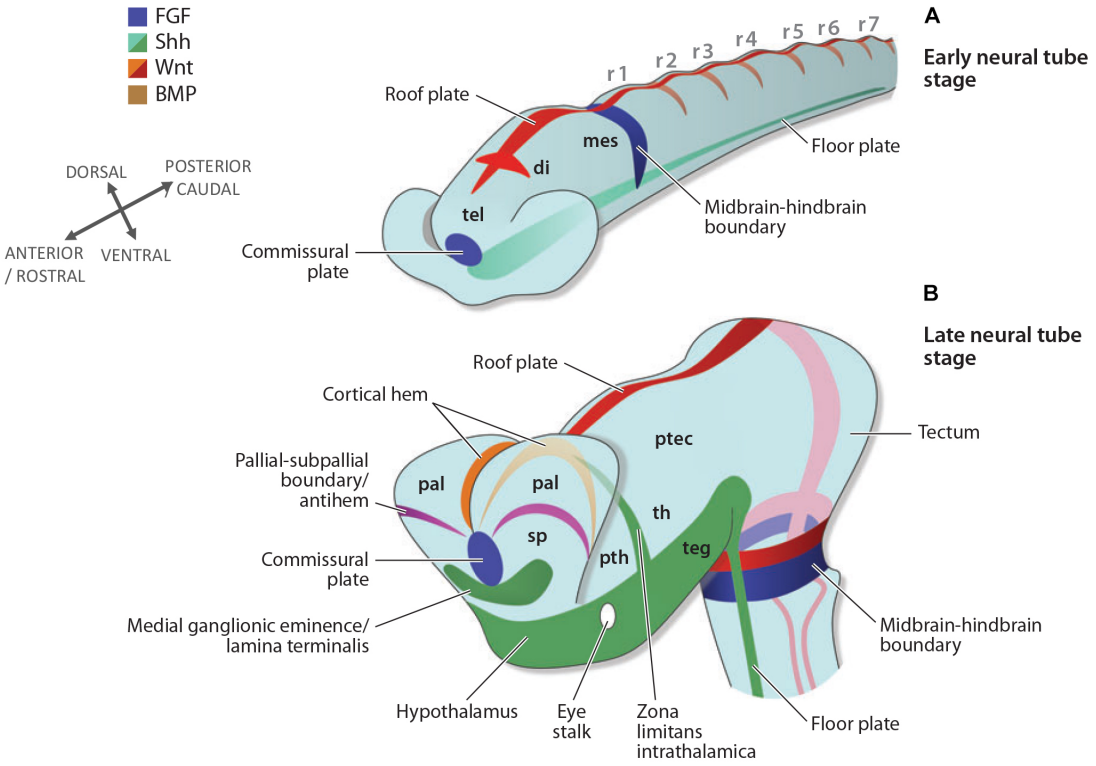

Figure 1.2 Schematic representation of regions where the major morphogens are expressed in the early and late neural tube stages in amniote embryos. (A) At early neural tube stage, prior to the formation of the ZLI, Shh is produced and released by the floor and basal plate (green). The other major morphogens being produced and released at this age are the Wnts at the dorsal midline (red) and the Fgfs at the commissural plate and midbrain-hindbrain boundary (blue). The expression of the Wnts comes in a gradient of caudal-high and rostral low, due to the repression of expression by Wnt antagonist such as Dkk1 in the rostral telecephalon. **(B)** At late neural tube stage, the three prosomeres of the diencephalon (P1-P3) had developed into the pretectum (ptec), the thalamus (th) and epithalamus, and prethalamus (pth). The zona limitans intrathalamica (ZLI) is a wedge-shaped structure with its Shh expression appears to be a distinct spike, which extends from the floor plate through the alar plate, towards the roof plate. Shh is also produced and released by the floor plate and the medial ganglionic eminence at this stage. Figure adapted from reference: (11).

Similar to the other regions of the developing CNS, the morphogen Shh in the diencephalon is also produced and released ventrally by the floor and basal plate (24). However, Shh released dorsally by the wedge-shaped structure of the ZLI that extends into the alar and roof plate is an additional source (4,13). So far, the mechanisms underlying the positioning and formation of the ZLI still remain elusive.

It is hypothesised that the ZLI initiates at the ventral midline where the prechordal neural plate (expressing transcription factor Six3) and the epichordal neural plate (expressing transcription factor Irx3) meet (20). Later, several studies questioned the advocated critical role of Six3 and Irx3 in establishing the ZLI domain. Scholpp and Lumsden thus proposed that instead of Six3 and Irx3, transcription factor Fez and Otx in the prechordal and epichordal plate should be the determinants of ZLI initiation (2). Analysis of expression patterns showed that the domain of Otx1 and Otx2 abut that of Fez's in the developing zebrafish neural plate whereas loss of function analysis indicated that both Fez and Otx are required for ZLI initiation (25,26). However, evidence from these studies only proved that in vivo interaction of the prechordal and epichordal domain itself was sufficient to initiate formation of ZLI, indicating the possibility that transcription factors other than Fez and Otx might also contribute to ZLI initiation.

Interestingly, the ZLI is also the only place in the neural tube where the expression domain of Shh expands dorsally to form a distinct spike (24). It was widely speculated that the mechanism underlying ZLI development was a progressing expansion of Shh domain from the Shh-positive basal plate to the roof plate (2). However, fate map analysis failed to identify the anticipated dorsally migrating cells, whereas zebrafish lacking the Shh-expressing basal plate established a nearly normal ZLI (27). One reasonable explanation is the weakening of repression against Shh expression from the dorsal portion (28). For example, studies in chick embryos have found that early expression of Wnt8b in the ZLI antagonises the expression of Gli3, an inhibitor of Shh

signalling, therefore creating a permissive area for Shh expression within the ZLI later on (28). Additionally, in Zebrafish, canonical Wnt signalling initiated by Wnt3 and Wnt3a inhibits apoptosis and promotes proliferation of cells in the ZLI primordium (29). Furthermore, retinoic acid (RA), a signalling molecule expresses in the diencephalic roof plate, can block Shh expression in diencephalic explants. Therefore, inhibition of RA can create a permissive region for dorsal development of the ZLI (30,31). However, exactly how this is achieved needs more thorough investigations.

1.1.4 Patterning and cell fate specification of the developing diencephalon

1.1.4.1 Shh

During development, the ZLI produces and releases several morphogenetic signals into the neighbouring tissue that play critical roles in specifying the intricate details of the diencephalic development (8). While Wnts, fibroblast growth factors (FGFs), RA and bone morphogenic proteins (BMPs) instruct the development of dorsal structures in the diencephalic epithelium, Shh is the primary signal that acts ventrally (8,32).

The ZLI's expression of Shh is one of the key sources of signals that pattern the diencephalon as abolishing Shh expression in chick and zebrafish results in the loss of cell identity and morphogenetic transcription factors in the prethalamus and thalamus (2,24). On the other hand, ectopic expression of Shh by way of activation of the Shh receptor (smoothened, SmoM2) promotes the expression of several thalamic markers such as Gbx2, Neurog2, Olig2 and Olig3 in the mouse pretectum (33). These results not only proved the qualification of the ZLI as a local organiser but also highlighted the central position of Shh in directing diencephalon development. Kiecker et al. further demonstrated that Shh is both necessary and sufficient for initiating expression of Dlx2 and Gbx2, which are markers for prethalamus and thalamus respectively (24). So how does a common morphogen initiate the acquisition

of entirely different identities among neighbouring cells? This is due, at least in part, to the different competencies of adjacent cells that have been established prior to the expression of Shh (2). For example, different Wnt signalling gradients that express dorsally set up a coarse prepattern of competence in respective areas by inducing transcription factors such as FezF1, FezF2 anteriorly and Irx posteriorly (34). Ectopic expression of Irx in prethalamus against a Shh-expressing background results in ectopic expression of thalamic markers such as Sox14 and Gbx2 (24), while the Fez genes in combination with Shh expression seems to have similar effects in initiating ectopic expression of prethalamic markers (25).

A small rostral thalamic progenitor region immediately caudal to the ZLI, which is exposed to relatively high levels of Shh, is referred to as pTH-R (Figure 1.3B) (35). pTh-R expresses marker genes such as Ascl1 (also known as Mash1) and Nkx2.2 (22). Unlike the majority of the thalamic progenitors, pTh-R generates mostly GABAergic neurons (4). Shh is crucial for specifying the pTh-R, as specific deletion of Shh in the ZLI resulted in the loss of pTh-R and expansion of the pTh-C (22). On the other hand, expansion of pTh-R was observed in Pax6 mutant mouse embryos where Shh expression was elevated (22,33,36). Caudal to the pTH-R, a larger thalamic progenitor region is referred to as pTH-C, which expresses marker genes such as Ngn2 and Olig3 and generate glutamatergic neurons that innervate the cortex (Figure 1.3B) (22,35).

1.1.4.2 Wnts

Various genes involved in the Wnt signalling pathways are expressed in the developing diencephalon in a temporally and spatially restricted manner (28,37,38). In this context, the Wnt/β-catenin signalling has been most extensively studied.

Before the onset of neurogenesis, the Wnt/β-catenin signalling plays pivotal roles during formation of the ZLI and subsequently facilitates the expression of Shh within the ZLI (28,29,32,39). Braun et al. have shown that high levels

of Wnt3 and Wnt3a in the posterior neural tube specify the caudal forebrain fate by inducing the expression of Irx3. However, in the anterior neural tube, canonical Wnt activities are suppressed by DKK1 released from the underlying prechordal plate. Low levels of canonical Wnt activities anteriorly enable the expression of Six3, which further specifies the rostral forebrain fate. This opposition and mutual repression of Irx3 and Six3 can further contribute to locating the position of the future ZLI (39).

During and after neurogenesis, canonical Wnt signalling continues to modulate the development of the diencephalon. The nuclear β-galactosidase reporter (BAT-gal) mice transcribe the LacZ gene under the control of the β-catenin/TCF responsive elements, upon active canonical Wnt signalling (40). These mouse embryos showed distinct and highly contrasting levels of canonical Wnt activities within the diencephalon, with thalamus, ZLI, and a small prethalamic region directly rostral to the ZLI being highly active, whereas a small gap between the ZLI and the thalamus, and the rest of prethalamus lack canonical Wnt signalling (36). These results are in concordance with others' findings that the expressions of mediator and reporter genes for canonical Wnt signalling, such as Axin2, Lef1 and Tcf7l2 are highly localised within the thalamus (36,38,40). Regarding Wnt ligands themselves, Wnt3, Wnt3a, Wnt8b and Wnt5a are all expressed strongly in the ZLI and at weaker levels in the thalamus, whereas Wnt7b is expressed in ventral regions of the thalamus as well as the prethalamus (36–38,41,42).

These highly localised expressions of Wnt and Wnt-related genes in the ZLI and thalamus at stages beyond patterning indicates other functions of this signalling pathway in the developing diencephalon. Indeed, studies have revealed that ectopic expressions of Wnt3 and Wnt3a were sufficient to induce the expression of thalamic marker Gbx2 in chick forebrain explants, via activation of the caudal forebrain marker Irx3 (39). On the other hand, inactivation of canonical Wnt signalling in pTh-C by selective deletion of β-catenin in this region has shown upregulation of marker genes for pTh-R and

prethalamus in the mantle zone of the pTh-C (36). Additionally, in mice lacking the LRP5/6 co-receptor, ectopic expressions of prethalamic markers such as Dlx2 were found in the mantle zone of the thalamus (32), whereas in mice lacking Tcf7l2, severe reduction of thalamic post-mitotic markers such as Rora and Hs6st2 was observed, along with expansion of habenular markers such as Robo3, Irx1 and Irx2 into the caudal thalamus (43). These findings highlight the significance of Wnt/β-catenin pathway in specifying caudal thalamic progenitor fate during neurogenesis.

1.1.4.3 FGF8

Fibroblast growth factor 8 (FGF8) is expressed in the dorsal part of the diencephalon, in a region towards ZLI but slightly anterior to the Shh domain (44). pTh-R, the area that flanks ZLI posteriorly with the characteristic marker of Nkx2.2 and Sox 14 seems to be controlled by Fgf8 expression (16). Studies utilised in utero electroporation to manipulate Fgf8 expression in the developing diencephalon of mouse revealed that Fgf8 activates expression of the pTh-R marker Ascl1 while it represses that of the pTh-C marker Ngn2 in a Shh and Wnt-independent way (16,32). The above information indicates that in addition to the prominent effect of Shh-expression on thalamic patterning, the expression of Fgf8 might act as another restraining factor that fine-tunes the intricate structures of at least the thalamus. Such a mechanism might be well adopted in other parts of the diencephalon to secure its correct patterning during development.

1.1.5 Specification of neuronal identities and early circuit formation of the diencephalic nuclei

1.1.5.1 Region-specific expressions of transcription factors specify diencephalic nuclei

As a result of these interplays between morphogens and transcription factors, the diencephalon is subdivided into distinct areas that express specific transcription factors (4,8,14,32). These transcription factors further convey

information of cell fate specification and direct the differentiation and migration of diencephalic cells into nuclei with distinct functions, connections and architectonic features (cell density and morphology) (4,8). Therefore, recognising the genes and TFs expressed in specific diencephalic subpopulations will help us understand the underlying mechanisms of how these nuclei are formed and how they function.

The diencephalon is a piece of highly heterogeneous tissue (4,8,14,45). Gene expression profiles of P1, P2 and P3 showed distinct expression boundaries correlated with morphological boundaries (8,13,14). The thalamus and prethalamus display rather different expression profiles of genes and transcription factors, although they reside on either side of the ZLI and hence are under the influence of the same morphogens (8,14,32). In both the thalamus and prethalamus, progenitor cells in the ventricular zone mostly exhibit different expression profiles of genes than post-mitotic cells that have started migrating away from the VZ (8,14,22,35,46,47). For example, In the thalamus, the transcription factor Olig3 is expressed in the pTh-C, pTh-R and the ZLI, with its ventral boundary abutting the dorsal boundary of prethalamus directly (4,22,35). On the other hand, Olig2 is expressed in the ventricular zone of the prethalamus, with its dorsal boundary abutting the ventral boundary of Olig3 directly (22,48). Olig2 is also expressed in the pTh-C, in a rostral-ventral high gradient (35). Interestingly, Dbx1 is expressed in the caudal-dorsal part of pTh-C, which complimented the gradient of Olig2 (35). Dbx1 is also expressed in the rostral half of P1 pretectum (35). Transcription factor Neurogenin1 (Ngn1) is also expressed in the pTh-C, whereas Neurogenin2 (Ngn2) is expressed in pTh-C and further maintained in the pTh-C derived thalamic neurons (35,36,49). Ngn1 and Ngn2 are both target genes of canonical Wnt signalling (36). Previous studies have shown that their expressions are crucial to antagonise ectopic expression of pTh-R and prethalamic markers in the pTh-C and its mantle zone area (36). Other pTh-C markers include Fgf15 (rostrodorsal), Irx5 (rostrodorsal), Ebf3, Barhl2 and Shox2 (4,47,50) (Figure 1.3B-C).

pTh-C gives rise to glutamatergic projecting neurons, whereas the pTh-R give rise to GABAergic interneurons that, although they do not project to the cortex, will integrate with the glutamatergic projecting neurons and become part of the thalamic nuclei (4,22,35). The pTh-R expresses a selection of transcription factors unique to itself, such as Ascl1, Nkx2.2, Helt2, Gata2, Gata3, Tal1, Tal2 and Sox14 (4,22,35,51) (Figure 1.3B-C). It is known that the interaction between Helt and Ascl1 is required to maintain pTh-R fate (51).

Although Shh is always used as a marker for the ZLI, the expressions of other transcription factors can also outline the ZLI and its surrounding regions. For example, Ngn2 is expressed in the caudal part whereas Dbx1 is expressed in the rostral part of the ZLI (Figure 1.3B-C) (22). Neurons derived from the ZLI contribute to both the thalamic nuclei, such as the dorsal lateral geniculate thalamic nuclei (dLGN) and prethalamic nuclei, such as the ventral lateral geniculate thalamic nuclei (vLGN) (35,52,53).

As development proceeds, the expression profiles of thalamic progenitor cells change accordingly (4,8,47,50). For example, pTh-C derived post-mitotic cells turn on their Gbx2 expression, which is one of the first genes identified as a thalamic marker (35,54). Global disruption of Gbx2 leads to ectopic expression of marker genes of P1-derived neurons, defective maturation of thalamic neurons, malformation and mispositioning of the distinct thalamic nuclei (4,55,56). Other TFs expressed specifically by pTh-C derived neurons, which are under the transcriptional regulation of Gbx2, are Rorα, Id4, Chst1, Glr1, Cd47, Slc18a2 (also known as Vmat2), Gas7, Hs6st2, Epha3 and Prokr2 (4,47,55). In addition to Gbx2, Lhx2 and Lhx9 are both expressed in the post-mitotic derivatives of pTh-C, whereas Foxp2, Nhlh2 and Kitl are expressed in the lateral pTh-C-derived mantle zone (47,49,50). The very few transcription factors, whose expressions are maintained from thalamic progenitor cells to post-mitotic cells are Sox2, Shox2 and Ngn2 (35,47,50). Sox2 is expressed in

the pTh-C and by E16.5, its expression becomes restricted to post-mitotic neurons in a rostral-lateral high manner (4,35) (Figure 1.3B, D).

Unlike the thalamus, detailed analysis of gene expression profiles in prethalamic subpopulations, and how each of these subpopulations further develops into individual nuclei is much less studied. Several transcription factors known to mark specific prethalamic regions include Pax6, Gsx2, Dlx1, Dlx2, Isl1, Six3, Arx, Olig2 and Ascl1 (8,22,45,48,57). As mentioned above, in the thalamus, the expression of Pax6 displays a gradient in the ventricular zone as its intensity increases with distance from the ZLI (22). However, in the prethalamic ventricular zone, Pax6 is expressed in a homogeneous level (22,58). Additionally, Pax6's expression is maintained in some of the prethalamic post-mitotic cells (22,58,59). Interestingly, the level of Pax6 expression in the prethalamic post-mitotic cells is much higher than that in the prethalamic progenitors (58)(60). Dlx1 and Dlx2 are both expressed in the ventricular zone of the prethalamus, with Dlx1 expression maintained by post-mitotic cells in the dorsal prethalamus, close to the ZLI (16,48,51) (Figure 1.3B-C).

Prethalamus also produces GABAergic interneurons, which unlike thalamic projecting neurons that innervate the cortex, project to and only innervate the neurons in the thalamic nuclei (8). Gsx2, a marker for progenitors with GABAergic fate, is expressed in all the ventricular zone of the prethalamus (22,59,61). The expression pattern of glutamic acid decarboxylase 67 (GAD67), which functions to mediate GABA synthesis, complimented that of Gsx2's and is found in the post-mitotic cells of the prethalamus (16,62). In addition to Gsx2, expressions of Olig2 and Ascl1 are also found only in the ventricular zone of the prethalamus, as mentioned above (22,48). Isl1 is expressed in the medial-lateral post-mitotic region of the prethalamus, with its dorsal border slightly overlapping with the ventral border of Pax6's expression (60). Six3 and Arx are expressed in both the VZ and post-mitotic region of the ventral prethalamus (16,50,63) (Figure 1.3B, D). Notably, in addition to

GABAergic neurons, a small region that is close to the VZ in the dorsal prethalamus produce a subpopulation positive for tyrosine hydrolyse (TH), which will further develop into A13 sub-nucleus that harbours dopaminergic neurons (8,45,57,64).

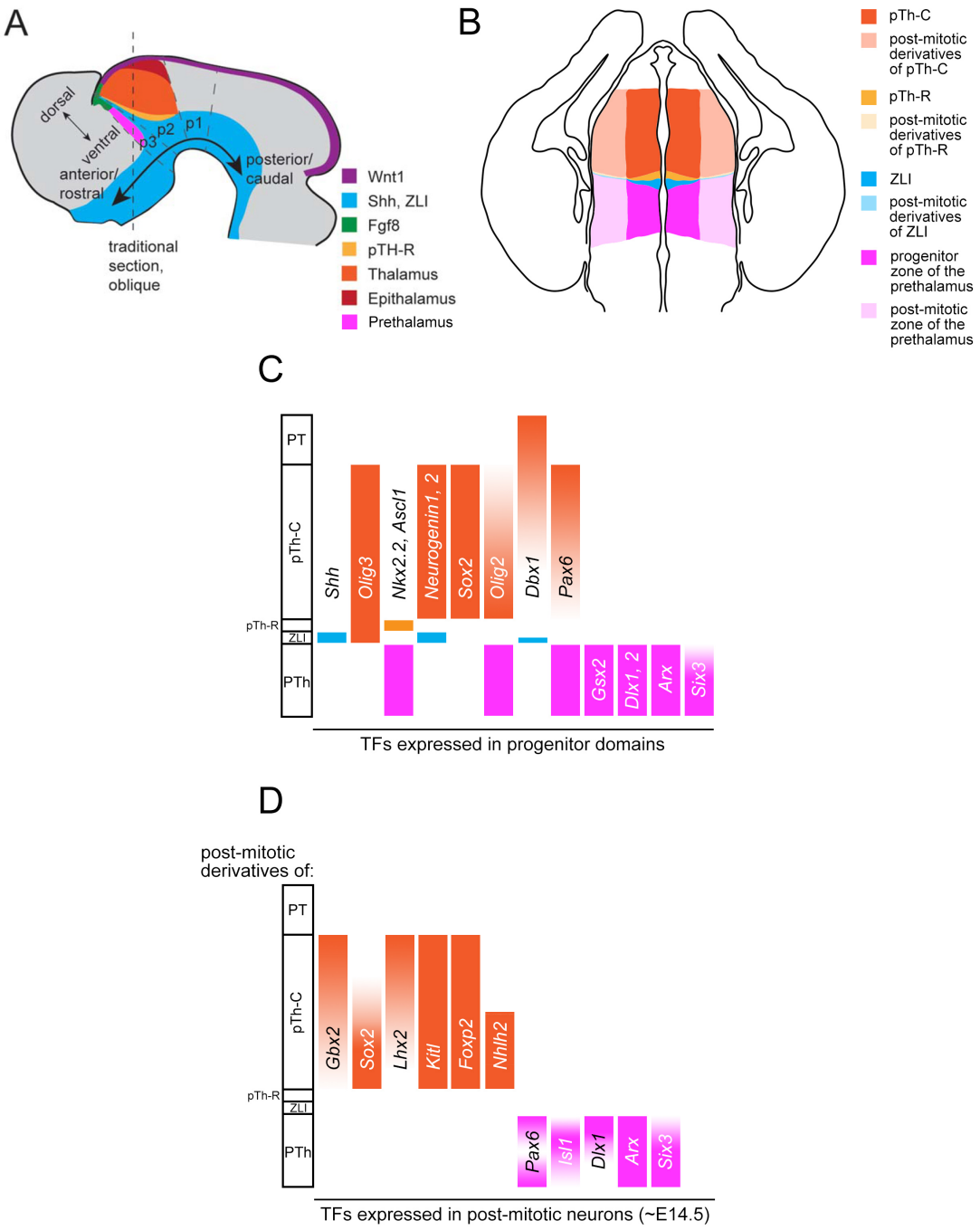

Figure 1.3 Schematic representation that summarizes early domain specification and different nuclei in the developing diencephalon. (A) Scheme of sagittal section through the early developing brain with prosomere 1-3 and key morphogens indicated. **(B)** Schematic representation of coronal view of the neural tube sectioned at the level indicated by the dash line in (A). Different regions of the diencephalon were indicated with areas marked with different colours. **(C)** Progenitor domains and transcription factors expressed in ventricular zone (VZ) of the diencephalon. **(D)** A selection of transcription factors expressed in thalamic and prethalamic neurons around E14.5, region of expression indicated. PT pretectum, PTh prethalamus. ZLI zona limitans intrathalamica. Figure (A), (C), (D) adapted from (4).

1.1.5.2 The thalamic nuclei

Under the instructions of combinational expressions of specific transcription factors, most thalamic cells start to differentiate and further organise into various thalamic nuclear complexes at about E15.5 (4). Together, they form one of the most important sensory information relay stations to the cortex (1,2).

The thalamic nuclei derived from the P2 alar plate are named and classified according to their topographic positions within the thalamus and by their function (4,8). The posterior nuclei (Po), derived from the Sox2 positive thalamic progenitors, are involved in pain transmission, visual orientation, eye movement and accommodation, as well as auditory and visual information relay (4,8,35,65). The ventral posterior nucleus, which can be further divided into posterolateral (VPL) and posteromedial (VPM) sections, also derives from the thalamic Sox2 lineage and is related to sensorial systems (4,8). The medial dorsal thalamic nuclei (MD) and the centromedian nuclei (CM) both derive from thalamic Dbx1 lineage progenitors and express Gbx2 stably (4,6,35). MD functions to modulate emotional arousal and the expression of emotional based behaviour, memory and feelings of pleasure (8). CM, together with intramedular, regulate excitability levels within the cerebral cortex, thus play significant roles in arousal and alertness in tune with circadian rhythm (8). The ventral lateral (VL) and ventral anterior (VA) nuclei modulate motor function whereas the anterior nuclei (AN) resides at the rostral pole of the thalamus, functions to modulate alertness, learning and memory (4,8). The medial geniculate thalamic nuclei (MGN) relays impulses from auditory structures to auditory centres of the cerebral cortex (8). The ventral MGN (MGv) is derived from thalamic progenitors positive for both Sox2 and Gbx2 expression (4,35). Other thalamic markers explicitly enriched in the MGv include Foxp2 and Shox2 (53). The lateral geniculate thalamic nuclei (LGN) process visual information and send it on to the visual cortex (Figure 1.4) (8).

The other P2 alar derivative, the epithalamus, further differentiates into habenular nuclei, stria medullaris tract and pineal body. The habenular nuclei

participate in motor and cognitive actions while the pineal gland (epiphysis) controls the internal circadian clock by way of melatonin secretion (8).

1.1.5.3 The prethalamic nuclei

Likewise, postmitotic neurons of the prethalamic derivative of P3 also form nuclei of characteristic functions (8). However, in contrast to the thalamus's relay of information to the cortex, nuclei of prethalamic origin possess no projection to the cortex whereas they mostly establish efferent connections with the thalamic nuclei, the striatum, the red nucleus and the substantia nigra (SN) (8).

In rodents, the main prethalamic derivatives of the P3 alar plate include the reticular thalamic nucleus (RTN), the zona incerta (ZI), the intergeniculate leaflet (IGL), the subgeniculate nucleus (SGN) and the ventral lateral geniculate nucleus (vLG) (Figure 3E) (8). Noted that the vLG has a mixed origin of cells from the prethalamus, pTh-R, ZLI, and thalamus, with thalamic neurons contribute to the dorsoventral region of vLG (4,53,66). The Ret, vLG and ZI together connect with other thalamic nuclei, modulating all incoming and outgoing information of the thalamus (8). Almost all the neurons in the RTN and most neurons in the vLG and ZI are GABAergic, apart from the A13 sub-nucleus in the ZI that accommodates dopaminergic neurons (45,64,66,67). Gene expression analysis of P0 mouse coronal sections showed that Dlx2, Isl1 and Six3 are expressed in both ZI and RTN at this age, whereas TH is only expressed in the A13 sub-nucleus and GAD67 is only expressed in the TRN and ventral ZI (57). Postnatally, Pax6 expression is maintained mainly by neurons in the TRN, ZI and SGN (68) (Figure 1.4).

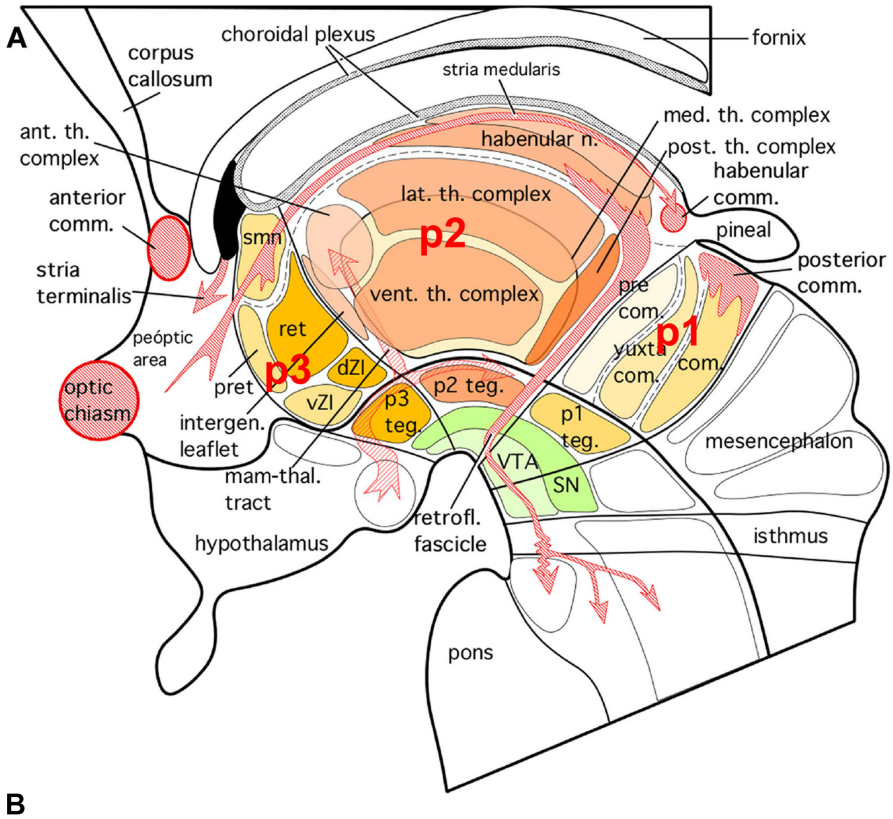
A
choroidal plexus
fornix
corpus
callosum
stria medularis
med. th. complex
ant. th.
complex
habenular n.
post. th. complex
habenular
comm.
anterior
comm.
lat. th. complex
p2
pineal
smn
posterior
comm.
stria
terminalis
vent. th. complex
pre
com.
p1
ret
peóptic
area
p3
dZl
vuxta
com.
com.
optic
chiasm
pret
vZl
p2 teg.
p3
teg.
p1
teg.
intergen.
leaflet
mesencephalon
VTA
SN
mam-thal.
tract
retrofl.
fascicle
isthmus
hypothalamus
pons

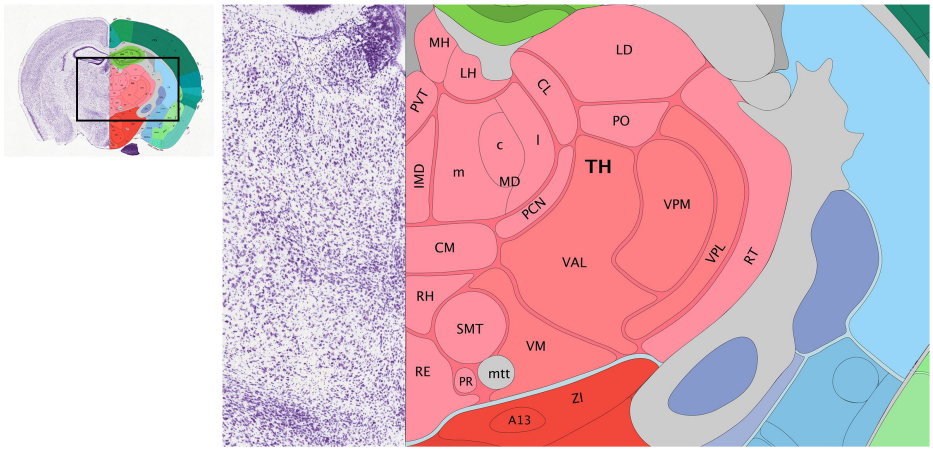
B
MH
LH
LD
CL
PVT
PO
c
l
IMD
m
MD
TH
PCN
VPM
CM
VAL
VPL
RT
RH
SMT
VM
RE
PR
mtt
ZI
A13

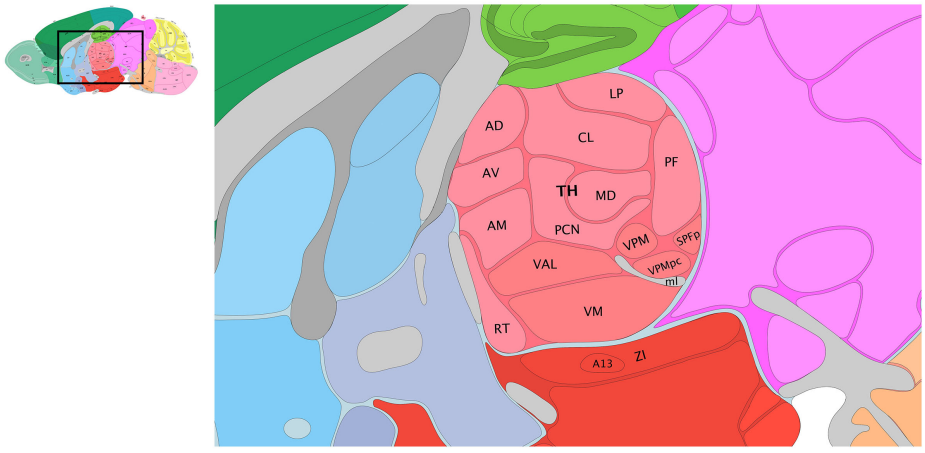
C
LP
AD
CL
PF
AV
TH
MD
AM
PCN
VPM
SPFp
VAL
VPMpc
ml
VM
RT
A13
ZI

Figure 1.4 Schematic representation of the diencephalic nuclei.

(A) Summary of the different nuclei and structures in the mammalian diencephalon. Major axon tracts were also presented. The P1 alar plate further develops into, from rostral to caudal, the precommissural pretectum (PTp), the yuxta commissural pretectum (PTy), and the commissural pretectum (PTc). The alar derivatives of P1 function to process afferent visual information as well as regulates visual reflexes formation, while the basal derivatives of the P1, which include the anterior pole of ventral tegmental area (VTA), substance nigra (SN) that involves in movement control, and the interstitial nucleus of Cajal (IC) that functionally involves in head orientation reflexes. The thalamic nuclei derived from the P2 alar plate can be further grouped into the lateral thalamic complex, which is responsible for somatosensory relay and motor control; the medial thalamic complex that extends projection to the prefrontal cortex, the striatum and the part of the cerebral cortex that innervate the same part of the striatum; the anterior thalamic complex, which participates in information relay from the mammillary nuclei to the limbic cortex; the posterior thalamic complex, which is involved in pain transmission, visual orientation, eye movement and accommodation, and auditory and visual information relay. The prethalamic derivatives of the P3 alar plate include: the reticular thalamic nucleus (Ret), the ventral lateral geniculate nucleus (vLGN), the subgeniculate nucleus (SG), the zona incerta (ZI), the intergeniculate leaflet (IGL) and the caudal pole of vLGN. The Ret, vLGN, SG and ZI together connect with other thalamic nuclei, modulating all incoming and outgoing information of the thalamus. P1 teg, P2 teg and P3 teg represents the tegmental parts of prosomeres 1-3.

(B) (B-C) Atlas of the diencephalic nuclei in the postnatal day 56 mouse brain from the coronal view (B) and sagittal view (C). Noted that not all the diencephalic nuclei mentioned in the text could be found at this level of sectioning.

Abbreviations for nuclei in the (B) but not mentioned in the text: nuclei derived from the epithalamus: medial habenula (MH), lateral habenula (LH); thalamic nuclei: intermediodorsal nucleus of the thalamus (IMD), medial dorsal thalamic nuclei central part (MDc), medial part (MDm) and lateral part (MDl), paraventricular nucleus of the thalamus (PVT), central lateral nucleus of the thalamus (CL), lateral dorsal nucleus of the thalamus (LD), paracentral nucleus (PCN), ventral anterior-lateral complex of the thalamus (VAL), ventral medial nucleus of the thalamus (VM), rhomboid nucleus (RH), nucleus of reuniens (RE), submedial nucleus of the thalamus (SMT), perireunensis nucleus (PR); prethalamic nuclei: reticular nucleus of the thalamus (RT); axon tract: mammillothalamic tract (mtt).

Abbreviations for nuclei in the (C) but not mentioned in the text: thalamic nuclei: anterodorsal nucleus (AD), anteroventral nucleus of thalamus (AV), anteromedial nucleus (AM), lateral posterior nucleus of the thalamus (LP), parafascicular nucleus (PF), subparafascicular nucleus, parvicellular part (SPFp), ventral posteromedial nucleus of the thalamus, parvicellular part (VPMpc); ml represents one of the fibre tracts.

Figure adapted from: (A) from reference (12). (B-C) from Allen Brain Atlas, Mouse Brain, Reference Atlas.

1.2 Neuronal morphogenesis underlying functional neural circuit formation

1.2.1 Neuronal morphogenesis

After cell fate specification, newborn neurons undergo active migration to reach their final destination, acquire their specific morphology and eventually form synapses with appropriate partners (1). This process is known as neuronal morphogenesis. Due to technical difficulties in visualising neuronal morphogenesis in vivo, the majority of our current knowledge was obtained from in vitro systems. Initially characterised in cultured neurons, neuronal morphogenesis can be roughly divided into five stages (69,70). Shortly after being plated in culture, the morphologically undifferentiated neurons start to extend circumferential actin-rich lamellipodia and filopodia (Stage 1, Figure 1.5) (69,70). During the transition from Stage1 to Stage2, neuritogenesis happens as the actin-rich lamellipodia, and filopodia further protrude and become engorged by microtubules and thus turn into minor neurites. Upon the completion of neuritogenesis, neurons typically display multiple minor neurites that undergo continuous protrusion and retraction, and all of them have the potential to become axons (Stage2, Figure 1.5) (70,71). If no external cues are present at this stage, intrinsic mechanisms break neuronal symmetry by activation/inhibition of localised cytoskeletal effectors, which further influence microtubule stability and actin dynamics in the growth cone at the tip of each neurite. As a result, the neurite with a larger and more dynamic growth cone will elongate more rapidly and become the axon (70,72). This process is known as axon specification, whose occurrence marks the neurons' transition from Stage2 to Stage3 and bestows upon the developing neurons' polarity (Stage3, Figure 1.5) (70,73). The axonal region further suppresses elongation of other neurites, which thus remain short and only develop into dendrites at later stages (70). At Stage4, the axon continues to elongate and differentiate, whereas other neurites acquire their dendritic identities and start to grow and arborise. Further on, at Stage5, neurons start to make synapses, develop dendritic spines and form neuronal circuits (Stage4-5, Figure 1.5) (70).

Recent advances in tissue culture and imaging techniques have shown that some of the typical morphologies described in cultures are analogous ex vivo. For example, several studies have reported that newborn cortical neurons displayed multiple processes when they migrate to the subventricular zone (SVZ) of the cortex (74–76). These processes were in a constant state of extension and retraction, which highly resembled the multiple neurites in cultured neurons at Stage2 (74,75). Upon exit of the SVZ, morphological transitions that resembled neuronal polarity establishment were also recorded as these cortical neurons displayed morphological changes from multipolar to unipolar (74,76). However, to date, a truly definitive in vivo description of neuronal morphogenesis is still missing (70).

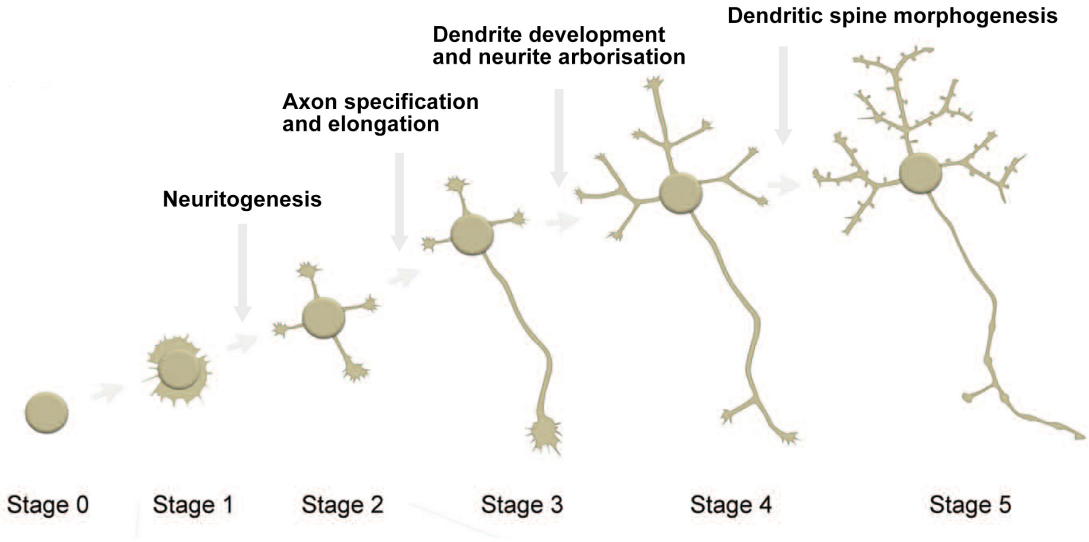

Figure 1.5 Neuronal morphogenesis can be divided into a series of stages which were initially characterized in cultured neurons, but also seem to occur in vivo. Figure adapted from (70).

1.2.2 Reorganization of the cytoskeleton during neuronal morphogenesis by effector genes

In vivo, an array of extracellular cues direct neuronal morphogenesis by coordinating the establishment of neuronal polarity and axon specification in addition to the intrinsic mechanisms and guide the axons towards proper target destinations for innervation (77). The external cues do so by binding with specific membrane receptors in the growth cones, which then activate various signalling pathways (77,78). Such reactions are then relayed to different cytoskeletal effectors that eventually carry out extensive remodelling of the actin and microtubule cytoskeleton (77).

Take nerve growth factor (NGF), an inductive signal for neuronal polarisation and axon elongation, as an example. Although being incompletely defined, it is proposed that the binding of NGF with tyrosine receptor kinases (Trks) on the growth cone cell membrane activates PI3K, the latter then phosphorylates phosphatidylinositol-4,5-bisphosphate (PIP2) to produce phosphatidylinositol-3,4,5-trisphosphate (PIP3) in the cell membrane (Figure 1.6B). Local activation of PI3K and accumulation of PIP3 then activate their downstream targets, such as protein kinase B (PKB, also known as AKT) and Rho-GTPases. One of AKT's functions is to phosphorylate and inactivate glycogen synthase kinase 3β (GSK3β). GSK3β inactivates the activity of several microtubule-associated proteins (MAPs) on a post-translational level by phosphorylating these MAPs. Upon being phosphorylated, GSK3β substrates such as Tau, adenomatous polyposis coli (APC) and Collapsin-response mediator protein-2 (CRMP-2) lose their abilities to stabilise microtubule or assembling tubulin dimers onto the growing microtubules. Thus, localised inactivation of GSK3β by the PI3K-AKT pathway results in microtubule polymerisation and cytoskeletal remodelling that precedes neuronal polarity establishment (79). Besides, localised activation of PI3K can also activate the PI3K–partition defective protein (Par) complex. The core of the Par polarity complex is composed of Par3, Par6 and atypical protein kinase C (aPKC). The Par complex also functions to specify axons from neurites by regulating activities of the MAPs,

whereas aPKC itself can also phosphorylate GSK3β, thereby antagonise GSK3β's action (78) (Figure 1.6B).

While signalling pathways converging on GSK3β mainly influence microtubule dynamics, regulations of the actin cytoskeleton upon neuronal polarity establishment are mostly carried out by three Rho-GTPases (Rho, Rac and CDC42). Binding of inductive signals with membrane receptors leads to the activation of different kinds of guanine nucleotide exchange factors (GEFs) or GTPase activating proteins (GAPs). The former activates whereas the latter inactivates specific Rho GTPases. Activations of Rac and CDC42 by GEFs such as the DOCK family proteins antagonise the activity of the RhoA-ROCK pathway and further lead to activation of specific actin-binding proteins (ABPs) that increase actin cytoskeleton dynamics and facilitate actin bundling (77). Additionally, signalling pathways relaying onto PI3K and the Par polarity complex can also influence actin cytoskeleton remodelling thus coordinating cytoskeletal changes among the actin and microtubule systems (Figure 1.6B) (78).

The special cytoskeletal arrangements within the growth cone enable it to respond to these external cues with corresponding behaviours. The growth cone thus serves as a sensory and motile organelle that directs neurite/axon pathfinding and target recognition for precise wiring of the neural circuitry (80). In response to inductive guidance cues, the actin cytoskeleton in the periphery of the growth cone bundles together to support protrusion of nascent lamellipodia and filopodia, whose stability is further enhanced by engorgement with microtubules. As a result, the once motile proximal section of the growth cone consolidates and becomes a new section of the extending axon, whereas the distal part of the growth cone ventures further. The actin and microtubule cytoskeleton in the growth cone are continuously engaged in this three-step cycle of protrusion, engorgement and consolidation in response to gradients of external cues, thus achieving growth cone advancement hence axon elongation towards target destinations (77).

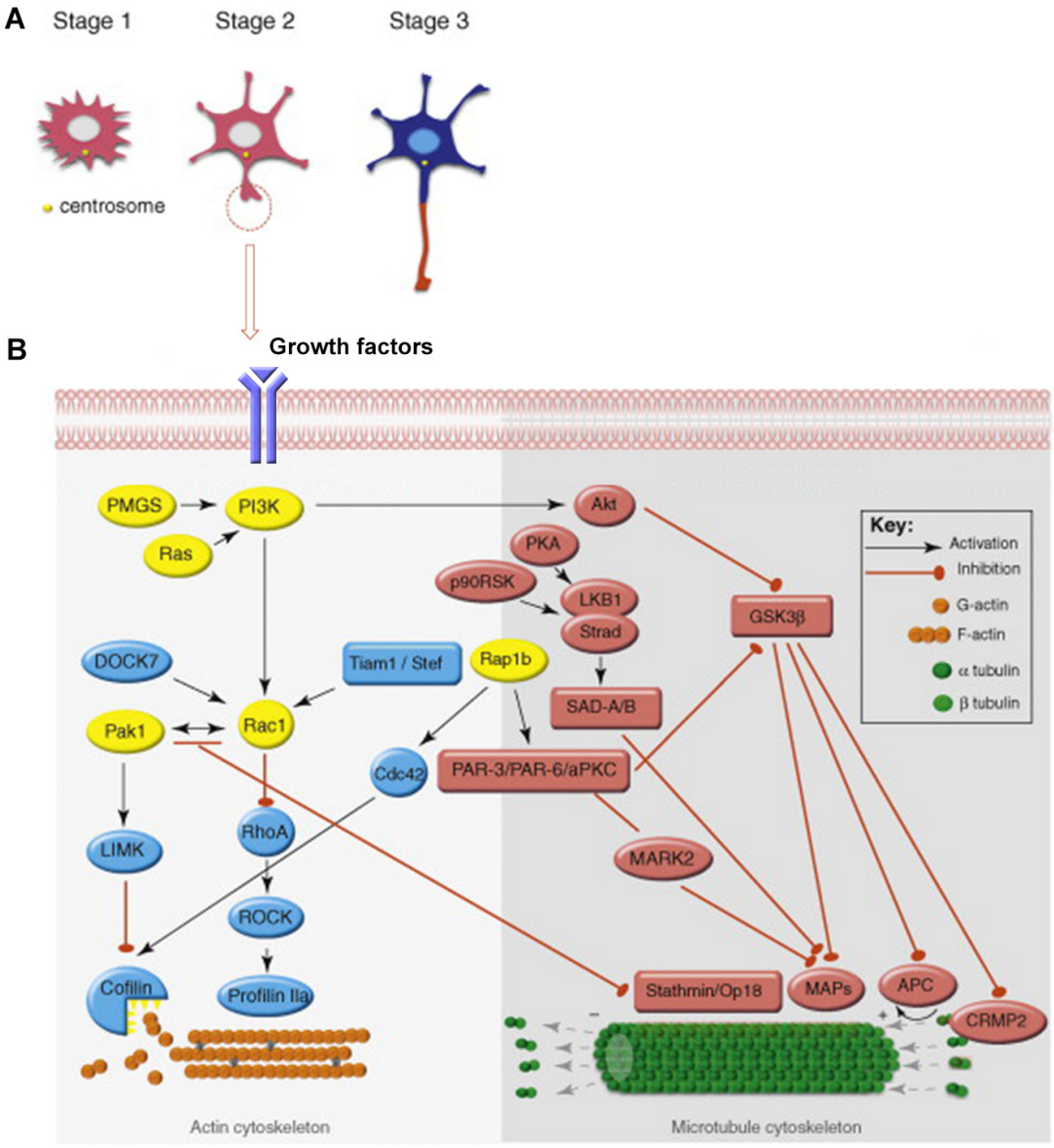

Figure 1.6 Schematic representation of key molecular pathways in regulation of neuronal polarity establishment. (A) Stages of development of cultured neurons showing the breaking of symmetry that begins in stage 2 neurons with the enlargement of the growth cone of the presumptive axon, followed by the accelerated growth of the axon (red) during stage 3. The red circle and arrow both point to the enlargement of a sub-membranous domain in the growth cone of the future axon as shown in (B). **(B)** The coordination of various molecular pathways underlies axon specification during establishment of neuronal polarity. The process requires the contribution of actin cytoskeleton remodelling factors (blue), such as cofilin, and factors that regulate the dynamics of microtubules (red), such as MAPs. Some factors stand at the crossroads of the microtubule and actin cytoskeleton regulations, such as PI3K (yellow). Figure adapted from (78).

1.2.3 Axon initial segment maintains neuronal polarity and determines the excitability of neurons

Neurons are highly polarised in terms of their morphology, directions of information transmission and subcellular structures as ion channels, organelles and protein complexes, which are restricted to distinct membrane domains or cellular compartments (81,82). Neuronal polarities as such are established during neuronal morphogenesis, under the combinational influence of intrinsic and extrinsic mechanisms, and will be maintained throughout the lifetime of the neurons (81,83). All the above forms of neuronal polarity are regulated and exemplified by the axon initial segment (AIS), which is a subcellular structure located at the proximal end of the axon that serves as both a physiological and a physical bridge between the somatodendritic and axon domains (Figure 1.7A-A') (81). A range of cytoskeletal proteins, cell adhesion molecules and voltage gated ion channels are meticulously arranged within the AIS (81,82). For example, fasciculated microtubules and actin rings are the cytoskeletal backbones of the AIS. Cell adhesion molecules, voltage-gated Na+ and K+ channels at the cell membrane of the AIS region are tethered to this cytoskeletal backbone via the other two cytoskeletal proteins βIV Spectrin and Ankyrin G (AnkG, also known as Ank3) (81,82) (Figure 1.7C). It has been shown that Na^+ channel density in the AIS is about 40-50 times that in the soma or proximal dendrites (81,84,85). As a result, this high degree of subcellularly polarised enrichment of Na+ channels facilitates a high Na^+ influx upon stimulation (84,86). Therefore, the AIS is usually where the action potential initiates, and its specific structure and molecular constituents determine the excitability and electrophysiology profile of the neurons (81,86,87).

The AIS was first described more than 50 years ago (88). However, until today, many crucial steps during AIS assembly remain elusive (82). For example, we are still trying to understand how the location and length of the AIS are determined, and how the ion channels are recruited to the AIS during development (81,82). Nevertheless, it is known that the AIS assembly is an

intrinsic property of the neurons as no extracellular or glial-dependent cues are required (81,89). The cytoskeletal scaffold protein AnkG plays a determining role during AIS assembly due to its modular structure (81,82,90). AnkG has a membrane binding domain, a spectrin-binding domain, a serine-rich domain, a tail domain and a carboxyterminal domain (Figure 1.7B) (82,91). With its membrane binding domain, AnkG can bind to the cytoplasmic portion of the transmembrane Na^+ channels, K^+ channels and cell adhesion molecules (CAMs) such as NrCAM and Neurofascin 186 (NF 186). With its spectrin binding domain, AnkG is able to tether itself to the underlying cytoskeletal scaffold protein βIV spectrin and αII spectrin. One end of the spectrin protein is anchored on the actin ring backbone of the AIS, whereas the other end is tethered to the overlying plasma membrane (82). As a result, by binding to the voltage-gated ion channels, cell adhesion molecules and spectrin proteins, AnkG is able to enrich the distribution of voltage-gated ion channels within the AIS region while also securing such a specialised structure to the overlaying plasm membrane, the underlying cytoskeleton and also the surrounding environment (Figure 1.7C). Besides, AnkG is also essential for the long-term stability of the AIS in mature neurons (81,82). Suppression of AnkG expression in hippocampal neurons using short hairpin RNA (shRNA) results in disassembly of the AIS with diminished expressions of Na^+ channels, βIV spectrin and the AIS adhesion molecules NrCAM and NF 186 (92).

In neuronal cultures, AnkG clusters along the proximal axon early during development (about 3-4 days in vitro (DIV)), which further directs AIS assembly by recruiting the other AIS components such as ion channels, CAMs and βIV spectrin (82,93). However, little is known about the mechanisms that guide the concentrated distribution of AnkG to the putative AIS region (81). It has been shown that soon after the establishment of neuronal polarity and axon elongation, the periodic actin rings can be seen prior to the assembly of AIS (94). These actin rings likely coordinate the micro-architecture within the AIS, and serve as the initial scaffold, on which the future AIS will be assembled (94,95). However, actin rings as such are not sufficient to restrict the AIS

complex to the proximal axon, as they are present throughout the entire axon (95). The actin rings at the proximal axon are organised by βIV spectrin whereas the actin rings at the distal axon are organised by βII spectrin. While βIV spectrin tethers AnkG, βII spectrin tethers Ankyrin B (AnkB) (94,95). It is known that AnkG and AnkB compete against each other and this competition between them functions to enhance AnkG targeting to the proximal axon and regulate the length of AIS (93). However, it is not essential for localised distribution of AnkG at the putative AIS site in the first place (96).

Findings from two recent studies have shed more light on this issue. Stephen L. Berger et al. have found that diphosphorylated myosin light chain (pMLC) is enriched in the putative AIS region before the localised expression of AnkG in the primary cultures of rat hippocampal and cortical neurons (97). Myosin light chains are part of the hexameric structure of the contractile Myosin II, which is a classical actin-directed motor protein complex (98). Increased phosphorylation of MLC resulted in ectopic AnkG expression in the distal axon (97). In the other study, M. Tapia et al. showed that phosphorylated β-catenin is also enriched at the putative AIS region in the cultured hippocampal and cortical neurons, before the localised expression of AnkG. Additionally, enriched expression of GSK3αβ was also found in the AIS. Inhibition of GSK3 function by lithium chloride and pharmacological inhibitors, as well as reducing the expression level of β-catenin by shRNA resulted in reduced AnkG and voltage-gated Na^+ channels at the AIS (99). It remains to be determined how these different molecules and phosphorylation systems coordinate to facilitate AIS assembly. However, a very intriguing message conveyed by these studies is that although AIS assembly is a cell-autonomous event, various signalling pathways can affect the details of the AIS structure via controlling the activities of kinases and phosphatase, as a method to regulate the development of neuronal excitability and fine-tune neuronal plasticity in the mature brain.

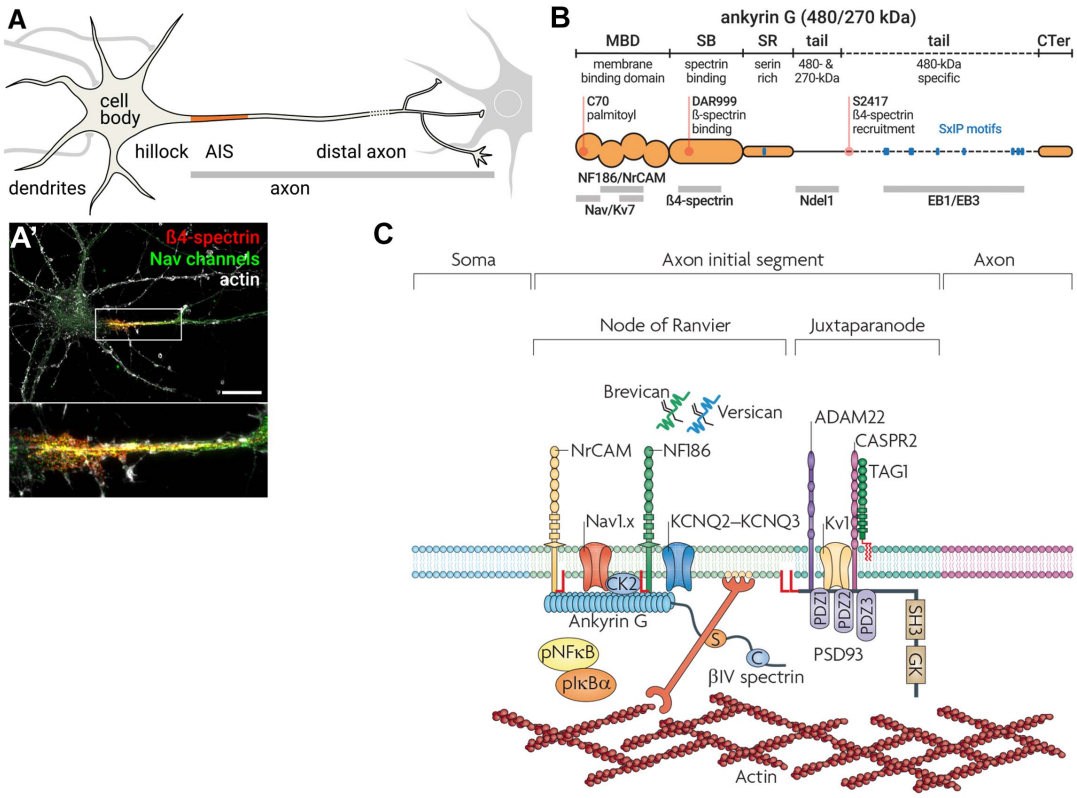

Figure 1.7 The molecular structure of the AIS and Ankyrin G. (A) A typical neuron receives input on the cell body and dendrites (left). The hillock leads to the axon, which contains the AIS (orange). The distal axon contacts downstream neurons (right). **(A')** Hippocampal neurons after 22 d in culture labelled for the AIS components NF-186 (green) and β4-spectrin (red). The somato-dendritic compartment is labelled using an anti-MAP2 antibody (blue). Scale bar, 50 µm. **(B)** Modular structure of ankyrin G, which exists as isoforms of 480 and 270. Important residues (red) and EB-binding SxIP motifs (blue) are indicated. Binding sites of partners are indicated below the protein (gray bars). Figure (A), (A') and (B) adapted from reference (82). **(C)** The molecular organization of the AIS. The AIS is comprised of ion channels (Nav1.x, KCNQ2–KCNQ3 and Kv1.x), cell adhesion molecules (neuronal cell adhesion molecule (NrCAM), neurofascin 186 (NF186), a disintegrin and metalloproteinase domain-containing protein 22 (ADAM22), transient axonal glycoprotein 1 (TAG1, also known as contactin 2) and CASPR2), extracellular matrix molecules (brevican and versican), cytoskeletal scaffolds (AnkG, βIV spectrin and postsynaptic density protein 93 (PSD93)) and other signalling proteins. GK, guanylate kinase; PDZ, PSD95/discs large/zonula occludens; SH3, SRC homology 3. Figure adapted from reference (81).

In neurons that fire repeatedly, the summation of synaptic inputs into bursts of action potentials is carried out by the AIS, given the high densities of voltage-gated Na^+ and K^+ channels at the AIS (81). As a result, the various characteristics of each AIS, such as its location, length, populations and locations of the voltage-gated ion channels, as well as their expression levels within the AIS, are all closely linked to the electrophysiology profile of that

neuron (81,87,100). For example, previous studies have shown that the AIS size and its distance from the soma are considerably variable across the substantia nigra pars compacta (SNc) dopaminergic neuronal population (101). Extracellular recording of these neurons in the SNc and corresponding staining of AnkG showed that their rate of tonic firing is positively correlated with AIS length, but negatively correlated with the distance between AIS and soma(101) . Besides, increased expression of the Na+ channel NaV1.6, AnkG and increased lengths of the AISs were observed in pyramidal neurons in the hippocampal CA1 area of the Angelman Syndrome mouse model, which was correlated with more hyperpolarised resting membrane potential, more hyperpolarised threshold potential, larger amplitudes and maximum rates of action potentials (102). Last but not least, when AnkG expression was diminished in the AIS due to a reduced level of β-catenin by shRNA, Tapia et al. further showed that these neurons were less excitable, with lower amplitudes of action potentials and densities of sodium currents (99).

1.2.4 Excitability and electrophysiology profiles of the thalamic and prethalamus-derived neurons

Diencephalic-derived neurons show distinct electrophysiology properties in comparison to cortical neurons, as diencephalic neurons are known to display two distinct response modes of action potential firing- tonic and burst firing (67,103,104). Cortical neurons that are involved in the thalamocortical relay circuits only fire in the tonic mode (104). To elaborate, I will take neurons from the lateral geniculate nucleus (LGN) as representatives for the thalamic neurons and neurons from the thalamic reticular nucleus (TRN) as representatives for the prethalamus-derived neurons. The LGN, as mentioned before, is the thalamic relay of retinal information to the cortex and provides a reasonable model for all thalamic nuclei (4,103). The TRN might be one of the most studied nuclei of prethalamic origin. Hence there is more comprehensive electrophysiological analysis on the TRN in the existing literature than any other prethalamus-derived nuclei.

When a neuron fires in the tonic mode, the cell responds with a stream of unitary action potentials as long as the stimulus is suprathreshold for firing (Figure 1.8A) (103). On the other hand, when a neurons fires in the burst mode, which is usually in response to more hyperpolarised stimuli, the cell fires with short-lasting (up to 100ms) high-frequency bursts of action potentials riding on the crest of an overshoot (Figure 1.8A') (67,103). An inward Ca^{2+} current that is known as I_T, which is mediated by the T-type low-threshold Ca^{2+} channels, is responsible for the burst firing mode (103,105,106). Unlike the voltage gated Na^+ channels and K^+ channels, which are tethered by AnkG at the AIS, the T-type low-threshold Ca^{2+} channels are located in the membranes of the soma and dendrites (103,107–109). The threshold voltage that activates the T-type low-threshold Ca^{2+} channels are more hyperpolarised than the threshold voltages that activate the Na+ channels (110,111). Therefore, when a neuron is hyperpolarised, a depolarising stimulus is more likely to activate the T-type low-threshold Ca^{2+} channels instead of the voltage-gated Na^+ channels (111). Consequently, I_T is activated and the inflow of Ca^{2+} causes depolarisation of

the cells. The latter further activates a burst of conventional action potentials mediated by Na^+ and K^+ channels (103,110,111). As a result, which mode of firing the neurons undergo is determined by both the types and abundance of membrane bound voltage-dependent ionic channels and the state of resting membrane potentials (103,110,111). When a neuron is relatively depolarised, the T-type low-threshold Ca^{2+} channels are inactivated (110,111). The neuron thus responds to depolarising stimuli with voltage-gated Na+ channels and fire in the tonic mode. However, when the neuron is relatively hyperpolarised, T-type low-threshold Ca^{2+} channels are de-inactivated, and therefore the neurons will fire in the burst mode (103,110,111).

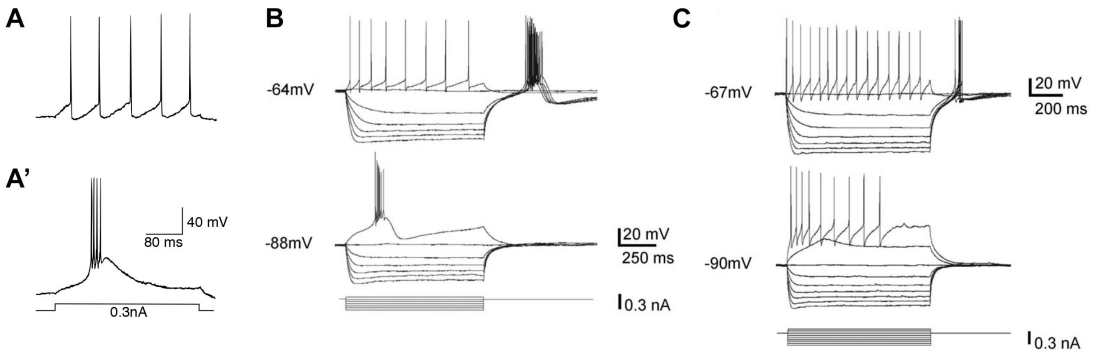

Figure 1.8 Tonic and burst firing of neurons in the LGN and TRN. (A) and **(A')** Responses of one LGN neuron to the same depolarising current pulse delivered intracellularly are shown, but from two different initial holding potentials. **(A)** I_T is inactivated, and the cell responds with a stream of unitary action potentials as long as the stimulus is suprathreshold for firing. This is the tonic mode of firing. **(A')** When the cell is relatively hyperpolarized, I_T is de-inactivated, and the current pulse mediated by the low-threshold Ca2+ channels further activates the voltage gated Na+ channels, leading to four action potentials. This is the burst mode of firing. Adapted from (103). **(B)** and **(C)** Two functionally different types of TRN cells. **(B)** This type is a bursting cell since it usually emits a high-frequency burst of action potentials at both the offset of hyperpolarizing current pulses and the onset of depolarizing pulses (from a strongly hyperpolarized level). **(C)** That unit is a tonic cell since it does not fire a burst discharge of action potentials at both the offset of hyperpolarizing current pulses and the onset of depolarizing pulses (from a strongly hyperpolarized level). Adapted from (67).

All thalamic relay cells exhibit both the tonic and burst firing modes (103). They can switch between these two modes depending on the specific afferent stimuli from the peripheral sensory organs, prethalamus-derived nuclei and cortex (67,103,104). However, this is not the case in the prethalaic nuclei such as the TRN (67). In the TRN, neurons can be divided into two functionally different types- the ones that can fire in both the tonic and burst modes and the ones that can only fire in the tonic mode (Figure 1.8B-C) (67,112). Also, thalamic neurons and prethalamus-derived neurons that can fire in both the tonic and burst modes display several other differences in terms of their firing characteristics. Firstly, the transient Ca^{2+} conductance mediated by the T-type low-threshold Ca^{2+} channels inactivates much more slowly in the TRN cells than the thalamocortical (TC) neurons (113). Secondly, the low-threshold current of the TRN cells has different voltage dependence features to those recorded in the TC cells (67). Thirdly, in urethane-anaesthetised or lightly narcotised rats, TRN cells transiently fire at both the onset and offset of whisker deflection and display robust tonic firing during sustained whisker deflection. However, to compare, the TC neurons of the corresponding somatosensory thalamic nucleus display a weaker tonic pattern and usually exhibit tonic suppression (67,114,115). Finally, in vitro intracellular recording found evidence of electrical coupling between two adjacent TRN neurons- current pulses that evoke tonic firing in cell1 can induce attenuated voltage oscillation (set of spikelets) in cell2 and vice versa (116). Whether such electrical coupling also exists between TC neurons remains to be confirmed.

So why are the diencephalic neurons programmed to fire in two modes? How does each mode contribute to the functionality of the neural circuitries? In general, tonic firing is known to afford better linearity, whereas burst firing supports better signal detection (103,105,111). For thalamic neurons, such as the ones in the LGN, both tonic and burst firing serve as effective relay modes in the awake state in rodents, cats, monkeys and humans (103,117–120). Therefore, tonic firing might be utilised to support a more faithful reconstruction of the visual world as it can minimise nonlinear distortion in the relay, while

burst firing can serve as some sort of ‘wake-up call’ when something has changed in the environment as it can maximise initial stimulus detection (67,103). As for prethalamus-derived neurons, such as the ones in the postnatal TRN, either tonic or burst firing would trigger inhibitory postsynaptic potentials (IPSPs) and further results in hyperpolarisation in a TC neuron due to the inhibitory nature of the GABA neurotransmitter produced by neurons in the TRN (67,104,121). Therefore, the TRN appears poised to induce a switch from tonic to burst firing of the TC neurons due to its ability to hyperpolarise TC neurons (104,122). However, the exact effects and functions of tonic and burst firing of TRN neurons on the responsiveness of the TC neurons remain elusive.

One thing to keep in mind is that the very roles of tonic and burst firing in both thalamic and prethalamus-derived neurons need to be considered within the big picture of what type of neural circuitries they are involved in. For example, open-loop arrangements between the thalamus and TRN have been found, in which the TRN receives input from regions of the thalamus that do not receive returning axons from the TRN (104,123,124). Adam M. Willis et al. have simulated a simple neural circuit, in which the TC cells innervate both the TRN and layer4 (L4) cortex, and either the TRN innervate reciprocally with TC cells to create a closed-loop arrangement or the TRN do not project to the TC cells to create an open-loop arrangement. In the closed-loop arrangement, tonic input to the TC cells can induce rhythmic tonic spiking in the TC cells and the TRN cells, as well as an onset response in the L4 neurons. However, in the open-loop arrangement, when tonic stimulations were applied to the TC cells, the latter can only fire intermittent spikes, which further drive tonic firing in the L4 cells, with occasional failures of stimulation not being able to be recapitulated in the L4 cells. Nevertheless, when another tonic input was added to the TRN cells along with the tonic stimulation as above on the TC cells in the open-loop arrangement, TC cells occasionally bursts in addition to the individual spikes of tonic firing, which further led to a higher total number of spikes in the L4 cells (104). Therefore, how these neural circuitries are

constructed impacts profoundly on how the neurons within would respond to the same stimuli. Although neurons in the TRN only send axons to and innervate neurons in different thalamic nuclei, it receives monosynaptic glutamatergic inputs mainly from both the cerebral cortex and the thalamus, as well as GABAergic, cholinergic and monoaminergic inputs from other parts of the brain, such as basal forebrain and the amygdala (67). All these afferent inputs affect which firing mode the TRN neurons undergo, and further determine how the nervous system as a whole would respond and react.

1.3 The Pax6 gene

1.3.1 Structure and transcription regulation of the Pax6 gene

The Pax6 gene encodes a highly conserved transcription factor from the paired box (Pax) family (125–127). Both the human PAX6 and mouse Pax6 gene contain 16 exons that span over 30 kb of the genomic DNA, and the human and mouse PAX6 proteins being produced share the identical amino acid sequence (128–130). PAX6 contains a paired domain (PD) and a paired-like homeodomain (HD) (125). Although both the PD and HD can bind to specific DNA target sites, only the PD is crucial for most of the well-known functions of Pax6, including regulation of proliferation, neurogenesis, telencephalic regionalisation, the formation of the pallial-subpallial boundary (PSPB), and so on (131–135). Four transcriptional initiation sites have been identified in the mouse Pax6 gene (Figure 1.9A) (128,136–139). With P0 and P1 giving rise to the primary transcripts of Pax6 (MW 46kDa) and an alternatively spliced variant Pax6(5a) (MW 48kDa), the two internal initiation sites, Palpha and P4, produce transcripts that encode for truncated PAX6 proteins that lack the PD (128,136,140). The Pax6(5a) variant includes 14 additional amino acid residues encoded by the exon 5a, which also results in disruption of DNA binding properties of the PD (128,140–142) (Figure 1.9B). Quantitative studies have revealed that in embryonic mouse tissues, the expression ratio of Pax6 and Pax6(5a) was around 8:1 (141).

A number of regulatory elements that regulate tissue-specific expression of Pax6 are within the vicinity of the Pax6 coding region (128,137,140,143). For example, the long non-coding RNA (lncRNA) Paupar is located within about 25kb 5'- from the P0 promoter (140,144). Paupar is expressed in the brain and can regulate the expression of Pax6 and other genes located on other chromosomes (140,144). Subsequent studies based on analysis of evolutionarily conserved non-coding regions identify an ectodermal enhancer (EE) upstream from the P0 promoter, which contains an array of Meis1/2, Oct1 (Pou2f1), Pax6, Pknox1 (Prep1), Six3 and Sox1/2 binding sites (140). Indeed,

molecular and genetic evidence showed that Pax6 could autoregulate its expression, whereas Pax6 and Six3 have been shown to mutually regulate the transcription of each other during mouse lens development (140,145,146).

1.3.2 Function of the PAX6 proteins

PAX6 proteins recognise specific DNA sequences through a variety of mechanisms enabled by their HD, PD and alternative splicing (140). The PD contains two independent subdomains- the N-terminal (PAI) and C-terminal (RED) subdomains (Figure 1.9B) (128,131,140,147). Both of these subdomains can bind to DNA (142,147). As a result, binding of PD exhibits a bipartite feature, so do the DNA sequences that the PD binds (131,142,147). The current model proposed that PAX6 binds to DNA by both the HD and PD (135,148). However, the DNA-binding properties of the HD receive less attention, possibly due to the findings that subtle defects were observed in the mouse developing forebrain when a point mutation was introduced to abolish the HD of Pax6 specifically (135). As a result, it was proposed that Pax6 HD might primarily function as a protein-protein interaction domain (135,140). In Pax6(5a), the HD is the only DNA binding domain available as the inclusion of the extra 14 amino acid residues from exon 5a interfere with the DNA-binding function of the PD (148). Under this premise, Zhang et al. found that in adult ocular tissues (cornea, lens and retina), the ratio of Pax6 and Pax6(5a) had decreased from 8:1 as observed in the embryonic tissues to 1:1 and deletion of exon 5a in these tissues disrupted iris formation (141,149). These findings indicated tissue-specific functions of exon 5a and also the HD of PAX6(5a). On the other hand, more recent studies have identified DNA sequences that can be recognised by both HD and PAI subdomain, as well as HD-recognition sequence that locate immediately to the 5’ end of the PD binding sequence, therefore forming the Pax6 HD-PD recognition site (148,150). These findings have complicated the mechanisms of function of the PAX6 proteins.

Nonetheless, a recent genome-wide Pax6-ChIP sequencing study identified a total of 3514 and 3723 Pax6-containing peaks in mouse forebrain and lens

respectively, with about 70% of them found in both tissues (150). When linking these Pax6 peaks to their adjacent genes, Sun et al. found 1808 putative Pax6-target genes in the forebrain, and 2099 putative Pax6 target genes in the lens. When comparing these two lists of Pax6-target genes with previously found deferentially expressed genes in Pax6-null cortices and lens placodes, they further confirmed 90 and 191 genes directly regulated by Pax6 in the forebrain and lens respectively. The largest functional classes these genes are involved in include DNA-binding transcription factors, cell surface receptors including cell adhesion molecules and their ligands, intracellular signalling molecules and cytoskeletal proteins (150).

1.3.3 Expression patterns of Pax6 in the developing mouse forebrain

Pax6 exhibits a restricted spatiotemporal expression pattern in the CNS, eye and nose (151). It is first detected when the major components of the developing CNS start to emerge after neural tube closure (around E8.0), and its expression pattern changes considerably as major structures such as cerebral cortex specialise and expand (128). In the mouse neural tube at E13.5, Pax6 is expressed in the ventricular zone of the cerebral cortex, in a lateral-high, medial-low and rostral-high, caudal-low manner (128,152). However, in the diencephalon, Pax6 is expressed in the ventricular zone of the thalamus, in a gradient that increases with distance from the ZLI, and in both the ventricular zone and a subset of post-mitotic cells in the mantle zone of the prethalamus (Figure 1.9C) (22). This expression pattern in the prethalamus is unique as in the developing CNS, Pax6 is mostly expressed by neural progenitor cells, which then shut down Pax6's expression upon exit of the cell cycle and embark on their journey of migration and differentiation (68). Various studies have proved the pivotal functions of Pax6 in diverse developmental processes of the CNS. However, most of these identified functions come from the Pax6-positive progenitor cells within the CNS and retina (128,133,140,153). The functions of Pax6 in the post-mitotic cells remain largely unknown. The prethalamus thus provides us with a unique and excellent system for us to further unveil the functions of this master regulator gene.

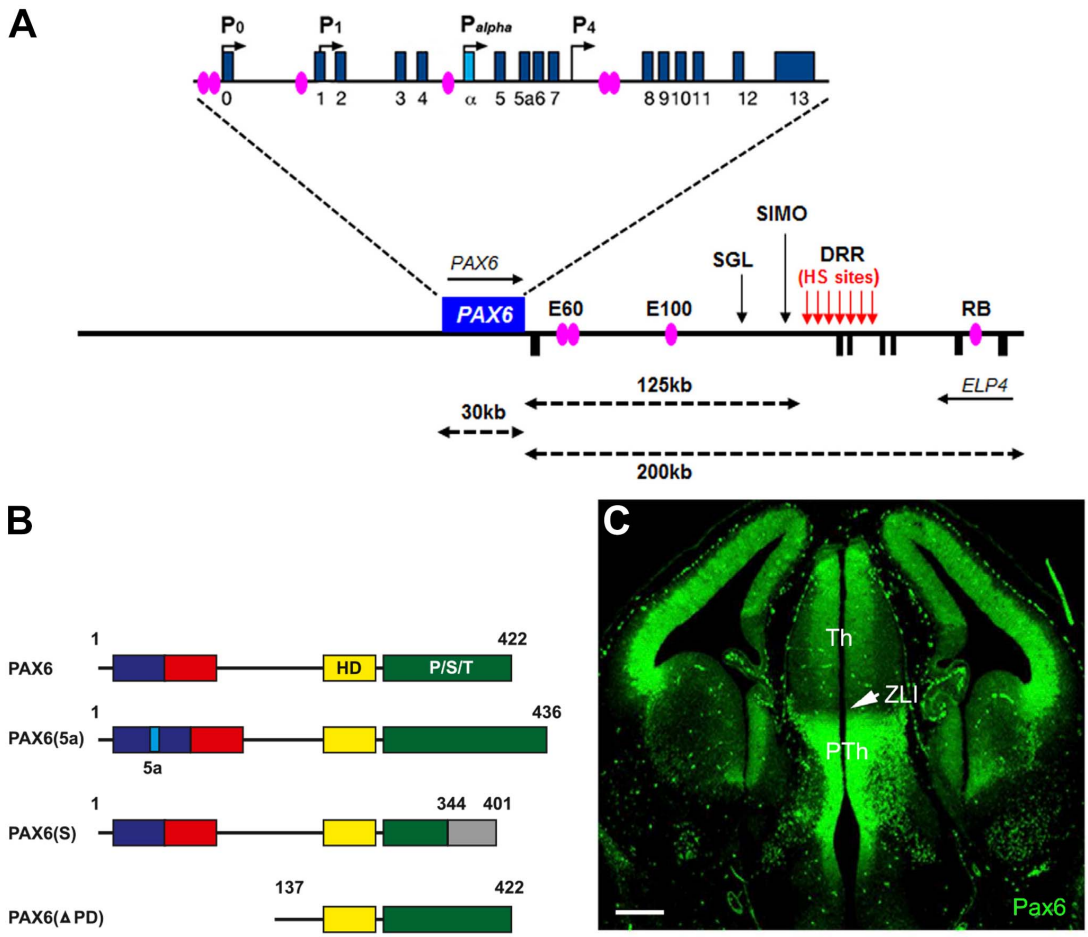

Figure 1.9 Structure of the Pax6 locus, the PAX6 proteins and the expression patterns of Pax6 in the mouse embryos. (A) Pax6 locus (exons marked by dark blue rectangles), promoters P0, P1, Palpha and P4, regulatory elements are marked by magenta ovals. Figure adapted from (128). **(B)** Diagrammatic representation of Pax6 proteins (PAX6, PAX6(5a), PAX6(S) and PAX6 (ΔPD)) due to alternative splicing and transcription initiation at different promotors. The bipartite paired domain of each PAX6 protein is represented by the rectangle on the left, with PAI subdomain being represented by the dark blue rectangle on the left (N-terminal) and the RED subdomain being represented by the red rectangle on the right, which is closer to the C-terminal. The homeodomain is represented by the yellow rectangle. The P/S/T domain where post-translational modifications usually take place is represented by the dark green rectangle. Figure adapted from (140). **(C)** Expression pattern of Pax6 in a coronal section of an E12.5 mouse embryonic brain. Pax6 is expressed in the ventricular zone of the cortex, in a gradient in the ventricular zone of the thalamus (Th), and in both the ventricular and mantle zone of the prethalamus (PTh). Pax6 expression is absent at the zona limitans intrathalamica (ZLI). Figure adapted from (22).

1.3.4 Pax6 acting as a master regulator of neural development

Since Pax6 sits at the top of the hierarchy of gene regulatory network, PAX6 proteins are classified as part of a rare group of 'master' regulators (128,133,140). These master regulators are capable of controlling cell fate specification and differentiation through regulating the expressions of 'secondary' transcription factors that further convey cell fate specification, and terminal differentiation products that underlie the functionalities of the mature cells (140). Therefore, disruption of the Pax6 gene can cause cascading defects in various processes during the development of the nervous system (128,133,140,154). For example, the Pax6 gene itself was first discovered and cloned by multiple groups that were trying to identify the genetic causes of congenital eye defects (125,133,155). Mutation or loss of one allele of Pax6 in human patients can lead to a spectrum of eye abnormalities such as Aniridia (i.e. lack of iris) and Peters' anomaly (thinning and clouding of the cornea) (156,157). In addition to eye defects, these patients also had symptoms associated with a range of neurological and psychiatric conditions including nystagmus, impaired auditory processing and verbal working memory, autism, and mental retardation (128,133). These conditions are linked to structural brain defects including a reduced size of the corpus callosum and anterior commissure, abnormalities of the cerebral cortex and cerebellum and absence of the pineal gland (128,140,154). Mouse models with Pax6 mutation share similar phenotypic defects, as haploinsufficiency of Pax6 in mice also leads to reduced sizes of eyes whereas loss of both alleles of Pax6 results in a complete absence of eyes (155,158). However, in Pax6 haploinsufficient mice, other parts of the developing central nervous system, such as the cerebral cortex and diencephalon, appeared to be normal, indicating divergence of Pax6's functions in evolution (134). Additionally, loss of both alleles of Pax6 in these mouse models is lethal as Pax6-null embryos die before birth with the absence of olfactory bulb, prethalamus, reduced size of cerebral cortex and cerebellum (22,128,152,153,155).

In the developing CNS, Pax6 plays crucial roles during various processes, including patterning of the neural tube, cell proliferation, migration of neurons, and formation of neural circuits (134). Mouse embryos with both copies of Pax6 alleles mutated display severe defects of dorsal-ventral patterning of the telencephalon (154). Decreased expressions of dorsal telencephalic markers such as Emx1, Ngn1, Ngn2, Tbr1 and Tbr2, along with ectopic expressions of ventral markers in the cortex, such as Gsh2, Mash1 (Ascl1), Dlx1, Vax1 and Six3 were observed in these embryos (151,154,159,160). Also, the boundary between the dorsal and ventral telencephalon, the pallial-subpallial boundary (PSPB), was severely impacted due to the loss of Pax6, as the expression levels of several PSPB markers are reduced or completely lost (151,154). What is more, due to Pax6's function to activate expression of specific adhesion molecules, such as R-cadherin, the loss of Pax6 further resulted in the loss of a mechanical palisade at the PSPB formed by radial glial cells (161). This palisade acts as a physical barrier to prevent mixing of the dorsal and ventral telencephalic progenitors. As a result, increased dorsal migration of ventral telencephalic cells was also observed upon loss of Pax6 (161). Apart from misspecification of dorsal-ventral identities, loss of innate structures and migration defects, these Pax6 mutant mice also have thinner cortices due to Pax6's function to increase cortical progenitor proliferation in a dosage-dependent manner (58,128,152). Loss of Pax6 in these mice caused increased cell cycle exit of cortical progenitors at early stages, which exhausted the progenitor cell pool prematurely and shifted the balance between proliferation and differentiation of the system towards the latter (152).

1.3.5 Pax6 removal causes severe defects in the developing diencephalon

1.3.5.1 Patterning defects and disruption of TCA formation

As mentioned above, Pax6 is expressed in a unique pattern in the diencephalon (22). At E12.5, Pax6 is expressed in a gradient in the ventricular zone of the thalamus, with its expression level increaseing with distance from the ZLI (22). This is likely due to the mutual repression of Pax6 and Shh released from the ZLI. In the prethalamus, Pax6 is expressed at a homogeneous level in the ventricular zone, and also in a subset of post-mitotic cells in the mantle zone (22). Previous studies have shown disruption of patterning and thalamocortical axons (TCAs) formation as the two major defects of the diencephalon after Pax6's removal. For example, Caballero et al., 2014 showed that Pax6 repress Shh expression in a cell-autonomous manner around the ZLI. Loss of Pax6 resulted in the expansion of markers of ZLI and pTh-R, such as Nkx2.2, Ascl1 and Gsx1, at the cost of reduction of pTh-C markers such as Sox2, Gbx2 and Ngn2 (22). In Pax6-null embryos, ectopic expression of some prethalamic genes (e.g., Lim1/Lhx1) are found in the prospective thalamic area, whereas other prethalamic markers, such as Sfrp2 that is expressed exclusively in the ventricular zone of the prethalamus, is completely lost (42,162). The physical structure of the prethalamus is hardly recognisable in the mouse line of constitutive Pax6 mutant, which lack Pax6 expression since conception (22,154). Additionally, previous studies have also shown that Pax6 is required in setting up a prepattern that contributes to the induction of pTh-R and pTh-C cell fate in the thalamic primordium in response to graded Shh concentrations (163). What is more, the loss of Pax6 would cause an anterior shift of mesencephalic markers, such as Dbx, into the prospective pretectum and the loss of several pretectum markers such as Gsh1, Lim1/Lhx1 and Wnt7b (164).

The thalamocortical axons are axonal projections sent by thalamic neurons to innervate the cerebral cortex (3,4). The TCA formation starts at about E12.5 in

mouse. TCAs extend rostral-ventrally through the adjacent prethalamus, then turned laterally to avoid the hypothalamus and enter the ventral telencephalon at about E13.5. After that, they turn dorsally into the cortex and innervate the correct cortical regions by about E18.5 (59,165,166). It is known that the deletion of Pax6 can cause defects in various key steps during this process, which all lead to the disrupted formation of the TCA (59,162,166,167). For example, in Pax6-null mouse embryos, the TCAs descend ventrally into the hypothalamus instead of turning laterally to enter the ventral telencephalon. The TCA bundle was more disorganised and showed a fan-out phenotype as the growth cones of the TCAs head towards different directions. Co-culture experiments using the thalamus explants of these embryos and wild-type ventral telencephalon showed the thalamic axons either fail to reach the medial part of the ventral telencephalon or turn dorsally towards the cortex (162,166). Additionally, loss of Pax6 resulted in disruption of thalamic patterning and miss-expressions of regional markers, axon guidance cues and receptors, which severely obstructed the process of TCA path-finding towards the cerebral cortex (59,162,166,167). Last but not least, Pax6-null rat embryos also showed abnormalities of Pax6-expressing cell clusters in the ventral prethalamus and amygdala, which lie along the path of TCAs and would usually guide them (167). Prior to the thalamic neurons sending out their axons rostral-ventrally to enter the prethalamus, the prethalamic neurons send out their axons caudal-dorsally into the thalamus (48,59,60). These axons act as scaffolds for the TCAs, which follows the prethalamic axons and descend into the prethalamus. Previous study in the lab has also shown that when Pax6 is conditionally knocked-out in the prethalamus, these ascending prethalamic axons have greatly reduced their numbers (unpublished data).

1.3.5.2 RNAseq data in the lab

So far, most of the studies on the functions of Pax6 during the development of the CNS comes from the progenitor cells, mostly in the cortex (128,140,153,154). Despite the unique expression patterns Pax6 displays in the prethalamus, the functions of Pax6 in the developing prethalamus,

especially in the post-mitotic cells of the prethalamus, remain largely unknown. However, due to its high position in the hierarchy of gene regulation networks, it is difficult to speculate and hypothesise the exact functions of Pax6 in the developing prethalamus. Data from the RNA sequencing study in the lab, which analysed the transcriptional changes of genes in the anterior cortex, the thalamus and the prethalamus upon acute deletion of Pax6, provided us with an unbiased starting point to answer these questions (58). In the experimental set up of this RNA sequencing study, the mouse model carries the tamoxifen-inducible Cre recombinase, which follows the ubiquitously expressed CAG promoter (CAGCreER). Therefore, the activity of the Cre recombinase will become active in every cell in these mouse embryos upon tamoxifen administration. This mouse model also carries the green fluorescent protein (GFP) reporter allele, and one (control) or two (mutant) copies of the floxed Pax6 (Pax6loxP) alleles, in which the loxP sites are flanking the 5, 5a and 6 exons of the Pax6 gene. As a result, upon activation of the Cre recombinase by tamoxifen, GFP expression will be activated, and the 5, 5a and 6 exons of Pax6 will be excised, giving rise to a truncated functionless PAX6 protein. The control embryos have the other Pax6 allele intact, therefore can still produce functional PAX6 proteins.

Analysis of differences between the transcriptomes of control and mutant prethalamus showed that there were over 3500 genes, whose expressions were significantly (adjusted $p < 0.05$) altered due to the loss of Pax6. Interestingly, this number is also the highest in comparison to the number of genes that showed significant differential expressions in the anterior cortex (over 2000 genes) or in the thalamus (over 1800 genes) after Pax6 deletion. Over half of these dysregulated genes were upregulated in the thalamus and prethalamus in response to the loss of Pax6 (Figure 1.10A). Gene ontology (GO) term enrichment analysis on all the genes that showed significant differential expressions in the prethalamus revealed 10 most highly enriched, non-redundant GO terms with obvious relevance to developmental processes. While the 10 most down-regulated GO terms could be roughly divided into two

categories- cell cycle (6/10) and translation (4/10), the 10 most up-regulated GO-terms were shared among differentiation (4/10), neuronal morphogenesis (3/10) and cell signalling (3/10) (Figure 1.10B). When all the significantly differentially expressed genes were hierarchically clustered according to the direction and magnitude of their log2 fold changes (LFCs) across all three tissues, we saw that most genes showed LFCs in the same direction in prethalamus and thalamus, but in an opposite direction in anterior cortex. Additionally, the prethalamus was the tissue with more extreme dysregulation of genes in both the downregulated clusters (cluster 1, 2 and 4) and the upregulated clusters (cluster 5, 6, 8 and 10). Interestingly, the GO terms related to neuronal morphogenesis (cluster 5, 7 and 8) also showed the most intense increase of LFCs. This indicated that there were not only quite a large number of neuronal morphogenesis related genes that are upregulated in the prethalamus when Pax6 is lost, they are also the most highly upregulated ones. Additionally, cluster 8 also showed enrichment for “Wnt signalling pathway,” indicating that this pathway might be explicitly upregulated in the diencephalon and more intensely in the prethalamus in the absence of Pax6 (Figure 1.10C).

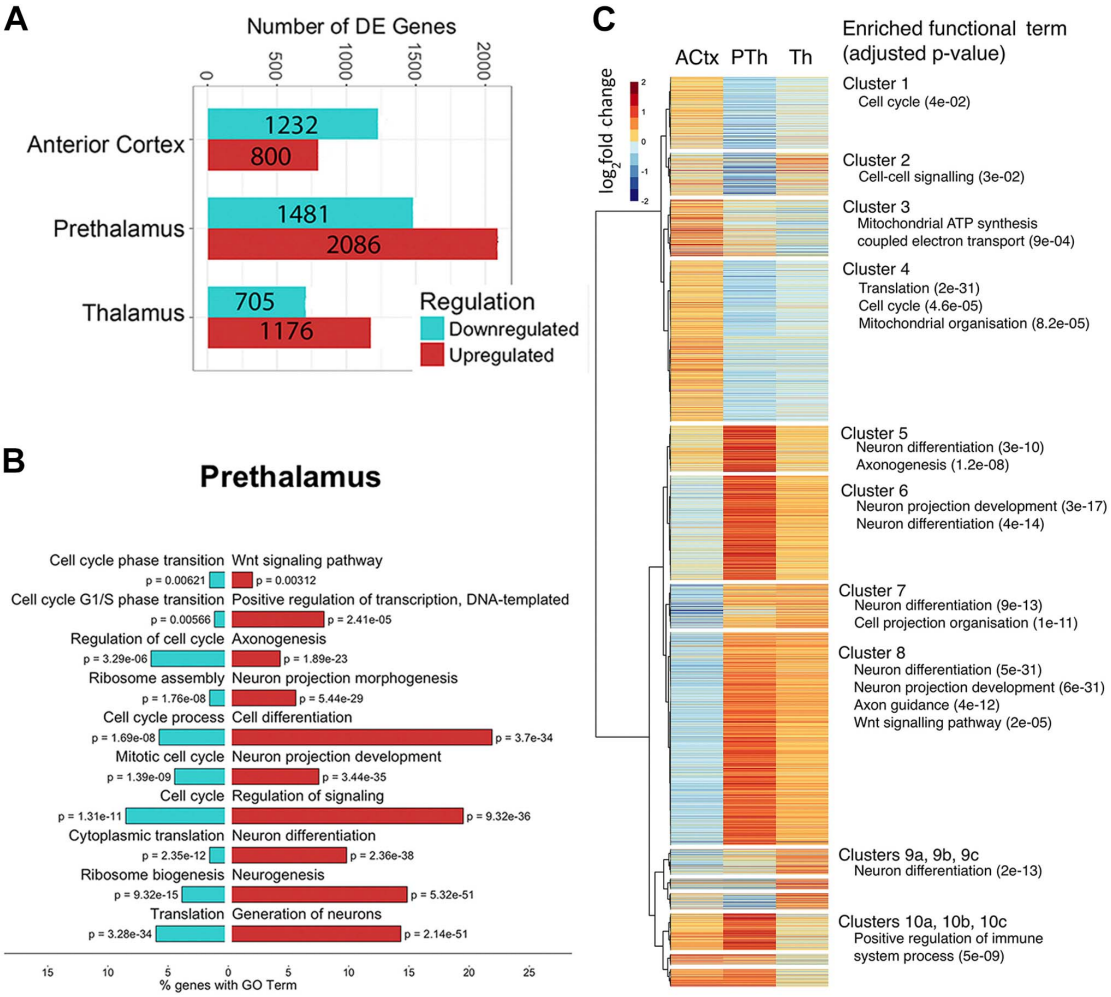

Figure 1.10 The Effects of Pax6 Deletion on the Transcriptomes of Prethalamic, Thalamic, and Anterior Cortical Cells. (A) An overview of the numbers of significantly differentially expressed (DE) genes resulting from Pax6 deletion in each region. **(B)** The 10 most highly enriched, non-redundant gene ontology (GO) terms with obvious relevance to developmental processes for up- and downregulated genes in the prethalamus. **(C)** Hierarchical clustering of all genes that showed significant differential expression in at least one tissue according to the direction and magnitude of their log2 fold change (LFC) across all three tissues. The dendrogram is cut to generate 14 clusters and enriched GO functional terms are listed against these clusters. Figure adapted from reference (55).

1.4 Aims of this thesis

The primary aim of this thesis is to utilise the information provided by the RNA sequencing experiment as a starting point and find out the novel functions of Pax6 during development of the prethalamus, especially in the prethalamic post-mitotic cells. As mentioned above, GO terms related to neuronal morphogenesis showed the most drastic upregulation in terms of the number of genes and levels of expressions. Therefore, in Chapter 3, by developing an in vitro culture system that allows me to observe neuronal morphogenesis of the prethalamic neurons, I aim to:

1. Characterise the process of neuronal morphogenesis of the prethalamic neurons in vitro
2. Investigate whether and how neuronal morphogenesis of the prethalamic neurons changes in the absence of Pax6

Based on the results from Chapter 3 and the RNAseq data, in Chapter 4, I further moved on to investigate the abilities of the prethalamic neurons to establish and maintain their neuronal polarity, aiming to test:

1. Whether the establishment of neuronal polarity is defective in the absence of Pax6
2. Whether the structure and components of the AIS, which is the key structure to maintain neuronal polarity, is altered in the absence of Pax6
3. Whether the excitability of the Pax6-null prethalamic neurons is changed due to altered AIS structure

According to the RNAseq data, the Wnt signalling pathway is also highly upregulated in the prethalamus when Pax6 is lost. Therefore, in Chapter 5, I aim to:

1. Determine the expression patterns of selected Wnt and Wnt-related genes in the prethalamus and how they change in response to the loss of Pax6

2. Further investigate the potential mechanisms by which Pax6 might be inhibiting Wnt signalling pathways in the prethalamus

Although the thalamus and prethalamus both reside on either side of the ZLI, hence receive the same dosages of morphogens released by this secondary organiser, the thalamus and prethalamus exhibit very different developmental profiles and produce neurons with very different morphologies and functions. The sharp difference of Pax6 expressions in the thalamus and prethalamus makes it an excellent candidate to test whether Pax6 can cause this regionally different development of the thalamus and prethalamus. Therefore, in Chapter 6, by utilising the existing RNAseq data, I aim to:

1. Test whether the Pax6-null prethalamus develops a thalamus-like expression profile of voltage-gated ion channels and AIS component genes
2. Find out the potential mechanism- whether this is due to loss of transcriptional control of Pax6 or upregulation of Wnt signalling pathway in the prethalamus

Chapter 2

Materials and Methods

2.1 Animals

2.1.1 Generation of the FP6CD1 line and mouse colony maintenance

All animal husbandry was conducted in accordance with the UK Animal (Scientific Procedures) Act 1986 regulations.

To generate conditional Pax6 knockout mice, I utilized the Pax6flox allele (167) in combination with the RCE: LoxP EGFP reporter allele (168) and the CAG-CreER allele (168). Homozygous $Pax6^{flox/flox}$ mice were crossed to CAG-$CreER^{+/-}$ mice to generate double heterozygous. CAG-$CreER^{+/-}$, $Pax6^{flox/+}$ males were selected in timed mating with $Pax6^{flox/flox}$ females to generate CAG-$CreER^{-/-}$, $Pax6^{+/+}$ or CAG-$CreER^{+/-}$, $Pax6^{flox/+}$ embryos as the control group (Ctrl) and CAG-$CreER^{+/-}$, $Pax6^{flox/flox}$ embryos as the Pax6-mutant experimental group (Hom or Pax6-null).

The Pax6flox allele have the 5, 5a and 6 exons of the Pax6 gene being floxed by the loxP sites. Therefore, with the conditional Pax6 knockout mice, upon the administration of tamoxifen, the 5, 5a and 6 exons will be excised, resulting in a truncated, functionless PAX6 protein.

For staging of embryos, the first day the vaginal plug was detected was designated as embryonic day 0.5 (E0.5).

To induce knockout of Pax6 in the CAG-$CreER^{+/-}$, $Pax6^{flox/flox}$ embryos, 10mg of tamoxifen was given to each female by oral gavage at E9.5. The oral gavage experiments were carried out by technicians from the animal unit of the Hugh Robson Building. All the mouse lines were managed by Dr. Martine Manuel.

The effectiveness of the tamoxifen induced Pax6 deletion was verified using the mouse monoclonal Pax6 antibody, which recognises the N-terminal of the PAX6 protein that is absent in the truncated PAX6 protein after the deletion of the 5, 5a and 6 exons (167). Figure 2.1 shows the effectiveness of Pax6

deletion, when I apply tamoxifen at E9.5 and harvest the embryos at E13.5. The examination of the effectiveness of Pax6 deletion was perform this way using one of the adjacent sections for every embryo that was sectioned with cryostat and processed for in situ hybridisation or immunohistochemistry. For embryos used for dissociated cell culture, genotyping for the floxed allele as described below was performed to examine the effectiveness of Pax6 deletion.

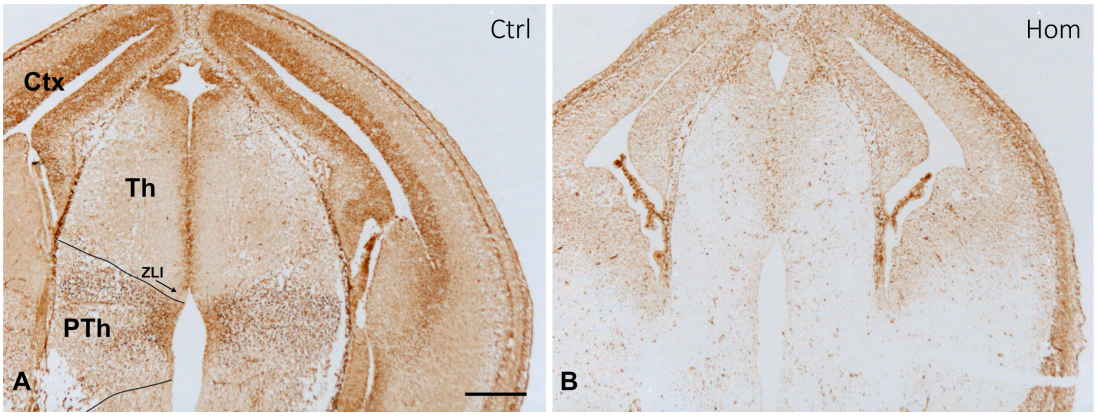

Figure 2.1 The expression of Pax6 is absent in the forebrain after 4 days of tamoxifen gavage. (A) In the control embryos (Ctrl, CAG-CreER$^{-/-}$, Pax6$^{+/+}$ or CAG-CreER$^{+/-}$, Pax6$^{flox/+}$), Pax6 is expressed in the ventricular zone of the cortex and thalamus, and in the ventricular zone and the post-mitotic cells of the prethalamus. **(B)** At E13.5, which is 4 days after tamoxifen gavage (at E9.5), no Pax6 protein was detectable in the forebrain of the mutant genotype (Hom, CAG-CreER$^{+/-}$, Pax6$^{flox/flox}$). Ctx, cortex; Th, thalamus; ZLI, zona limitans intrathalamica; PTh, prethalamus. Scale bar: 250μm.

2.1.2 Dissection and tissue fixation

All embryos were collected at E13.5. To minimize animal suffering, pregnant females were first treated with terminal anaesthesia followed by cervical dislocation according to the Code of Practice for Humane Killing of Animals under Schedule 1 to the Animals (Scientific Procedures) Act 1986 issued by the Home Office.

Embryos were placed in ice-cold PBS (pH7.4) after their dissection from the uterine horns. Embryos with GFP signal were selected under the GFP scope

followed by decapitation. For embryos used for dissociated cell culture, please refer to Chapter 4 for specific methodologies.

Tail nibs were collected and placed in 1.5ml Eppendorf tubes in -20°C until extraction.

2.2 Genotyping

2.2.1 Extraction of DNA

Extraction of DNA was performed according to the Hotshot method. Briefly, 75µl of Hotshot buffer was added to each 1.5ml Eppendorf tube containing the tail bud sample, which was followed by a 30-minute incubation at 95°C on a PCR machine. The Eppendorf tubes were left in the PCR machine to cool down to 4°C. Then 75µl of neutralization buffer was added to each tube for equilibrium. The extracted DNA was placed on ice for follow-up genotyping, otherwise it would be stored in -20°C freezer until genotyping.

2.2.2 Genotyping by Polymerase Chain Reaction

Reaction mix for each sample consists of 15.3µl ddH_2O, 2.5µl of 2.5mM dNTP mix, 5µl of the 5X PCR reaction buffer, 0.5µl Primer mix (Simpson et al. 2009, forward primer: 5'-AAA TGG GGG TGA AGT GTG AG-3'; reverse primer: 5'-TGC ATG TTG CCT GAA AGA AG-3'), 0.2µl Taq DNA polymerase (Qiagen) and 1.5µl of the extracted DNA to make up a total volume of 25µl. The themocycler (MJ Research PTC-225 Peltier Thermal Cycler) condition is shown in Table 2.1. PCR products were analysed with 2% agarose gel (Sigma) containing 3µl SYBRsafe (Invitrogen), ran at 115V for 70 minutes with a 100bp DNA ladder (New England Biolabs). PCR products were visualized with the IN GENIUS SYNGENE BIO Imaging machine and the Genesnap Imaging Acquisition Software.

The floxed allele fragment amplified with these primers was 195bp, whereas wild type allele was 156bp. Therefore, heterozygous condition (used as controls) was identified by two bands and the homozygous floxed allele condition (used as experimental groups, 'hom') was identified by one strong 195bp band.

Step 1	96°C for 2 minutes
Step 2	95°C for 30 seconds
Step 3	59°C for 30 seconds
Go back to Step2 for 30 cycles	
Step 4	72°C for 30 seconds
Step 5	4°C forever

Table 2.1. Thermocycling condition used for genotyping of the floxed Pax6 allele

2.2.3 Tissue embedding and sectioning

Selected tissues with desired genotypes were rinsed with 1x PBS for 3 times and cryoprotected in 30% sucrose (in 1x PBS) overnight at 4°C with rocking. Tissues were then equilibrated in 30% sucrose: OCT compound (50:50) at 4°C with rocking for 6 hours and embedded in the same solution in truncated moulds. The orientations of the tissues were adjusted to make sure that the snouts of the embryonic head were facing upwards for cutting coronal sections. The tissues were frozen on dry ice and stored at -80°C until cryostat sectioning at thicknesses of 10μm. Each slide of the tissue was transferred onto Superfrost (Thermo Scientific) and stored at -20°C if not use immediately.

2.3 *In situ* hybridization (ISH)

2.3.1 Probes used

DIG-labelled probes used were: Pax6 (from Michael Molinek). Wnt3a (kindly donated by Dr. Gareth Brady), Axin2 (kindly donated by Dr. Ondrej Machon, Oslo University Hospital), Lef1 (kindly donated by Dr. J. Galcerán, University of Alicante, Spain), Sfrp2 (kindly donated by Dr. Jeremy Nathans, JHU, USA), Dkk3 (synthetized from cDNA using primers specified in reference (168)), Ngn2 and Wht5a (kindly donated by Dr Thomas Theil, University of Edinburgh, UK). Except for DKK3, which was synthesized from primers for the use of this study, all the other probes as mentioned above were kept in the lab as plasmids.

2.3.2 Probe preparation

2.3.2.1 Amplification of target DNA sequence

To generate plasmids containing the DNA segments to make the probes, PCR reaction mix of a total volume of 50µl was prepared, which contained 32.6 µl ddH2O, 5µl of 2.5mM dNTPs, 10µl of 5X PCR reaction buffer, 1µl of 25mM primer mix, 0.4µl Taq DNA polymerase (Qiagen) and 1µl of cDNA (prepared by Dr. Idoia Quintana-Urzainqi). The same programme was run (Table 2.1) to amplify the target sequence. PCR products were analysed with 1% agarose gel (Sigma) containing 1µl SYBRsafe (Invitrogen), ran at 60V for 20 minutes with both the 100bp and 1kb DNA ladder (New England Biolabs). PCR products were visualized with the IN GENIUS SYNGENE BIO Imaging machine and the Genesnap Imaging Acquisition Software.

2.3.2.2 Gel extraction

The amplified DNA sequences with correct lengths were then excised from the gel under UV illumination. Gel extractions were performed using the

GENECLEAN® KIT (MP Biomedicals) according to the manufacturer's protocol. Concentrations of the DNA segments were measured with the Thermo Scientific Nanodrop 1000 after being eluted.

2.3.2.3 Ligation

Ligation of the DNA segments to the pGMT-easy (Promega) vectors was performed afterwards. The optimal amount of DNA segments and vectors for ligation was calculation using the following equation:

$$\frac{\left(\frac{kb\ of\ insert}{kb\ of\ vector} \times ng\ of\ vector\right) \times 3}{concentration\ of\ insert} = volume\ of\ insert\ in\ the\ ligation\ system$$

The ligation reaction mix contained 5µl of 2x rapid ligation buffer, 1µl T4 ligase, 1µl of pGMT-easy vector (all from Promega), the calculated volume of the specific inserts and lastly appropriate amount of ddH_2O to top up to a final volume of 10µl. This reaction mix was then placed in the 4°C fridge for ligation to happen overnight.

2.3.2.4 Transformation, plasmid amplification and extraction

After ligation, transformation was performed using competence cells (JM109, Promega) and the heat shot method. The cells were then plated onto agar plates coated with 100µl ChromoMax™ IPTG/X-GAL solution (Fisher Scientific) and cultured overnight in a 37°C oven. The next day, white single colonies were selected, amplified in overnight incubation at 37°C in agar medium supplemented with Ampicillin. Plasmid extraction using the Midiprep Kit (Qiagen) was performed according to manufacturer's protocol after the bacterial growth had reached certain confluency. The plasmid yielded was then sent for sequencing (Eurofins Genomics) to determine the orientation and the exact sequences of the inserts. The sequences of the inserts were matched against the whole mouse genome (Standard Nucleotide BLAST,

Mouse genomics plus transcripts (Mouse G+T), blastn, NCBI) to double check the specificity of the probes made from such DNA sequences. The concentration of the extracted plasmid was determined using the Thermo Scientific Nanodrop 1000.

2.3.2.5 Plasmid linearization

To linearize the extracted plasmid, a reaction mix of a total volume of 200µl was prepared, containing 10x CutSmart® Buffer and 5µl of either SacII or NdeI restriction enzyme (NEB Biolabs) depending on the orientation of the insert, 10µg of plasmid DNA, and lastly ddH_2O to top up to 200µl. Digestion of plasmid by restriction enzyme was carried out at 37°C for 3 hours on a thermocycler or at 4°C overnight in the fridge. The digestion product, i.e. the linearized DNA, was cleaned using the Qiagen Gel Extraction Kit according to manufacturer's protocol. 5µl of the digestion product was analysed with 1% agarose gel (Sigma) containing 1µl SYBRsafe (Invitrogen) ran at 60V for 30 minutes with both the 100bp and 1kb DNA ladder (New England Biolabs), and visualized with the IN GENIUS SYNGENE BIO Imaging machine and the Genesnap Imaging Acquisition Software, to check whether all the plasmid DNA had been linearized. The concentration of the linearized plasmid was determined with the Thermo Scientific Nanodrop 1000 after being eluted.

2.3.2.6 Transcription and DIG-labelling of the probes

Digoxigenin (DIG)-labelling of the probes was carried out by DIG RNA-labelling kit (Sigma-Aldrich) during in vitro transcription. Briefly, transcription mix was set up containing 3µg of linearized plasmid, 2µl of 10x solution, 2µl Sp6 or T7 RNA polymerase (Sigma-Aldrich, depending on the orientation of the insert), and ddH_2O to make up a final volume of 20µl. Transcription was carried out in the thermocycler at 37°C for 2 hours.

To eliminate the DNA template in the transcription mix, 2µl of DNAse was added and the transcription mix was placed back into the thermocycler to react

for 15 minutes at 37°C. Afterwards, 0.8µl EDTA (0.5M, pH 8.0), 7µl LiCl (5M), 75µl chilled 100% Ethanol were added to the mixture. The latter was placed in -20°C overnight.

The resulting mixture was then centrifuged at 4°C, 13000rpm for 15 minutes. The supernatant was carefully discarded, and the pellet was washed with 75µl Ethanol. The mixture was further centrifuged at 4°C, 13000rpm for 15 minutes, after which the supernatant was discarded, and the pellet was left to dry at room temperature (RT) for 1 hour. 20µl ddH2O was used to dissolve the pellet and the concentration for the probe was read by Nanodrop 1000 (Thermo Scientific). The probes were stored at -20°C before use.

2.3.3 Hybridization

In situ hybridizations were performed following a standard three-day protocol. On the first day, slides were taken out of the -20°C freezer and warmed to RT for at least 30 minutes. Probes were first diluted with hybridization buffer by 1:500 to make the stock solutions. Probe stock solutions were further diluted to desired working concentration, also using the hybridization buffer. The diluted probes were incubated in water bath above 85°C for at least 10 minutes to denature the diluted probes. Probe solutions were mixed thoroughly before applying to each slide (200µl/slide). A coverslip was placed onto each slide. Slides were then placed in a sealable plastic box containing 2 sheets of 3mm Whatman paper saturated with 50%Formamide/1X salt for overnight incubation at 72°C.

2.3.4 Post hybridization washes, blocking and antibody staining

Slides were retrieved from the humid box and incubated at 65°C in Coplin jars filled with fresh wash buffer for 3 times (30 minutes, 20 minutes and 20 minutes each time). Slides were then transferred to new Coplin jars containing 1X MABT buffer and washed with rocking for 30 minutes and another 2 hours.

A humidified box was prepared by lining the bottom of a Tupperware container with 3MM Whatman filter paper saturated with water. Slides were taken out from the 1X MABT buffer and dried around edges. Sections were outlined with hydrophobic pen (Vector Labs) and incubated with blocking solution at RT for at least 1 hour in the humidified box. After blocking, blocking solution was removed and anti-DIG antibody (1:2500 in blocking solution) was applied to each slide and incubated in the humidified box at 4°C overnight.

2.3.5 Post antibody washes and colour reaction

Slides were transferred to Coplin jars and washed with 1X MABT and subsequently pre-staining buffer at RT with rocking.

Slides were retrieved from pre-staining buffer and dried around edges. Staining buffer were added to each slide and incubated in the dark in a 37°C incubator for 3 hours or at 4°C over the weekend to develop the colour. Colour reaction was then stopped by washing the slides in Coplin jars with 1X PBS for several times.

For counter staining, slides were submerged in Nuclear Fast Red (Vector Labs) for 1 minute per slide. Then slides were quickly rinsed and washed with 1x PBS.

2.3.6 Mounting

Slides were first transferred to a slide rack and submerged in 50%, 70%, 90%, 95% and 100% ethanol successively (1 minute/concentration) at RT. Slides were further incubated in 100% ethanol, and two times in 100% xylene for 2 minutes. Slides were taken out of the xylene and dried around edges and were further left to dry. A few drops of DPX were applied to each slide and a coverslip was carefully placed on top of each slide. The mounted slides were left in the fume hood overnight to dry.

2.4 Fluorescence in situ hybridization

2.4.1 Hybridization, washes and antibody staining

Fluorescence in situ hybridization was performed as previously described. The hybridization step was the same as described above. Afterwards, slides were retrieved from the plastic box and incubated at 65°C in Coplin jars filled with fresh wash buffer for 3 times. Slides were then transferred to new Coplin jars containing TNT buffer and incubate at RT for 30 minutes with rocking for 2 times. Then slides were dried around edges and sections were outlined with hydrophobic pen and were blocked with TNB blocking buffer for more than one hour at RT. Anti-DIG POD antibody was diluted in blocking solution (1:1000) and applied to slides. Slides were incubated with antibodies in TNB buffer overnight at 4°C.

2.4.2 Detection

Slides were washed in TNT buffer. Cyanine 3 tyramide (Perkin Elmer) was taken out of the 4°C fridge 30 minutes before use and was diluted to a working concentration of 1:200 in amplification diluent. The diluent of Cyanine 3 tyramide was added to each slide (100µl/slide) and further incubate with the slides for 10 minutes at RT in the dark (slides were kept in the dark in steps onwards). Slides were then washed in TNT buffer and further counterstained with DAPI. Slides were then washed in 1X PBS and mounted with Vectashield Hard Set (Vector Labs). The slides were sealed with nail polish around the edges and stored in dark at 4°C until imaging.

2.5 Immunohistochemistry

Immunofluorescence was performed as previously described (28). Briefly, sections were warmed to RT and incubated in 37°C incubator for 30 minutes for better section attachment. Afterwards, sections were submerged in running

water for 5 minutes to rehydrate and subsequently washed in 1x PBS and further equilibrated and boiled in 10mM sodium citrate by microwaving for 4 times, 5 minutes each to increase tissue permeability and achieve antigen retrieval. Sections were incubated with blocking solution (PBS-0.1%Triton + 20% goat serum) for 1hr at room temperature, and then incubated with primary antibodies in antibody solution (PBS-0.1%Triton + 10% goat serum) at 4°C overnight. Sections were then washed with PBS-0.1%Triton and goat anti-mouse IgG biotinylated was used as secondary antibody and was incubated with the section for 1 hour at RT. Colour reactions were developed by submerging slides in DAB solution (150ml PBS, 1.5ml DAB 3%, 1.5ml 30% H2O2) for 5 minutes at RT in the fume hood. Sections were washed and then dehydrated and mounted with DPX.

2.6 Immunofluorescence

Immunofluorescence was performed as previously described. Steps before secondary antibody incubation were done in the same way as described in the immunohistochemistry section above. Afterwards, slides were incubated with fluorophore-conjugated secondary antibodies in blocking solution for 1hr at RT. Primary and secondary antibodies and their concentration used in this study are listed in Table 2.2 and 2.3. Slides were washed with PBS-0.1%Triton for 5 minutes, and counterstained with DAPI for 5 minutes. Slides were further washed with PBS for 3 times, 5 minutes each and mounted with AF1 mounting medium sealed with nail polish and stored at 4°C until imaging.

2.7 In situ hybridisation in combination with immunohistochemistry

In situ hybridization was performed first as described above. After colour reaction, the slides were washed in 1x PBS to get rid of all the residue of the

staining buffer. Then slides were transferred and washed in PBS-0.1%Triton and proceed for immunohistochemistry as described above.

To perform fluorescence in situ hybridization in combination with immunofluorescence, the slides were processed with FISH as described above. After colour reaction with Cyanine 3 tyramide, slides were washed with TNT buffer and further transferred to and washed with PBS-0.1%Triton and proceed for immunofluorescence as described above.

Primary antibodies	Source	Identifier
Rabbit polyclonal anti-Pax6 (1:200)	Biolegend	Cat#901301, RRID: AB_2565003
Mouse monoclonal anti-Pax6 (1:10)	A gift from Prof. V van Heyningen, AD2.38 Simpson *et al.*, 2009	N/A
Mouse monoclonal anti-Beta III tubulin (Tuj1) (1:200)	Abcam	Cat# ab18207, RRID: AB_444319
Mouse monoclonal anti-Ankyrin-G, clone N106/36 (1:200)	Antibodies Inc.	Cat# 75-146
Monoclonal Anti-Sodium Channel, Pan antibody produced in mouse (1:100)	Sigma-Aldrich	Cat# S8809-.1MG
Rabbit polyclonal Anti-Partitioning-defective 3 Antibody (1:100)	Millipore	Cat# 07-330
Goat polyclonal Anti-GFP antibody (1:200)	Abcam	Cat# ab6673
Chicken polyclonal Anti-GFP antibody (1:200)	Abcam	Cat# ab13970
Rat monoclonal anti-Sfrp2 antibody (1:1)	A generous gift from Dr. Stefanie Hauck	N/A

Table 2.2 Primary antibodies used in this study.

Secondary antibodies	Source	Identifier
Goat anti-mouse biotinylated secondary antibody (1:200)	Vector laboratories	Cat# BA-9200, RRID:AB_2336171
Goat anti-rabbit biotinylated secondary antibody (1:200)	Vector laboratories	Cat# BA-1000, RRID:AB_2313606
Donkey anti-mouse Alexa 568 secondary antibody (1:200)	Thermo Fisher Scientific	Cat# A10037, RRID:AB_2534013
Donkey anti-rabbit Alexa 647 secondary antibody (1:200)	Invitrogen	Cat # A-31573
Donkey anti-chicken Alexa 488 secondary antibody (1:200)	Stratech Scientific Limited	Cat# 703-545-155-JIR
Donkey anti-rabbit Alexa 568 secondary antibody (1:200)	Invitrogen	Cat # A10042
Donkey anti-goat Alexa 488 secondary antibody (1:200)	Invitrogen	Cat # A-11055
Donkey anti-rat Alexa 488 secondary antibody (1:200)	Thermo Fisher Scientific	Cat# A-21208, RRID:AB_141709
Streptavidin, Alexa Fluor 488 conjugate antibody (1:200)	Thermo Fisher Scientific	Cat# S11223, RRID:AB_2336881

Table 2.3 Primary antibodies used in this study.

Chapter 3

Pax6 regulates neuronal morphogenesis in the developing prethalamus

3.1 Introduction

3.1.1 Defects in neuronal morphogenesis and axon formation in Pax6-null neurons

In addition to the prethalamus, Pax6 is also expressed post-mitotically in the retinal ganglionic cells (RGCs), granule cells in the cerebellum and dopaminergic neurons of the olfactory bulb (169). The functions of Pax6 in these post-mitotic cells remain to be fully uncovered. Interestingly, several groups have reported defects in neuronal morphogenesis and axon formation in some of these Pax6-expressing post-mitotic cells when Pax6 is deleted.

For example, in the cerebellum, granule cells extend bipolar axons when migrating from the external germinal layer (EGL) to the internal granule layer (IGL). These bipolar axons are termed parallel fibres because the axon bundles they form are parallel to the pial surface. Yamasaki et al. (170) showed that in the rat Pax6-null (rSey2/rSey2) cerebellum, the parallel fibres are distorted and clustered together. When assessing cell morphology and migration of granule cells in in vitro tissue culture of the EGL, they found that the Pax6-null granule cells do not possess long neurites and they fail to follow specific trajectories during migration. The effects of Pax6's loss seemed to be cell-autonomous, as defects in morphology and migration of the Pax6-null granule cells were not rescued when they were co-cultured with the postnatal day 2 (P2) P2 wild-type (WT) EGL cells. However, when Pax6 expression was restored by transferring Pax6 cDNA into the cultured Pax6-null EGL, these Pax6-null EGL cells exhibited long neurites that resembled the morphology of the WT granule cells. These results indicate that Pax6 functions as an intrinsic factor and is required for the formation of bipolar axons and probably subsequent migration of granule cells in the developing rat cerebellum (170). In addition to rat granule cells, granule cells in mouse cerebellum seem to display similar defects in neuronal morphogenesis when Pax6 is lost. Swanson et al. (171) showed that in dissociated cell cultures of the E18.5 mouse cerebellum, the number of differentiated cells (Tuj1-positive) with at least one

neurite greater than twice the cell body diameter was significantly lower in the Sey/Sey cell culture. This result indicated that the post-mitotic cells' abilities to produce and/or maintain long neurites (or axons) were compromised when Pax6 is lost (171). Furthermore, Sebastian-Serrano et al. (169) showed that the axonal length of retinal ganglion cells could be augmented by the addition of the secreted protein SFRP1. However, knock-down of Pax6 in these cultured RGCs by shRNA blocks the SFRP1-stimulated growth of retinal axon. These results indicated that both extrinsic and intrinsic factors affect axon formation in the RGCs, and Pax6 might regulate axon formation by controlling the transcription of intrinsic factors downstream of the Sfrp1 signalling pathway (169). These observations raised the intriguing possibility that Pax6 might regulate neuronal morphogenesis, or more specifically, axon formation, in neurons that still maintain its expression postmitotically.

3.1.2 Aim of this chapter

As a subset of the prethalamic-derived neurons maintains the expression of Pax6 during and after neurogenesis, the developing prethalamus provides us with an ideal system to investigate the functions of Pax6 in post-mitotic cells. Interestingly, in our RNAseq data, GO terms such as axonogenesis, neuron projection development, cell projection organisation and axon guidance were among the most highly enriched and significantly upregulated in the prethalamus when Pax6 is lost.

Based on the analysis of the RNAseq data and previous studies in granule cells and retinal ganglion cells, I hypothesised that Pax6 promote neuronal morphogenesis and axon elongation in the Pax6-positive prethalamic neurons.

In this chapter, by developing an in vitro culture system that allows me to observe neuronal morphogenesis of the prethalamic neurons, I aim to:

1. Characterise the process of neuronal morphogenesis of the prethalamic neurons in vitro

2. Investigate whether and how neuronal morphogenesis of the prethalamic neurons changes in the absence of Pax6

3.2 Materials and Methods

3.2.1 Animal model

The animal model used in this study is the FP6CD1 mouse. Protocol for tamoxifen gavage and embryo collection remains the same as previously described where 10mg of tamoxifen was given to the pregnant female on E9.5 and embryos were collected on E13.5.

3.2.2 Dissection of the prethalamus

To dissect the prethalamus, embryos from E13.5 are collected and decapitated. The neural tube is separated from the epidermal and mesodermal tissue (Figure 3.1A) and cut in half along the dorsal and ventral midline (Figure 3.1B). From E9.5, morphologic segmentation of the diencephalon starts and the diencephalic prosomeres become apparent from E10-11 as ventricular ridges and lateral wall bulges appear (18). These morphological landmarks are used to distinguish prethalamus from the surrounding tissue (the thalamus and the eminentia thalami (EmT)) during dissection (Figure 3.1B arrows).

3.2.3 Dissociated cell culture

After being cut out, the two prethalamic pieces from the two halves of the neural tube of the same embryo were put together and chopped into smaller pieces for dissociated cell culture using the Papain Dissociation System (Worthington Biochemical Corp.) according to the manufacturer's protocol (Figure 3.1C-D). The prethalamus from each embryo was dissociated and cultured individually. The number of cells obtained after dissociation was measured using a haemocytometer. Additionally, trypan blue staining was used to determine the ratio of viable to damaged cells. To adjust the plating density of the cell culture, cells obtained after dissociation were resuspended using a certain amount of culture medium (Advanced DMEM/Neurobasal medium 1:1, supplemented with N2 (100x) and B27 (50x) neural supplement,

Thermo Fisher Scientific). 130µl of the culture medium containing the resuspended cells was then added onto the 9mm circular coverslips (Fischer Scientific) coated with Poly-L-lysine and Laminin (Thermo Fisher Scientific). Due to the surface tension of the culture medium, the culture medium containing the dissociated cells would stay within and fill up the realm of the coverslips. The cell cultures were then incubated at 37°C with 5% CO2 for 1 hour to allow the cells to attach to the coverslips. In this way, all the cells obtained after the dissociation was retained within the coverslip, and the exact cell density of plating could be calculated using the total amount of cells divided by the surface areas of the coverslips being used. After 1hr, 240µl of the culture medium was then added into each well of the 48-well plate (Greiner Bio-One) that contains the coverslip. The dissociated prethalamic cells were cultured for 1-6 days (Figure 3.1E). Light microscopy was used to monitor the condition of cell cultures every day.

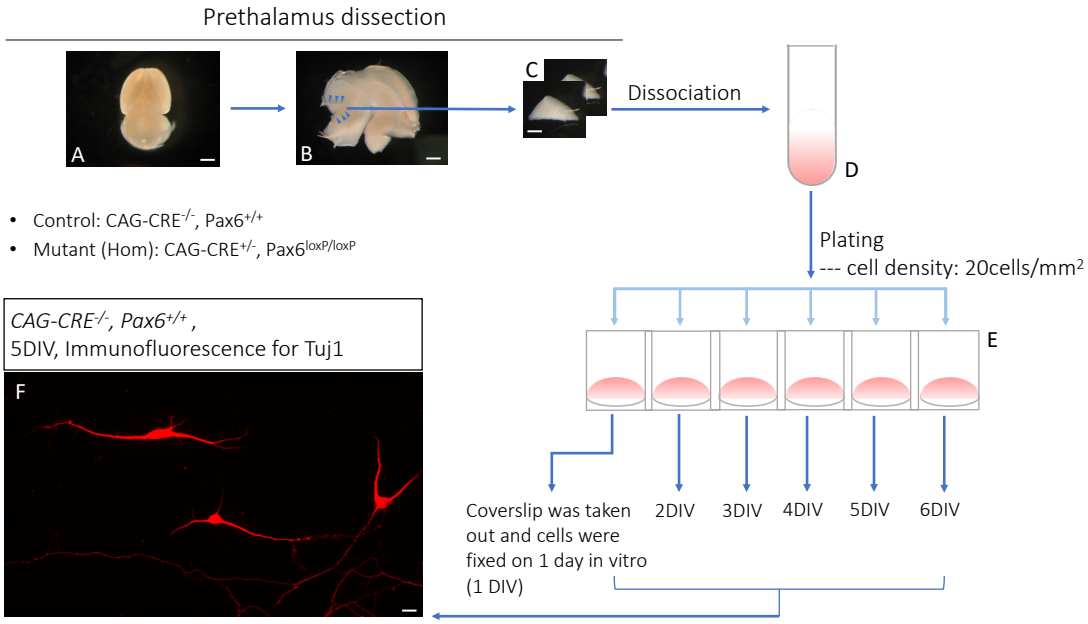

Figure 3.1. Steps of dissociated cell culture of the prethalamus. After the embryo was decapitated, the neural tube was isolated (A) and separated into two halves (B). Then, according to the morphological ridges and furrows (B, arrow heads), the prethalamus from both halves of the neural tube was cut out (C) and processed for dissociated using the Papain Dissociation System (Worthington Biochemical Corp.) according to the manufacturer's protocol, as one sample (From C to D). The numbers of cells yielded was determined by haemocytometer, and further diluted to make a final plating concentration of 20 cells/mm^2 (From D to E). Dissociated prethalamic cells from the same embryo were then plated onto coverslips and cultured for 1-6 days (E). On each individual day, the coverslip was taken out, and processed for fixation and further fluorescent immunohistochemistry with the Tuj1 antibody (F). Scale bar in F: 10μm.

3.2.4 Fluorescent immunohistochemistry for whole morphology of neurons

To stain for the whole morphology of neurons, the coverslips containing the prethalamic neurons were removed from the culture medium, rinsed with 1xPBS and fixed in 4% PFA for 20 minutes. These coverslips were then rinsed again in 1xPBS, and the cells were permeabilised in 0.1% Triton X-100 in 1xPBS (0.1% PBST) for 10 minutes. After that, 0.1% PBST was removed, and cells were washed with 0.1% PBST for three times and further blocked with blocking solution (20% goat or donkey serum in 0.1% PBST) for 2 hours. Then the blocking serum containing primary antibodies was added to the cells for overnight incubation. On the second day, cells were replaced with clean 0.1% PBST for washes and further incubated with blocking serum containing the corresponding secondary antibodies for 1 hour. Cells were then washed with 1xPBS, and further incubated with DAPI for counterstaining of the nucleus.

The expression patterns of GFP, Neurobiotin and Tuj1 in the dissociated prethalamic neurons were analysed and compared in order to decide which one is the most suitable marker to label the entire morphology of the neurons. As mentioned above, the animal model I use carry a cytoplasmic GFP reporter, which becomes active upon tamoxifen induction. Neurobiotin is an amino derivative of biotin, which can be taken up by the cytoplasm of the cultured neurons when added to the culture medium and visualised by fluorophore-conjugated streptavidin. Tuj1 labels the neuron-specific Class III β-tubulin of the cytoskeleton. Therefore, in theory, all three of them can be used as markers for the morphology of the neurons. In the end, I chose Tuj1 as the marker because its expression within the neurons highly correlated with that of GFP and Neurobiotin's (Figure 3.2A, B, C'). Unlike the Neurobiotin staining, whose efficiency depended on how much of the Neurobition was taken in and thus could vary among neurons (Figure 3.2A arrows), the neuronal morphology staining I got from Tuj1 was rather homogenous. Additionally, as it labels neuron-specific Class III β-tubulin, which is specifically expressed in newly generated immature post-mitotic neurons and differentiated neurons

(19), Tuj1 staining can also help us distinguish undifferentiated cells in the culture (Figure 3.1F).

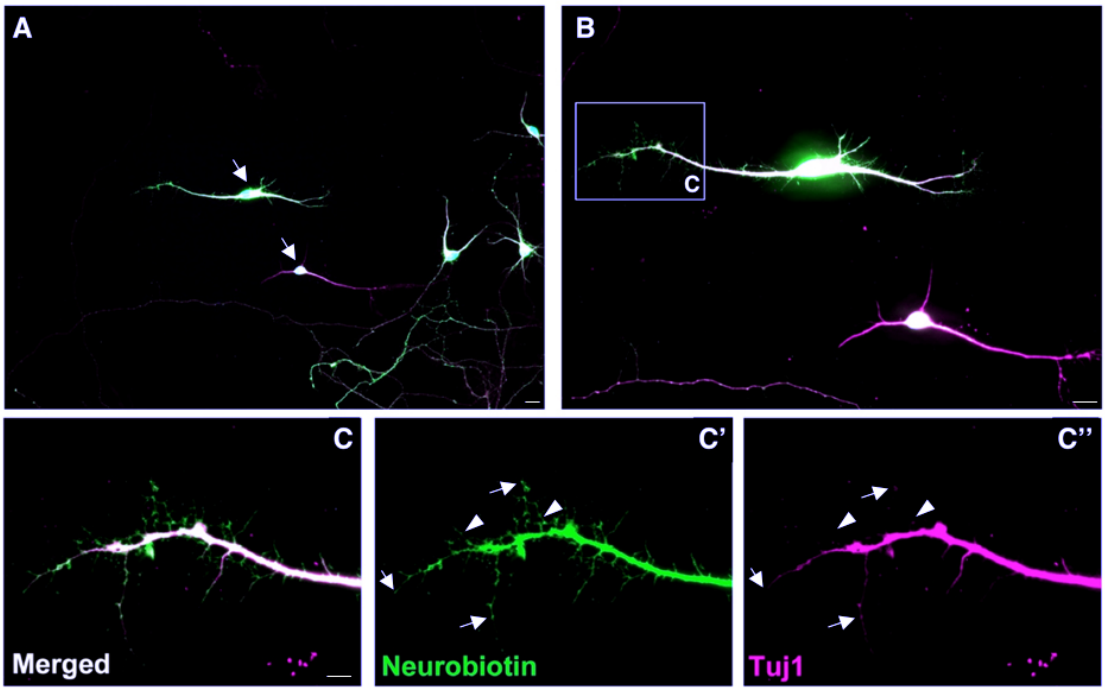

Figure 3.2 Comparison of neuronal morphologies labelled by Neurobiotin and Tuj1.
(A-B) Dissociated prethalamic neurons were fixed and immuno-reacted with Streptavidin-488 to detect Neurobiotin and antibody for Tuj1. The effectiveness of Neurobiotin staining for whole-neuron morphology depends on how well the neurons can absorb the Neurobiotin, which is heterogenous among the cultured prethalamic neurons (A, arrows).
(C) Enlargement of the boxed area in B.
(C') Neurobiotin staining was seen in the filopodia and small processes surrounding the growth cone (arrow heads).
(C'') Tuj1 staining was seen all the way to the end of the neurite and bigger protrusions (C', C'', arrows), but not in small filopodia and processes (C'', arrow heads).
Scale bars: 10μm (A-B); 5μm (C-C'').

3.2.5 Imaging

Fluorescence images of the dissociated cells were taken using a Leica DM5500B automated upright microscope connected to a DFC360FX camera. The route of acquiring images started from the upper-left corner towards the lower-right of the 9mm circular coverslip. Every image being taken was from an adjacent visual field of the previous image, in an attempt to cover as many cells on the coverslip as possible and without imaging the same cells twice.

3.2.6 Neurite tracing and cell counting

Images obtained were processed with Fiji-ImageJ. Three parameters were chosen to represent the dynamics of neuronal morphogenesis at each day of the cell culture - the number of neurites, the length of the longest neurite and the total length of neurites. All these three parameters were counted for each Tuj1-positive cell. A neurite was defined as a stable protrusion from the soma (Figure 3.3A-B). Protrusions from the soma which were thin and had vague Tuj1 staining were considered as either filopodia or artefacts. Filopodia mainly consist of F-actin, therefore were not considered as neurites. Length measurements were done by using the freehand line tool in Fiji. To measure the length of one neurite, the tracing would start at the edge of the soma, where neurite protrusion started and continued all the way to the furthest possible edge of the growth cone (Figure 3.3B, white line tracing). The longest neurite for each neuron was defined as the one with the highest reading for this measurement. All the other protrusions stemmed from that neurite were considered as branches. The length of each branch was measured from where it stemmed from the neurite to its furthest edge possible (Figure 3.3C, green line tracing). The total length of neurites for each neuron was calculated as the sum of the length of all the neurites and branches (Figure 3.3D).

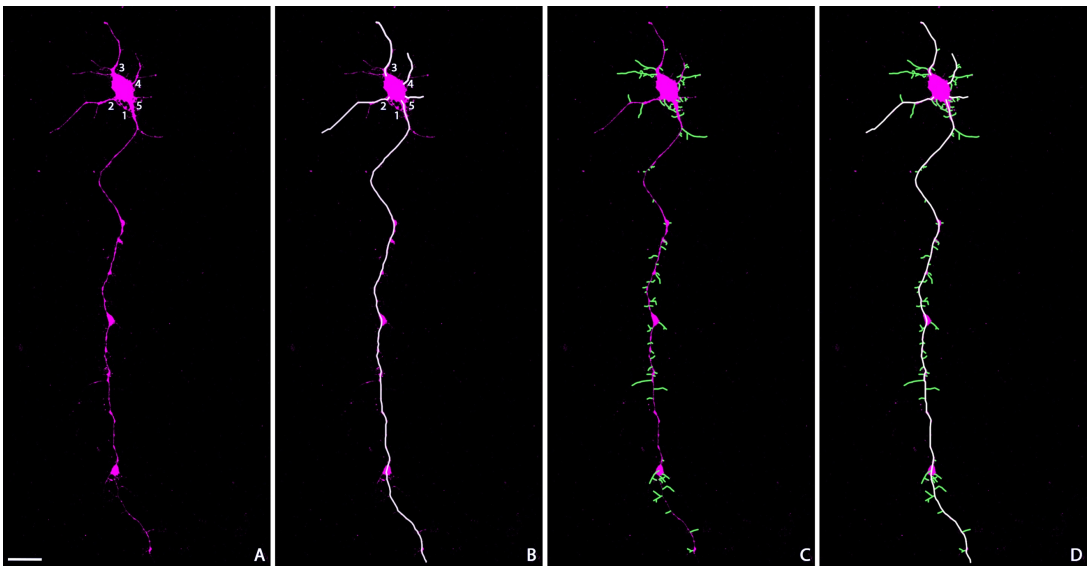

Figure 3.3 Example of how the measurements were carried out for each neuron. The images were processed with Fiji and the freehand line tool was used to measure the lengths. For our example neuron in **(A)**, five protrusions from the soma display strong Tuj1 staining. Therefore, we defined the number of neurites for this neuron to be 5. **(B)** To measure the length of each neurite, we would start the tracing with the freehand line tool at the edge of the soma and continue all along to the furthest point where the Tuj1 staining was detectable. **(C)** To measure the length of each branch, where that branch stemmed from the neurite would be considered as the start point, and the tracing would continue all the way to the furthest point where Tuj1 staining was detectable. **(D)** Total length of neurites was calculated as the sum of all the neurites and branches for each neuron. Scale bar: 10μm.

3.2.7 Statistics

Three independent experiments were performed using embryos from three litters (n=3). The dissociated prethalamic neurons from embryos from these three litters were cultured for 1-6 days. For each day of the cell culture, at least 100 neurons from the control genotype and 100 neurons from the Pax6-null genotype were measured. The data I collected consisted of two fixed effects- days and genotype, one random effect- litters and three output variables- the length of longest neurite, the total length of neurites and number of neurites. We then processed these data sets for mixed-effect models for statistic test.

To elaborate, as the data set of the length of longest neurite and the total length of neurites consisted of continuous numerical data, they were first tested for best distribution fit using Quantile-Quantile plots, and the best fit was gamma distribution. The data set of the number of neurites consisted of discrete numerical data, therefore was fitted to the Poisson distribution.

As shown in Figure 3.4, both sets of data for the length of the longest neurite and total length of neurite fitted well with the gamma distribution. However, the data set of the number of neurites did not fit well with the Poisson distribution. Nevertheless, we still proceeded for mixed-model with all three data sets. From there, type III ANOVA was applied to test which factors, and which interactions affect the data. With such information, the data sets were further processed for Tukey comparisons. To elaborate, one-way ANOVA tests were first performed to see if there was any evidence that the means of populations differ. If the ANOVA led to the conclusion that there was evidence of differences between the group means, we then considered the pair-wise factors and further investigate which of the means are different. Statistics for mixed-model were performed by Zrinko Kozić.

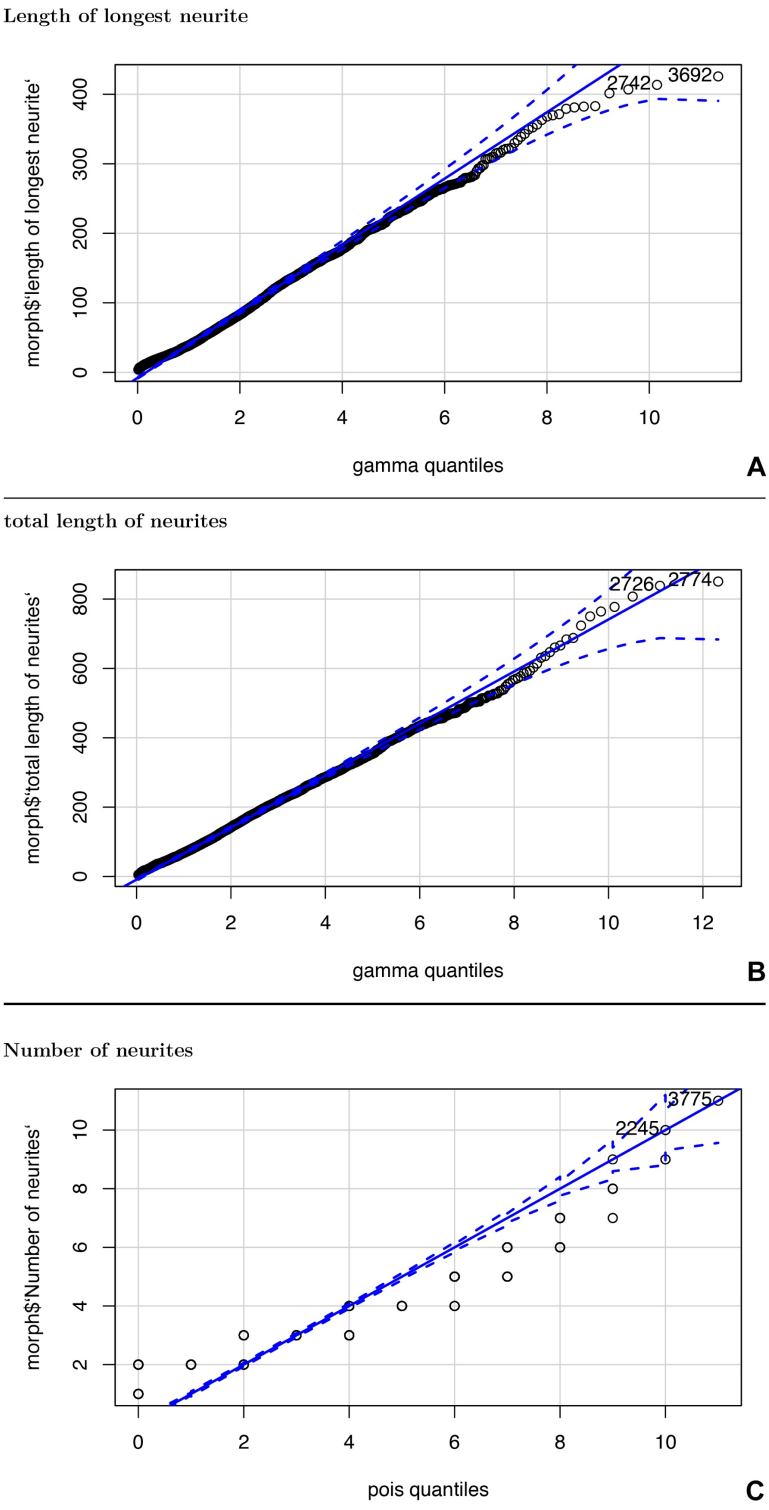

Figure 3.4 Quantile-Quantile plots showing the best fitted distribution for the data sets of length of the longest neurite, the total length of neurites and the number of neurites. Fitting the data sets Data points for length of longest neurite **(A)** and total length of neurites **(B)** fitted gamma distribution. Data points for number of neurites did not fit the Poisson distribution very well **(C)**.

3.3 Results

3.3.1 Genes involved in regulating cytoskeletal reorganisation in favour of neuritogenesis and axon elongation are up-regulated in the prethalamus when Pax6 is lost.

To understand how neuronal morphogenesis might have changed in the prethalamus when Pax6 is lost, I first looked into the genes in the neuronal morphogenesis related GO-terms, which were highly enriched and significantly upregulated in the RNA-seq data. Candidate genes were cross-referenced from reviews and research articles addressing cytoskeletal regulation during neuronal morphogenesis (neuritogenesis, axon specification and elongation). The results showed upregulation of effector genes involved in both actin and microtubule cytoskeleton modification that underlie increased actin nucleation, actin bundling, microtubule assembly and bidirectional intracellular transportation, which have been shown to augment axon/neurite elongation. Besides, genes involved in relaying extracellular signals to both the actin and microtubule cytoskeleton are also upregulated. These include several GEFs that relay membrane-signalling activities to members of the Rho GTPases, and several Rho GTPases themselves. Genes that function to manipulate membrane curvature in order to accommodate cytoskeletal changes during neurite outgrowth are also upregulated. Table 3.1 shows a selection of these genes, their functions during neuronal morphogenesis in other systems, their mean-base expression level in the prethalamus, and their LFCs of expression levels in the absence of Pax6.

The above data indicate that cytoskeletal organisation is influenced when Pax6 is deleted in the prethalamus. Surprisingly, they also seem to imply that, opposite to defective axon formation and decreased axon/neurite length observed in granule cells and retinal ganglion cells, axon formation may be augmented in the prethalamic post-mitotic cells upon Pax6's loss.

To find out exactly how neuronal morphogenesis might have been impacted, I then turned to the in vitro culture system, to observe the process of neuronal morphogenesis in the dissociated prethalamic neurons in the presence and absence of Pax6.

Gene Name	Base mean	Log2 fold change
GEFs for Rac		
Dock4	1190.45	1.03
Dock2	62.19	0.86
Dock3	887.12	0.68
Dock9	99.98	0.66
Dock10	82.01	0.76
Dock8	36.44	0.95
Scafold for GEFs		
ELMO1	1686.98	0.87
GEFs for CDC42		
Fgd1	835.78	0.57
Fgd5	176.05	1.04
Fgd6	144.76	0.66
GAP for Rho and Rac		
srGAP3	4396.61	1.80
Rac		
Rnd1	356.24	0.78
Actin bundling		
Ablim1	1065.46	0.59
Ablim3	1201.84	1.20
Ablim2	37.54	0.91
Strip2	27.04	1.81
Anti-capping for actin		
Enah	2801.44	0.68
Membrane curvature		
Pacsin1	241.30	0.82
Microtubule polymerisation/bundling		
Mapt (tau)	15146.60	1.16
Map2	27419.65	0.33
Map6	5846.83	0.71
Map9	1923.74	0.61
Apc2	9112.11	0.86
Apc	3736.29	0.79
Crmp1	30626.71	0.32
Crmp2	2395.25	0.50
Dpysl5	12540.05	0.67
Clip1	716.53	0.82

Table 3.1 Log2-fold change (LFC) of representative genes involved in the process of neuritogenesis, axon specification and elongation.

In terms of actin cytoskeleton regulation, for example, the Rho family GTPase1- Rnd1, which has been shown to regulate axon extension by enhancing microtubule destabilising activities, is upregulated by a LFC of 0.779. Overexpression of Rnd1 induces the formation of multiple axons (172). Members of the Dock180-related proteins, which function as GEFs for Rac and/or CDC42, were upregulated. The included (ranked according to their LFC changes) Dock4 (LFC 1.03), Dock8 (LFC 0.95), Dock2 (LFC 0.86), Dock10 (LFC 0.76), Dock3 (LFC 0.68) and Dock9 (LFC 0.66). Studies on Dock4 have indicated that it functions to transduce several upstream signals such as Wnt, RhoG towards the activation of Rac1. In hippocampal neurons, upregulation of Dock4 expression resulted in dendritic elongation (173,174). Dock2's binding with the scaffold protein ELMO1, which was also upregulated in the RNAseq data (LFC 0.87), is critical for Dock2-mediated Rac1 and Rac2 activation that result in cytoskeletal reorganisation during neutrophil chemotaxis (175). Dock3 enhances axonal outgrowth through activating Rac1 and stimulating membrane recruitment of the WASP family verprolin-homologous (WAVE) protein complex. The WAVE proteins function to relay activated Rac1 and CDC42 signalling to Arp2/3 that eventually result in actin nucleation (176). Interestingly, WAS protein family member 1, also known as WAVE-1, is also upregulated by a LFC of 0.759. Several actin cytoskeletal effector proteins regulating actin elongation and bundling were also upregulated. For example, the murine and avian Ena ortholog Mena (mammalian Enabled), which is a member of the Ena/VASP family, functions to out-compete capping proteins and subsequently recruits Fascin to generate nascent filopodia (177). The expression of Mena was upregulated by a LFC of 0.677. In C. elegans, it has been shown that in addition to Arp2/3's function in growth cone filopoia initiation, Enabled and the actin binding LIM protein (Ablim) function in similar fashions but in parallel pathways to Arp2/3 (178). Notably, expressions of Ablim3 (LFC 1.195), Ablim2 (LFC 0.913) and Ablim1 (LFC 0.594) were all upregulated.

In terms of microtubule effector genes, several microtubule binding proteins (MBPs), which bind directly to the microtubules and modify their organisation, were upregulated in the prethalamus in the absence of Pax6. For example, members of the type II family of MAPs, Tau and Map2 showed upregulated expression of LFCs of 1.16 and 0.326 respectively. Map2 is particularly important for the initial phases of neurite outgrowth, as suppressing its expression abolishes neurite outgrowth and extension in cerebellar neurons. Suppressing Tau expression, on the other hand, only prevent axonal elongation, indicating Tau's specific role in axonal growth. Other studies showed that elevating Tau's expression can increase the number and length of axons (69). The expression of the microtubule dimer binding protein Crmp-2 is upregulated by a LFC of 0.495. CRMP-2 associates with kinesin and functions to deliver free tubulin dimers to the plus ends of the microtubules. It also transports effectors for actin organisation such as WAVE proteins to the distal tip of the protruding filopodia. CRMP-2 thus can facilitate microtubule and F-actin assembly and promote growth cone advancement (69,179). In addition, +TIPs such as APC (LFC 0.78), APC2 (LFC 0.86) and CLIP1 (LFC 0.815) are also upregulated.

Genes that functions to manipulate membrane curvature in order to accommodate cytoskeletal dynamics during neurite outgrowth were also upregulated. These included Syndapin/Pascin1 (LFC 0.81) and srGAP3 (LFC 0.92) (180)(181).

3.3.2 Progression of neuronal morphogenesis of individual prethalamic neurons can be observed in the dissociated cell culture system

Morphogenesis of dissociated prethalamic cells started soon after the cells were plated onto the coverslips and attached to the coverslip surfaces. When cells were fixed after 24 hours after plating (1DIV), neuritogenesis had already happened, and the majority of the dissociated prethalamic cells had transited from stage 1 to stage 2 or even later stages (Figure 3.5A-A'). At 1DIV, Pax6-positive and Pax6-null prethalamic neurons, which were positive for Tuj1 staining, and mostly display 2-3 short neurites with similar lengths (Figure 3.5A-A'). From 2DIV onwards, most Pax6-positive and Pax6-null prethalamic neurons displayed one longest neurite, which was presumably the developing axon, and several shorter neurites (Figure 3.5B-F'). The progression of neuronal morphogenesis of the prethalamic neurons generally followed the in vitro model that previous studies proposed. However, branching of neurites in the prethalamic neurons took place prior to the establishment of neuronal polarity and later, alongside neurite elongation (Figure 3.5A-C'). Interestingly, the longest neurites the prethalamic neurons displayed also developed a lot of branching and small protrusions, especially at later stages (Figure 3.5D-F'). By visual inspection, the general morphologies of the Pax6-null prethalamic neurons were similar to those displayed by their control counterparts (Figure 3.5A-F').

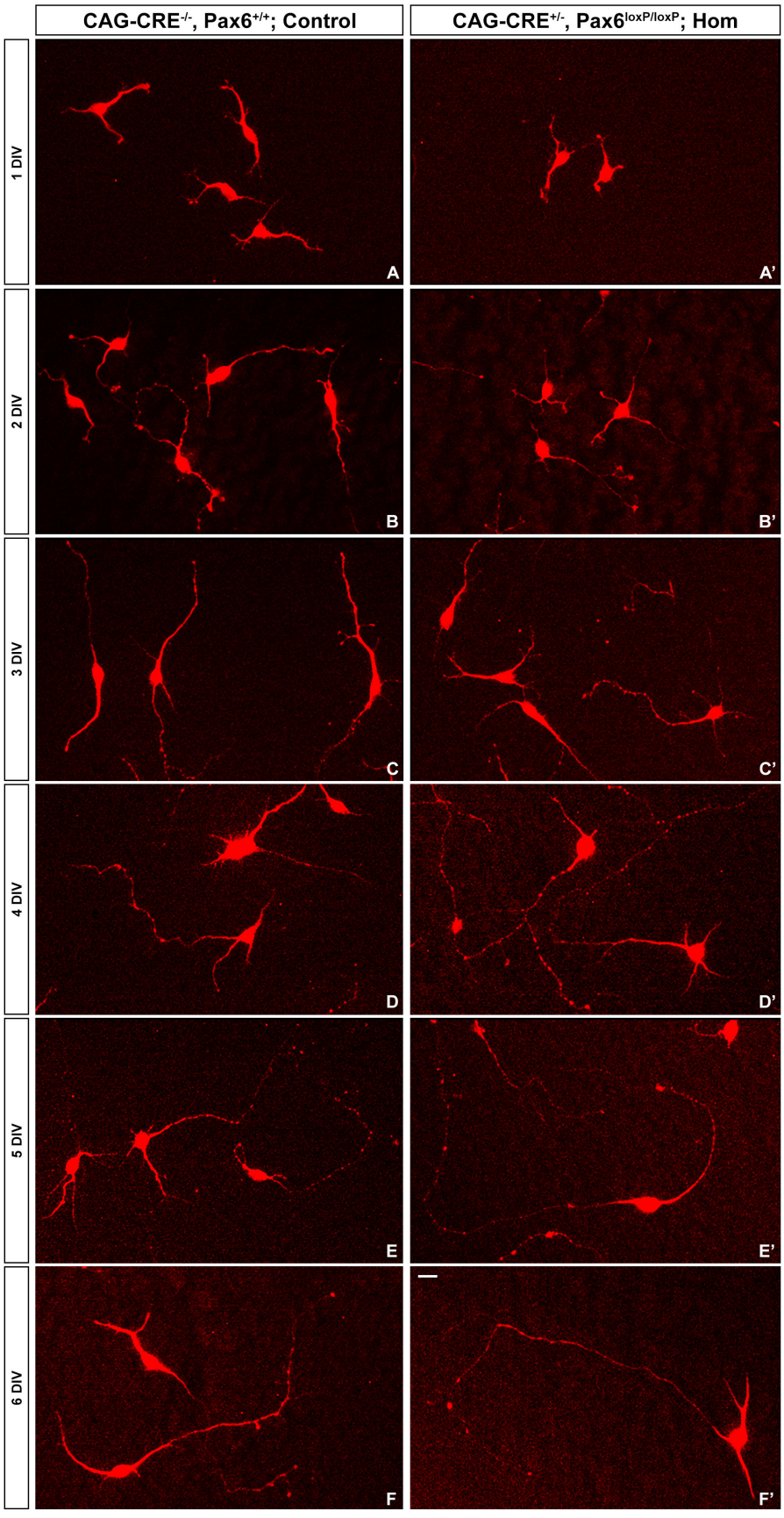

Figure 3.5 Dynamics of neuronal morpho-genesis of prethalamic neurons in the dissociated cell culture system. (A-F') Example morphologies the control (A-F) and Pax6-null (A'-F') prethalamic neurons displayed on each of the 6 days of the cell culture. Scale bar: 10 μm.

3.3.3 Neuronal morphogenesis is highly heterogeneous among the primary neurons of the prethalamus at the same age of cell culture.

To find out if the dynamics of neuronal morphogenesis was affected when Pax6 was deleted from the prethalamus, I measured the length of longest neurite, the total length of neurites and the number of neurites in each individual Pax6-positive and Pax6-null prethalamic neurons. Scatter plots were used to demonstrate whether there were any correlations between the length of the longest neurite and total length of neurites among the prethalamic neurons being measured. Interestingly, on the averaged population level, it seemed that both Pax6-positive and Pax6-null prethalamic neurons distributed nearly half of their cytoskeletal contents to make up the stem of the longest neurite, as the ratio of the length of longest neurite over the total length of neurites always ranged from 0.4 to 0.5 across the 6 timepoints examined (Figure 3.6A-F). Another interesting result showed by these scattered plots was that the morphologies of prethalamic neurons, when represented by correlation of these two parameters, exhibited high levels of heterogeneity, especially at later stages when the neuronal morphologies are more mature (Figure 3.6D-F). Additionally, Pax6-null prethalamic neurons seemed to display shorter longest neurites and lower total length of neurites at earlier stages (Figure 3.6A-C). However, at later stages, the Pax6-null population seemed to be more spread out than the control cells, and the averaged the longest neurite, and total neurite length seemed to have surpassed the control cell population (Figure 3.6D-F).

In terms of the number of neurites, the majority of the prethalamic neurons constantly display 2-3 neurites throughout the time points examined (Figure 3.7A-F'). However, the Pax6-null prethalamic neurons seemed to have a larger proportion of cells displaying lower numbers of neurites than the Pax6-positive prethalamic neurons (Figure 3.7A'-F'). The number of neurites displayed by both the Pax6-positive and Pax-null neurons increased as neuronal morphogenesis proceeded (Figure 3.7A'-F'), indicating that unlike what the conventional model of neuronal morphogenesis in vitro proposes,

neuritogenesis of prethalamic neurons can also happen at later stages, such as beyond the stages of establishment of neuronal polarity and axon elongation.

The above observations indicated that although the general morphologies the Pax6-null prethalamic neurons displayed were similar to that of the Pax6-positive prethalamic neurons, the dynamics of neuronal morphogenesis might differ. Therefore, we further performed statistical tests on the data I collected on the length of the longest neurite, the total length of neurites and the number of neurites from the control and Pax6-null prethalamic cells. As mentioned above, the prethalamic cells collected from these six days of cell culture came from the prethalamus of a single embryo. Moreover, on each day of the cell culture, images of at least 100 cells were processed for measurement of the three morphological parameters. Therefore, to accommodate the fact that the cells on each day of the cell cultures were not independent, and to avoid creating pseudo-replications in our statistical tests, we performed mixed-effect models on the data collected, to verify if loss of Pax6 can significantly alter any of these three parameters, and thus affect the dynamics of neuronal morphogenesis in the prethalamic neurons.

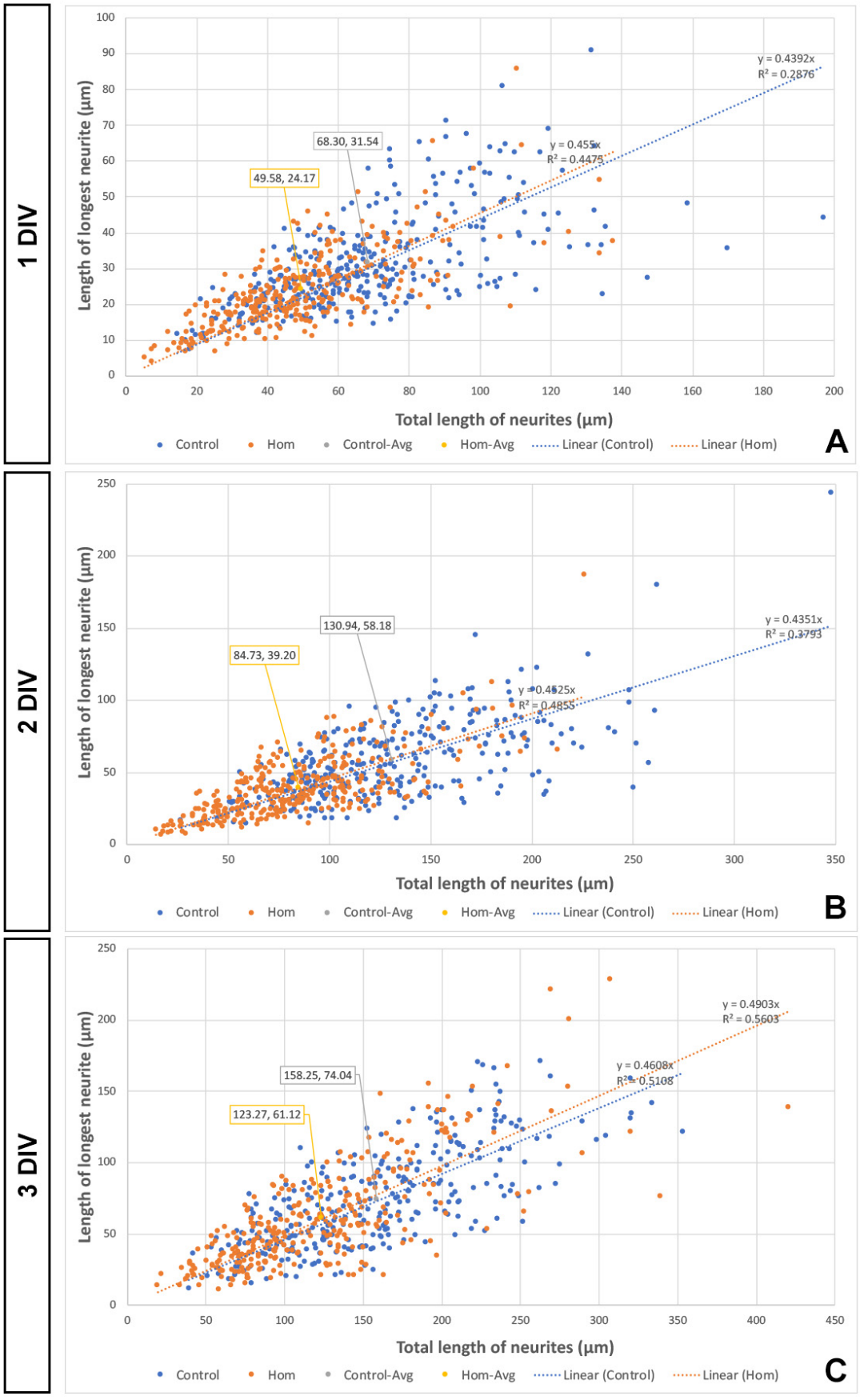
1 DIV
Length of longest neurite (µm)
Total length of neurites (µm)
y = 0.4392x
R² = 0.2876
y = 0.455x
R² = 0.4479
68.30, 31.54
49.58, 24.17
Control
Hom
Control-Avg
Hom-Avg
Linear (Control)
Linear (Hom)
A
2 DIV
Length of longest neurite (µm)
Total length of neurites (µm)
y = 0.4351x
R² = 0.3793
y = 0.4525x
R² = 0.4855
130.94, 58.18
84.73, 39.20
Control
Hom
Control-Avg
Hom-Avg
Linear (Control)
Linear (Hom)
B
3 DIV
Length of longest neurite (µm)
Total length of neurites (µm)
y = 0.4903x
R² = 0.5603
y = 0.4608x
R² = 0.5108
158.25, 74.04
123.27, 61.12
Control
Hom
Control-Avg
Hom-Avg
Linear (Control)
Linear (Hom)
C

4 DIV

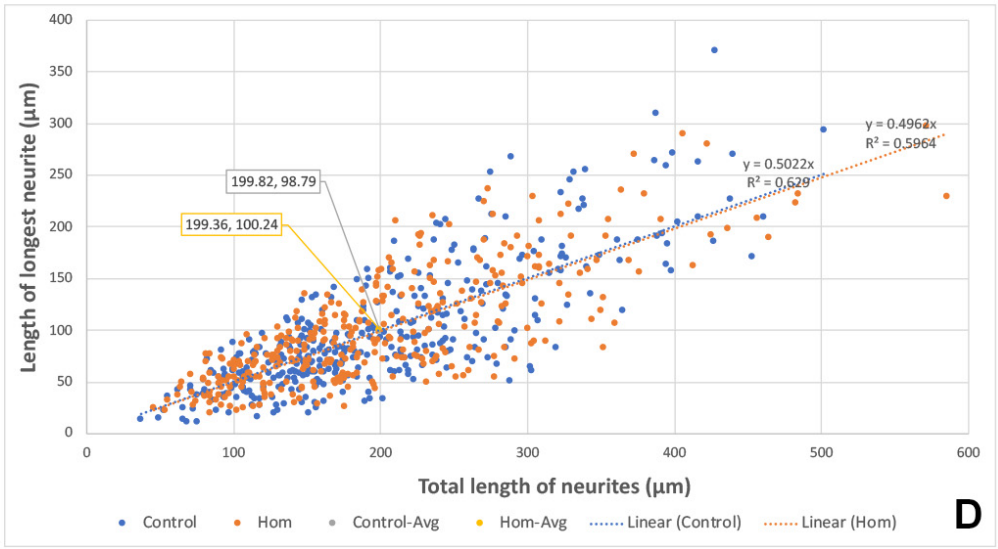

5 DIV

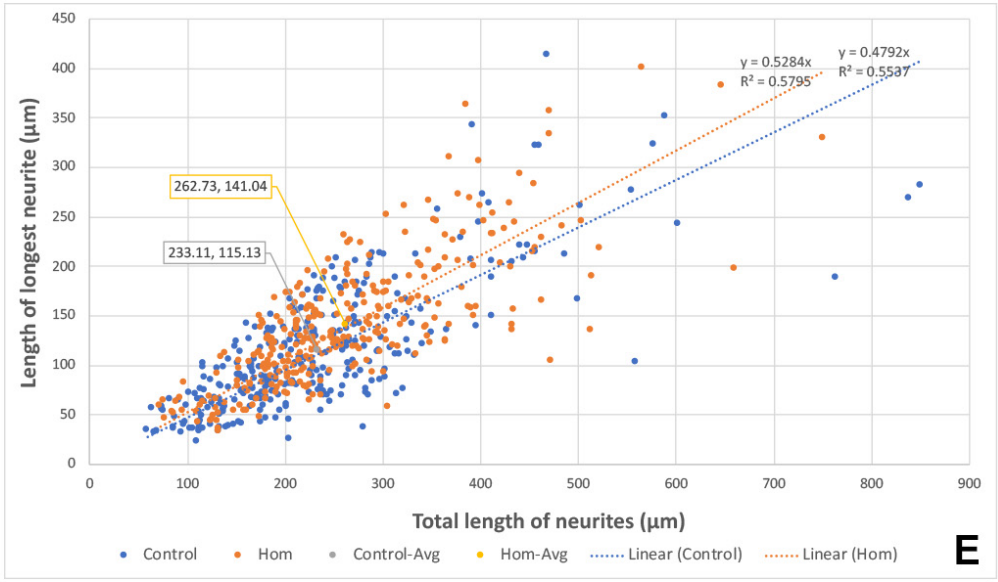

6 DIV

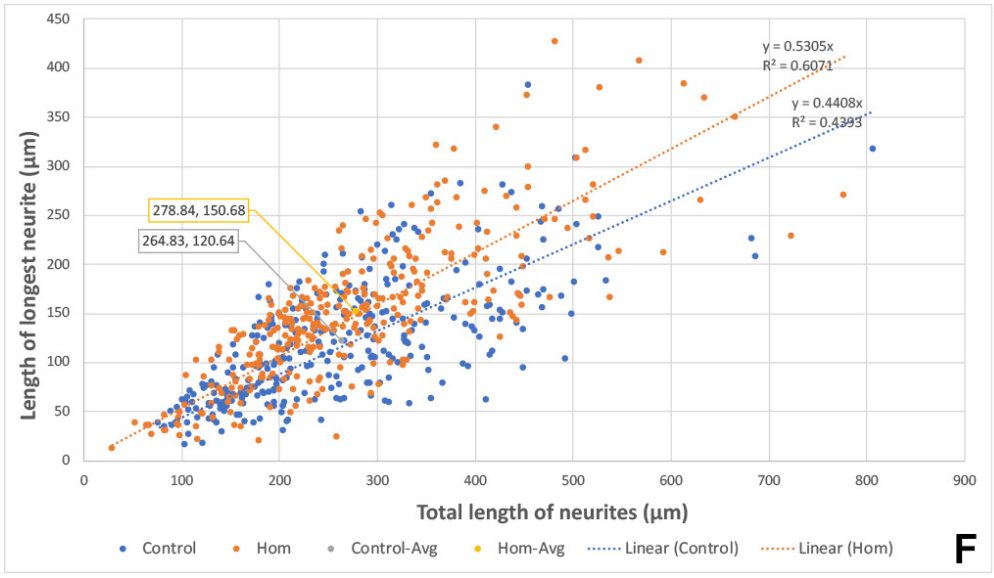

Figure 3.6 Scatter plots showing correlation between length of longest neurite and total length of neurites in each of the neurons measured (Page 85-86). (A-F) Neurons cultured for 1-6 DIV. At least 100 prethalamic neurons from each litter of both the control and Pax6-null genotype were measured on each of the six days of the cell culture. Measurements of prethalamic neurons from three litters were pulled together to make up each scatter plot. Linear trendlines with a set intercept of zero were calculated with Excel to fit for the two measurements in both genotypes of prethalamic neurons on each day of the cell culture. The closer the R2 values were to 1, the better the trendlines were fitting and representing the population. The mean values of length of longest neurite and total length of neurites for each genotype on each day of the cell culture was also plotted and shown in the scatter plots.

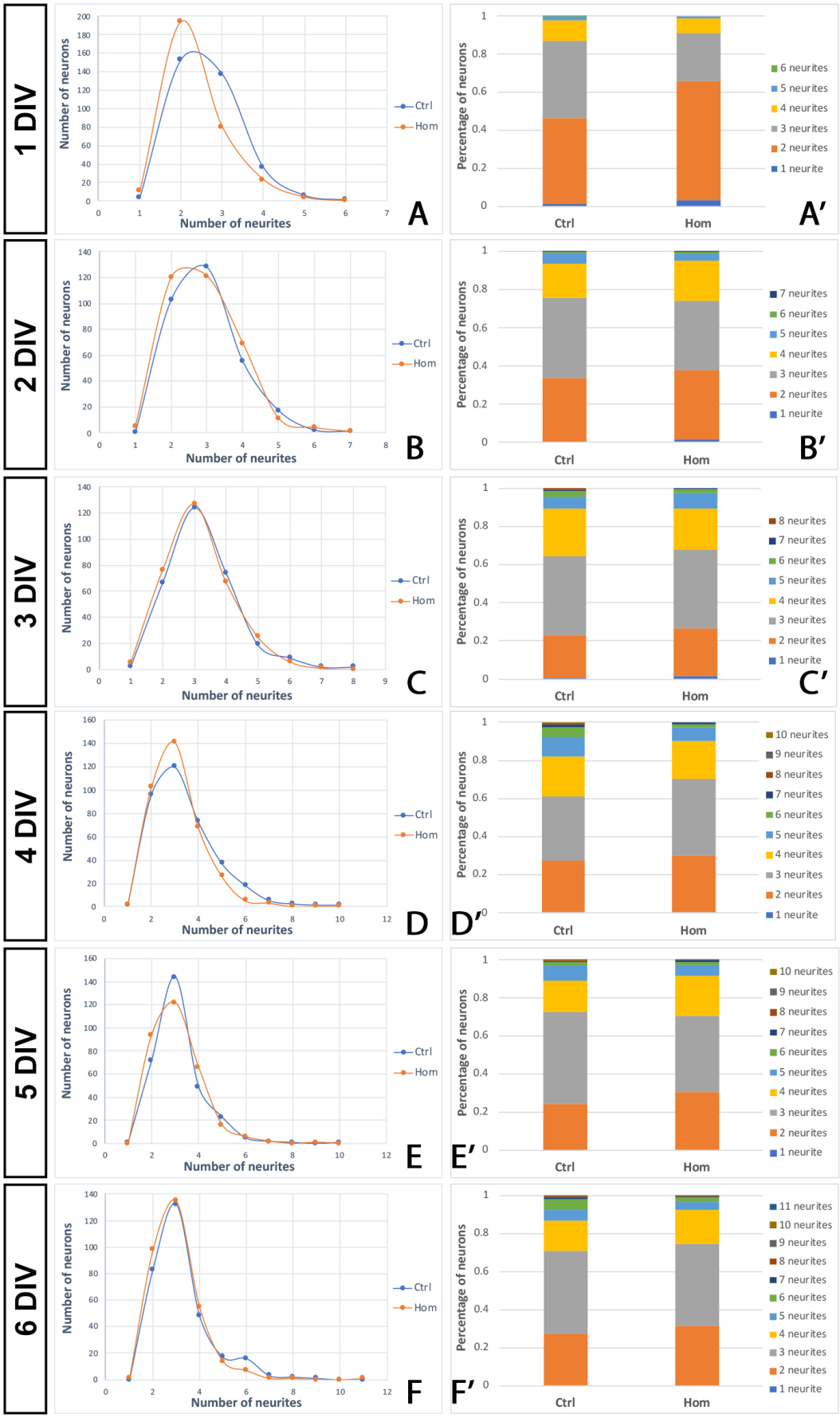
1 DIV
2 DIV
3 DIV
4 DIV
5 DIV
6 DIV
Number of neurons
Number of neurites
Ctrl
Hom
A
B
C
D
E
F
Percentage of neurons
6 neurites
5 neurites
4 neurites
3 neurites
2 neurites
1 neurite
7 neurites
8 neurites
10 neurites
9 neurites
11 neurites
A'
B'
C'
D'
E'
F'

Figure 3.7. Number of neurites displayed by prethalamic neurons of the control and Pax6-null genotypes on each of the six days of the cell culture. The neurons being measured were the same as the ones that were used for measurements of length of longest neurite and total length of neurites. Therefore, at least 100 prethalamic neurons were measured for both genotypes and measurements of numbers of neurites in neurons from three litters were pulled together to make each one of the scatter plots (A-F) and stacked column graphs (A'-F'). (A-F) Scatter plots with smooth lines and markers showed the number of neurons displaying a set number of neurites on each day of the cell culture. (A'-F') Stacked column graphs showed the percentage of neurons displaying a set number of neurites on each day of the cell culture.

3.3.4 Loss of Pax6 affects neuronal morphogenesis dynamics in the prethalamic neurons.

For the data sets of the length of longest neurite and the total length of neurites, fixing a mixed model with litter as random effect made the model unable to converge, meaning that the parameters of the model (days, genotypes and output variables) cannot be estimated correctly. Therefore, we left out the litter effect from the model. Analysis of deviance by Type III ANOVA showed significant effects of days and genotype ($P < 2.2 \times 10^{-16}$), as well as their interaction. From this, the pairwise comparison can be made between genotypes within the same days for data collected for the length of the longest neurite and total length of neurites.

Data points of the three data sets were processed for box plots, to show the distributions of the data of each genotype on each individual day. The upper and lower edge of each box indicated the 75th percentile and 25th percentile, while the horizontal line inside the box indicated the median and the cross inside the box indicated the mean value of each data set. The whiskers were drawn according to the Tukey method. Briefly, the difference between the 25th and the 75th percentile was calculated and termed interquartile range (IQR). The upper whisker was drawn by adding 1.5 times of IQR on top of the 75th percentile, and the lower whisker was drawn by deducing 1.5 times of IQR from the 25th percentile. Any value greater than the value of the upper whisker or lower than the value of the lower whisker was plotted as individual points in the box plots. If no values in a data set were higher than the value of the 75th percentile plus 1.5 times of IQR, or no value was lower than the 25th percentile minus 1.5 times of IQR, the upper or lower whisker was drawn as the highest or lowest value in that data set.

As shown in Figure 3.8 and 3.9, Pax6-null prethalamic neurons constantly displayed shorter length of longest neurite and the total length of neurites from 1-3 DIV, indicating that neuronal morphogenesis might have been delayed in the prethalamic neurons at early ages of cell culture (1-3 DIV) when Pax6 is

lost (Figure 3.8A-C, Figure 3.9A-C). However, the rate of neurite elongation increased dramatically from 3-5 DIV (Figure 3.8D-F, Figure 3.9D-F), and this lack of neurite growth was soon caught up by the Pax6-null prethalamic cells as at 4DIV, as no difference was seen in the length of longest neurite and the total length of neurites between the control and the Pax6-positive prethalamic neurons (Figure 3.8D, Figure 3.9D). Additionally, at 5 and 6 DIV, the Pax6-null prethalamic neurons display longer length of the longest neurite, and on 5DIV, they also displayed a longer total length of neurites (Figure 3.8E-F, Figure 3.9E-F).

In terms of numbers of neurites, although on all six days of the cell culture, Pax6-null prethalamic cells always displayed a larger proportion of cells possessing lower numbers of neurites, these differences were not significant except for 1 DIV (Figure 3.10).

These results showed that when Pax6 is lost from the prethalamus, the process of neuronal morphogenesis was affected in the prethalamic neurons as in the early stages, neuronal morphogenesis was delayed but soon caught up and overshot at later stages (Figure 3.11A-B).

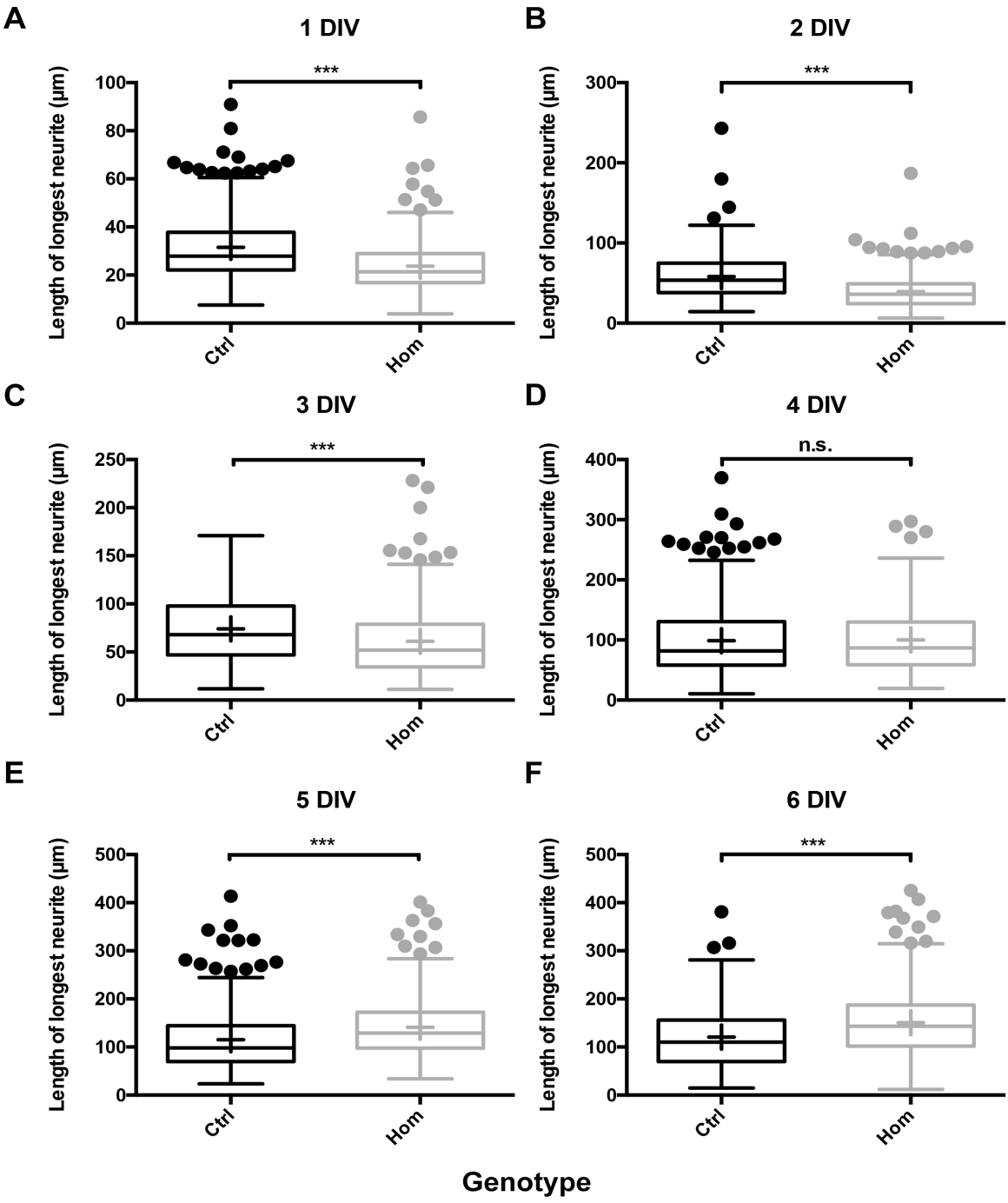

Figure 3.8 Pax6-null prethalamic neurons displayed different dynamics of extending their longest neurites during neuronal morphogenesis. (A-C) From 1-3 DIV, Pax6-null prethalamic neurons had shorter length of longest neurites. **(D)** At 4 DIV, Pax6-null prethalamic neurons showed similar length of longest neurites as the control prethalamic neurons, indicating an increased rate of neurite elongation from 3-4 DIV. **(E-F)** At 5 and 6 DIV, Pax6-null prethalamic neurons showed longer length of longest neurites. Data were analysed with mixed-model, measurement of length of longest neurite from at least 100 neurons of both genotypes were collected from each litter on each of the six days of cell culture. Three litters in total (n=3). ***: P<0.001.

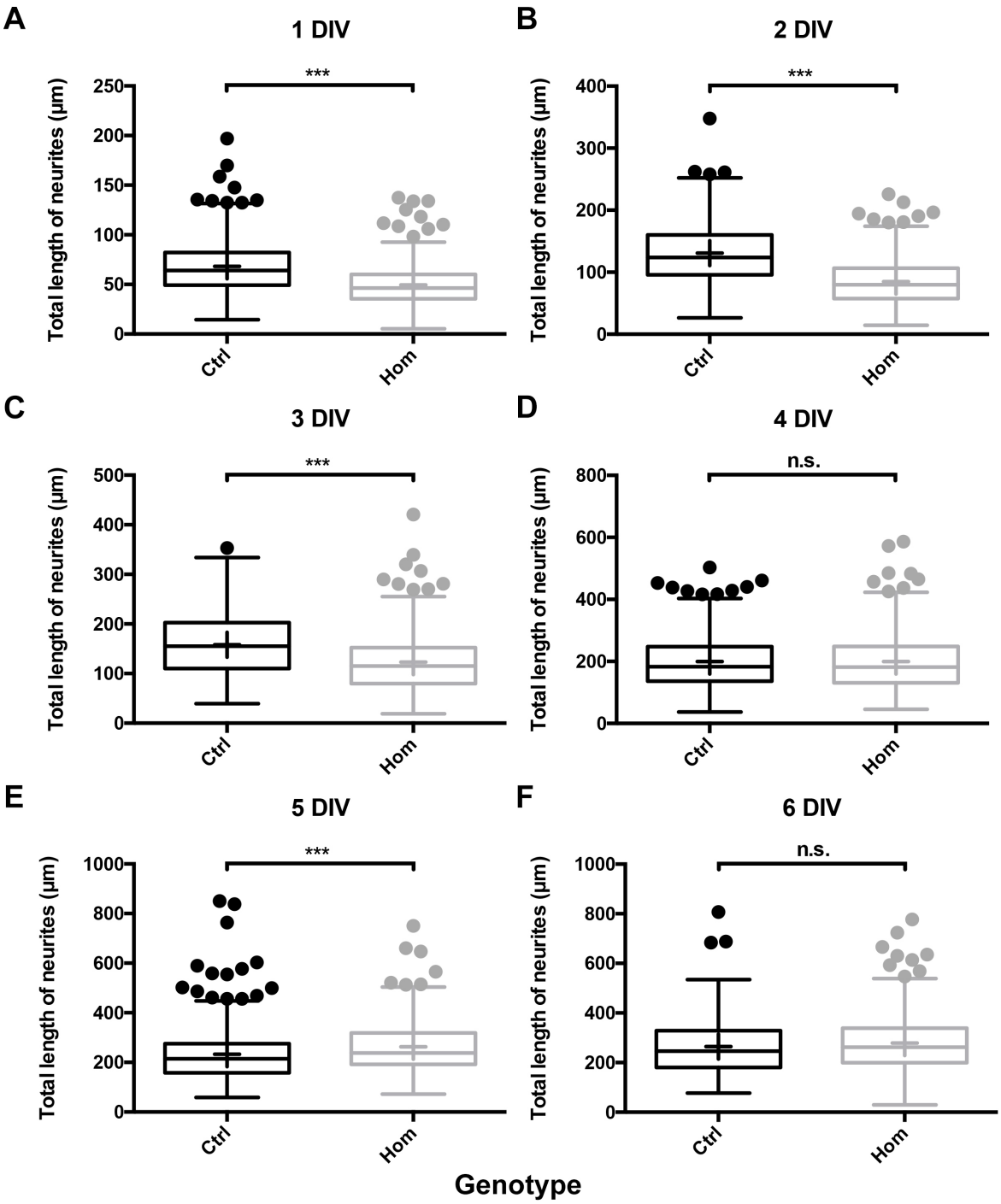

Figure 3.9 Similar to length of longest neurite, Pax6-null prethalamic neurons also showed different dynamics when extending all of their neurites. Total length of neurites in the Pax6-null prethalamic neurons were shorter at 1-3 DIV **(A-C)**, whose extending rate also seemed to have increased during 3-4 DIV and displayed similar length to the control prethalamic neurons on 4 DIV **(D)**. **(E)** On 5DIV, Pax6-null prethalamic neurons displayed significantly longest length of total neurites. Although the average lengths of total neurites were still higher in the Pax6-null prethalamus, the difference was not significant on 6 DIV **(F)**. Data were analysed with mixed-model, measurement of length of longest neurite from at least 100 neurons of both genotypes were collected from each litter on each of the six days of cell culture. Three litters in total (n=3). ***: P<0.001.

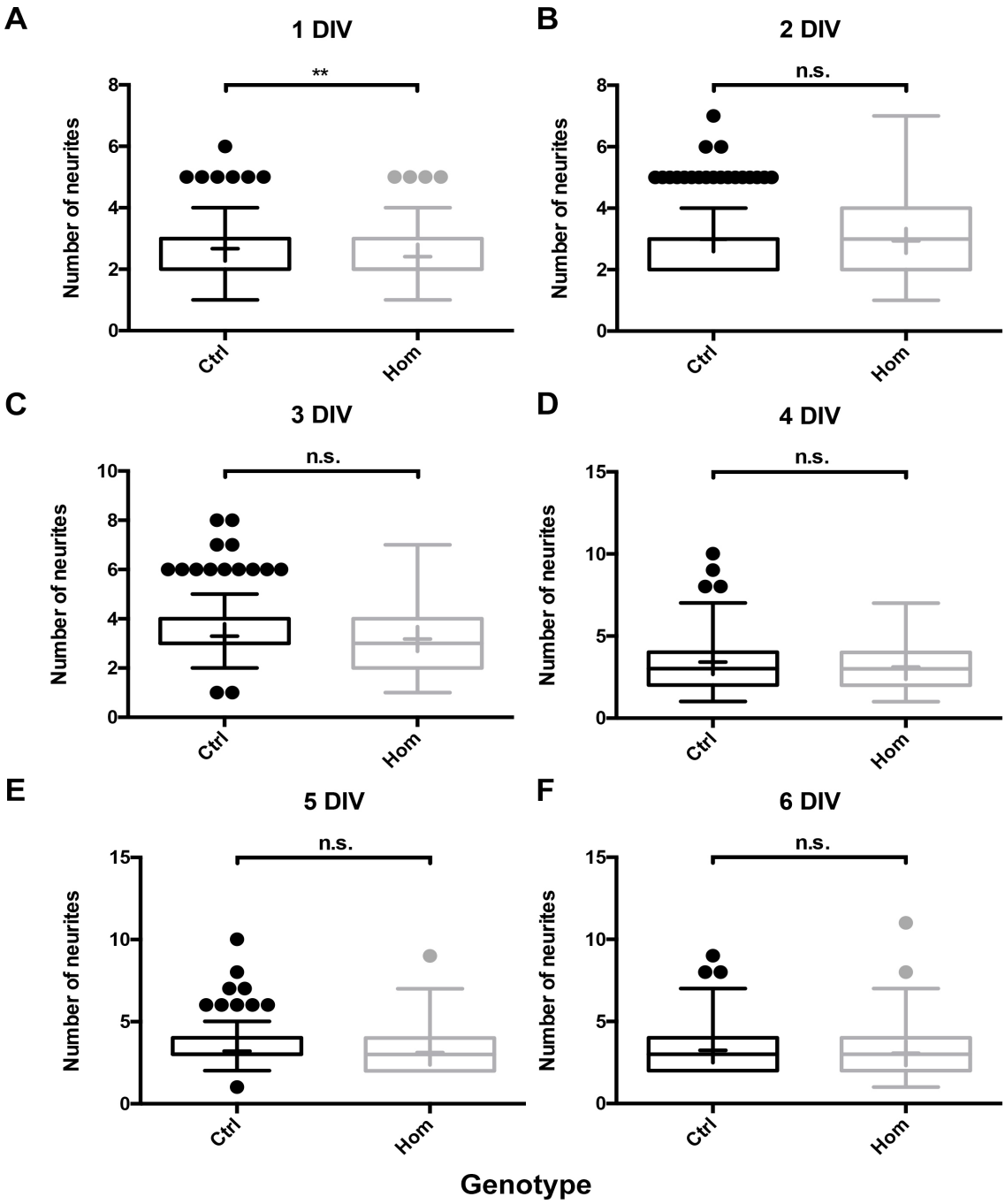

Figure 3.10 Pax6-null prethalamic neurons displayed slightly lower number of neurites during neuronal morphogenesis. Across the six days measured, only on the first day of the cell culture (1DIV) **(A)** that the number of neurites differed significantly between the control and the Pax6-null neurons. In the rest of the days tested **(B-F)**, Pax6-null neurons constantly displayed lower averaged number of neurites on a populational scale, but such difference was not significant. Data were analysed with mixed-model, measurement of number of neurites from at least 100 neurons of both genotypes were collected from each litter on each of the six days of cell culture. Three litters in total (n=3). **: 0.001<P<0.01.

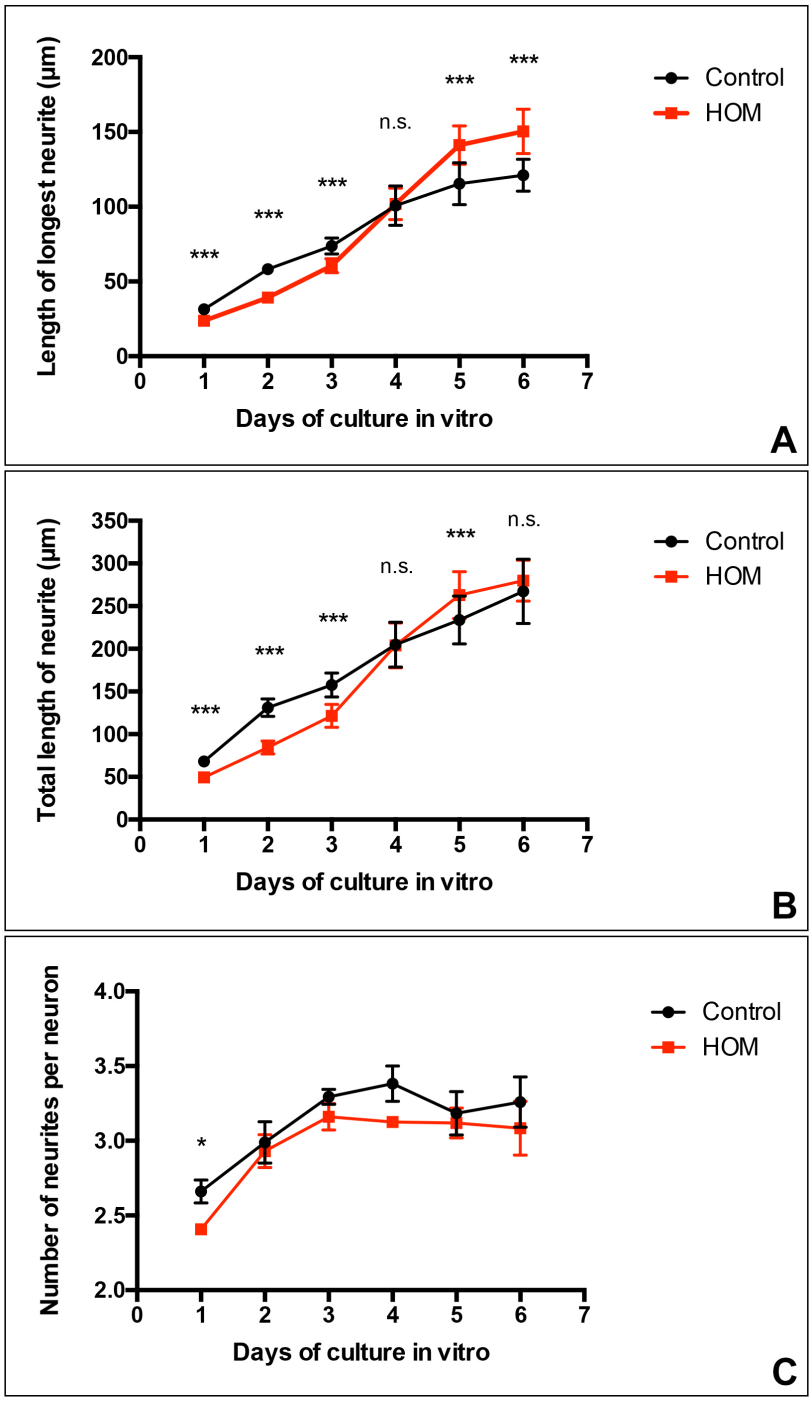

Figure 3.11 Summary of neuronal morphogenesis of prethalamic neurons in culture through time. (A-B) Neuronal morphogenesis was delayed in the Pax6-null prethalamic neurons as they displayed shorter length of longest neurite and total neurites from 1-3DIV, and these differences were significant for both parameters from 1-3DIV. From 3-5DIV, the rate of axon elongation in the Pax6-null prethalamic cells increased dramatically, and they displayed longer longest neurite and total neurite length in later stages (5-6DIV). These differences were significant for both parameters on 5DIV. **(C)** The average number of neurites per neurons was constantly less in the Pax6-null prethalamic cells, and such difference were only significant on 1DIV. Mixed-effect model, at least 100 neurons of both genotypes were collected from each litter on each of the six days of cell culture. Three litters in total (n=3). **: 0.001<P<0.01, *: 0.01<P<0.05

3.4 Discussion

In this chapter, I utilised the dissociated cell culture system to study neuronal morphogenesis of prethalamic neurons in vitro. Three parameters- length of the longest neurite, the total length of neurites and the number of neurites were chosen to represent the dynamics of neuronal morphogenesis as primary prethalamic neurons mature. By comparing these three parameters in control and Pax6-null prethalamic neurons, I found that Pax6-null prethalamic neurons displayed different dynamics when extending their neurites during neuronal morphogenesis. At earlier stages (1-3 DIV), neuronal morphogenesis was delayed in the prethalamic neurons as they showed a shorter length of the longest neurite and total neurites. However, the rate of neurite extension increased dramatically from 3-5 DIV and the Pax6-null prethalamic neurons displayed longer length of the longest neurite and total neurites at later stages (5-6 DIV).

The prethalamus is one of the very few places in the neural tube where Pax6 is expressed post-mitotically (22). Previous researches investigating the relationship between Pax6 and neuronal morphologies in granule cells of the cerebellum and retinal ganglionic cells have pointed out a possible general trend of Pax6 facilitating these neurons in extending their neurites or axons (169–171). However, in the prethalamic neurons, Pax6 seemed to play a role in limiting axon elongation, at least during the later stages of the cell culture when the morphologies of the prethalamic neurons were more mature. This has once again pointed out an intriguing but quite frequently observed situation, in which the same transcription factor plays opposite roles in different tissues during development of the nervous system (58).

Unlike the thalamic neurons, which receive afferent sensory input (except olfactory) and relay them onwards by projecting to and innervating specific regions of the cortex, prethalamic neurons only project to and innervate the neighbouring thalamus and form close or open circuitries with thalamic

neurons to fine tune the latter's excitability (12,104). Prior to the formation of the thalamocortical axons (TCA), prethalamic axons that innervate the thalamus would act as scaffolds for the descending of the TCA into the prethalamus before the TCA exit the ventral diencephalon and turn for the cortex. Misroute of the TCA has been a known phenotype of the Pax6 mutant mice, and previous studies have shown that in these Pax6 mutant mice, prethalamus failed to send out as many pioneer axons to the thalamus (unpublished data) (59). Indeed, dysregulated expressions of guidance molecules within the diencephalon might be one significant contributor (60,165,166). However, by confirming that Pax6 can regulate morphogenesis of the prethalamic neurons in a cell-autonomous manner, my findings provided another potential explanation and a new insight into how TCA formation could be disrupted in the Pax6 mutants. If what I showed in vitro reflects what happens in vivo, then disrupted dynamics of morphogenesis of the prethalamic neurons might cause the prethalamic axons to arrive at the thalamus at an incorrect timepoint or even not arriving at the thalamus at all, therefore failing to support the formation and descending of the TCA.

Different attempts of visualising neuronal morphogenesis of the prethalamic neurons in vivo had been made during this PhD. For example, as the animal model I used carries a GFP reporter for the activities of the tamoxifen-dependent Cre recombinase, lowering the dose of the tamoxifen enables me to create a mosaic deletion of Pax6 and activation of GFP expression. If this dosage is low enough, I will be able to see a random set of Pax6-null cells with cytoplasmic GFP expression lighting up their entire morphology. Additionally, when the dose of tamoxifen is so low, these Pax6-null cells would still be in a Pax6-positive environment, meaning that the environmental information for neuronal morphogenesis in vivo would still be more or less correct. Therefore, this set up creates an ideal in vivo counter-situation to the in vitro culture system, that would allow me to study the cell-autonomous effect of Pax6 on neuronal morphogenesis if any of the prethalamic neurons were randomly hit by the tamoxifen. Unfortunately, despite the repeated effort of trying different

dosages of tamoxifen and different length of time for the low-dose tamoxifen to activate the Cre-recombinase, I was not able to set up this mosaic system to study neuronal morphogenesis in vivo. The reason was that the dose of tamoxifen needed to activate the GFP reporter was way lower than the dose needed to excise the floxed Pax6 exons effectively. As a result, when the dose of tamoxifen was low enough for me to visualise the clear morphology of single neurons, that neuron still had at least one of its Pax6 allele intact despite it was also positive for GFP expression.

To compensate this, another effort I made to visualise neuronal morphogenesis in vivo was to perform intracellular filling of cells using microinjection electrodes in fixed diencephalic sections of the same mouse model. The technique worked for what I needed, which was to outline the entire morphologies of a few prethalamic neurons selectively. However, due to the difficulty of performing this technique, it was time-wise unrealistic to use this technique in an attempt to collect enough numbers of prethalamic neurons for statistical analysis. For future experiments to visualise and trace the morphologies of prethalamic neurons at different developmental stages, I might be able to utilise in utero electroporation. To elaborate, a low concentration of plasmids containing a cytoplasmic marker different than GFP can be injected into the third ventricles of the control and Pax6-null embryos of the same mouse model, followed by electroporation. That way I might be able to selectively label the morphologies of a subset of prethalamic neurons for further analysis.

How does Pax6, as a transcription factor, regulate neuronal morphogenesis in a cell-autonomous manner remains elusive. One possibility might be that Pax6 directly controls the expression of the cytoskeletal regulatory genes in the Pax6-positive prethalamic neurons. This remains to be confirmed. Another possibility might be that through activation or inactivation of other signalling pathways. In our RNAseq data, the Wnt signalling pathway was also highly enriched and upregulated in the prethalamus when Pax6 is lost. Both

canonical and noncanonical Wnt signalling were known to be able to regulate cytoskeletal reorganisation during neuronal morphogenesis. Therefore, could the change of neuronal morphogenesis dynamics in the Pax6-null prethalamic neurons be a result of altered Wnt activities? Which Wnt signalling pathway exactly and also in which prethalamic cells? On the other hand, it is known that canonical Wnt signalling plays a role in specifying cell fate of the pTh-C derived neurons. Could the change of neuronal morphogenesis simply be a result of changes in cell fate of the prethalamic neurons due to this upregulation of canonical Wnt signalling in the prethalamus? These are all interesting questions that need to be further pursued in the future.

The upregulated expressions of cytoskeletal regulatory genes found in the RNAseq data after Pax6 deletion might be the reason for the overshoot of the length of the longest neurite and total neurites. However, it remains exceptionally intriguing why at early stages of the cell culture, neuronal morphogenesis was slower in the Pax6-null prethalamic neurons.

Due to my experimental design, when I applied tamoxifen gavage at E9.5, almost all the cells in the neural tube at this age were progenitors. Therefore, I started deleting Pax6 in the prethalamic progenitor cells, and these progenitors carried the impacts of absence of Pax6 during and after they become post-mitotic cells. As a result, one possibility to explain the delayed neuronal morphogenesis in the early stages of the cell culture might be that I saw a total effect of Pax6's deletion throughout the development of the prethalamic cells, from when they were still progenitors to when they have become neurons. Could this be the underlying reason why the Pax6-null prethalamic neurons develop their morphologies slower at the early stages of the cell culture?

In order to distinguish the effect of loss of Pax6 in progenitor cells and post-mitotic cells, I attempted to delete Pax6 only in the prethalamic post-mitotic cells. However, as we did not have a mouse model which initiate the

expression of the Cre-recombinase only in the post-mitotic cells, this experiment was done in the dissociated prethalamic cell cultures. To elaborate, embryos of CAG-Cre$^{+/-}$, Pax6$^{+/loxP}$ and CAG-Cre$^{+/-}$, Pax6$^{loxP/loxP}$ were collected at E13.5, and their prethalamus were dissected out and processed for dissociated cell culture as described above. Unlike my experimental design for observing neuronal morphogenesis, these embryos had not experienced tamoxifen. After the dissociated cells have attached to the coverslips and rested for 2 hours, 4OH-tamoxifen was added into the cell culture to active the Cre-recombinase in these prethalamic primary cell cultures. As most of the cells in the prethalamus at E13.5 have already exited the cell cycle, by applying active tamoxifen directly into the cell culture, I made sure to delete Pax6 almost only in the prethalamic post-mitotic cells. Unfortunately, the prethalamic primary cells in culture were susceptible to 4OH-tamoxifen. Also, when I lower the dose of 4OH-tamoxifen to a level that cell viability could be achieved, it was too low for the Cre-recombinase to excise the floxed Pax6 exons effectively. GFP expression, however, could still be activated under this dose of 4OH-tamoxifen, a scenario similar to the in vivo mosaic experiment described above.

In addition to low tamoxifen dosage that was not high enough to excise the floxed Pax6 exons, another complication I encountered when I attempted to delete the Pax6 in only post-mitotic cells was that it seemed that a high Pax6 deletion efficiency was much harder to achieve in the post-mitotic cells than progenitor cells. Previous work done in the lab has shown that when applying tamoxifen gavage at E9.5 to these FP6CD1 mice, Pax6 deletion can reach approximately 80% or above even just after two days (58). However, when I tried to delete Pax6 only in the post-mitotic cells by applying tamoxifen at E13.5 to the pregnant females, Pax6 expression could still be found in prethalamic derivative neurons at P0. Interestingly, when I cross the FP6CD1 mouse with the constitutive Pax6 mutant mouse to generate embryos carrying one allele of constitutively mutated Pax6 and one allele of floxed Pax6, the efficiency of Pax6 deletion did not increase much in comparison to the embryos carrying

two alleles of floxed Pax6. It remains to be determined whether this persistence of Pax6 expression in the post-mitotic cells was due to the inability of Cre-recombinase to excise the Pax6 gene from the chromosome, or extremely low level of turnover of the PAX6 protein. Nevertheless, with the mouse model available, I could not proceed any further on investigating the deletion of Pax6 only in the post-mitotic cells and how that might impact on neuronal morphogenesis of the prethalamic neurons.

Another possibility to explain the delay of neuronal morphogenesis in the Pax6-null prethalamic neurons might be the disruption of the establishment of neuronal polarity. As what people previously proposed, one of the speed-limiting steps during neuronal morphogenesis was the establishment of neuronal polarity. In cultured hippocampal neurons, for example, the establishment of neuronal polarity can take up to 24-48 hours (33). To find out whether this is the reason for the delayed neuronal morphogenesis I observed in the Pax6-null prethalamic neurons, I next moved on to study the establishment and maintenance of neuronal polarity in the prethalamic neurons.

3.5 Summary

In this chapter, by analysing the most highly enriched and upregulated GO terms in the prethalamus in the absence of Pax6, I further set out to investigate whether neuronal morphogenesis of the prethalamic neurons was disrupted when Pax6 is deleted. By comparing the length of longest neurites, total length of neurites and number of neurites the control and Pax6-null prethalamic neurons displayed from 1-6 days of the cell culture, I found that the dynamics of neuronal morphogenesis in the Pax6-null prethalamic neurons altered as they displayed slower rate of extension for lonest neurite and also total neurites at early stages of the cell culture (1-3 DIV). This delay in neuronal morphogenesis was then soon caught up from 3-5 DIV and the Pax6-null prethalamic neurons displayed an overshot for the length of longest neurite and total neurites at later stages when the morphologies of the neurons were more mature (5-6 DIV).

Chapter 4

The roles of Pax6 in regulating the establishment and maintenance of neuronal polarity during the development of the prethalamic neurons

4.1 Introduction

The primary function of neuronal cells, which is to receive, process and propagate electrical signals in a unidirectional manner, is tightly linked to their unique and complex morphological features (83,182). A mature neuron usually displays a single extended axon and an elaborated web of dendrite arbours that have different membrane composition and cytoskeletal structures (73). Such distinctions, called neuronal polarity, are established during neuronal morphogenesis and maintained throughout the lifetime of the neuron (70,83,182).

4.1.1 The PAR3/6 complex plays vital roles during the establishment of neuronal polarity

During the establishment of neuronal polarity, the developing neurons integrate the spatial and intrinsic cues and ultimately convert them to cytoskeletal rearrangements that give rise to the axons and dendrites (83). The PAR3/6 complex is a core component of polarity determination in many tissues and cells (183). Recent studies have shown that it also plays a vital role during the establishment of neuronal polarity (182,184,185). It is composed of the scaffold proteins PAR3 and PAR6, and various protein kinases that are tethered to them (183). For example, the small GTPase cdc42 and the guanine exchange factor (GEF) Tiam1/STEF are both components of the PAR3/6 complex (183). Upon activation of the PI3K-PIP3 pathway by growth factors or adhesion molecules, CDC42 and Tiam1/STEF can be activated and further modulate the actin cytoskeleton in favour of neurite protrusion and axon elongation (182). Another type of kinase involved in the PAR3/6 complex is the atypical forms of protein kinase C (aPKC: PKC λ and ζ) (183). Activation of aPKC by CDC42 or Dishevelled (DVL) due to increased activity of Wnt signalling pathways can both phosphorylate Lethal Giant Larvae 1 (Lgl1), thus promoting membrane insertion at the nascent axon; and inactivate MARK-2, causing microtubule stabilisation and growth (Figure 4.1) (182). As a result, the PAR3/6 complex can mediate rearrangements of cytoskeleton and plasma

membrane structures in response to localised activation of membrane receptors, hence achieving polarised modification of cellular morphology. This is why the function of the PAR3/6 complex is highly dependent on its subcellular localisation in the polarised cells (83,182).

Indeed, the kinesin motor protein KIF3A has been shown to interact directly with PAR3 and direct the transportation and accumulation of PAR3 and aPKC to the tip of growing axons in cultured rat hippocampal neurons (185). The expression of a dominant-negative form of PAR3 and fragmented KIF3A inhibited the accumulation of PAR3 and aPKC at the axonal tip and induced sprouting of multiple neurites with similar lengths, indicating that the establishment of neuronal polarity was disrupted (184,185).

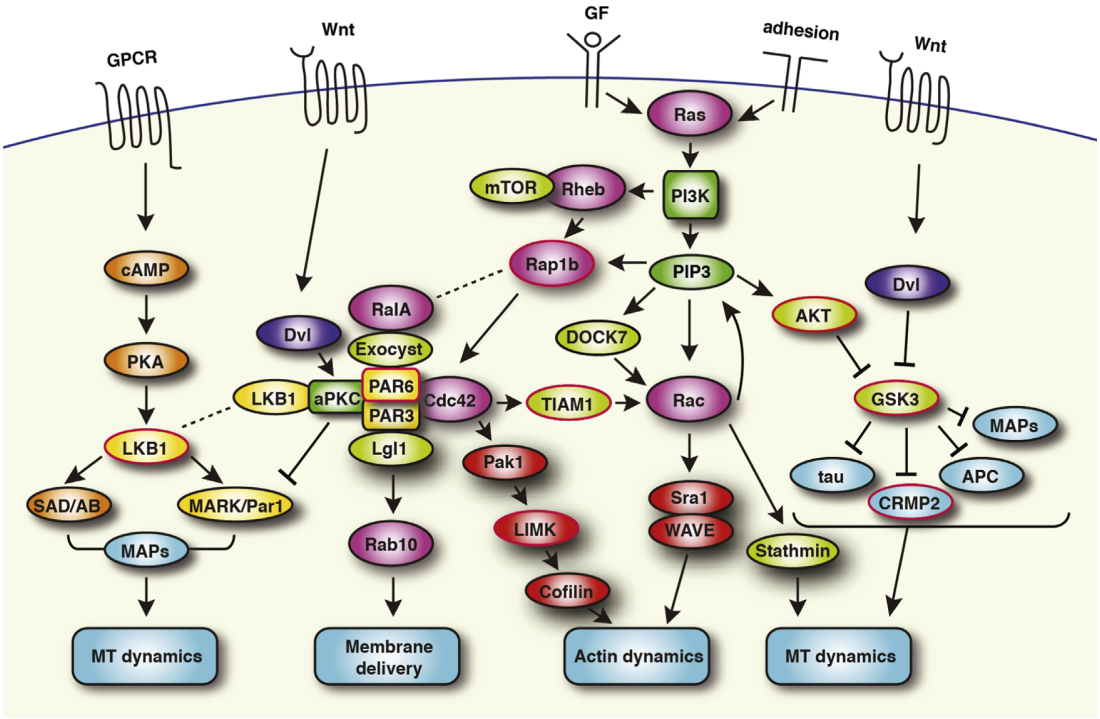

Figure 4.1 Schematic depiction of key signalling events regulating neuronal polarity. Following Ras activation after growth factor/adhesion signals, PI3K activation and PIP3 accumulation trigger a series of signaling events: 1) Akt activation and GSK3 inhibition resulting in microtubule stabilization; 2) activation of Rac regulating actin and microtubule dyamics; 3) Rheb-Rap1b-Cdc42 activation leading to activation of aPKC in the PAR complex, promoting actin cytoskeletal remodeling and polarized membrane delivery. Local activation of RalA and the exocyst complex also favour proper localisation of PAR complex at the tip of the nascent axon. cAMP-dependent activation of PKA leads to activation of LKB1, which in turn phosphorylates SAD kinases and MARK/PAR1, regulating microtubule dynamics via modulating the affinity of MAPs for microtubules. The Wnt pathway may regulate polarity via Dvl by activating aPKC and/or inihibiting GSK3. Figure adapt from (182).

4.1.2 The AIS is a crucial indicator of maintenance of neuronal polarity in the mature neuron

As mentioned before (Chapter 1), one of the critical indicators of maintenance of neuronal polarity is the axon initial segment (AIS) (81,82). The AIS is strategically located at the most proximal part of the axon, and functions as both a physiological and a physical bridge between the somatodendritic and axonal domains (81). With its specialised ultrastructural features, such as fasciculated microtubules and periodically arranged actin rings, and its unique molecular constituents, such as the highly concentrated cytoskeletal molecules of AnkG, βIV-spectrin and various voltage-gated Na+ and K+

channels, the AIS functions as the nexus of neuronal polarity in the mature neuron (81).

4.1.3 Aim of this chapter

In Chapter 3, I found that, although axon and neurite elongation was augmented in the Pax6-null prethalamic neurons at later stages of the cell culture, which might be due to the increased expressions of various cytoskeletal effector genes, neuronal morphogenesis was initially delayed in the prethalamic neurons when Pax6 is lost. Interestingly, RNAseq data in the lab showed significantly increased expression of components of the PAR3/6 complex and the AIS, which indicated that the establishment and maintenance of neuronal polarity might be disrupted in the prethalamic neurons upon Pax6 removal. Therefore, in this chapter, I moved on to investigate the abilities of the prethalamic neurons to establish and maintain their neuronal polarity, aiming to test:

1. Whether the establishment of neuronal polarity is defective in the absence of Pax6, and if that can contribute to the delayed neuronal morphogenesis of the Pax6-null prethalamic neurons

2. Whether the structure and components of the AIS, the key structure to maintain neuronal polarity, is altered in the absence of Pax6

3. Whether the excitability of the Pax6-null prethalamic neurons is changed due to altered AIS structure and components

4.2 Materials and methods

4.2.1 Fluorescent Immunohistochemistry on dissociated cell cultures of the prethalamic neurons

The animal model used in this study was still the FP6CD1 mouse. Protocol for tamoxifen gavage and embryo collection remains the same as previously described. 10mg of tamoxifen was given to the pregnant female on E9.5 and embryos are collected on E13.5. Dissection of the prethalamus and dissociated cell cultures of the prethalamic neurons were performed in the same way as previously described in Chapter 3.

Prethalamic neurons used for investigating the establishment of neuronal polarity were collected on 3 DIV of the cell culture, whereas neurons used for investigating the AIS were collected on 5, 7 and 9 DIV of the cell culture. At each one of these time points, the coverslips containing these cells were removed from the cell culture, rinsed with 1x PBS and the cells were further fixed with 2% PFA/4% sucrose for 10 minutes at room temperature. Both the 1x PBS and the 2% PFA/4% sucrose were warmed to 37°C before applying to the cells.

After fixation, cells were processed for fluorescent immunohistochemistry in the same ways as described in chapter 4. Primary antibodies and secondary antibodies used were listed in Chapter 2, Table 2.2 and Table 2.3.

4.2.2 Imaging

Fluorescence images of the dissociated cells used to test PAR3 distribution were taken using the Zeiss LSM800 confocal microscope with Airy Scan.

Fluorescence images of the dissociated cells used to test the AIS structures and measurements of intensity profiles were taken using the Andor Revolution XDi Spinning disk confocal microscope.

4.2.3 Measurement of PAR3 distribution

Dissociated prethalamic neurons cultured for 3DIV were fixed and stained with antibodies for PAR3, GFP for whole-cell morphology and DAPI for counterstaining of the nucleus (Figure 4.2A), in order to measure the amount of PAR3 and compare its distribution within the cytoplasm of the control and Pax6-null prethalamic neurons. With such staining, I first masked out the cytoplasmic volume of each neuron using signals from the GFP channel with IMARIS software (Bitplane, version 9.1.2). To elaborate, I first utilised the surface function of IMARIS to create a new GFP channel (Figure 4.2B). To do so, I manually adjusted the signal intensity threshold based on the specific situation of each neuron so that IMARIS was able to detect the space where the GFP signal is above that set threshold. This threshold was determined by fitting and adjusting different threshold values so that the GFP-positive space IMARIS detected optimally matched the actual cytoplasmic volume and included almost all the neurites and cytoplasmic protrusions. Places where their GFP signals were above this threshold but resided outside of the cytoplasm were manually deleted. In this way, I was able to create a new GFP channel, which only included and highly resembled the entire cytoplasm of the neurons (Figure 4.2B). Then I created a new PAR3 channel using this new GFP channel as the template of the cytoplasmic volume of that neuron to exclude any Par3 staining outside of the cytoplasm (Figure 4.2C). With this new PAR3 channel, I was then able to find out the value of the highest intensity of PAR3 expression within the cytoplasm. I then set different thresholds for IMARIS to detect the cytoplasmic volumes in which the PAR3 intensities were above 75%, 50%, 25%, 20% and 10% of its own highest intensity value (Figure 4.2D_1-D_5). This allowed me to quantify the cytoplasmic volume that had higher expression levels of PAR3 at each of these thresholds, and also visualise the distribution of different intensities of PAR3 within the cytoplasm. By comparing the values of these volumes between the control and Pax6-null prethalamic neurons, I was then able to determine if the expression level and distribution of PAR3 showed any difference between genotypes.

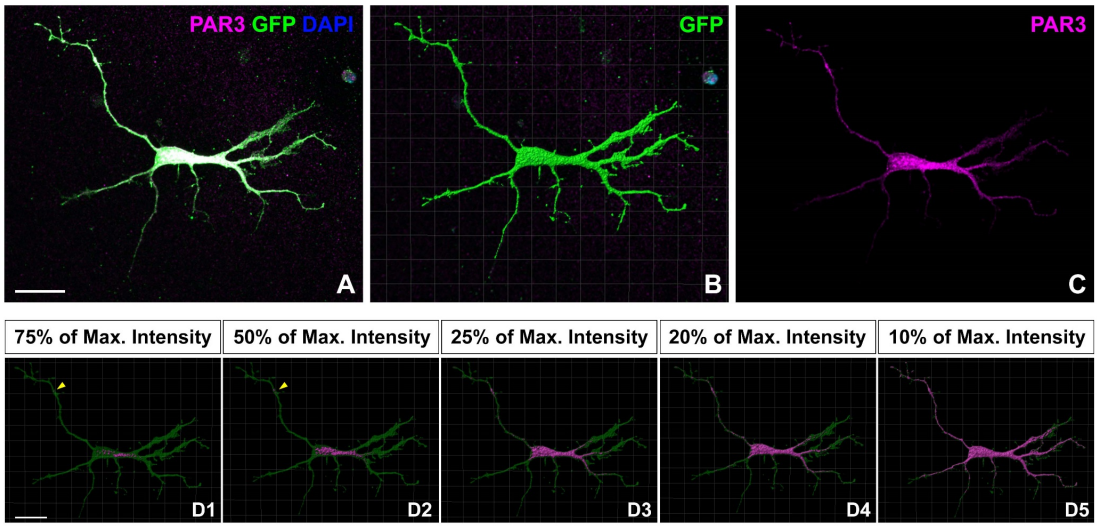

Figure 4.2 Setting the different intensity thresholds to detect PAR3 distribution within the cytoplasm of the prethalamic neurons. (A) Prethalamic neurons cultured for 3DIV were stained with antibodies detecting PAR3, GFP and DAPI for counterstaining of the nucleus. **(B)** A new GFP channel was created for each neuron by fitting the detection threshold so that the GFP-positive space IMARIS detected optimally matched the actual cytoplasmic volume and included almost all the neurites and cytoplasmic protrusions. **(C)** A new PAR3 channel was created by excluding any PAR3 staining outside the new GFP channel. By doing this, we obtained a new PAR3 channel, which only included the cytoplasmic PAR3. **(D_1-D_5)** PAR3-positive cytoplasmic volume detected when the threshold was set at 75%, 50% 25% 20% and 10% of the maximum intensity of the PAR3 channel respectively. Scale bar: 10μm for all images.

4.2.4 Measurement of the intensity profile of the axon initial segment marked by either AnkG or sodium channels

The axon initial segment of a prethalamic neuron was marked by a segment of concentrated expression of either AnkG or voltage-gated Na+ channels at the proximal part of a neurite. The neurite bearing such AnkG or sodium channel staining would then be recognised as the axon, regardless of whether the position of the AIS is somatic or dendritic (Figure 4.3A).

The intensity profiles of the axon initial segments were measured by tracing down the axons of the prethalamic neurons using the freehand line tool in Fiji-ImageJ. The tracing would start at the edge of the soma (Figure 4.3B, arrowhead) and follow the track of the axon for at least 80μm (Figure 4.3B, yellow line). If the AIS is dendritic, i.e. the position of the AIS is on a branch of the axon, tracing of the AIS intensity profile would then follow that specific branch instead of the stem of the axon as we did for measuring the length of longest neurite in Chapter 3. All the AISs being measured this way were within the 80μm length limit. Fiji was then able to measure the intensity of expressions of either AnkG or sodium channels at each pixel along the line drawn by the freehand line tool when tracing down the axon. The intensity profile of the AIS of each prethalamic neuron was thus created by corresponding the intensity of AnkG or sodium channels with the distance from the soma (Figure 4.3C).

Three independent experiments using embryos from three litters were performed (n=3). Within each litter, the prethalamus from one embryo of the control genotype and the prethalamus from one embryo of the Pax6-null genotype were processed with dissociated cell culture. Neurons were cultured for 5 days, 7 days and 9 days in vitro. 30 neurons from each embryo of control or Pax6-null genotype, at each time point, were measured. The intensity profiles were created by plotting the intensity of each pixel (Y-axis) along the line traced by the freehand line tool, against the distance of that pixel from the soma (X-axis). 80μm was set as the limit for the distance from soma as all the

neurons measured have their AISs located within this distance. The representing line for the intensity profile at each time point for each genotype was the averaged intensity profiles of all neurons from three litters (90 neurons). The error bars represent 95% confidence interval.

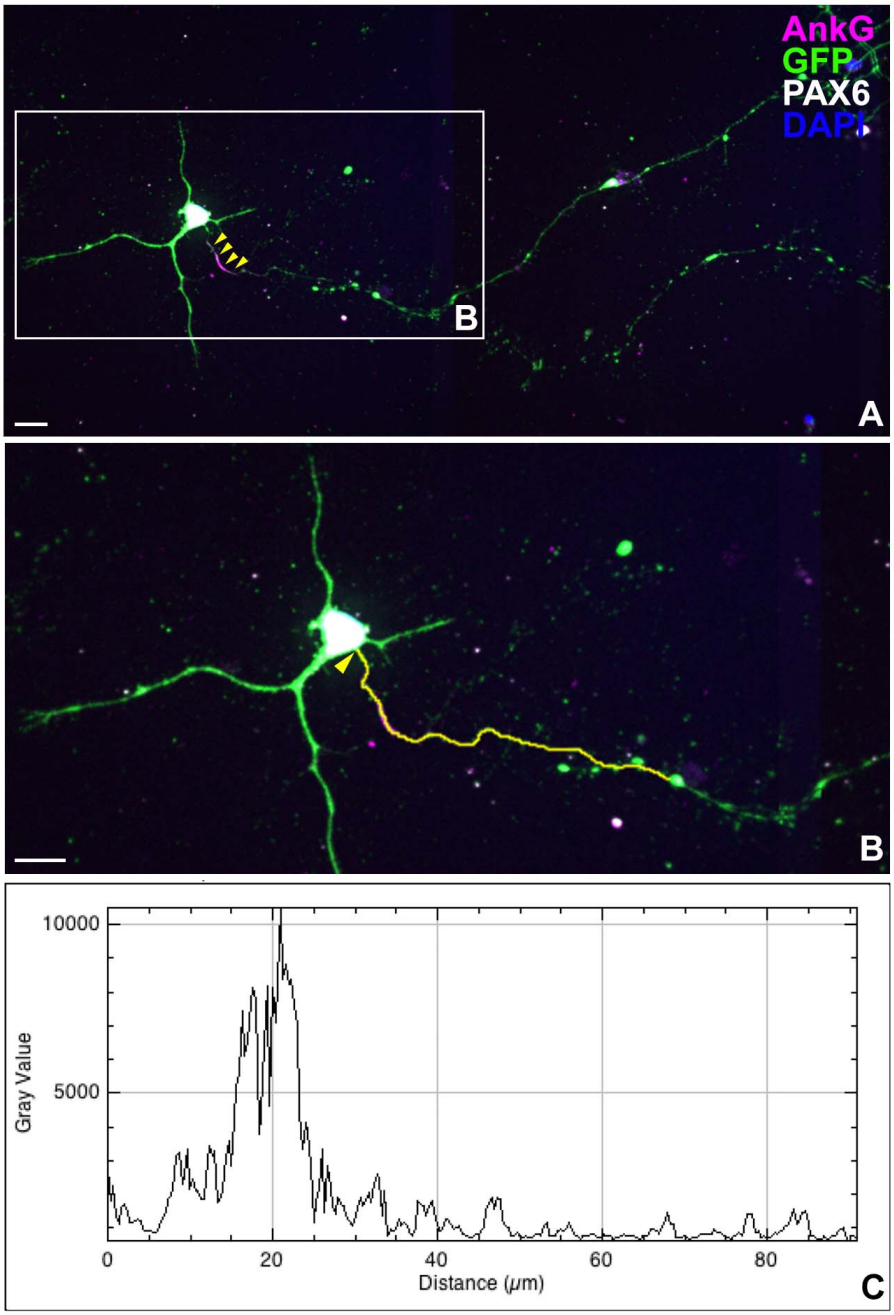

Figure 4.3 How intensity profiles of AIS, marked by either AnkG or voltage-gated Na+ channels staining, are generated. (A) A Pax6-null prethalamic neuron cultured for 9DIV and stained for AnkG, GFP, PAX6 and DAPI was used as an example. The axon is indicated by the presence of the AIS, which was shown by a clear concentrated distribution of AnkG in this case (the magenta segment, yellow arrowheads). **(B)** Zoomed in view of (A). Intensity profiles were measured by tracing down the axon using the free-hand line tool in Fiji-ImgeJ. The start point of every tracing was at the edge of the soma where the axon (or the stem of a dendrite, if the AIS is on a dendritic branch) initiated (yellow arrowhead). The tracing will follow the axon for at least 80μm. **(C)** The intensity profile generated by Fiji-ImageJ. After tracing down the axon, Fiji-ImageJ can read out the intensity of each pixel on the axon that overlapped with yellow line that was drawn and generate a scatter plot with 2D-line with distance from soma (μm) as the X-axis and intensity of the pixels at the Y-axis. Fiji-ImageJ call also generate an excel file of such readings, which were used for further analysis. Scale bar for all images: 10 μm.

4.2.5 Electrophysiology recording

4.2.5.1 Preparation of cells for electrophysiology recording

Dissociated prethalamic neurons cultured for 7 DIV were prepared in the same way as described in Chapter 3. After being retrieved from the incubator, the coverslips containing the cultured prethalamic neurons were placed directed into the external solutions for further electrophysiological recording.

4.2.5.2 External and internal solutions

All the chemicals were purchased from Sigma-Aldrich Company Ltd.

External

Table 4.1. External solution composition (in mM)

NaCl	150
KCl	2.8
HEPES	10
CaCl2	2
MgCl2	1
Glucose	10

The pH of the solution was set to 7.3 by addition of 1M NaOH. The solution was kept at room temperature during electrophysiology recording.

Internal

Table 4.2. Internal solution composition (in mM)

K-gluconate	130
Glucose	4
HEPES	10
EGTA	0.1

CaCl2	0.025
Sucrose	20

The pH of the solution was set to 7.2 by addition of 1M KOH, and the osmolarity was adjusted to around 300 mOsm.L-1 by addition of sucrose. The solution was kept at room temperature during electrophysiology recording.

4.2.5.3 Stimulation programmes

Three protocols were applied to the cultured prethalamic neurons sequentially.

In the first protocol, I switched the amplifier to no current input (I=0) for 30 seconds to record the resting membrane potential of these neurons.

In the second protocol, I applied current steps to the prethalamic neurons for 28 cycles, where each cycle lasts for 1400ms. Within these 1400ms, the first 100ms the cells were clamped at -70mV with no current input. In the first cycle, within the next 1000ms, a current input of -30pA was applied. Then the current input was again returned to 0, and the neurons were clamped and stabilised at -70mV for the next 300ms. For the following cycles, the current inputs in the 1000ms were increased 10pA per cycle, while the conditions in the first 100ms and the last 300ms stayed the same (Figure 4.4A).

In the third protocol, the neurons were clamped at -70mV for 100ms with no current input. Then, a hyperpolarising current pulse of -70pA was applied to the neurons for 500ms. After that, such current was withdrawn, and the neurons were clamped at -70mV for another 200ms. Each repeat was composed of these three consecutive steps, and 20 repeats were applied to each neuron being measured (Figure 4.4B).

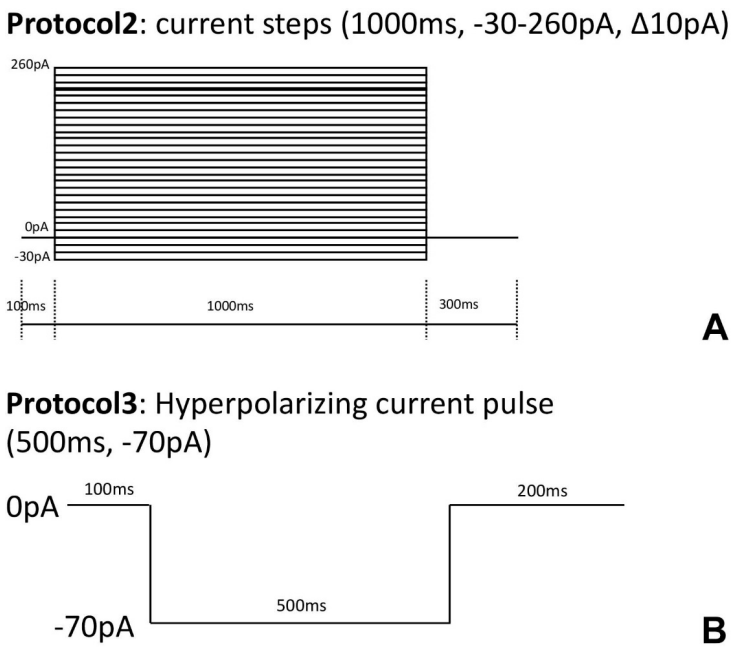

Figure 4.4 Schematic representation of stimulation protocols. (A) Details of the cycles of the current steps. **(B)** Details of each repeat of the current pulse.

4.2.6 Statistics

4.2.6.1 PAR3 intensity and distribution

Three independent experiments were performed using embryos from three litters (n=3). The dissociated prethalamic neurons from embryos of these three litters were cultured for 3 days. For each litter, 10 neurons randomly selected from the control genotype and 10 neurons from the Pax6-null genotype were measured. For each neuron, I measured the total cytoplasmic volume and the cytoplasmic volumes that the PAR3 expressions within were above 75%, 50%, 25%, 20% and 10% of the maximum PAR3 intensity. Therefore, there were 10 data sets to be analysed- cytoplasmic volumes that PAR3 expressions were above 75%, 50%, 25%, 20% and 10% of its maximum intensity (PAR3 volume at different percentage threshold); and the ratio of such cytoplasmic volume against the total cytoplasmic volume (PAR3 volume at different percentage threshold /total cytoplasm volume).

These data sets consisted of two fixed effects- genotype and percentage. Litter and cell are nested random effects, whereas PAR3 volume at different percentage threshold and PAR3 volume at different percentage threshold /total cytoplasm volume are output variables to be tested based on effects.

As the data sets of PAR3 volume at different percentage threshold and PAR3 volume at different percentage threshold /total cytoplasm volume consisted of continuous numerical data, they were first tested for best distribution fit using Quantile-Quantile plots. As shown in Figure 4.5, both data sets didn't exactly fit any of the standard distributions but seemed to fit normal distribution well enough.

We then processed these 10 data sets for mixed-effect models for statistical analysis. From there, type III ANOVA tests were applied to test which factors, and which interactions affect the data. If the type III ANOVA leads to a conclusion that there is a significance of variance introduced by factors

(effects), we then considered the pair-wise comparisons (Tukey comparison) and further investigate which of the means are different. Statistics for mixed-model were performed by Zrinko Kozić.

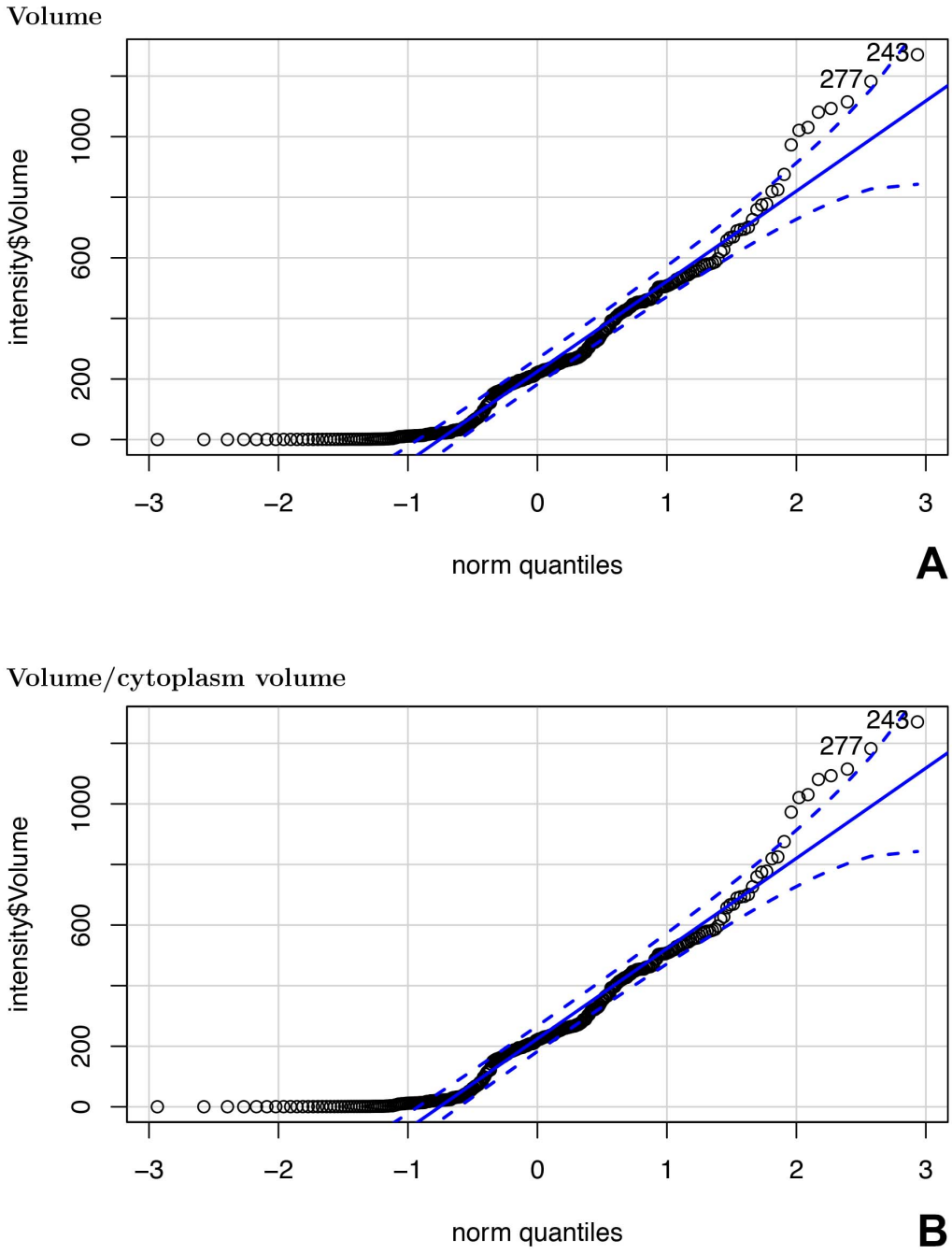

Figure 4.5 Data points of PAR3 volume at different percentage thresholds. **(A)** and PAR3 volume at different percentage thresholds /total cytoplasm volume **(B)** fitted quite well with normal distribution.

4.2.6.2 Electrophysiological data analysis

Analysis of electrophysiology results was carried out with a MATLAB (Version R2018b, The MathWorks, Inc.) plug-in programme developed and kindly provided by Dr Adam Jackson. With this programme, from protocol 1 and protocol 2, I was able to calculate the resting membrane potentials and rheobases in the neurons I patched.

One neuron per genotype per litter was subjected for whole-cell patch clamp recording. Neurons from three litters of embryos were patched (n=3). Paired student t-test was performed to test if resting membrane potentials and rheobases in the prethalamic neurons differ significantly between the control and Pax6-null genotype.

4.3 Results

4.3.1 Expressions of components of the PAR3/6 complex and the axon initial segment were significantly upregulated in the prethalamus when Pax6 was lost.

To have an idea of whether and how establishment and maintenance of neuronal polarity might have changed in the absence of Pax6, I first cross-referenced with literature that identified the components of the PAR3/6 complex and AIS and compared that with the list of significantly dysregulated genes in our RNAseq data. Interestingly, the results showed that most of the component genes of the PAR3/6 complex and AIS showed significantly upregulated expressions in the prethalamus when Pax6 is lost.

For example, Par-3 Family Cell Polarity Regulator Beta (Pard3b), the paralog B of the mammalian Par3 gene, was upregulated by a log2-fold change (LFC) of 1.03 in the prethalamus when Pax6 is lost. PARD3B can interact with PARD6B to mediate specification of cell polarity. Other known components of PAR3/6 complex, such as aPKC- PKCζ, Tiam1, the GTP activating protein (GAP) p190RhoGAP and the ubiquitin ligase Smurf1 all showed different levels of upregulation. Additionally, genes encoding for proteins that have shown to interact with the PAR3/6 complex and direct its localised distribution at the nascent axon tip, such as the kinesin motor protein KIF3A and scaffold protein APC, were also upregulated in the RNA seq data. The only known PAR3/6 complex components whose gene expression level was significantly downregulated were STEF (LFC -0.61) and the transforming growth factor receptor 1 (TGFβR1) (LFC -0.40) (Table 4.3).

Expression of various component genes of the AIS also showed significant upregulation in the RNA seq data. These include genes encoding for the cytoskeletal proteins, voltage-gated Na+ channels and K+ channels. AnkG, the master regulator gene for AIS assembly, was upregulated by a LFC of 2.01 in the prethalamus when Pax6 is lost. The expression of βIV-Spectrin, which

is the cytoskeletal protein that links AnkG to the actin cytoskeleton and plasma membrane, showed an upregulation of 1.73 LFC. Expression levels of other β-Spectrins were also upregulated. Voltage-gated Na+ channels consist of the core α subunits, which conduct Na+ passage in a voltage-dependent manner, and β subunits, which associate with α subunits and regulate channel gating and linkage with the cytoskeleton or the extracellular matrix. Genes encoding for both the α and β subunits showed upregulated expression in the prethalamus when Pax6 is lost (Table 4.4). On the other hand, voltage-gated K+ channels also consist of the α subunits, which form the actual conductance pore, and β subunits that associate with α subunits and modulate the activities of K+ channels. The majority of α subunits and all β subunits of K+ channels that showed dysregulated expressions were upregulated. As voltage-gated K+ channels have not been studied in this thesis, the exact voltage-gated K+ channel subunit genes were not included in Table 4.4 for simplicity.

The above information indicated that the protein levels of these PAR3/6 complex and AIS component genes might have also increased in the Pax6-null prethalamic neurons. However, in order for the PAR3/6 complex and the AIS to initiate the establishment and maintenance of neuronal polarity, the proteins of all these component genes need to be assembled into specific functional structures that take specific locations within the neurons. Therefore, with fluorescent immunohistochemistry, I further stained for the PAR3, AnkG and voltage-gated Na+ channels to find out if their distributions and expression levels differed in the prethalamic neurons in the absence of Pax6.

PAR3/6 complex components		
Gene name	Base mean	Log2-fold change
aPKC- PKC λ	TBC	-
aPKC- PKC ζ	1718.2	0.44
CDC42	TBC	-
KIF3A	2586.5	0.53
Tiam1	464.7	0.80
Tiam2 (STEF)		-0.61
PTEN	TBC	-
p190RhoGAP	6558.6	0.72
LGL	TBC	-
inscuteable	TBC	-
Smurf1	2022.0	0.61
Smurf2	TBC	-
TGFβR1	112.6	-0.40
Pard3b	111.7	1.03
APC	3736.3	0.79

Table 4.3 Log2-fold changes of genes encoding for proteins reported to exist in the PAR3/6 complex.

Axon initial segment component		
Gene name	Base mean	Log2-fold change
Cytoskeletal protein		
Ank3	1323.66	2.01
Sptbn1	3405.69	1.37
Sptbn4	149.05	1.72
Sptb	57.92	1.65
Voltage-gated Sodium channels		
Scn1a	73.16	0.92
Scn2b	156.66	0.67
Scn3a	1764.88	0.45
Scn3b	3089.21	0.81

Table 4.4 Log2-fold changes of axon initial segment component genes.

4.3.2 PAR3 distribution in the cytoplasm of the prethalamic neurons was not significantly affected when Pax6 is lost

I used the PAR3 protein as the marker for the PAR3/6 complex, and with fluorescent immunohistochemistry, I was able to reveal the distribution of PAR3 proteins within the developing prethalamic neurons in vitro. As shown in Figure 4.6A-D, PAR3 was present in both the soma and neurites. However, the expression level of PAR3, unlike what has been emphasised by previous studies, showed the highest expression levels within the soma (Figure 4.6C-D). This was further confirmed when I tried to measure the cytoplasmic volume being occupied by PAR3, whose expression level was above a certain percentage of the maximum intensity of the PAR3 channel. As shown in Figure 4.6E-F, when the threshold was set at 75% of the maximum intensity of the PAR3 channel, the cytoplasmic volumes being occupied by PAR3 above this threshold were always located within the soma. Outside the soma, some neurons also showed PAR3-positive cytoplasmic volumes only in their most extended neurites (Figure 4.6E1, 4.6F1, yellow arrowheads). However, the locations of these PAR3-positive cytoplasmic volumes were not always at the tip of the longest neurite. This highly concentrated presence of PAR3/6 complex localised only in the longest neurite was in concordance with what people have described in other systems (184,185). When the threshold was set at 50% of the maximum intensity of the PAR3 channel, the cytoplasmic volumes being occupied by PAR3 above this threshold increased within the soma, as well as propagated further towards the distal part of the longest neurite (Figure 4.6E2, 4.6F2, yellow arrowheads). Interestingly, PAR3-positive volume started to appear in the proximal part of other neurites (Figure 4.6E2, 4.6F2, grey arrowheads) at this threshold. When the threshold was set at 25% of the maximum intensity of the PAR3 channel, the PAR3-positive volumes reached the tip of the longest neurites (Figure 4.6E3, 4.6F3, yellow arrowheads), while PAR3-positive volumes in the other neurites further propagate towards the neurite tips (Figure 4.6E3, 4.6F3, grey arrowheads). Additionally, PAR3-positive volumes started to appear in the rest of the neurites (Figure 4.6E3, 4.6F3, blue arrowheads). When the threshold was set

at 20% of the maximum intensity of the PAR3 channel, PAR3-positive volumes occupied more cytoplasmic space and propagated further towards the neurite tips (Figure 4.6E4, 4.6F4, grey and blue arrowheads). When the threshold was set at 10% of the maximum intensity of the PAR3 channel, PAR3-positive volumes could be seen in almost all the tips of neurites and protrusions (Figure 4.6E5, 4.6F5 orange arrowheads).

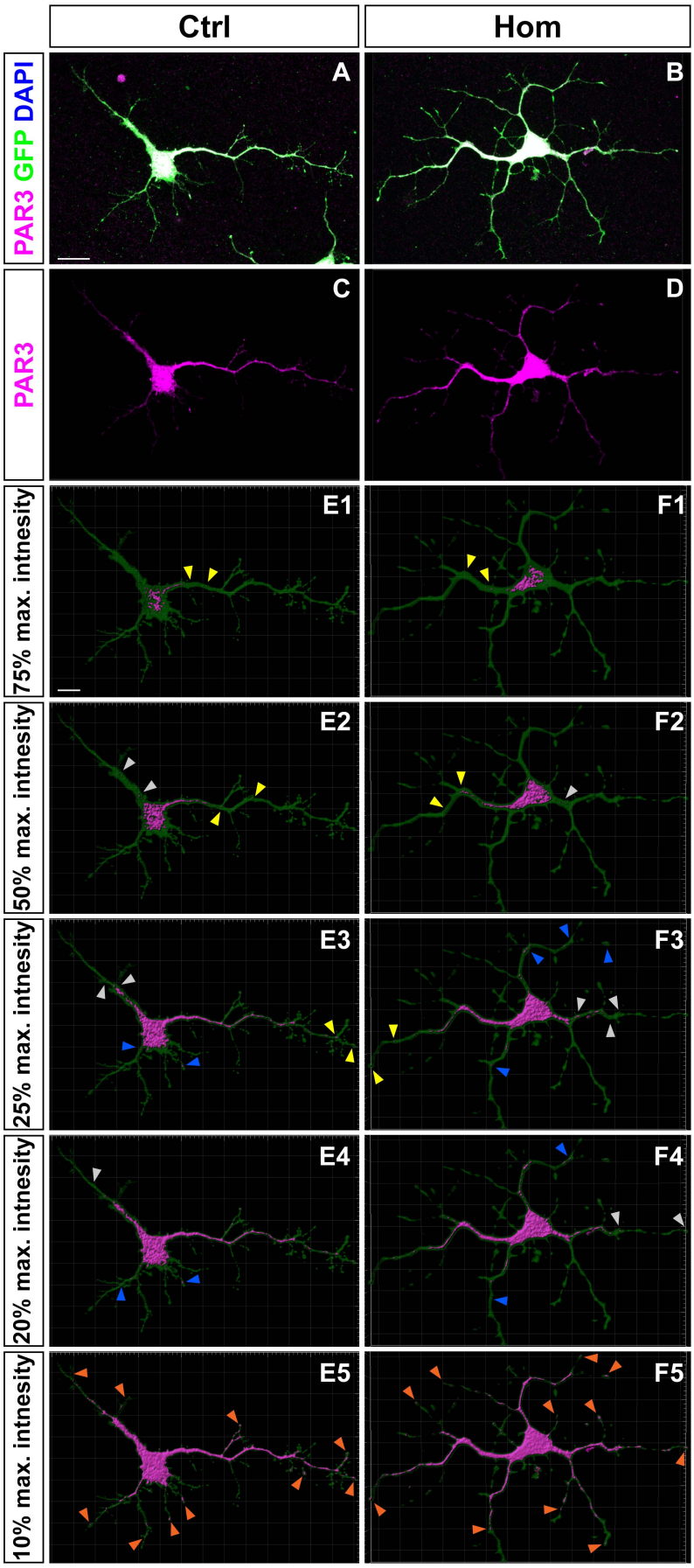
Ctrl
Hom
PAR3 GFP DAPI
A
B
PAR3
C
D
75% max. intnesity
E1
F1
50% max. intnesity
E2
F2
25% max. intnesity
E3
F3
20% max. intnesity
E4
F4
10% max. intnesity
E5
F5

Figure 4.6 Distribution of PAR3 proteins within the developing prethalamic neurons in vitro. (A, B) Prethalamic neurons from the control (A) and Pax6 mutant (B) embryos were cultured for 3DIV and stained for PAR3, GFP and DAPI. **(C, D)** PAR3 expression within the cytoplasm of the neurons. **(E1-F1)** PAR3 expression within the cytoplasm when the intensity threshold was set at 75% of the maximum intensity of the PAR3 channel. The majority of the PAR3 volumes were distributed within the soma. However, PAR3 volumes were also found in the stem of the longest neurites (yellow arrowheads). **(E2-F2)** PAR3 expression within the cytoplasm when the intensity threshold was set at 50% of the maximum intensity of the PAR3 channel. More PAR3 volumes were detected in the soma, the stem of the longest neurites (yellow arrowheads), as well as in other neurites (grey arrowheads). **(E3-F3)** PAR3 expression within the cytoplasm when the intensity threshold was set at 25% of the maximum intensity of the PAR3 channel. PAR3 volumes within the cytoplasm continued to increase. PAR3 volumes could be found at the tip of the longest neurites (yellow arrowheads) and other neurites (grey and blue arrowheads). **(E4-F4)** PAR3 expression within the cytoplasm when the intensity threshold was set at 20% of the maximum intensity of the PAR3 channel. **(E5-F5)** PAR3 expression within the cytoplasm when the intensity threshold was set at 10% of the maximum intensity of the PAR3 channel. PAR3 volumes had filled up the cytoplasm and could be found at almost all the tip of the neurites and protrusions (orange arrowheads). Scale bars: A-D, 15μm, E1-F5, 10μm.

To find out if the distribution of PAR3 as described above changed significantly due to the loss of Pax6, I compared the PAR3-positive cytoplasmic volumes at different thresholds between the control and Pax6-null prethalamic neurons using the mixed-effect model.

As the data fitted quite well with a normal distribution, we further processed the five data sets of PAR3 volume at different percentage threshold with Type III ANOVA, in order to find out if interactions between any of the effects (fixed effects- genotype and percentage; random effects- litter and cell) were significant. Overall, there is a significant effect of percentage, i.e. that the differences of PAR3 volumes at different thresholds were significant regardless of genotype. The interaction between genotype and PAR3 volume at different percentage threshold was not significant, meaning that the effect of genotype did not change when the thresholds were set at any of the different percentages (Figure 4.7A-D). This can be shown with pairwise comparisons which will all show insignificant effect, except for the PAR3 volume at 10% percentage threshold. When the threshold was set at this percentage, the PAR3-positive volume was significantly higher in control prethalamic neurons (Figure 4.7E).

As the functions of the PAR3/6 complex are highly dependent on its localised distribution, in addition to the absolute PAR3 volume at different percentage threshold, it was also worth finding out whether the ratio of PAR3 volume at different percentage threshold against the total cytoplasmic volumes showed any significant difference in the absence of Pax6. To elaborate, if the absolute PAR3 volumes at a particular threshold of two neurons (neuron A and neuron B) are the same, but neuron A has a smaller total cytoplasmic volume, then the PAR3 volume in A will occupy a relatively larger cytoplasmic space. This might affect the accessibility of resources to the available PAR3/6 complex and hence further impact on how the neurons respond to intrinsic and extrinsic signals during the establishment of neuronal polarity. For this aim, I calculated the ratio of PAR3 volume at different percentage threshold against total

cytoplasmic volume. We then processed the resulting data sets with Type I ANOVA. As shown in Figure 4.8, the interaction between genotype and PAR3 volume/ total cytoplasmic volume was not significant at the threshold set at any percentage. Nevertheless, the effect of percentage was still significant, i.e. PAR3 volume/ total cytoplasmic volume differed significantly across thresholds set at different percentages, regardless of genotype. Interestingly, Pax6-null prethalamic neurons seemed to have smaller cytoplasmic volumes. The delayed neuronal morphogenesis that I discovered in Chapter3, that Pax6-null prethalamic neurons at this stage showed a shorter length of longest neurite and the total length of neurites, might be the underlying reason.

The above results indicated that, although the RNAseq data showed upregulated expressions of component genes of the PAR3/6 complex, the distribution of the PAR3/6 complex, marked by PAR3, was not affected in the prethalamic neurons when Pax6 is lost. From here, I can only conclude that the establishment of neuronal polarity, marked by the distribution of PAR3, seemed to not have been affected in the Pax6-null prethalamic neurons.

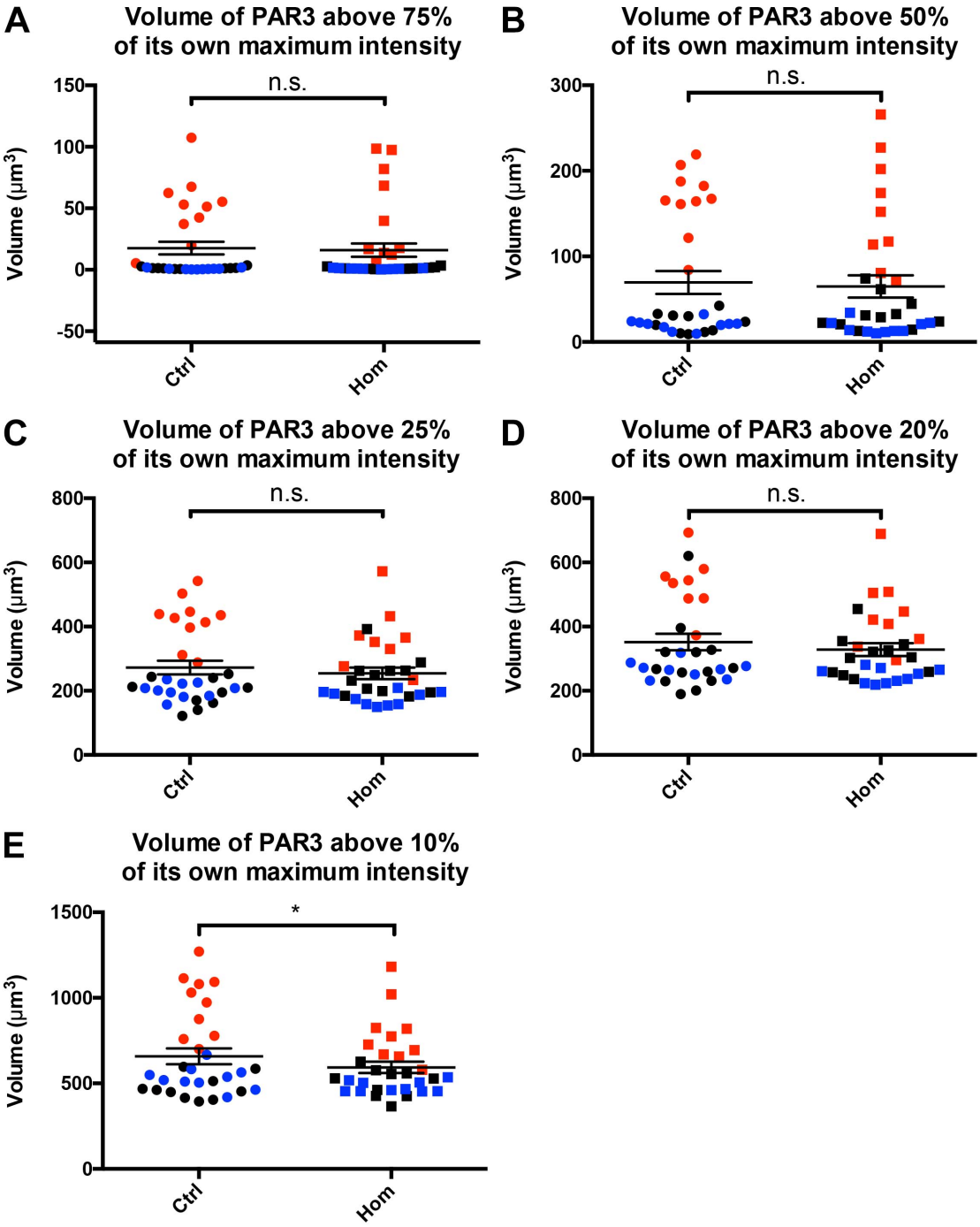

Figure 4.7 PAR3 volume at different percentage thresholds did not differ significantly between the control and Pax6-null prethalamic neurons. (A-D) When the thresholds were set at 75%, 50%, 25% and 20% of the maximum intensity of the PAR3 channel, the PAR3 volume within the cytoplasm of neurons did not differed between the control and Pax6-null genotype. **(E)** When the thresholds were set at 10% of the maximum intensity of the PAR3 channel, the PAR3 volume within the cytoplasm of control prethalamic neurons was significantly higher than that in the Pax6-null prethalamic neurons. The error bar represented the value of standard error of the mean (SEM). PAR3 volume at different percentage thresholds from 10 neurons from the control and Pax6-mutant genotypes were measured. Three litters in total (n=3). Each dot (data point) represented the value of PAR3 volume from each neuron at a specific threshold. The data points of the neurons from the

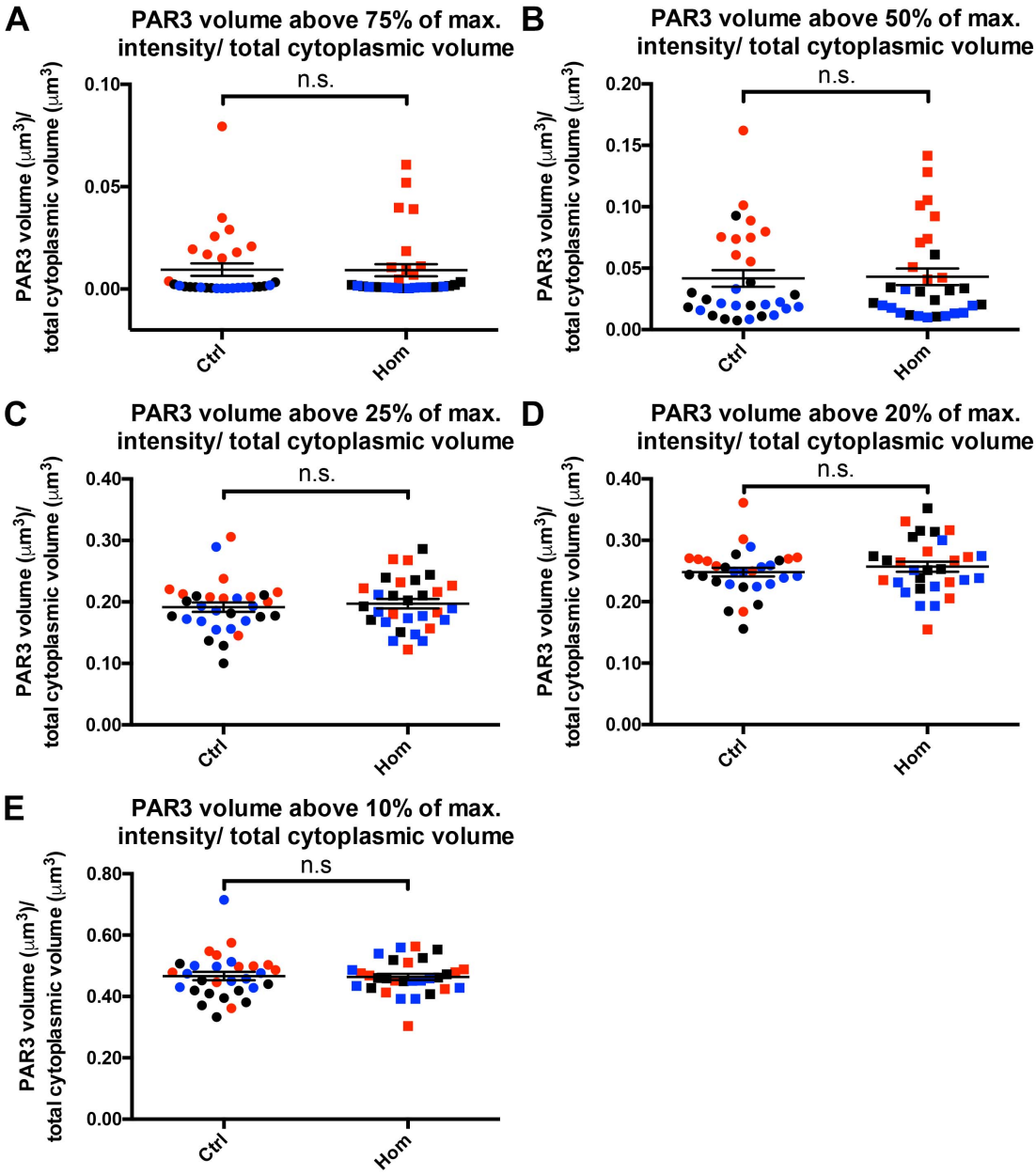

Figure 4.8 PAR3 volume at different percentage thresholds/ total cytoplasmic volume did not differ significantly between the control and Pax6-null prethalamic neurons. When the thresholds were set at 75% (A), 50% (B), 25% (C), 20% (D) and 10% (E) of the maximum intensity of the PAR3 channel, the cytoplasmic PAR3 volume/ total cytoplasmic volume did not differed between the control and Pax6-null genotype. The error bar represented the value of standard error of the mean (SEM). PAR3 volume at different percentage thresholds, as well as the total cytoplasmic volumes from 10 neurons from the control and Pax6-mutant genotypes were measured. Three litters in total (n=3). Each dot (data point) represented the value of PAR3 volume/ total cytoplasmic volume from each neuron at a specific threshold. The data points of the neurons from the same litter were marked with the same colour. Data were analysed with mixed-model. *: $P<0.05$.

4.3.3 Pax6-null prethalamic neurons showed altered AIS structures with increased expressions of AnkG and voltage-gated Na+ channels

I chose the axon initial segment (AIS) as the primary indicator of maintenance of neuronal polarity in the prethalamic neurons. AnkG and voltage-gated Na+ channels were used to mark the AIS due to their highly concentrated localisation within this structure. As the AIS is formed at the later stages of neuronal morphogenesis, and it is also a feature of mature neurons, I performed fluorescent immunohistochemistry to detect the distribution of AnkG and voltage-gated Na+ channels in the prethalamic neurons cultured for 5, 7 and 9 days. The antibody I used to detect voltage-gated Na+ channels recognises all the α subunits of the voltage-gated Na+ channels. Therefore, the readout of this staining would be the sum of all the α subunits expressed within the neurons. This way, I was able to find out whether the prethalamic neurons are able to form AISs, whether the number of AISs per neuron, the structure and components of the AIS, and the rate of AIS formation differed in any ways in the prethalamic neurons when Pax6 was lost.

Prethalamic neurons in culture were able to develop single AISs, which were marked by the signature localised expressions of AnkG and voltage-gated sodium channels at the proximal end of a neurite (Figure 4.9A, C, E and Figure 4.10A, C, E, magenta segments). The exact locations of the AISs varied among the prethalamic neurons- some neurons have their AIS located on a somatic neurite (axon), while others have their AIS located on a dendritic branch (compare the location of the magenta segments in Figure 4.10C, E). Previous studies in cultured hippocampal neurons suggested that AnkG acts as the master regulator of AIS formation and localised AnkG expression at the putative AIS region further facilitates localised distribution of voltage-gated Na+ and K+ channels (81,82). Therefore, localised expression of AnkG at the putative AIS should happen before localised expressions of voltage-gated Na+ channels. I found that this is exactly the case in cultured prethalamic neurons. At 5DIV, AnkG expression started to show localised distribution at the proximal end of neurites and its intensity profile exhibited a gentle rise, which then

plateaued and decreased with distance from the soma (Figure 4.9A, G, blue line). However, at 5 DIV, expressions of voltage-gated sodium channels did not show any localised distribution and its intensity only decreased with distance from the soma (Figure 4.10A, G, blue line). At 7DIV, AIS marked by AnkG showed more of a distinct peak in its intensity profile in comparison to 5DIV, indicating more AnkG localisation and the AISs being more mature at this stage (Figure 4.9C, H, blue line). At 7DIV, AIS marked by voltage-gated sodium channels showed a gentle peak in its intensity profile, indicating the recruitment and assembly of voltage-gated Na+ channels to the AIS region at this stage (Figure 4.10C, H, blue line). Interestingly, the locations of the AnkG and Na+ channels peaks seemed to be colocalising, as both peaks in the intensity profiles showed similar distances from the soma and similar widths (Figure 4.11C, D blue lines). At 9DIV, the AnkG intensity profile showed a decreased level of AnkG localisation at the AIS, although the position remained more or less the same as 5 and 7 DIV (Figure 4.9E, I, blue line). The localisation of Na+ channels at the AIS, however, showed a drastic decrease as the peak seen in 7 DIV in the Na+ channel intensity profile was dismissed at 9 DIV (Figure 4.10E, I, blue line).

When Pax6 is deleted, the prethalamic neurons were still able to develop and form AISs, as staining for AnkG and voltage-gated sodium channels showed clear concentrated localisation of both at the proximal end of neurites (Figure 4.9B, D, F and Figure 4.10B, D, F, magenta segments). The Pax6-null prethalamic neurons also displayed somatic or dendritic locations of AISs and these locations of AISs also varied among individual neurons (compare the locations of the magenta segments in Figure 4.9B and 4.9D). At 5 DIV, AnkG started to show localised distribution at the putative AIS region in the Pax6-null prethalamic neurons (Figure 4.9B, G, orange line). The location of the putative AIS overlapped with the putative AIS location in the control prethalamic neurons with AnkG staining. However, in the Pax6-null neurons, the length of the putative AIS seemed to be slightly longer (Figure 4.9G). Similar to the situation in the control neurons, at this stage of cell culture, voltage-gated Na+

channels have not yet displayed localised distribution either. However, the expression level of Na+ channels was higher in the putative axons of the Pax6-null prethalamic neurons (Figure 4.10B, G orange line). At 7 DIV, the intensity profiles of AnkG of Pax6-null neurons also showed more of a distinct peak in comparison to 5DIV, indicating that AIS in the mutant neurons were also being formed during this period of cell culture (Figure 4.9D, H, orange line). The highest intensity of AnkG in the AIS of the Pax6-null prethalamic neurons was comparable to that of the control neurons. However, the location of the AIS seemed to have shifted further away from the soma, whereas the length of the AIS seemed to be slightly shorter in the mutant neurons (Figure 4.9H). The intensity profile of Na+ channels at this stage also showed a clear peak, indicating that recruitment and assembly of voltage-gated Na+ channels were also taking place during this period of cell culture in the mutant neurons (Figure 4.10D, H, orange line). However, the intensity of Na+ channels was once again higher in the AIS region and axons of the Pax6-null prethalamic neurons (Figure 4.10H). Additionally, the location of AIS marked by AnkG and Na+ channels did not colocalise in the Pax6-null prethalamic neurons, indicating that the tethering of Na+ channels by AnkG might have been faulty in the absence of Pax6 (Figure 4.11C, D). At 9 DIV, the AIS region marked by AnkG was still further away from the soma in the mutant neurons. Additionally, the mutant neurons also showed a higher intensity of AnkG expression in the AIS (Figure 4.9F, I, orange line). Similarly, expression of Na+ channels also showed a drastic drop in the Pax6-null prethalamic neurons (Figure 4.10F, I, orange line).

These results indicate that loss of Pax6 did not affect the ability of the prethalamic neurons to form AISs. However, the locations of the AISs in the Pax6-null prethalamic neurons were further away from the soma and their lengths seemed slightly shorter in more mature neurons. Additionally, these AISs showed higher expressions of AnkG and voltage-gated Na+ channels, in concordance with our RNAseq data.

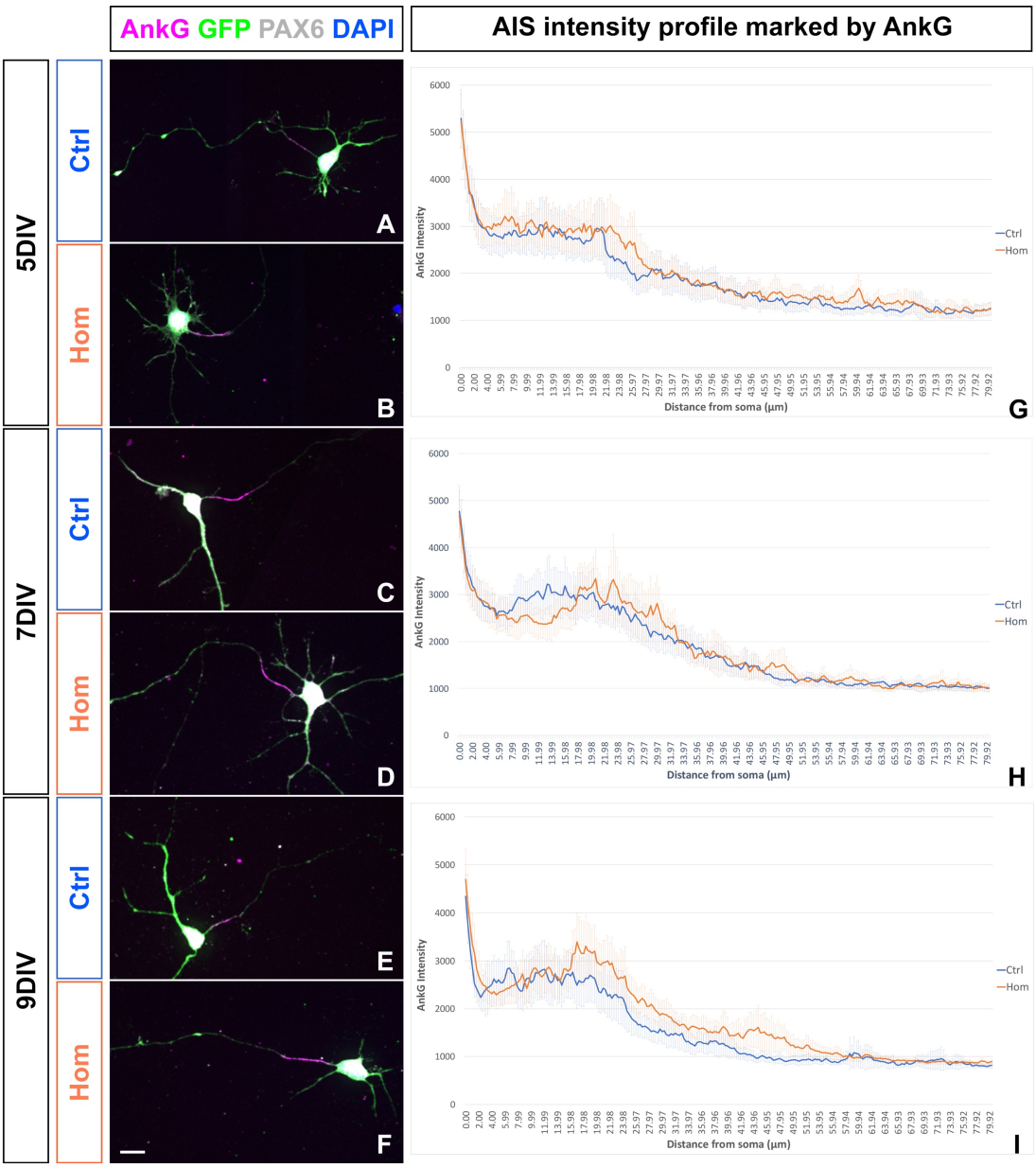

Figure 4.9 Development of AIS marked by AnkG expression through time in the cultured prethalamic neurons. Morphological representation of AIS marked by AnkG staining in the control (A, C, E) and Pax6-null (B, D, F) prethalamic neurons cultured for 5 DIV (A-B), 7DIV (C-D), 9 DIV (E-F). (G-I) The intensity profile of AIS marked by AnkG in prethalamic neurons cultured for 5 DIV (G), 7DIV (H) and 9DIV (I). 30 neurons per embryo per genotype were processed for intensity profile measurement. For each litter, one control embryo and one Pax6-null embryo was processed for dissociated cell culture to generate prethalamic neurons as above. Three litters in total (n=3). The blue and orange lines were the averaged intensity for the intensity profile of 90 neurons. The scale bars represented the 95% confidence interval. Scale bar for A-F: 10μm.

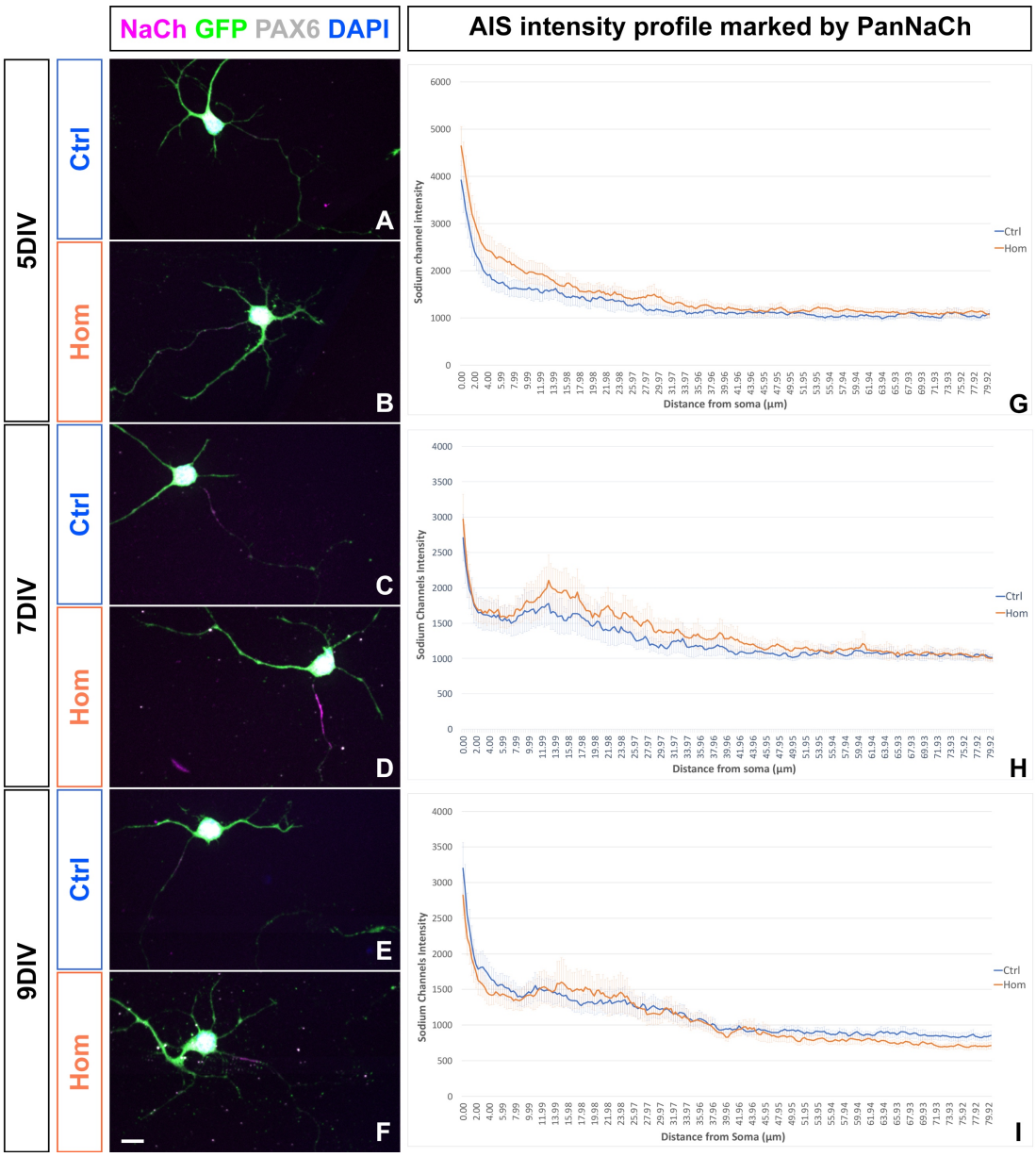

Figure 4.10 Development of AIS marked by voltage-gated Na+ channels expressions through time in the cultured prethalamic neurons. Morphological representation of AIS marked by voltage-gated Na+ channels staining in the control (A, C, E) and Pax6-null (B, D, F) prethalamic neurons cultured for 5 DIV (A-B), 7DIV (C-D), 9 DIV (E-F). (G-I) The intensity profile of AIS marked by voltage-gated Na+ channels in prethalamic neurons cultured for 5 DIV (G), 7DIV (H) and 9DIV (I). 30 neurons per embryo per genotype were processed for intensity profile measurement. For each litter, one control embryo and one Pax6-null embryo was processed for dissociated cell culture to generate prethalamic neurons as above. Three litters in total (n=3). The blue and orange lines were the averaged intensity for the intensity profile of 90 neurons. The scale bars represented the 95% confidence interval. Scale bar for A-F: 10μm.

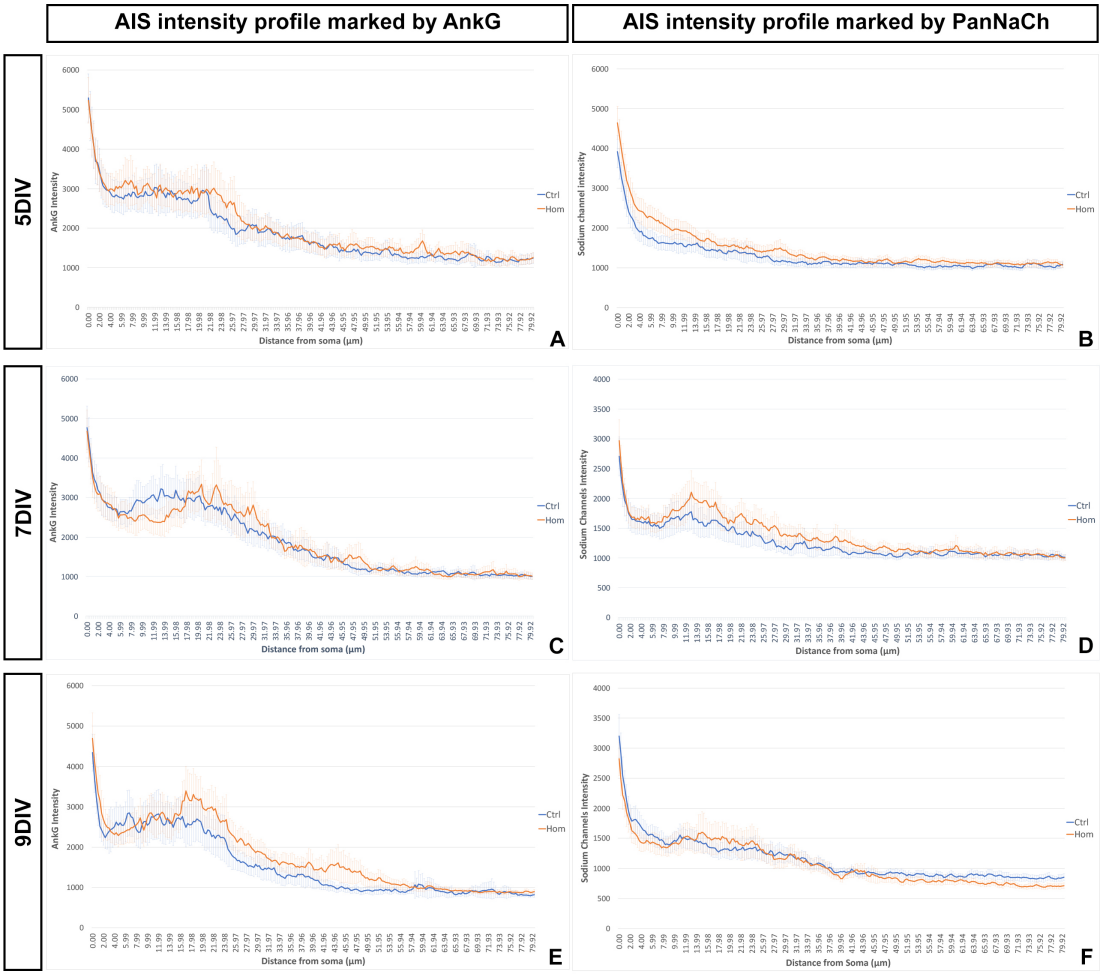

Figure 4.11 Comparison of AIS intensity profiles marked by AnkG or voltage-gated Na+ channels through time in the cultured prethalamic neurons. Intensity profile of prethalamic neurons at 5DIV (A-B), 7DIV (C-D), and 9DIV (E-F).

4.3.4 Prethalamic neurons are more excitable in the absence of Pax6

In addition to its ability to maintain neuronal polarity, the AIS is also where action potentials are being shaped and fired. Changes in the location, structure and components of the AIS have been linked to altered electrophysiological properties in other neurons in vivo and in vitro. To find out whether these changes in the AISs of the Pax6-null prethalamic neurons can affect how these neurons fire their action potentials, and further impact their functionality, I performed whole-cell patch clamp in cultured prethalamic neurons at 7DIV.

By switching the amplifier to no current input, I was able to record the resting membrane potential of the cultured prethalamic neurons. Previous studies have recorded the average resting membrane potential in neurons of the thalamic reticular nucleus in vivo to be around -57mV (104). As shown in Figure 4.12E, the resting membrane potentials in the prethalamic neurons did not show a significant difference between the control and Pax6-null genotypes. However, the average resting membrane potentials displayed by prethalamic neurons from both genotypes were around -30mV, which were much higher than what other people described in the TRN neurons in the postnatal brain in vivo.

By stimulating the neurons with increased current steps as described in protocol 2, I was able to find out if the cultured prethalamic neurons can fire action potentials and also what would the rheobases of these neurons be. Rheobase is defined as the minimum current amplitude to elicit at least one action potential. Therefore, rheobase reflects how excitable the neurons are. As shown in Figure 4.12A, B, prethalamic neurons from both genotypes were able to fire action potentials. As mentioned in the Introduction chapter, when TRN neurons fire in tonic mode, they normally display a train of action potentials (67). However, the cultured prethalamic neurons fire only one action potential once the rheobases were reached, regardless of genotype nor further increment of current amplitudes. Interestingly, Pax6-null prethalamic neurons displayed much lower rheobases in comparison to the control neurons (Figure

4.12F). Although paired Student t-test showed that such a difference was not significant with a P value of 0.0766, these results indicated that the prethalamic neurons might be more excitable when Pax6 is lost. Previous studies have reported that a longer AIS that is closer to the soma, with increased levels of AnkG and voltage-gated Na+ channels are associated with higher levels of excitability in various types of neurons (99,101,102). In the cultured Pax6-null prethalamic neurons, AIS structures were slightly shorter and further away from the soma. However, they displayed higher levels of expressions of AnkG and voltage-gated Na+ channels. How and whether such changes of the AISs might contribute to changes in the rheobases of Pax6-null prethalamic neurons deserve immediate further investigation.

To find out if the prethalamic neurons in culture can fire in the burst mode and whether the deletion of Pax6 can affect that, I applied a hyperpolarising current pulse to these neurons. If enough T-type low-threshold Ca2+ channels are present, I should be able to see rebound firing of action potentials at the offset of these hyperpolarising current pulses. Depending on the number and frequency of the action potentials being fired, I can then determine whether this prethalamic neuron is a tonic cell or a bursting cell. As shown in Figure 4.12C-D, no firing of action potentials was observed in all the three control neurons that were patched. However, one of the Pax6-null neurons was able to fire an action potential at the offset of the hyperpolarisation current pulse at the 18th repeat. Noted that this neuron did not fire more action potentials in the next 19th and 20th repeats. Due to the low numbers of neurons being recorded and inexperience with electrophysiology recording, immediate further repeats of this experiment are needed in order for us to draw any solid conclusions.

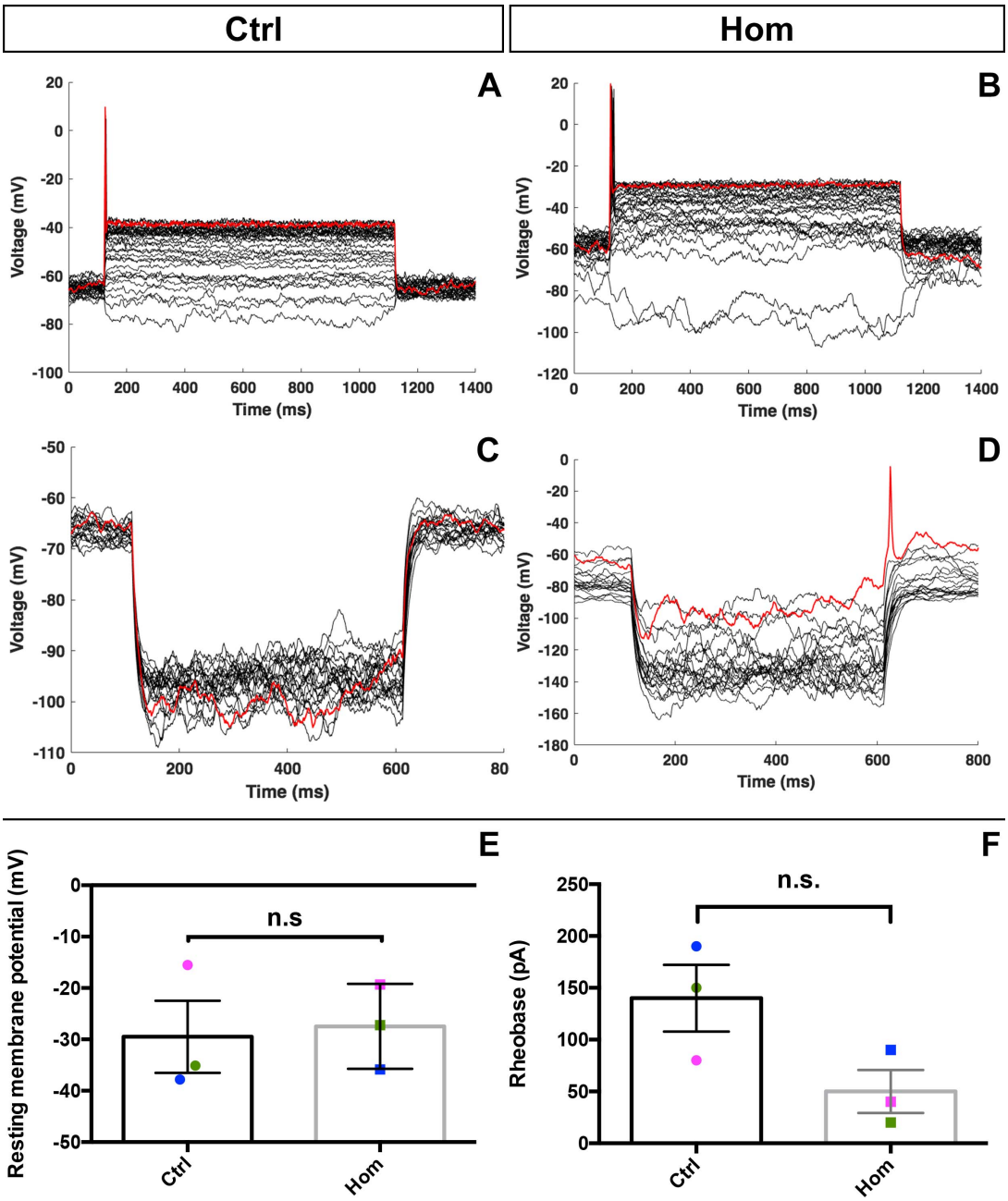

Figure 4.12 Analysis of electrophysiological properties of the prethalamic neurons cultured for 7DIV. Both the control (A) and Pax6-null (B) prethalamic neurons were able to fire action potentials. Noted that (A) and (B) showed the complete responses of a representative control (A) and Pax6-null (B) prethalamic under the stimulus from Protocol 2. The red line showed the first action potential fired in (A) and (B). (C-D) The complete responses of a control (C) and Pax6-null (D) prethalamic neuron to hyperpolarisation current pulses (Protocol 3). Noted that the red line in (C) and (D) highlighted the response of the neurons at the 18th sweep of the hyperpolarisation current pulses. Also noted that (D) might not be a representative as only one out of three for Pax6-null prethalamic neurons were able to a fire action potential at the offset of this hyperpolarising stimuli. One neuron per genotype per litter was subjected for whole-cell patch clamp recording. Neurons from three litters of embryos were patched (n=3). (E-F) Resting membrane potentials and rheobases recorded in these prethalamic neurons. Neurons the same litter were marked with the same colour. Paired student t-test.

4.4 Discussion

4.4.1 Comments on the PAR3 experiment

In this chapter, I recorded in detail the distribution of PAR3 proteins within the cytoplasm of prethalamic neurons by setting up different intensity thresholds. Interestingly, the results showed the highest intensity of PAR3 expression was in the soma and the proximal part of the most extended neurites. When the intensity thresholds were set at lower values, the PAR3-positive volumes started to propagate towards the tips of the longest neurites and appeared in the proximal part of other neurites. As PAR3 functions to direct polarised modification of neuronal morphology in an expression level-dependent manner, this consecutive appearance of PAR3-positive volumes in different areas of the neurons as the set intensity threshold dropped can also serve as an indicator of the hierarchy of the neurites. In studies where pinpointing the identities of the neurites were necessary, researchers usually utilise axon and dendrite markers. These markers are usually linked to the specialised cellular, membranous and cytoskeletal structures axons and dendrites display, which become fully developed only after the establishment of neuronal polarity. For example, in my cultured primary prethalamic neurons, the frequently used axonal marker Tau and the dendritic marker MAP2 showed clear regional segregation of expression within the neurons after 5 DIV. However, the morphological distinctions among neurites in the cultured prethalamic neurons started to appear after 1DIV. Therefore, there is a gap in the neuronal morphogenesis timeline, where many of the frequently used morphological markers could not be applied. Detailing the PAR3 distribution at different intensity thresholds as above might be able to fill this gap, and serve as indicators of the putative axon, the primary dendrite, the secondary dendrite and so on.

One puzzling phenomenon in my PAR3 analysis was that the PAR3-positive cytoplasmic volumes were much higher in one of the litters. This was more obvious when the thresholds were set at higher values and could be seen in

neurons of both genotypes (Figure 4.7 and Figure 4.8A-B, compare the values of the red dots and squares with the black and blue dots and squares). Note that neurons from the control and mutant genotypes of the same litter were processed and imaged at the same time. And although the experiments that led to these results were performed independently for the three litters, all the conditions were kept the same among experiments. If such variations among litters were not due to human error, then it is intriguing how PAR3 expression can change so drastically among litters on the same days of the cell culture. One possible explanation for this result would be that although the neurons were collected on the same day of the cell culture (all on 3DIV), the actual development of the neurons might have varied among experiments, which might have led to the different expression levels of PAR3. (And that one day has 24 hours, therefore, that particular litter might be a bit older than the others because the embryos could have been several hours older.) The primary reason for me to choose to test PAR3 expression and distribution at 3DIV was that according to my analysis on neuronal morphogenesis of the prethalamic neurons, this is the age when most of the neurons had formed a distinct longest neurite, but neurite extension of the mutants was still lagging. Judging by the results of PAR3 analysis as above, it is worth stepping back and examining PAR3 expression and distribution at earlier time points such as 1 and 2 DIV. This will allow us to track PAR3 distribution and correlate the establishment of neuronal polarity with morphological changes through time. Additionally, it will also allow us to compare the expression and distribution of PAR3 across different time points and give us a clue of whether such variation among litters as above was caused by a difference in maturation of the neurons. Last but not least, it is also worth increasing the N number of the above experiments, to find out if variations among litters can be seen in more than one litter.

PAR3 is not the only indicator for neuronal polarity. Therefore, expression of other polarity markers within the prethalamic neurons, such as other components of the PAR3/6 complex and the kinesin motor protein KIF3A, which had been shown to display polarised distribution during the

establishment of neuronal polarity can be further tested. Notably, the antibody I used in the PAR3 analysis recognises the mammalian PAR3 protein (PARD3), which differs from the PARD3B protein. It was the mRNA level of the latter that was upregulated in the RNAseq data in the prethalamus when Pax6 was lost. Pard3b is the paralog B of the mammalian Par3 gene, whose protein cannot be recognised by the PAR3 antibody. By interacting with PARD6B, PARD3B can also mediate the specification of neuronal polarity. Therefore, it is also worth repeating the above experiments with antibodies for the PARD3B to find out if expression and distribution of this particular protein shows any difference in the Pax6-null prethalamic neurons.

4.4.2 Statistical analysis for the intensity profile of AIS

No statistical analysis was performed on the data sets of the AIS intensity profiles, due to the unique nature of these data sets. When measuring the intensity profiles, the readout for each neuron was a scatter plot. Each dot on that scatter plot contained one reading on the X-axis and one reading on the Y-axis, which were correlated. Additionally, all the dots on that plot were not independent of each other, because they resemble the intensity readout of each pixel on the same axon. What is more, 30 neurons from each embryo were measured. Therefore, the 30 scatter plots (intensity profiles) obtained were not independent of each other either. This further complicated the situation, and no present statistical tests can satisfy the criteria for such data sets. One of the very few publications that studied the AIS in the same way with measurements of intensity profiles used the Kruskal-Wallis test with Dunn's correction for multiple comparisons (97). However, the Kruskal-Wallis test studies distributions, and if the samples being tested originate from the same distribution (186). Therefore, the data points themselves that make up such distributions should be independent of the others. However, this is not the case for the intensity profile data sets, as the intensity profile from one neuron is already a population of numerical data that shows certain trends of distribution, and these numerical data points are all related to each other.

One possible solution that can apply to such complicated data sets is to simulate how the intensity profiles of AIS behaves using mathematic models. However, within the time frame of this PhD, this was not managed. This is one of the most immediate follow-up experiments to do.

4.4.3 High expression of PAR3, AnkG and voltage-gated sodium channels in the soma

Instead of the tip of the neurite or the AIS, in my study, I found that PAR3, AnkG and voltage-gated Na+ channels showed the highest expression levels in the soma. Previous studies have repeatedly emphasised the importance of polarised expressions of PAR3 at the neurite tips in the establishment of neuronal polarity and concentrated expressions of AnkG in the formation of the AIS (81,82,184,185). The significance of the highest intensity of these proteins in the soma remains to be further determined. Interestingly, previous studies that used the same antibody as in my study to reveal the distribution of PAR3 also showed high level of PAR3 expression within the soma (184,185). These studies utilised hippocampal neurons prepared from E18 rat embryos, which were cultured for 2-3DIV, and showed strongest selective accumulation of PAR3 within the soma and at the tip of only one of the immature neurites of the neurons (184,185). However, the authors only emphasised the significance of PAR3 accumulation at the tip of only one neurite. They did not mention the possible meaning and function of PAR3 expression within the soma, let alone measured the level of PAR3 within the soma and compared that to the level of PAR3 expression at the tip of the neurites (184,185). It would be crucial to our understanding of the mechanism of action of the PAR3/6 complex during establishment of neuronal polarity if we can further confirm whether the PAR3 proteins within the soma are as functional as the PAR3 proteins at the tip of the neurites, when and how the PAR3/6 complex is assembled after the PAR3 proteins are produced in the soma, and how the PAR3/6 complex are selectively transported towards the putative axon. In addition to the high-PAR3-expressing neurite, these studies also found lower levels of PAR3 expression at the tip of other neurites, a scenario similar to

what I found in the cultured prethalamic neurons (184,185). In my study, instead of selective PAR3 accumulation at the tip of one of the neurites, I found the strongest selective PAR3 accumulation at the proximal end of the stem of one of the neurites. This discrepancy of PAR3 distribution during establishment of neuronal polarity might arise from different types of neurons (prethalamic neurons versus hippocampal neurons), different species of neurons (mouse versus rat), different maturation speed in culture of different neurons and also different starting timepoint of embryonic tissue in culture (E13.5 versus E18).

In terms of high AnkG and voltage-gated Na^+ channels expression within the soma, one possible explanation is that the prethalamic neurons were still developing and such proteins were still under production and sorting as the neurons become more polarised. A simple experiment that I can do to verify this is to stain for AnkG and voltage-gated sodium channels in embryonic, neonatal and postnatal mouse brain sections, and check if their expression and distribution differ in any ways in the prethalamus-derived neurons, such as neurons in the TRN.

4.4.4 Improvement on future electrophysiology recordings

Results from whole-cell patch clamp recording showed intriguing changes in the excitability of the Pax6-null prethalamic neurons. However, several improvements need to be applied in future experiments before I can draw any solid conclusion. First of all, the sample size was too small. The above results were obtained from one neuron per litter per genotype and a total of three litters were recorded (n=3). Second of all, the conditions of the neurons changed during recording, therefore within each protocol, I saw fluctuation of membrane potentials across cycles (Protocol 2, Figure 4.12A, B) and repeats (Protocol 3, Figure 4.12C, D). This greatly complicated the analysis of such recording and also impacted on the credibility of the results. In future experiments, a small negative current (-5pA) will be first applied to the neurons to stabilise their membrane potentials, and adjustments will be made during

the recording to make sure that the membrane potentials of the neurons are clamped at a certain voltage throughout the protocol. Third of all, I will further improve the culture conditions to improve the viability of the neurons. With the current cell culture protocol, I was able to keep the primary prethalamic neurons viable for as long as 13 DIV. However, as shown by Figure 4.9E, I and 4.10E, I, AnkG and voltage-gated Na+ channel staining, the AIS seemed to be disassembling at 9DIV, as the prethalamic neurons of the control genotype showed drastic decreases in AnkG and Na+ channel intensity in the AIS region. Additionally, electrophysiology recordings showed that the resting membrane potentials in the cultured prethalamic neurons were much more depolarised than what was normally recorded in other neurons (Figure 4.12E). These results indicated that the conditions of the neurons might not have been ideal or as healthy as their in vivo counterpart. In my dissociated cell culture, I plated the prethalamic neurons purposefully at a density of 20 cells/mm2, to make sure that the neurites of the neurons do not cross each other so that I can observe the entire morphology of the mature neurons. Previous protocols of dissociated thalamic cell cultures indicated that if the plating density is below 3000 cells/mm2, the dissociated thalamic neurons were not healthy, and they died within a few days of cell culture (187). Therefore, in future experiments, I will try to improve neuron viability by first increasing the plating density. Additionally, it would also be interesting to see if the prethalamic neurons are able to form synapses and communicate with each other once the plating density has increased.

4.5 Summary

In this chapter, I analysed the ability of the prethalamic neurons to establish and maintain their neuronal polarities, in the presence and absence of Pax6. I found that the establishment of neuronal polarity, indicated by PAR3 expressions and distributions within the neurons, was not impacted in Pax6-null prethalamus. In terms of maintenance of neuronal polarity by the AIS, the Pax6-null prethalamic neurons can form single, functional AISs as they mature, and they can also fire action potentials upon depolarising current inputs. However, the AISs in the Pax6-null prethalamic neurons were slightly shorter in length and further away from the soma. Additionally, these AISs have higher expressions of AnkG and voltage-gated Na+ channels, which might have contributed to the lower rheobases and higher excitability recorded in the Pax6-null prethalamic neurons.

Chapter 5

Pax6 inhibits the activities of Wnt signalling pathways in the prethalamus

5.1 Introduction

5.1.1 Wnt signalling pathways

The Wnt signalling pathways are crucial and versatile. During neurodevelopment, the functions of Wnt signalling pathways include patterning of the neural tube, promoting proliferation of neural progenitors, specifying cell fates, regulating the establishment of polarity and cytoskeletal remodelling during neuronal morphogenesis, etc. (32,188,189). Recent findings also unveil novel functions of Wnt signalling pathways in maturing neurons in postnatal brains, in which they control transcriptional activation of voltage-gated ion channels and regulate the molecular composition of the axon initial segment, thereby fine-tuning the electrophysiological properties of these neurons and having further impact on the functionality of the nervous system (99,190).

WNTs are secreted glycoproteins with a conserved cysteine residue being palmitoylated. This unusual post-translational modification restricts long-range diffusion of the WNTs (99,188). Therefore, although acting as morphogens, the range of the effects of the WNTs usually is within the distance of a few cells.

There are 19 WNTs and 9 Frizzled receptors expressed in the mouse genome. Depending on what downstream signalling cascades the WNTs initiate, they are classified into two categories: (1)- the canonical WNTs, including WNT1, WNT3A, WNT7B and WNT8B and (2) non-canonical WNTs, including WNT4, WNT5A and WNT11 (188,191,192).

In the case of the canonical or Wnt/β-catenin pathway, binding of WNTs to the transmembrane Frizzled receptors and the co-receptor LRP5 (low-density lipoprotein receptor-related protein 5) or LRP6 further activates the scaffold protein Dishevelled (DVL). Activation of DVL inhibits the functions of glycogen synthase 3β (GSK-3β) and also induces the disassembly of the destruction

complex composed of adenomatosis polyposis coli (APC), AXIN and GSK-3β. This subsequently leads to the accumulation of cytoplasmic β-catenin, which can then be translocated into the nucleus, where it binds to and activate the functions of the transcription factors T-cell specific transcription factor (TCF)/ lymphoid-enhancing factor (LEF) (188,189).

Axin2 is a direct target of the Wnt/β-catenin pathway, whose transcription can be activated by the TCF/LEF transcription factors. Axin2 is a scaffold protein that together with APC and GSK3β, compose the destruction complex. The latter binds to and phosphorylate cytoplasmic β-catenin, resulting in ubiquitylation and degradation of β-catenin. Therefore, Axin2 is part of the negative feedback mechanism to limit the activities of canonical Wnt signalling. Lef1, on the other hand, is part of the positive feedback loop to boost the effect of canonical Wnt signalling locally, as it is a direct target and acts as a downstream transcriptional activator of Wnt/β-catenin pathway (193,194).

In addition to transcriptional activation, the canonical Wnt signalling pathway can also initiate cytoskeletal remodelling as inhibition of GSK-3β can also activate multiple cytoskeletal effector proteins (188,195). In the absence of WNTs or the presence of antagonists for the Wnt signalling pathways, GSK-3β phosphorylates the cytoplasmic β-catenin, resulting in the latter's ubiquitylation and degradation (Figure 5.1a) (188,189).

Similar to the canonical Wnt signalling pathway, the other two Wnt signalling pathways- the Planar cell polarity pathway (PCP pathway) and the WNT/calcium pathway also begin with the binding of the WNT ligands to the Fz receptors and activation of the DVL proteins (189). However, in the PCP pathway, activated DVL relays the signal through Rho GTPases (Rho or Rac or both). These Rho GTPases function to modify cytoskeletal structures directly or through activation of the c-Jun amino (N)-terminal kinase (JNK). The PCP pathway, therefore, has been found to direct cell and tissue polarity and dendritogenesis (Figure 5.1b) (196,197). On the other hand, in the

WNT/calcium pathway, activated DVL induces the intracellular release of Ca2+ and activation of protein kinase C (PKC), which can eventually result in changes of cell fate and cell movement (Figure 5.1c) (198).

Wnt signalling pathways can be blocked at multiple levels. Wnt antagonists such as Cerberus, Wnt inhibitory factor 1 (WIF1), secreted Frizzled-related proteins (SFRPs) and Dickkopf-related proteins (DKKs) can inhibit the signalling relay from the very beginning, by either binding directly to the WNT ligands themselves or to the LRP5/6 co-receptors. SFRPs, for example, can bind to the secreted WNTs, rendering the latter unable to bind with the Fz receptors. Therefore, SFRPs are capable of inhibiting both canonical and non-canonical Wnt signalling pathways. DKKs, on the other hand, is only capable of blocking the canonical Wnt signalling pathway by occupying the LRP5/6 co-receptors (192,199–201).

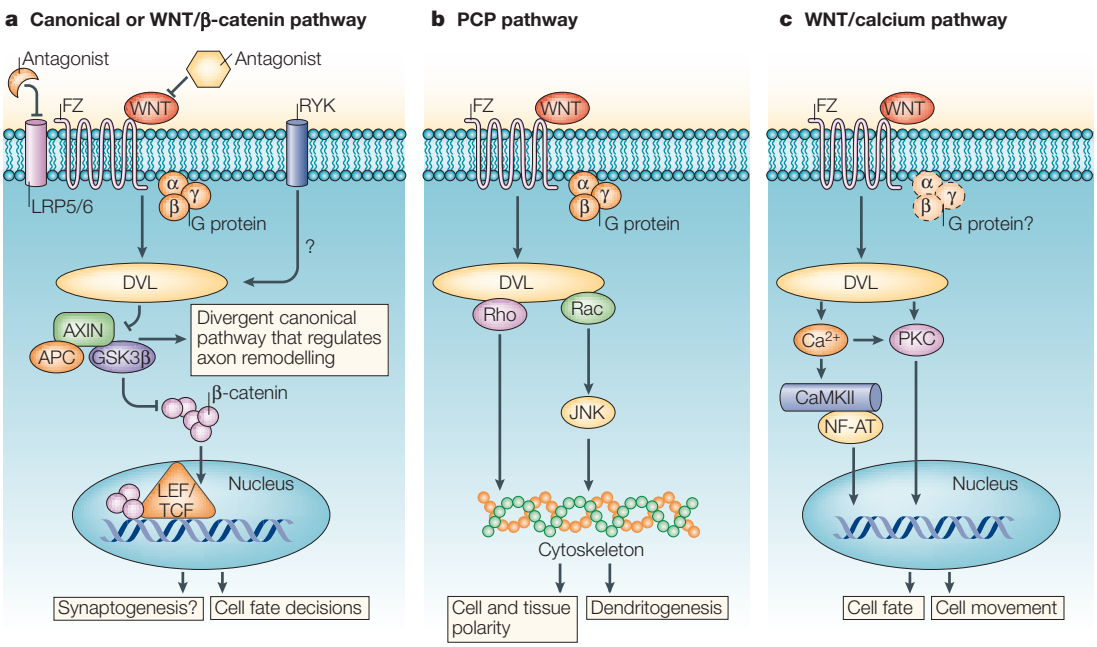

Figure 5.1 Schematic representation of the three branches of Wnt signalling pathways. Depending on the downstream signalling effects, the Wnt signalling pathways can be categorized into Canonical or WNT/β-cantenin pathway **(a)**, planar cell polarity (PCP) pathway **(b)** and WNT/calcium pathway **(c)**. **(a)** Activation of Canonical or WNT/β-cantenin pathway relies on signalling relay that results in stabilized β-cantenin, which then enters the nucleus and activate the TCF/LEF transcription factors. The functions of WNT/β-cantenin pathway have been implicated in cell fate decision, proliferation, etc. A divergent of this pathway, downstream of GSK3β, has also been shown to affect cytoskeletal remodelling during neuronal morphogenesis. **(b)** The PCP pathway controls cellular behaviours such as cell and tissue polarity, dendritogenesis by modulating cytoskeletal structures through Rho GTPases and/or JNK. **(c)** In the signalling relay of WNT/calcium pathway, activation of DVL induces the release of Ca^{2+} into the cytoplasm, which triggers the activities of protein kinase C (PKC) and calcium/calmodulin-dependent protein kinase II (CaMKII). This pathway has been implicated to function during cell fate determination and cell movement. Figure adapted from reference (185).

5.1.2 Activity of Wnt signalling in the prethalamus

Although it has been established that canonical Wnt signalling is crucial for correct patterning and cell fate specification of the thalamus, little is known for its roles during prethalamic development. The minimal amount of evidence so far points to a scenario in which there needs to be a low Wnt activity environment for correct prethalamic development (32). This remains to be further confirmed. More importantly, if that is the case, why and how is that achieved? Just like the thalamus, the prethalamus directly abuts ZLI, which is the primary source of Wnt ligands within the diencephalon. How the thalamus and prethalamus display such a distinct difference in Wnt signalling activity remains unclear. Additionally, previous studies have only focused on the effects of canonical Wnt signalling in diencephalic development. The functions of the other Wnt signalling pathways remain to be elucidated as non-canonical Wnt ligands such as Wnt5a are also expressed in the ZLI.

5.1.3 Aim of this chapter

Pax6 displays a unique expression pattern in the developing diencephalon. It is expressed in the ventricular zone of the thalamus in a gradient, with the level of Pax6 increasing with distance from the ZLI (22). In the prethalamus, however, Pax6 is expressed in a homogeneous level in the ventricular zone. Besides, Pax6 is also expressed in a subset of prethalamic post-mitotic cells (22,60). Various evidence has shown differential expressions of Wnt and Wnt-related genes in the prethalamus in mouse models when expression of Pax6 was disturbed (39,42,202). In addition, RNAseq data in the lab showed that genes involved in the GO-term of Wnt signalling pathway were among the most highly up-regulated genes in the prethalamus when Pax6 is lost (58).

Based on the above, in this chapter, I aim to:

1. Determine innate Canonical Wnt activities in the prethalamus under control conditions

2. Determine the expression patterns of selected Wnt and Wnt-related genes in the prethalamus and how they change in response to the loss of Pax6
3. Further investigate the potential mechanisms by which Pax6 might be inhibiting Wnt signalling pathways

5.2 Results

5.2.1 Expression of specific Wnt and Wnt-related genes was dysregulated in the prethalamus in the absence of Pax6

To have an idea of how the activity of Wnt signalling might have changed in the prethalamus when Pax6 is lost, I first cross-referenced with literature that identified components of the Wnt signalling pathways with the list of differentially expressed genes in out RNAseq data. What I found was that the expression of several Wnt ligands, Fzd receptors and Wnt effector genes was significantly upregulated whereas several Wnt antagonist genes were significantly downregulated in the prethalamus when Pax6 is lost (Table 5.1). Specifically, transcription of the Wnt3a gene showed a Log2-fold change (LFC) of 2.206, which ranked as the third most upregulated among the over 3000 differentially expressed genes. On the other hand, the Wnt antagonist genes Sfrp2 and Dkk3 showed LFCs of -3.03 and -2.05 respectively, which were among the most downregulated genes in the RNA-seq data. Additionally, Wnt effector genes Axin2 (LFC 0.808), Lef1 (LFC 1.005) and Tcf7l2 (LFC 1.262), together with Frizzled receptor genes (Fzd5 LFC 0.927, Fzd10 LFC 0.846) and scaffold protein Dishevelled (Dvl3 LFC 0.723) all showed significantly upregulated expressions in the absence of Pax6 in the prethalamus. All these seemed to point to a general trend of upregulated canonical Wnt signalling in the prethalamus when Pax6 is lost.

Gene	Base mean	Log2-fold change
Wnt genes		
Wnt3a	**280.1**	**2.206**
Wnt5a	**900.3**	**0.918**
Wnt9a	111.9	0.796
Wnt4	74.0	0.705
Wnt7b	**6768.9**	**-0.585**
Wnt7a	419.1	-0.619
Wnt5b	38.9	-0.680
Frizzled receptor genes		
Fzd5	18.9	0.927
Fzd10	260.6	0.846
Fzd8	187.9	-0.534
Fzd2	904.4	-0.609
Fzd7	597.8	-2.1376
Scaffold protein Dishevelled (Dvl)		
Dvl3	1014.2	0.723
Wnt effector genes		
Axin2	**648.7**	**0.808**
Lef1	**344.5**	**1.005**
Tcf7l2 (Tcf4)	**1350.3**	**1.262**
Wnt antagonist genes		
Sfrp1	620.9	0.892
Sfrp2	**1144.8**	**-3.03**
Dkk2	557.4	0.907
Dkk1	28.0	-0.881
Dkk3	**1202.3**	**-2.05**

Table 5.1. Selective Wnt and Wnt-related genes showed significantly differential expressions in the prethalamus when Pax6 is lost.

5.2.2 Activities of the Wnt/β-catenin pathway expand ventrally into the ventricular zone of the prethalamus when Pax6 is lost

5.2.2.1 Prethalamus displayed low activity of Wnt/β-catenin pathway under normal conditions

To test how the activities of canonical Wnt signalling are altered in the prethalamus when Pax6 is lost, and more importantly in which prethalamic areas these changes might have happened, we first turn to the TCF/Lef: H2B-GFP reporter line to find out how active the canonical Wnt signalling is in the prethalamus under normal conditions. The reporter construct of the TCF/Lef: H2B-GFP line consists of six TCF/Lef binding sites and a minimal promoter followed by a GFP gene fused with the histone H2B gene. Therefore, it allows us to visualise Wnt/β-catenin signalling activity by expression of the nuclear-localised GFP (203).

Immunofluorescence staining detecting GFP and PAX6 showed their expressions in the diencephalon at E13.5 mutually exclusive. Pax6 is a known marker for the prethalamus. It is expressed in the ventricular zone of the prethalamus, where its dorsal boundary directly abuts the ZLI, and a subset of cells in the mantle zone (Figure 5.2A-D). GFP expression, on the other hand, showed the highest levels in the mantle zone of the thalamus and hypothalamus. However, expression of GFP was barely detectable in the prethalamus (Figure 5.2A-B, E-F). As the expression pattern of GFP and PAX6 seemed complementary, these results indicated a low canonical Wnt environment in the prethalamus under normal condition, which is in concordance with what others have found using the BAT-gal reporter line or Wnt effector genes (36,38,40,43).

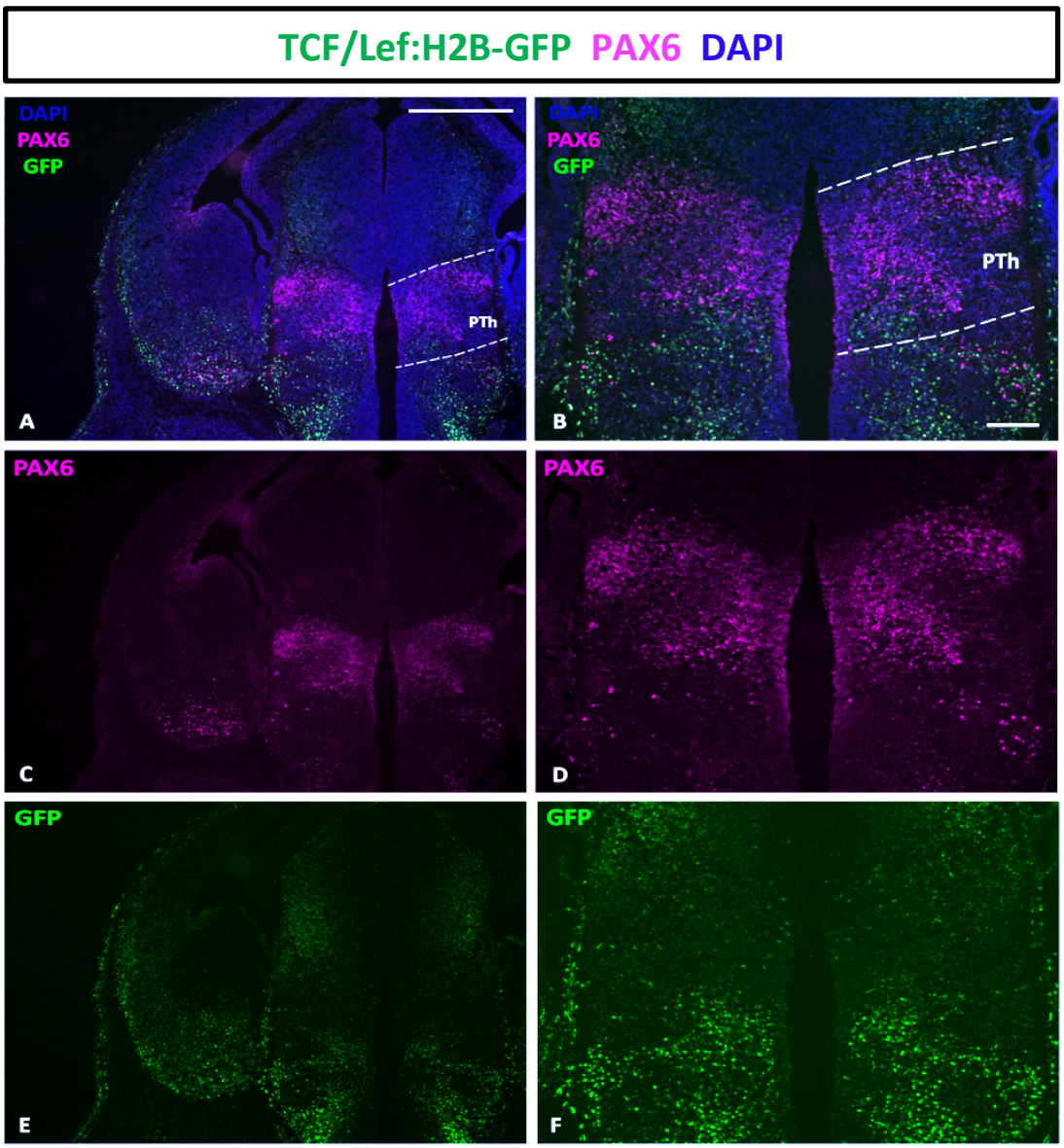

Figure 5.2 Activities of canonical Wnt signalling is low in the prethalamus, shown by the TCF/Lef:H2B-GFP reporter line. (A-F) Fluorescent immunohistochemistry detecting PAX6 (red) and GFP (green) in coronal sections of the TCF/Lef:H2B-GFP reporter mouse line at E13.5, sections were also counter-stained with DAPI (blue). **(A, B)** Merged channels for PAX6, GFP and DAPI, the two dashed lines demarcated the boundaries of the prethalamus based on PAX6 expression. The expression patterns of PAX6 and GFP seem mutually exclusive in the diencephalon. Single channels for PAX6 **(C-D)**, and GFP staining **(E-F)**. **(C-D)** PAX6 expression is strong in the prethalamic area. **(E-F)** GFP expression reporting for canonical Wnt activity shows to be strong in the post-mitotic cells of thalamus and hypothalamus, but weak in the prethalamus. Embryos from 3 litters of TCF/Lef:H2B-GFP reporter mouse line were analysed, n=3. Abbreviations: PTh, prethalamus. Scale bars: 500μm **(A, C, E)**, 250μm **(B, D, F)**.

5.2.2.2 Wnt3a expression expanded into the prethalamic ventricular zone when Pax6 is lost

To find out where the significantly differentially expressed Wnt and Wnt-related genes are expressed in the diencephalon under normal conditions and upon acute Pax6 deletion, we performed in situ hybridisation to detect the presence of their mRNAs in coronal sections of the FP6CD1 mouse brain at E13.5. Due to the structural complexity of the developing diencephalon, without any regional markers, it would be difficult for us to pinpoint the exact locations of the finer diencephalic regions such as the ZLI and pTh-R. Therefore, for each gene tested, we also performed in situ hybridisation against Ngn2 in adjacent sections (Figure 5.3B). Ngn2 is a known marker for specific diencephalic regions- it is expressed in the ZLI, pTh-C and the mantle zone of pTh-C (24). Therefore, by comparing with Ngn2 expressions in adjacent sections, we will be able to locate where exactly the gene to test is expressed in the diencephalon. The expression patterns of each gene tested were examined in sections throughout the entire caudal-rostral axis of the diencephalon. Representative sections for the caudal, medial and rostral levels were selected for presentation (Figure 5.3A').

In the control embryos, the expression of Wnt3a showed the highest intensity in the ZLI. In the ventricular zone of the thalamus, Wnt3a is expressed in pTh-R as well as pTh-C (Figure 5.3C-H). However, this expression seemed to display a gradient as its intensity decreases with distance from the ZLI (Figure 5.3C-E). Wnt3a expression was also found in the mantle zone of the thalamus, but only at more rostral levels (Figure 5.3E, H). Notably, no expression of Wnt3a was observed in the prethalamus (Figure 5.3C-H). In the absence of Pax6, however, Wnt3a expression showed a distinct expansion into the prethalamic ventricular zone. The average level of Wnt3a expression seemed to have been elevated in the mantle zone of the prethalamus as well (Figure 5.3I-N). Wnt3a expression in the ZLI and pTh-R also seemed to have expanded (Figure 5.3L-N).

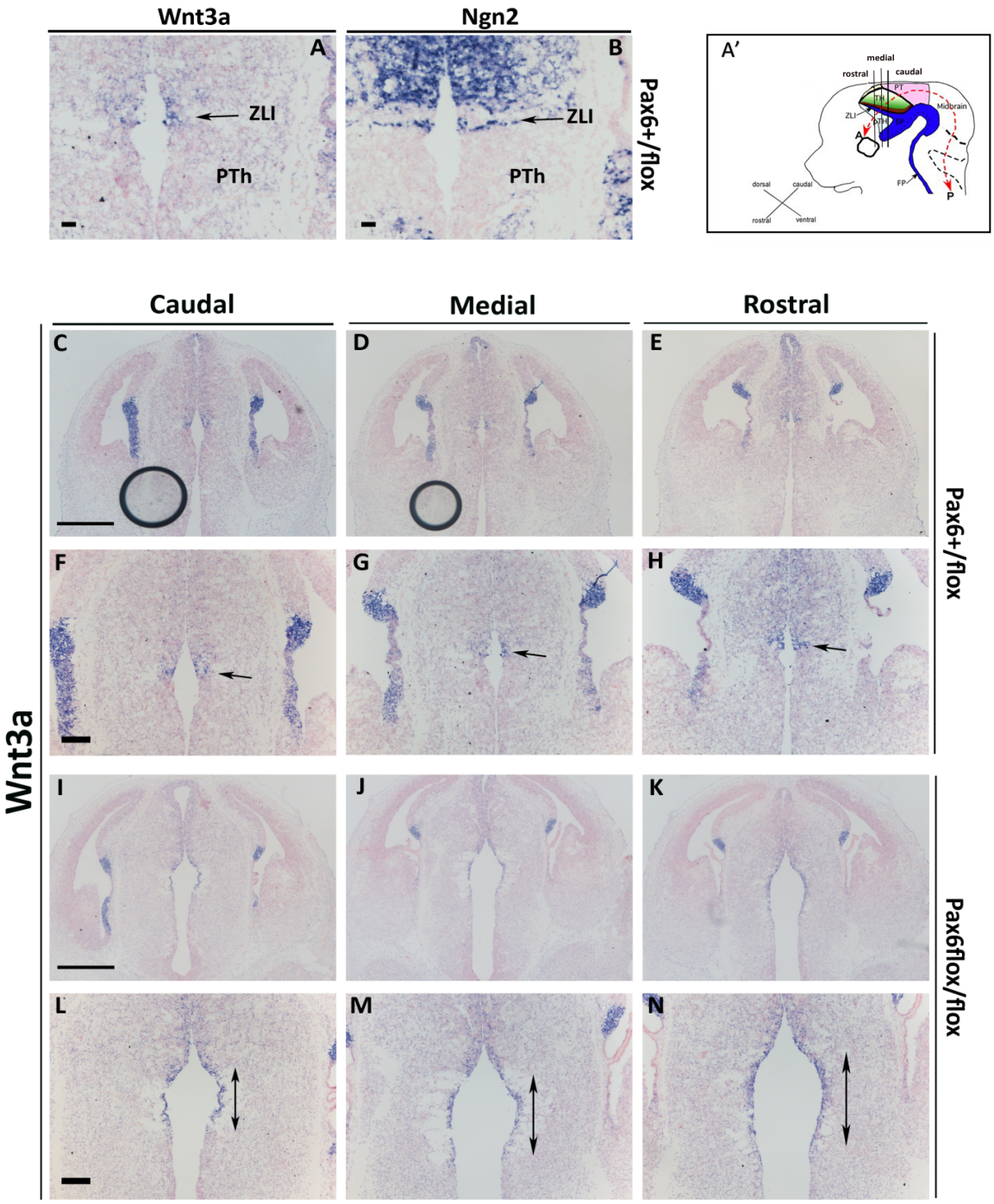

Figure 5.3. Expression pattern of Wnt3a in coronal sections at caudal, medial and rostral levels of Pax6$^{+/flox}$ and Pax6$^{flox/flox}$ embryos at E13.5. High magnification images of **(A)** Wnt3a and **(B)** Ngn2 expression in medial sections of Pax6$^{+/flox}$. Single arrows indicate the position of the ZLI. **(F-H)** Single arrows point to the highest intensity of Wnt3a expression in the diencephalon of Pax6$^{+/flox}$. **(L-N)** Double arrows indicate expansion of Wnt3a expression into the prethalamic ventricular zone of Pax6$^{flox/flox}$. **(A')** Schematic representation of the sagittal view of the mouse neural tube. The vertical lines indicate the proximate location of the representation sections at the rostral, medial and caudal levels. One control and one Pax6-null embryo were obtained from each litter, three litters (n=3). **(C-D)** Black circles are bubbles created during mounting. PTh, prethalamus; ZLI, zona limitans intrathalamica. Scale bars: 500μm **(C-E, I-K)**, 250μm **(F-H, L-N)** and 125μm **(A-B)**.

5.2.2.3 Readout genes for Wnt/β-catenin pathway showed upregulated expressions in the prethalamus in the absence of Pax6

The expansion of Wnt3a expression into the prethalamic ventricular zone indicates potential upregulation of canonical Wnt activities in this region. To find out whether that was the case, we selected Axin2 and Lef1, two known readout genes for the canonical Wnt signalling that also showed upregulated expressions in the RNA-seq data and examined their expression patterns using in situ hybridisation.

In control embryos, Axin2 was expressed in the ventricular zone of the thalamus, the ZLI, as well as the mantle zone of the ZLI (Figure 5.4A-B, C-H). Additionally, Axin2 expression was found in the ventricular zone of the dorsal-most part of the prethalamus, abutting the ZLI (Figure 5.4G, double arrows). This expression appeared higher in the medial level of the diencephalon. In the absence of Pax6, Axin2 expression was elevated in the prethalamus (Figure 5.4I-N) and expanded even more ventrally to occupy almost the entire ventricular zone of the prethalamus (Figure 5.4M, double arrows).

Similar to Wnt3a and Axin2, Lef1 expression in the control embryos seemed most robust in the ZLI (Figure 5.5A-B). However, in the thalamus, the level of Lef1 expression was low in pTh-R and pTh-C, but higher in the mantle zone of the pTh-C (Figure 5.5C-H). In the prethalamus, Lef1 is also found to be expressed in the ventricular zone of the dorsal-most prethalamic region (Figure 5.5A-B, 5.5G, double arrows). Interestingly, Lef1 was also expressed in the ventricular zone and subventricular zone of the hypothalamus (Figure 5.5C-E).

In the absence of Pax6, Lef1 expression was also found to have expanded ventrally, closing the gap of the Lef1-null region in the ventricular zone of the prethalamus observed in the control embryos (Figure 5.5I-N, 5.5M double arrows). Additionally, the low-Lef1 region, which was initially the pTh-R, have also expanded in the Pax6 mutant.

The above results showed that the ZLI was one of the primary sources of releasing ligands of the Wnt/β-catenin pathway, in concordance with previous studies. Detailed analysis of the expression patterns of Wnt3a, Axin2 and Lef1 as above revealed differential expressions of these genes in different structures of the diencephalon- pTh-R and the ventral prethalamus display low canonical Wnt activity, whereas pTh-C and the dorsal ventricular zone of the prethalamus display high canonical Wnt activity. Acute deletion of Pax6 led to region-specific increased activities of canonical Wnt in the ventricular zone of the prethalamus.

In contrast to the upregulated expressions of Wnt ligands and Wnt effector genes, several Wnt antagonist genes showed significantly downregulated expressions in the prethalamus when Pax6 is lost. Based on this information, we hypothesised that Pax6 inhibits the activity of Wnt signalling pathways by promoting the expressions of Wnt antagonists. To test this hypothesis, we examined the expression patterns of Wnt antagonists- Sfrp2 and Dkk3 by in situ hybridisation.

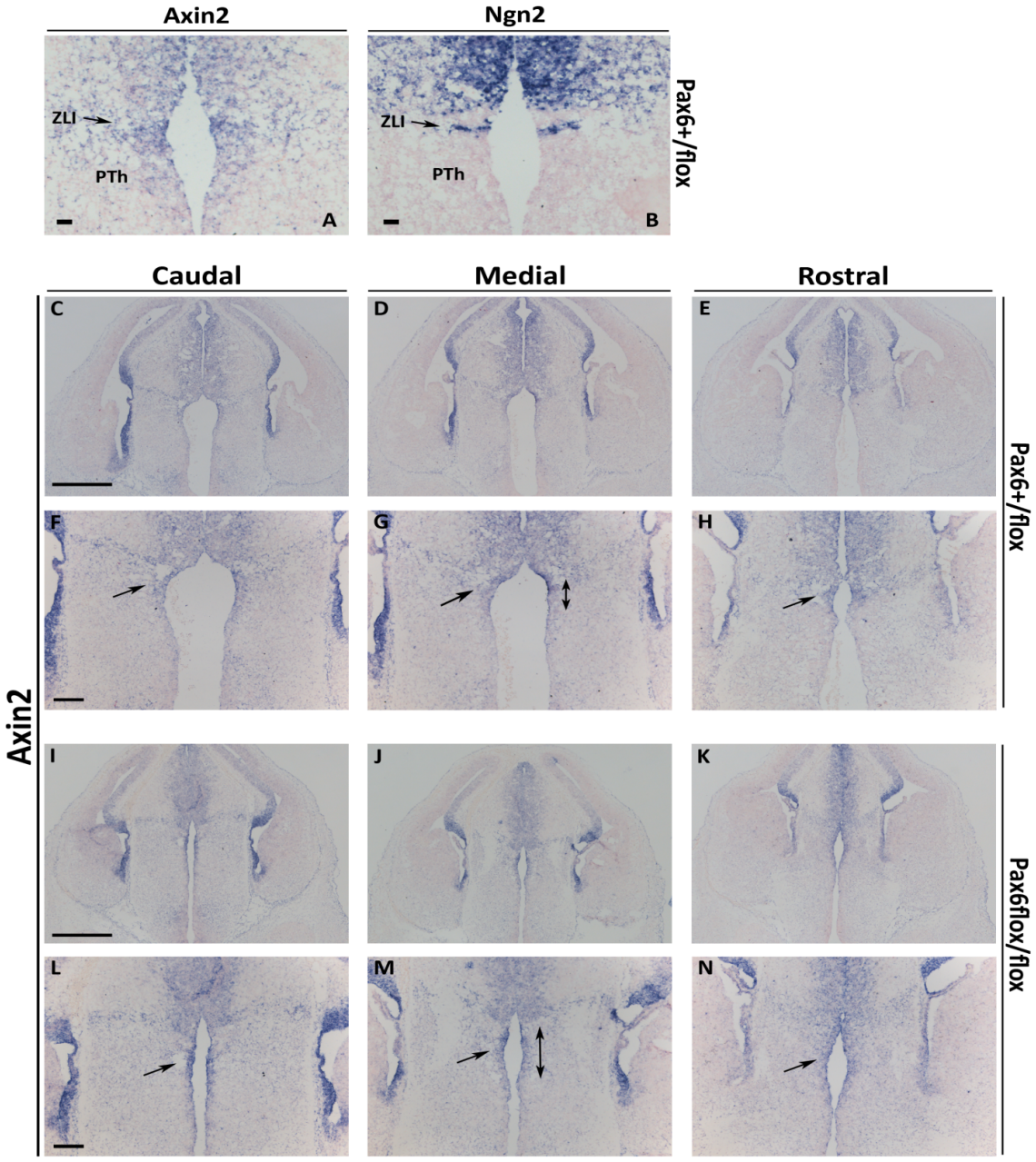

Figure 5.4. Expression pattern of Axin2 in coronal sections at caudal, medial and rostral levels of Pax6$^{+/flox}$ and Pax6$^{flox/flox}$ embryos at E13.5. High magnification images of **(A)** Axin2 and **(B)** Ngn2 expression in medial sections of Pax6$^{+/flox}$. Single arrows indicate the position of the ZLI in the sections. **(F-H, L-N)** Single arrows point at Axin2 expressions in the prethalamus of Pax6$^{+/flox}$ and Pax6$^{flox/flox}$ respectively. Double arrow in **(G and M)** indicates the area of Axin2 expression in the prethalamic ventricular zone. At least one control and one Pax6-null embryo were obtained from each litter, three litters were analysed (n=3). Abbreviations: PTh, prethalamus; ZLI, zona limitans intrathalamica. Scale bars: 500μm **(C-E and I-K)**, 250μm **(F-H and L-N)** and 125μm **(A and B)**.

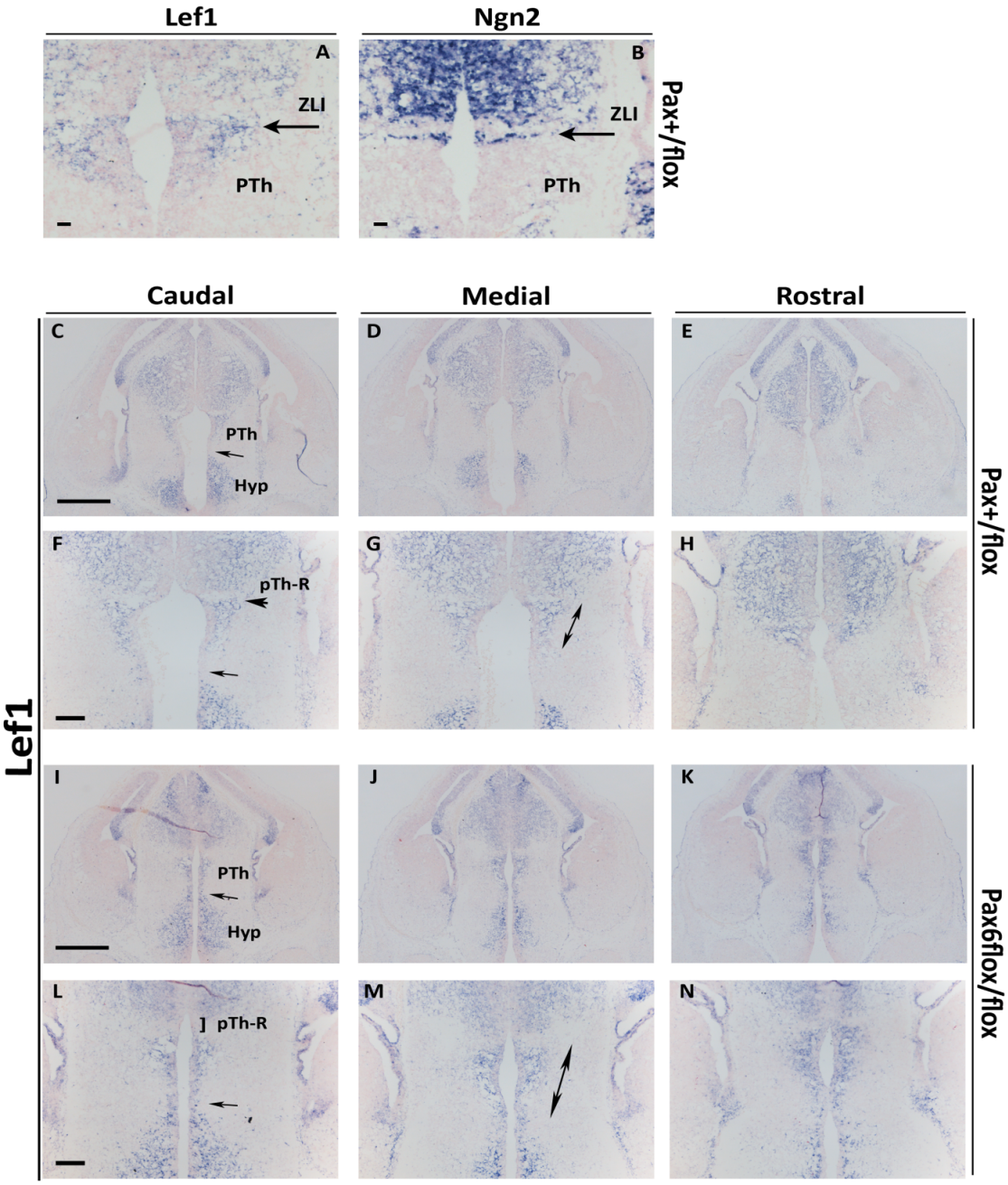

Figure 5.5. Expression pattern of Lef1 in coronal sections at caudal, medial and rostral levels of Pax6$^{+/flox}$ and Pax6$^{flox/flox}$ embryos at E13.5. High magnification images of **(A)** Lef1 and **(B)** Ngn2 expression in medial sections of Pax6$^{+/flox}$. Single arrows indicate the position of the ZLI in the sections. **(C, F, I, L)** Single arrows indicate the disappearance of the Lef1-null gap between the prethalamus and the hypothalamus when Pax6 is lost. **(F)** Arrowhead points at the pTh-R with low Lef1 expression. **(L)** Bracket indicates the expansion of the pTh-R. **(G)** Double arrows indicates the expression of Lef1 in the Pax6$^{+/flox}$ prethalamus. **(M)** Double arrow indicates the area of stronger and expanded Lef1 expression in the Pax6$^{flox/flox}$ prethalamus. At least one control and one Pax6-null embryo were obtained from each litter, three litters were analysed (n=3). Abbreviations: PTh, prethalamus; ZLI, zona limitans intrathalamica; Hyp, hypothalamus. Scale bars: 500μm **(C-E and I-K)**, 250μm **(F-H and L-N)** and 125μm **(A and B)**.

5.2.3 Wnt antagonists are expressed in the ventricular zone of the prethalamus, which were almost completely abolished when Pax6 is lost

When looking into the RNA-seq data, Wnt antagonists Sfrp2 and Dkk3 were among the most highly down-regulated genes in the prethalamus when Pax6 is lost. SFRP2 and DKK3 are both soluble inhibitors of Wnt signalling pathways. By binding directly to the Wnt ligands themselves, SFRP2 is thus able to inhibit the signalling relay of all three Wnt pathways. DKK3, on the other hand, functions to bind with the LRP5/6 co-receptor, therefore inhibits explicitly the activities of the canonical Wnt signalling pathway (192,199–201).

In control embryos at E13.5, strong Sfrp2 expression was found in the ventricular zone of the prethalamus (Figure 5.6C-E, F-H double arrows), with its dorsal limit abutting the ZLI (Figure 5.6A-B). The intensity of this Sfrp2 expression increased as it descended ventrally, but then dialled down as it reached and passed the ventral boundary of the prethalamus and hypothalamus (Figure 5.6F-H).

In the absence of Pax6, Sfrp2 expression was almost completely lost in the ventricular zone of the prethalamus (Figure 5.6I-N). Interestingly, the expression of Sfrp2 seemed to have been upregulated in the ventricular zone of the thalamus at the medial level (Figure 5.6J).

SFRP2 is a soluble inhibitor (204). Therefore, to better understand the range of its effects, I tried to further find out the range of its diffusion by studying the distribution of the protein itself. Due to technical difficulties, fluorescent immunohistochemistry detecting the SFRP2 protein could not be combined with fluorescence in situ hybridisation detecting the Sfrp2 mRNA. Therefore, these two experiments were done in parallel, in adjacent sections to compare the expression patterns of the Sfrp2 mRNA and SFRP2 protein. As shown in Figure 7, the distribution of the SFRP2 protein highly resembles the expression pattern of the Sfrp2 mRNA (Figure 5.7A-B). Expression of the Sfrp2 gene

seemed to be limited to only the cells in the ventricular zone of the prethalamus, so did diffusion of the SFRP2 protein (Figure 5.7A-B, 5.7A', 5.7A'', 5.7B', 5.7B''). These results indicated that the effect of the SFRP2 protein was also short-ranged and limited to a distance of only a few cells from its source, which is similar to the diffusion mechanisms of the Wnt ligands as previous studies proposed (99,188).

In addition to Sfrp2 expression, Dkk3 expression in the control embryos also showed the strongest staining in the ventricular zone of the prethalamus. The dorsal limit of Dkk3 expression seemed to be abutting the ZLI as well; however, at a much lower level than Sfrp2 expression in this area (Figure 5.8A-B). The intensity of Dkk3 expression also displayed a gradient, which increased with distance from the ZLI. The ventral limit of Dkk3 also seemed to have passed the prethalamic boundary and descended into the hypothalamus (Figure 5.8C-D, 5.8F-H, double arrows).

Interestingly, in the absence of Pax6, Dkk3 expression also suffered a drastic drop in its intensity, as its expression was merely detectable in the ventricular zone of the prethalamus.

The overlapping expression patterns of Sfrp2, Dkk3 in the ventricular zone of the prethalamus in the presence of Pax6, and the region-specific upregulated activity of canonical Wnt signalling in this area in the absence of Pax6 suggested that our hypothesis might be correct.

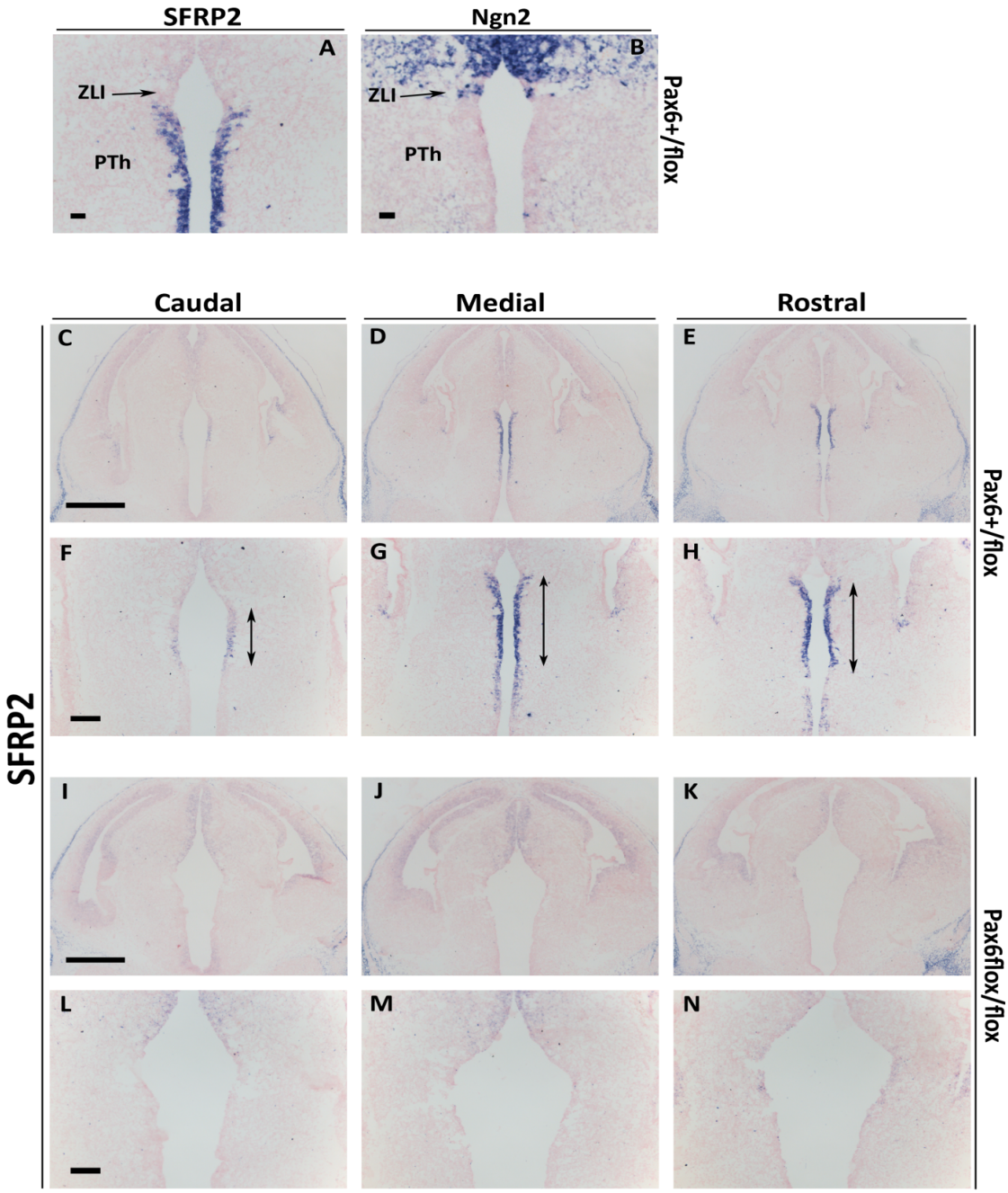

Figure 5.6 Expression pattern of SFRP2 in coronal caudal, medial and rostral diencephalic sections of Pax6$^{+/flox}$ and Pax6$^{flox/flox}$ embryos at E13.5. (A) SFRP2 and **(B)** Ngn2 expression in medial sections of Pax6$^{+/flox}$. Single arrows indicate the position of the ZLI in the sections. **(F-H)** Double arrows indicate the expression of SFRP2 in the ventricular zone of the prethalamus of Pax6$^{+/flox}$. At least one control and one Pax6-null embryo were obtained from each litter, five litters were analysed (n=5). Abbreviations: PTh, prethalamus; ZLI, zona limitans intrathalamica. Scale bars: 500μm **(C-E and I-K)**, 250μm **(F-H and L-N)** and 125μm **(A and B)**.

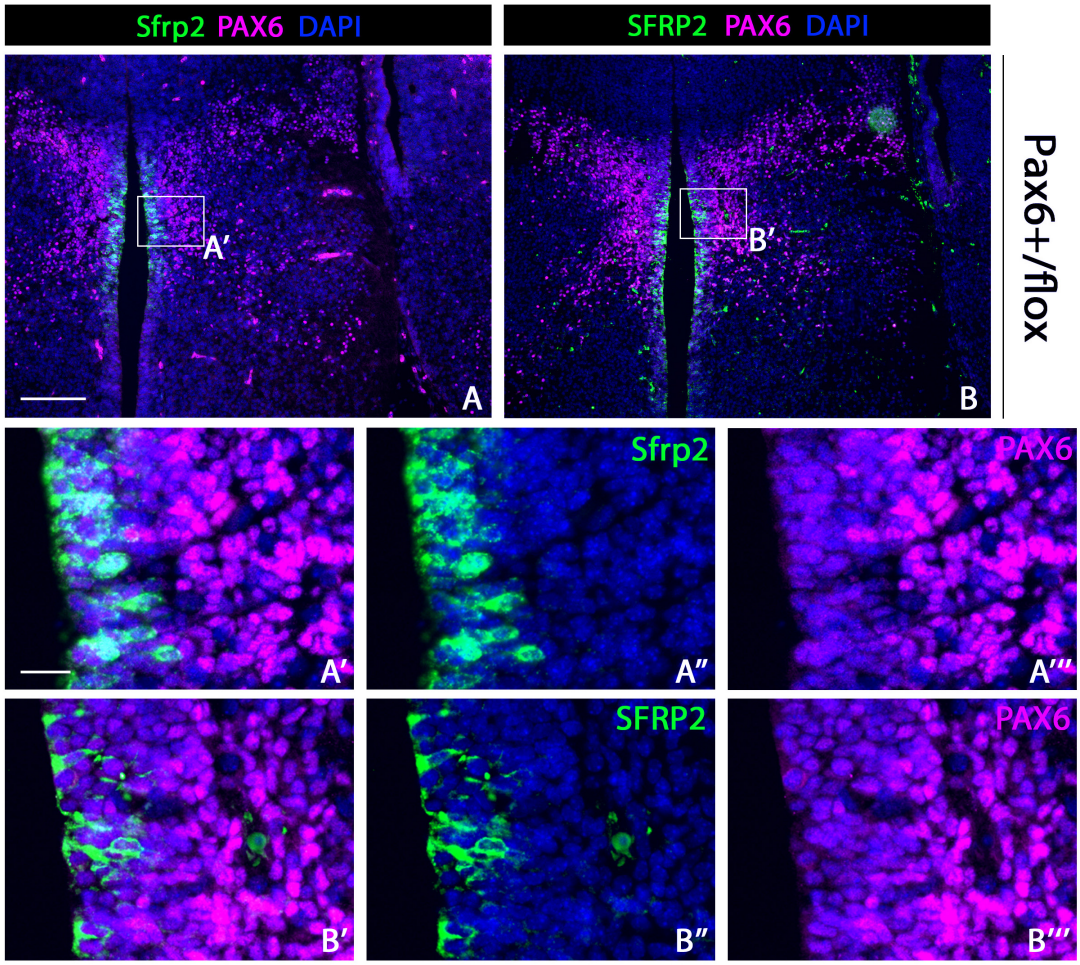

Figure 5.7. Comparison of expression patterns of Sfrp2 mRNA and SFRP2 protein in parallel sections. (A) Fluorescent in situ hybridization detecting Sfrp2 mRNA in combination with fluorescent immunohistochemistry detecting PAX6 protein in coronal section of the E13.5 mouse brain at medial level. **(B)** Fluorescent immunohistochemistry detecting SFRP2 and PAX6 protein in parallel section of (A). **(A', B')** Zoomed in images of the areas within the rectangular in (A) and (B), section in (A') were stained to detect Sfrp2 mRNA and PAX6 protein distribution; section in (B') were stained to detect SFRP2 and PAX6 protein distribution. **(A'', A''', B'', B''')** Single channel images for (A') and (B'). One control and one Pax6-null embryo were obtained from each litter, three litters were analysed (n=3). Scale bars: 300μm **(A-B)**; 30μm **(A'-B''')**.

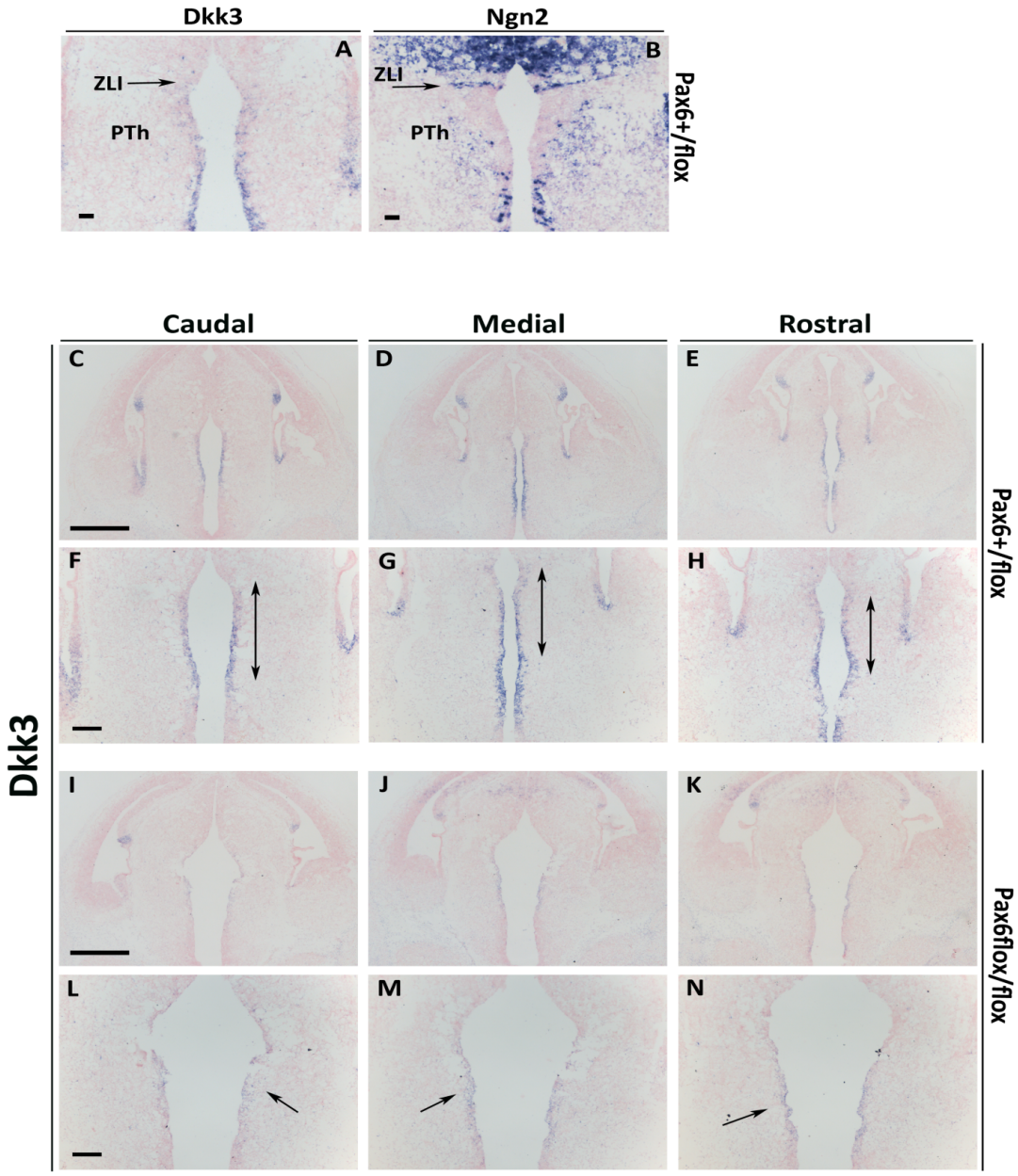

Figure 5.8. Expression pattern of Dkk3 in coronal caudal, medial and rostral diencephalic sections of Pax6$^{+/flox}$ and Pax6$^{flox/flox}$ embryos at E13.5. (A) Dkk3 and **(B)** Ngn2 expression in medial sections of Pax6$^{+/flox}$. Single arrows indicate the position of the ZLI in the sections. **(F-H)** Double arrows indicate the expression of Dkk3 in the ventricular zone of the prethalamus of Pax6$^{+/flox}$. **(L-N)** Single arrows point areas of low expression of Dkk3 in the prethalamus of Pax6$^{flox/flox}$. At least one control and one Pax6-null embryo were obtained from each litter, three litters were analysed (n=3). Abbreviations: PTh, prethalamus; ZLI, zona limitans intrathalamica. Scale bars: 500μm **(C-E and I-K)**, 250μm **(F-H and L-N)** and 125μm **(A and B)**.

5.2.4 Wnt5a expression is upregulated in the ventricular zone as well as a subset of post-mitotic cells of the prethalamus when Pax6 is lost

In addition to Wnt3a, another Wnt gene- Wnt5a also showed upregulated expression in the prethalamus when Pax6 is deleted. WNT5a is normally considered as a non-canonical Wnt ligand. However, when co-expressed with Fzd5 receptor, it can also activate the canonical Wnt pathway (200,205). Additionally, previous studies have shown strong Wnt5a expression in the ZLI during diencephalic development (37,38,41). To determine the exact expression pattern of Wnt5a in our mouse model at this particular age of diencephalic development, we also performed in situ hybridisation to detect the expression of Wnt5a mRNA in coronal sections.

In control embryos, Wnt5a is also expressed most strongly in the ZLI (Figure 5.9A-B, 5.9C-E arrowhead). In the thalamus, Wnt5a is expressed in a rather homogeneous level in the ventricular zone (Figure 5.9C-E). Interestingly, Wnt5a is also expressed by a small group of post-mitotic cells in the prethalamus at the caudal and medial levels (Figure 5.9F-G, rectangle). Additionally, Wnt5a is also expressed in the ventricular zone of the hypothalamus, a group of post-mitotic cells in the subpallium, as well as the cortical hem.

In the absence of Pax6, Wnt5a expression has expanded, not only ventrally into the ventricular zone of the prethalamus (Figure 5.9I-K, double arrows), but also laterally as more post-mitotic cells in the caudal and medial levels of prethalamus now express Wnt5a (Figure 5.9L-M, rectangle).

To find out whether Wnt5a expressions in the post-mitotic cells of the prethalamus correlate with Pax6 expressions in this area, we performed in situ hybridisation against Wnt5a mRNA in combination with immunohistochemistry detecting the PAX6 protein. The PAX6 antibody used in these experiments detects the last 20 amino acids on the C-terminal of the PAX6 protein. Due to the presence of an internal initiation site, a truncated PAX6 protein with its C-

terminal intact can still be produced after the floxed Pax6 exons had been excised from the genome (32). Hence, we can utilise this antibody to detect cells with active transcriptions for the Pax6 gene, regardless of whether the protein being produced will be complete and functional or not.

Colour reaction of the Wnt5a in situ hybridization was performed with BCIP (5-bromo-4-chloro-3-indolyl-phosphate) in conjunction with NBT (nitro blue tetrazolium), hence giving out the signal in blue, whereas colour reaction of the immunohistochemistry detecting PAX6 was performed with the DAB (3, 3 - diaminobenzidine) HRP substrate, which produces a dark brown reaction product. As shown in Figure 5.10, in control embryos, the population of Wnt5a positive cells mainly resides in the very lateral mantle zone of the prethalamus. Expression patterns of Wnt5a and PAX6 are highly mutually exclusive as most of the Wnt5a-high cells express low levels of PAX6, and vice versa (Figure 5.10C, arrows). Only a few cells co-expressing Wnt5a and Pax6 were found in the mantle zone of the prethalamus (Figure 5.10C, arrowheads). However, in the absence of Pax6, not only had this Wnt5a-positive population expanded within the mantle zone of the prethalamus, but cells within this population also expressed higher levels of Wnt5a. Additionally, more cells in this population were now co-express Wnt5a and PAX6 (Figure 5.10D, arrowheads). Adjacent sections were processed in parallel with immunohistochemistry detecting PAX6 using the antibody recognising the N-terminal of PAX6, which is absent in the truncated PAX6 in the mutant embryos (153). Figure 10E confirmed that within the mantle zone of the prethalamus in the Pax6flox/flox embryos, most of the cells had lost their PAX6 expression. There were still a few PAX6-positive cells detected, possibly due to a variation of responses towards tamoxifen from different cells. Nonetheless, this does not affect the Pax6-null phenotype, and we can conclude from the above that loss of Pax6 induced increased expression of Wnt5a in the ventricular zone and mantle zone of the prethalamus, and the inhibition of Wnt5a expression by Pax6 in the mantle zone of the prethalamus might be cell-autonomous.

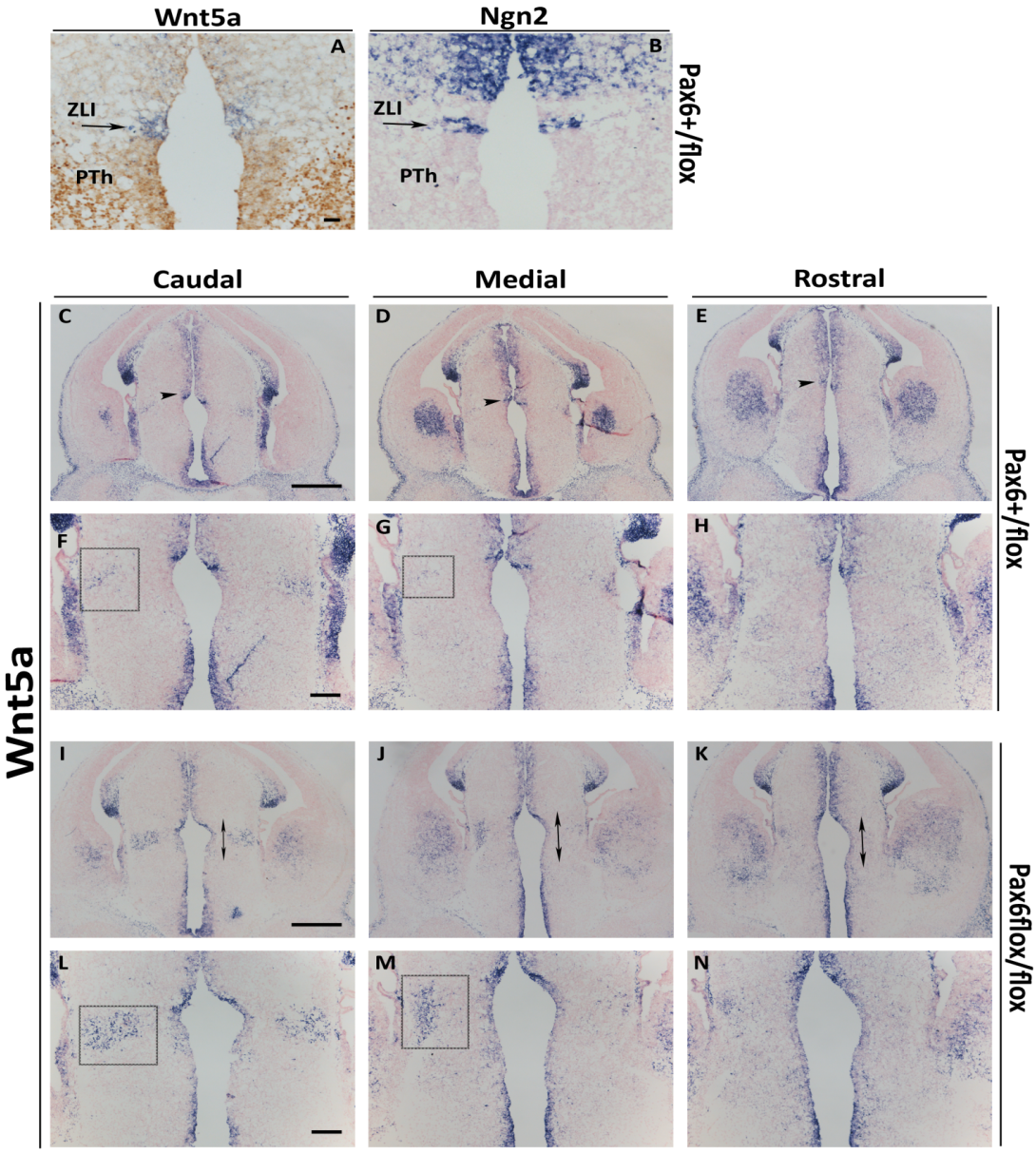

Figure 5.9. Expression pattern of Wnt5a in coronal caudal, medial and rostral diencephalic sections of Pax6$^{+/flox}$ and Pax6$^{flox/flox}$ embryos at E13.5 after *in situ* hybridization. (A) Wnt5a and **(B)** Ngn2 expression in medial sections of Pax6$^{+/flox}$. Single arrows indicate the position of the ZLI in the sections. **(F, G, L and M)** Rectangles indicate the cell population expressing Wnt5a in the mantle zone of the prethalamus. **(C-E)** Arrowheads point the expression of Wnt5a in the ZLI in Pax6$^{+/flox}$. **(I-K)** Double arrows indicate Wnt5a expression in the ventricular zone of the prethalamus of Pax6$^{flox/flox}$. At least one control and one Pax6-null embryo were obtained from each litter, three litters were analysed (n=3). Abbreviations: PTh, prethalamus; ZLI, zona limitans intrathalamica. Scale bars: 500μm **(C-E and I-K)**, 250μm **(F-H and L-N)** and 125μm **(A and B)**.

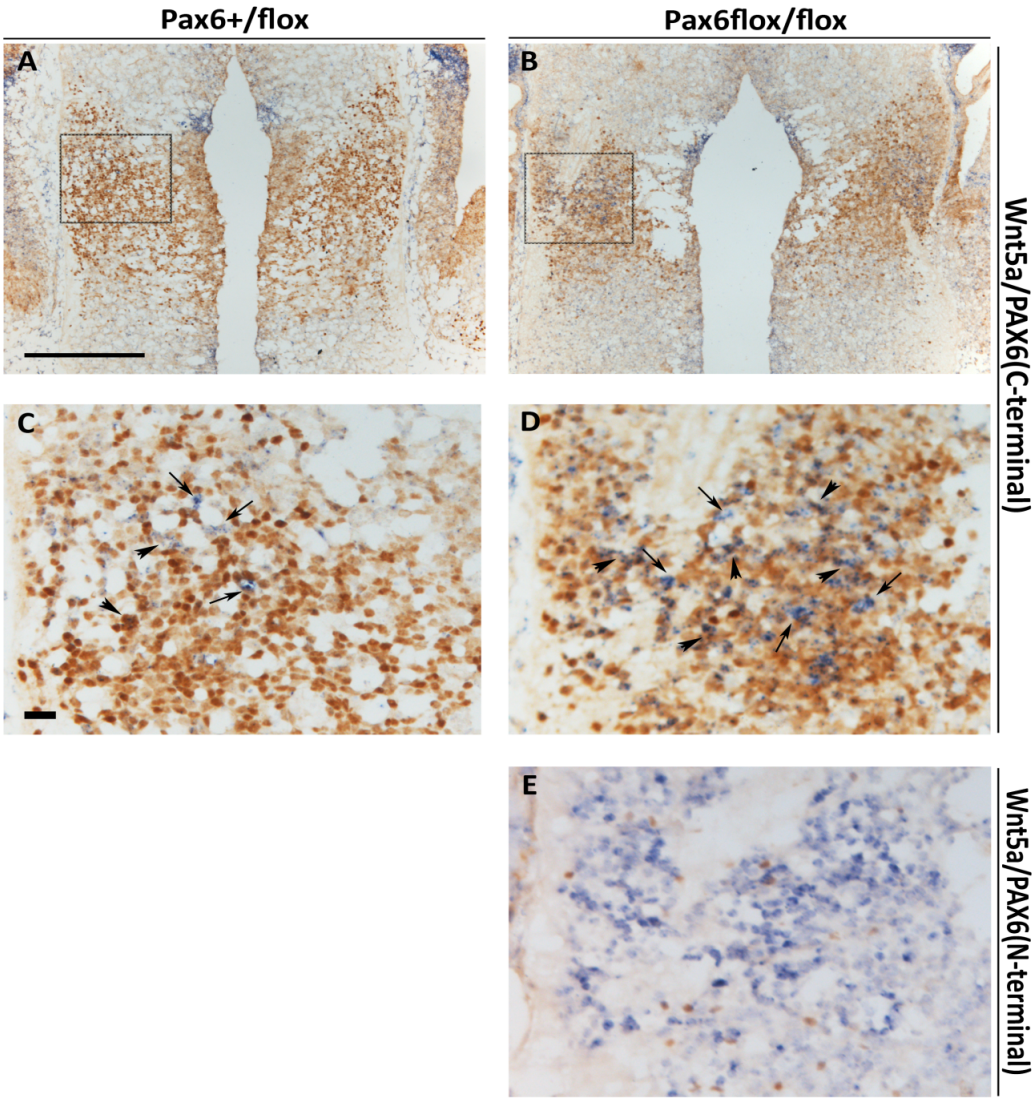

Figure 5.10 Expression pattern of Wnt5a and Pax6 in coronal medial diencephalic sections of Pax6$^{+/flox}$ and Pax6$^{flox/flox}$ embryos at E13.5 after DAB Immunohistochemistry. (A-D) Wnt5a (blue) and Pax6 (brown) expression in the prethalamus. **(C-D)** Single arrows indicate Wnt5a-expressing cells in the mantle zone. Arrowheads point to overlapping Wnt5a-Pax6 cells in the mantle zone. **(E)** Wnt5a and Pax6 expression in the mantle zone of the prethalamus of Pax6$^{flox/flox}$. At least one control and one Pax6-null embryo were obtained from each litter, three litters were analysed (n=3). Scale bars: 250μm **(A and B)**, 65μm **(C, D and E)**.

5.3 Discussion

The functions of Wnt signalling pathways are essential for the normal development of the forebrain. Recent studies have also revealed new roles of canonical Wnt signalling in directing the development of the diencephalon, with most emphasis on the thalamus. These studies have validated various thalamic developmental defects when canonical Wnt signalling was removed (28,29,32,36,38,41,43). However, the impacts of Wnt signalling pathways on the development of the prethalamus were seldom mentioned. It had been established, although, without much in-depth investigation, that inhibition of canonical Wnt signalling is required for the normal development of the prethalamus (32). However, this remained to be confirmed, and the underlying mechanisms are still poorly understood. RNAseq data in the lab showing differential expressions of genes revealed a general increase of activities of Wnt signalling pathways in the diencephalon, and especially in the prethalamus, after acute deletion of Pax6. However, as the diencephalon at this age of investigation is compacted with fine structures such as pTh-C, pTh-R, ZLI etc., it was hard to draw any solid conclusions without knowing the specific expression patterns of particular genes involved in the Wnt signalling pathways.

Based on this, in this chapter, we analysed the expression patterns of several Wnt and Wnt-related genes by in situ hybridisation, to find out how the activities of Wnt signalling pathways were affected in specific regions of the diencephalon in the presence and absence of Pax6. This has enabled us to elucidate the involvement of Wnt signalling pathways in prethalamic development and further shed light on the potential mechanisms of Pax6's control over Wnt signalling pathways in this particular region.

5.3.1 Working model: Pax6 inhibits the activities of Wnt signalling pathways in the prethalamus by promoting the expressions of Wnt antagonists

As shown above, canonical Wnt signalling is highly active in the thalamus but inert in the prethalamus under normal conditions (Figure 5.2). In the absence of Pax6, increased and expanded expressions of Wnt3a, Wnt5a, Lef1 and Axin2 were observed specifically in the ventricular zone of the prethalamus, along with a drastic decrease of expressions of Wnt antagonists Sfrp2 and Dkk3 in this region. These results have allowed us to propose a simple working model. As shown in Figure 5.11, in the ventricular zone of the prethalamus, Pax6 might be indirectly inhibiting the canonical Wnt signalling pathway by promoting the expressions of Wnt antagonists such as Sfrp2 and Dkk3. Indeed, previous studies have shown that Pax6 can directly bind to the promoter of Sfrp2 and activate its transcription, in order to inhibit canonical Wnt signalling during retinal development. Kim et al. had also shown the disappearance of Sfrp2 expression in the Sey/Sey mutant, the mouse model with the natural loss of function mutation of the Pax6 gene. Additionally, Pax6 was shown to be able to bind to the promotor of the Dkk1 gene (42,202).

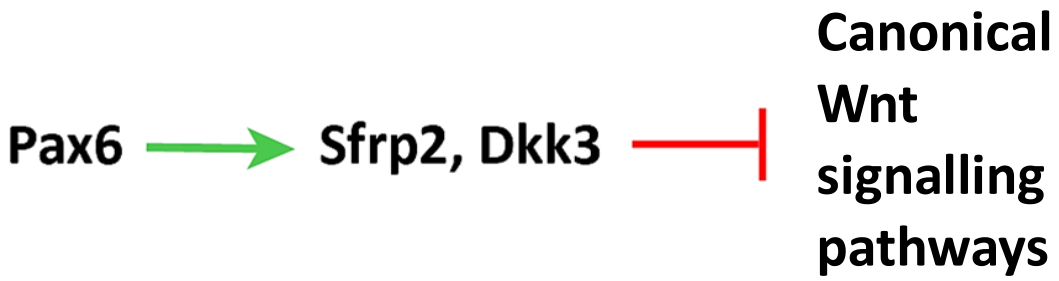

Figure 5.11. Diagram showing the proposed working model of Pax6's inhibition on the canonical Wnt signalling in the ventricular zone of the prethalamus at E13.5. By directly promoting the expressions of Wnt antagonists such as Sfrp2 and Dkk3, Pax6 thereby indirectly inhibit the activities of the canonical Wnt signalling in the ventricular zone of the prethalamus.

Sfrp2 and Dkk3 can inhibit the activities of the canonical Wnt signalling by binding directly to the Wnt ligands themselves or to the LRP5/6 co-receptors, therefore stopping the signalling relay from the very beginning (192,199,200).

How the loss of this extracellular protein-protein interaction results in transcriptional activation of Wnt and Wnt-related genes remains to be elucidated. However, as shown in the case of the transcriptional activation of Wnt effector genes Axin2 and Lef1, it is reasonable to speculate that the canonical Wnt signalling in the ventricular zone of the prethalamus might be involved in positive feedback loops of transcribing genes that are themselves components of the signalling relay of this pathway.

In summary, we propose that Pax6 indirectly inhibits the activities of the canonical Wnt signalling pathway through directly promoting the expressions of Wnt antagonists in the prethalamic ventricular zone.

5.3.2 Activities of Wnt signalling pathways in the different regions of the developing diencephalon

Our detailed analysis of the expression patterns of Wnt3a, Axin2 and Lef1 have revealed differential expressions of these genes in different structures of the diencephalon- pTh-R and the ventral prethalamus display low canonical Wnt activities whereas pTh-C and the dorsal ventricular zone of the prethalamus display high canonical Wnt activities. These results were derived from the TCF/Lef: H2B-GFP reporter line as well as in situ hybridisation against Wnt and Wnt-related genes in the FP6CD1 line. Interestingly, the activities of canonical Wnt signalling on either side of the ZLI as we found was rather opposite to what was previously proposed. Both the pTh-R and the dorsal-most prethalamus situate directly on either side of the ZLI, hence should be receiving a similar amount of WNT ligands. However, the most ventral-rostral thalamic region, the pTh-R, showed low Lef1 expression, whereas the most dorsal prethalamic region showed high Axin2 and Lef1 expressions.

On either side of the ZLI, Pax6 expression was reported to be low, due to the mutual repression between Pax6 and Shh expressed by the ZLI (22). Low Pax6 expression in the ventricular zone of the dorsal-most prethalamus might explain why Sfrp2 and Dkk3 expressions were also lower in this particular

region, possibly as a result of lower levels of direct transcriptional activation of Pax6 over these genes. This might therefore further lead to elevated Axin2 and Lef1 expressions in this region. It would be interesting to find out how the derivative neurons from this region differ from the neurons generated in nearby prethalamic regions, in terms of cell identity and even electrophysiological properties.

Whether the pTh-R indeed displays low canonical Wnt signalling remains to be confirmed, as, in our study, we only looked at the expression of Lef1. The pTh-R might express other members of the TCF/LEF families of transcription factors, such as Tcf7l2, to carry out the final steps of canonical Wnt signalling. However, we also observed the Lef1-null gap within the thalamic region widened in the absence of Pax6. This might be due to the expansion of pTh-R in Pax6-null mutants, which was in concordance with what was previously described (22). This indicated that the absence of Lef1 expression in the pTh-R might be independent of Pax6. So far, the very limited evidence showed that deleting β-catenin in the ZLI and pTh-C at E10.5 and onwards does not affect the formation of the pTh-R. It does, however, results in an invasion of prethalamic and pTh-R markers in the mantle zone of pTh-C. On the other hand, deleting Shh expression under the same condition results in loss of pTh-R markers such as Helt, Gata2, Ascl1 and Nkx2-2. Lastly, deleting both Shh and β-catenin although restored expression of pTh-R markers close to ZLI, it also led to the invasion of prethalamic and pTh-R markers in the mantle zone of pTh-C. These results indicate an essential role of canonical Wnt signalling in maintaining the development of pTh-C and Shh in maintaining the development of pTh-R in the presence of high levels of canonical Wnt signalling (36). Therefore, in terms of the formation and development of the pTh-R, Shh signalling might be playing a more determining role than the canonical Wnt signalling. If this is true, then the remaining questions would be, what signalling pathway contributed to this and what are their interactions with the canonical Wnt signalling.

As the mid-diencephalic organiser, the ZLI is known to release morphogens such as Shh and Fgfs, which further direct the development of the neighbouring tissues as the thalamus and prethalamus (2,32). Interestingly, our results revealed that in addition of being the primary source of releasing Wnt ligands, such as Wnt3a and Wnt5a, ZLI is also where the two readout genes for canonical Wnt signalling, Axin2 and Lef1, most intensively expressed. This result indicated that although the prevailing notion proposes that organisers do not respond to the morphogens expressed by themselves (2), ZLI at this age might be able to respond to its own canonical Wnt signals. If this is truly the case, it would be extremely intriguing to test how canonical Wnt signalling might interact with ZLI's production of other morphogens such as Shh and Fgfs, and how that might affect the responses of neighbouring tissues to any of these signalling pathways.

Another interesting finding from this study was the expression of Wnt5a in the diencephalon. In the ventricular zone of the diencephalon, the expression pattern of Wnt5a highly correlates with that of Wnt3a's. However, Wnt5a is also expressed in a subset of post-mitotic cells in the prethalamus, which display either no or low levels of Pax6 expression. In the absence of Pax6, not only more prethalamic post-mitotic cells started to express Wnt5a, but also at a higher level. The functions of Wnt5a in the prethalamus remain elusive, and without the information of expression patterns of specific receptor genes for the Wnt signalling pathways, it is difficult to speculate what they might be. WNT5a is normally considered as a non-canonical Wnt ligand. However, in the presence of FZD5, it can also act as a canonical Wnt ligand and induce anterior-posterior axis formation by activating the canonical Wnt signalling pathway (200,206). Based on the unique expression patterns of Wnt5a in the prethalamus, one intriguing idea to propose would be that Wnt5a plays different roles in the progenitor and post-mitotic cells in the prethalamus. Notably, this group of Wnt5a-positive post-mitotic cells resides lateral to the thalamocortical tract in the control embryos. However, the expansion of this group of cells upon Pax6 deletion places them directly in the path of the TCA

in the mutant embryos. Given Wnt5a's involvement in the PCP pathway and directing axon guidance and neurite extension, it would be worthwhile to investigate further whether this elevated Wnt5a expression in the prethalamic post-mitotic cells also contribute to the misformation and misroute of TCA frequently observed in the Pax6 mutants (167).

In this study, we did test the expressions of Fzd5, Fzd7 and Fzd10 by in situ hybridisation. However, the signals were not specific and clear enough for us to distinguish them from the background staining. Therefore, they were not included in this thesis, and other attempts are needed.

5.3.3 Potential impact of upregulated Wnt signalling pathways on the development of the prethalamus (proliferation, the specification of cell fate and PCP pathways)

As we showed that the ventricular zone of the prethalamus is protected from the canonical Wnt signalling under normal conditions, an important question to ask would be why this is the case and what defects would the prethalamus display when canonical Wnt signalling is activated in the prethalamic progenitor cells, as what we saw in our Pax6 conditional knock-outs.

One possibility would be misspecification of cell fates of the prethalamic derivative neurons. As shown in the RNA-seq data, several prethalamic markers showed a drastic decrease of expressions, such as Isl1 (LFC -2.59), Gsx2 (LFC -2.15) and Six3 (LFC -1.3). In contrast, markers for epithalamus (Irx2, LFC 2.10; Robo3, LFC 1.93; Irx1 LFC 1.57), pTh-C and pTh-C derived post-mitotic cells (Gbx2, LFC 1.60; Irx3, LFC 1.24; Lhx2, LFC 0.70; Hs6st3, LFC 1.39; Rora, LFC 0.75), and pTh-R and pTh-R derived post-mitotic cells (Gata3, LFC 2.34; Sox14 LFC 2.39; Gata2 LFC 1.64) were upregulated in the prethalamus when Pax6 is lost (43,47). It would be interesting to see the exact locations of these upregulated expressions of marker genes in the prethalamus.

Canonical Wnt signalling has been shown to promote cell proliferation in various systems (189). Given that the prethalamus has a more differentiated profile than the thalamus at the same age, we wonder whether the specific blockage of canonical Wnt signalling in the progenitor cells of the prethalamus could contribute to that. However, recently published work in the lab has shown that deletion of Pax6 led to more cell cycle exit and less proliferation in the prethalamus, which is opposite to what the thalamus displays under normal conditions (58). Nonetheless, it would be interesting to perform a time course analysis on the expressions of Sfrp2, Dkk3, as well as Wnt3a and the effector genes Axin2 and Lef1, to see if the expressions of the antagonists and changes of expressions of Wnt3a, Axin2 and Lef1 are always restricted to the ventricular zone of the prethalamus. We know that the palmitoylation of the Wnt ligands renders their inability to diffuse far. Thus, Wnt signalling is considered to be effective locally. This also seemed to be the case for the Wnt antagonists such as SFRP2. Therefore, an intriguing hypothesis to propose would be that prethalamic progenitors are protected from Wnt because they are within the range of effect of canonical Wnt secreted from the ZLI, but once they are protected from the canonical Wnt signalling, their post-mitotic derivatives would be ‘immune’ and thus unaffected by the canonical Wnt signalling.

In addition to canonical Wnt signalling, the RNA-seq data also showed dysregulated expressions of components of the planar cell polarity pathways (196). For example, the Wnt ligands know to initiate the PCP pathway (Wnt5a, LFC 0.92; Wnt4, LFC 0.70), and transmembrane adhesive molecule maintaining the polarities (Vangl 2, LFC 0.54; Prickel1, LFC 0.68; Prickel2, LFC 1.16; Dishevelled 3, LFC 0.72; Celsr1, LFC 1.05; Celsr3, LFC 0.72); whereas Frizzled7 showed a -2.14 log2-fold change. The expression patterns of these genes and where their proteins are distributed in the prethalamus need to be determined, to unravel the location of action and disruption of the function of the PCP pathways in the developing prethalamus.

5.4 Summary

In this chapter, we analysed the expression patterns of several Wnt and Wnt-related genes in the E13.5 mouse diencephalon in the presence and absence of Pax6. According to these, we proposed that in the developing prethalamus, Pax6 might be indirectly inhibiting the activities of the Wnt signalling pathways by directly promoting the expressions of Wnt antagonists Sfrp2 and Dkk3.

Chapter 6

Pax6-null prethalamus develops a thalamus-like expression profile of voltage-gated ion channels and AIS component genes

6.1 Introduction

Although the thalamus and prethalamus both reside on either side of the ZLI, hence should receive the same dosages of morphogens released by this secondary organiser, the thalamus and prethalamus exhibit very different developmental profiles and produce neurons with very different morphologies and functions (12,32). The sharp difference of Pax6 expression in the thalamus and prethalamus makes it an excellent candidate to test whether Pax6 can cause this regionally different development of the thalamus and prethalamus.

Thalamic neurons derived from the pTh-C are glutamatergic, which send out long axons that travel through the prethalamus and the ventral telencephalon to innervate the cortex (4,12). Prethalamus-derived neurons, on the other hand, are mostly GABAergic, which develop much shorter axons that only innervate the thalamic nuclei nearby (12,67). Previous studies have pointed out that downregulation of Pax6 expression in the thalamic post-mitotic cells correlates with the time of thalamic axon outgrowth and TCA formation (162). However, whether this downregulation of Pax6 directly causes the rapid outgrowth of TCA remains to be confirmed. Interestingly, my analysis on neuronal morphogenesis showed that, in the absence of Pax6, the prethalamic neurons were able to develop longer neurites, evidenced by both the total length of neurites and length of the longest neurite. This result indicated that at least in the prethalamic neurons, normal expression of Pax6 in the post-mitotic cells might function to limit axon outgrowth and elongation. When Pax6 is removed from the prethalamus, the prethalamic neurons can develop longer axons, raising the possibility that the morphologies of prethalamic neurons resembled that of the thalamic neurons in the absence of Pax6.

In addition, in the absence of Pax6, we observed specific regional upregulation of activities of various Wnt signalling pathways in the prethalamus. Previous studies have identified the determining roles of canonical Wnt signalling in patterning, cell fate specification and transcriptional control of voltage-gated

ion channels in the developing thalamus. Could this ectopic expression of Wnt signalling moved the transcriptome profile of the prethalamus towards that of the thalamus?

What is more, I also discovered that the Pax6-null prethalamic neurons displayed altered structures of the AISs, which were shorter in lengths and located further away from the soma. In the absence of Pax6, these AISs also exhibited higher expression levels of AnkG and voltage-gated Na+ channels. How do the expression levels of these AIS component genes in the prethalamus differ from that in the thalamus in the presence and absence of Pax6?

The RNAseq data in the lab, which analysed the transcriptional changes of genes in the anterior cortex, the thalamus and the prethalamus upon acute deletion of Pax6, provided us with an unbiased starting point to answer the above questions.

Therefore, in Chapter 6, by utilising the existing RNAseq data, I aim to:

1. Test whether the Pax6-null prethalamus develops a thalamus-like expression profile of AIS component genes and voltage-gated ion channels

2. Reveal the potential mechanisms- by assessing whether this is due to the loss of direct transcriptional control of Pax6 or upregulation of Wnt signalling pathway in the prethalamus

6.2 Materials and methods

Heatmap of hierarchical clustering and principal component (PC) analysis were performed by Zrinko Kozić. RNAseq data were from reference (58); the gene list of putative TCF/LEF target genes was from reference (207).

Identification of potential Pax6 target genes was also performed by Zrinko Kozić, using the RNAseq data from reference (58) and ChIP-seq data from reference (150).

6.3 Results

6.3.1 Pax6 deletion in the prethalamus made its expression profile of AIS component genes and voltage-gated ion channels thalamus-like

To find out if deletion of Pax6 in the prethalamus would move its expression profile of AIS component genes and voltage-gated ion channels towards that of the thalamus, I first identified genes included in the GO terms of axon initial segment (GO:0043194), sodium channel activity (GO:0005272), potassium channel activity (GO:0005267) and calcium channel activity (GO:0005262). Then I identified the genes included in the above GO terms, which also showed significant dysregulation of expressions in any of the three pieces of tissues- the anterior cortex (ACtx), thalamus and prethalamus in our RNAseq data, to generate the overlapping genes (marked as red dots in Figure 6.1). After that, we carried out distance-based hierarchical clustering and principal component (PC) analysis specifically on these overlapping genes.

22 genes were included in the GO term of axon initial segment. As shown in Figure 6.1A, in the prethalamus, 6 of them showed significant dysregulation of expression in our RNAseq data and the expression levels of all six genes were upregulated in the prethalamus in the absence of Pax6. A similar situation happened with genes in the GO term of sodium channel activity. A total of 75 genes were included in this GO term, and 9 showed up in our RNAseq data, all of which showed significantly upregulated expression in the prethalamus when Pax6 was lost (Figure 6.1B). In terms of the GO term of potassium channel activity, a total of 160 genes were included in this GO term, and 27 of them showed significant dysregulation of expression in the prethalamus in our RNAseq data. Among these 27 genes, 24 of them were significantly upregulated, and 3 of them were significantly downregulated in the prethalamus following the loss of Pax6 (Figure 6.1C). The GO term of calcium channel activity included the highest number of genes among these four GO terms. 194 genes were included in this GO term, and 25 of them showed significantly dysregulated expressions in the prethalamus in our RNAseq data.

The expression levels of 24 genes were significantly upregulated, whereas the expression of only 1 gene was significantly downregulated in the Pax6-null prethalamus (Figure 6.1D). These results also highlighted an intriguing phenomenon that although Pax6 is expressed by three tissues, the prethalamus is the only one where these genes were almost exclusively upregulated, which could be due to the postmitotic actions of Pax6.

As shown in Figure 6.2A, 6.2C, 6.2E, and 6.2G, the heatmap of hierarchical clustering of the genes in the above four GO terms that were present in our RNA-seq data showed that, regardless of genotype, all six anterior cortical samples clustered together and separated from the diencephalic samples. PC analysis using the same set of genes showed the same trend, as cortical samples always clustered together and separated from the diencephalic sample along the axis of maximum variation, which represented 60%, 75%, 72% and 72% of the variance respectively for the above four GO terms (Figure 6.2B, 6.2D, 6.2F and 6.2H). These results revealed the drastic differences the anterior cortex and the diencephalon displayed in terms of expression profiles of AIS component genes and voltage-gated ion channels, and the loss of Pax6 did not change such differences.

Among the diencephalic samples, distance-based hierarchical clustering showed that the thalamic samples also always cluster together for all four GO terms, regardless of genotype (Figure 6.2A, 6.2C, 6.2E and 6.2G). PC analysis showed the same trend, as thalamic samples always clustered together and separated from the prethalamic control samples along the axis of the second highest variation, which represented 23%, 9%, 12% and 9% of variance respectively for the above four GO terms (Figure 6.2B, 6.2D, 6.2F and 6.2H). This indicated that within the diencephalon, the thalamic and prethalamic neurons also displayed rather different expression profiles of AIS component genes and voltage-gated ion channels, and the loss of Pax6 had little effect on the expression profiles of these genes in the thalamus. Such result was also in concordance with what was shown in Figure 6.1A-D. For all the genes that

were involved in these four GO terms, the thalamus had the least amount of them that showed significantly dysregulated expressions in the absence of Pax6.

However, when Pax6 was removed from the prethalamus, there was a general trend of the prethalamic expression profiles of the genes in these GO-terms to become thalamus-like. This was more obvious in the GO terms of axon initial segment and calcium channel activity. As shown in Figure 6.2A and 6.2G, Pax6-null prethalamic samples were clustered with the thalamic control and Pax6-null samples, and only at the third level in the dendrogram did the Pax6-null prethalamic samples separated from the thalamic samples. PC analysis showed the same results, as the Pax6-null prethalamic samples had moved (having as a reference the position of control prethalamic samples) from one end of the axis of the second highest variation and mixed with the thalamic samples (Figure 6.2B and 6.2H). Genes involved in the other two GO terms-sodium channel activity and potassium channel activity of the Pax6-null prethalamic samples - still clustered better with the control prethalamic samples in the distance-based hierarchical clustering (Figure 6.2C and 6.2E). Their PC analysis showed that same results, as they clustered first with their control counterparts. Nevertheless, the variances of expressions of genes in both of these GO terms displayed by the thalamus and prethalamus were smaller when Pax6 was removed from the prethalamus, as Pax6-null prethalamic samples in these two GO terms showed a trend of moving towards the thalamic samples (they were situated closer to the thalamic samples than the prethalamic controls) (Figure 6.2D and 6.2F).

These results showed that following the loss of Pax6, the variances of expression profiles of the AIS component genes and voltage-gated ion channels in the thalamus and prethalamus became smaller. This indicates that the Pax6-null prethalamus developed a thalamus-like expression profile for genes implicated in axon initial segment and calcium channel activity.

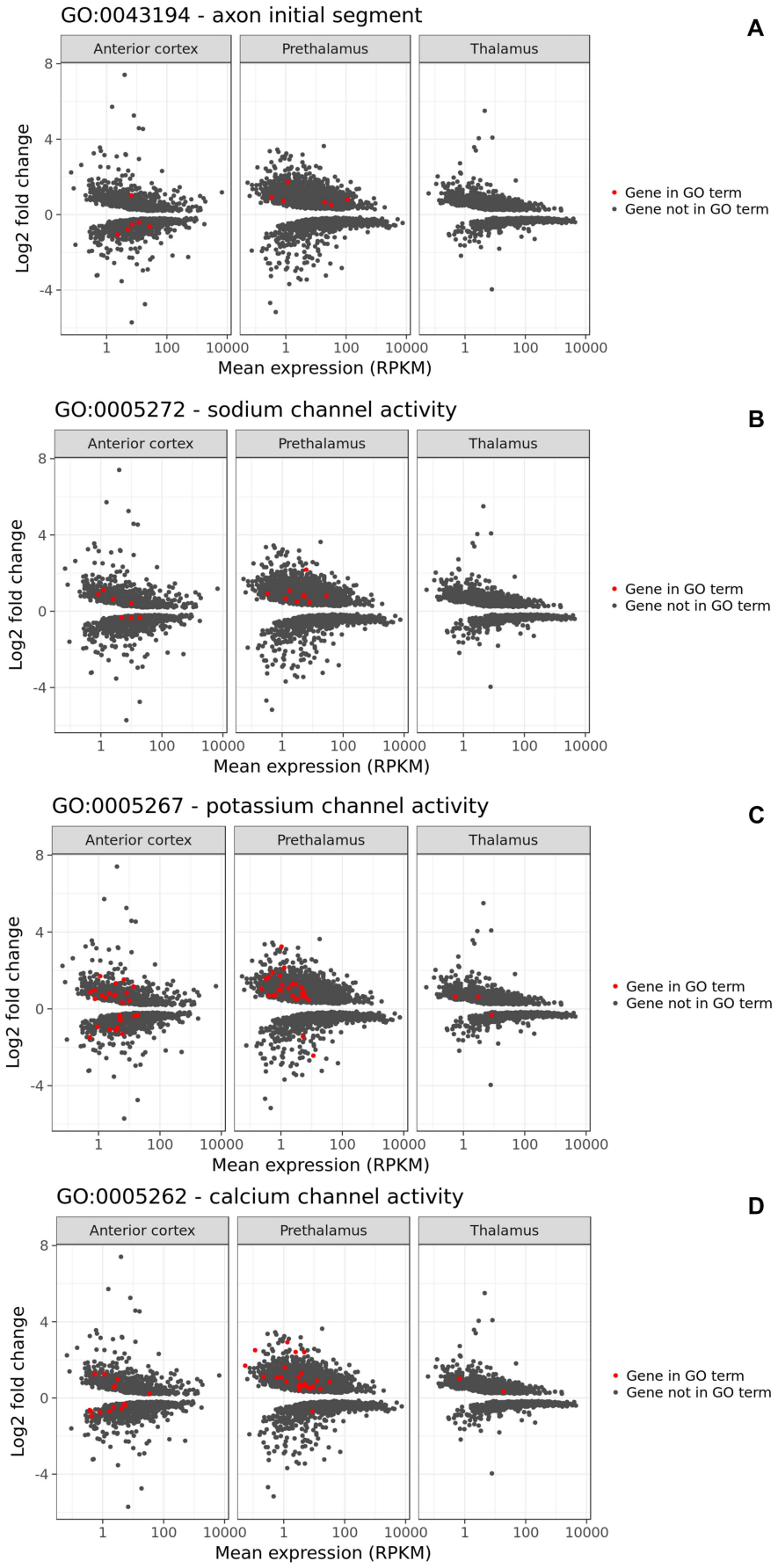
GO:0043194 - axon initial segment
A
Anterior cortex
Prethalamus
Thalamus
Log2 fold change
8
4
0
-4
1
100
10000
Mean expression (RPKM)
Gene in GO term
Gene not in GO term
GO:0005272 - sodium channel activity
B
GO:0005267 - potassium channel activity
C
GO:0005262 - calcium channel activity
D

Figure 6.1 Overlapping genes which are involved in the four GO terms of axon initial segment (A), sodium channel activity (B), potassium channel activity (C) and calcium channel activity (D) that were also significantly dysregulated in the anterior cortex, prethalamus and thalamus in the RNAseq data. All the black dots in the background for each piece of tissue represented all the genes, whose expressions were significantly dysregulated in the absence of Pax6. Each red dot represented one gene that was involved in that specific GO term, but also showed significant dysregulation in any of the three pieces of tissues in the absence of Pax6. **(A)** 6 overlapping genes were seen in the GO terms of axon initial segment; **(B)** 9 overlapping genes were seen in the GO terms of sodium channel activity; **(C)** 27 overlapping genes were seen in the GO terms of potassium channel activity and **(D)** 25 overlapping genes were seen in the GO terms of calcium channel activity.

Axon initial segment

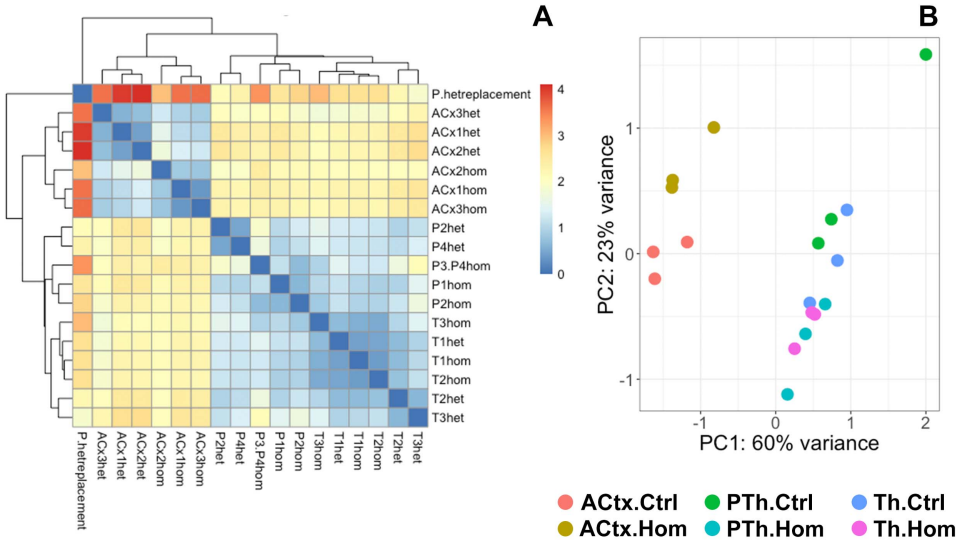

Sodium channels

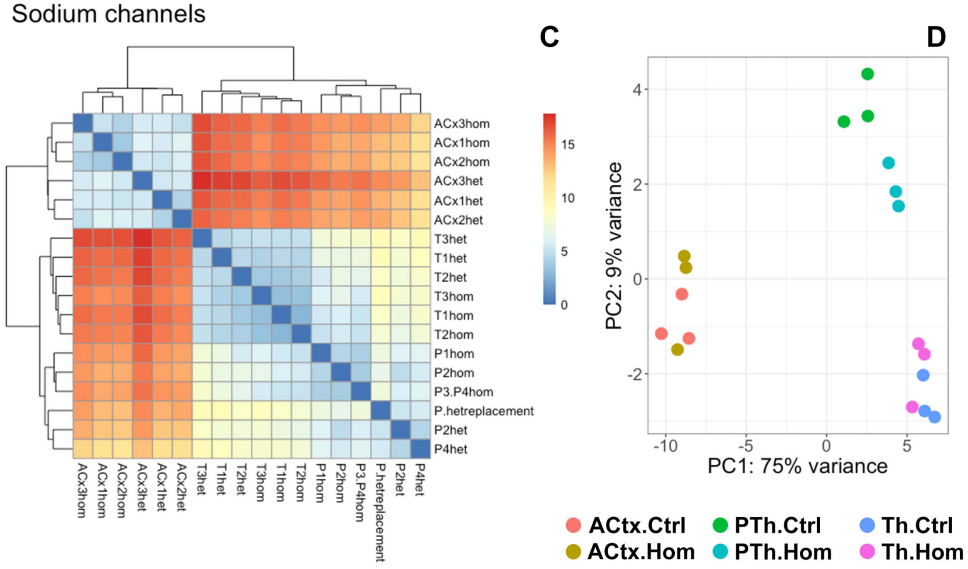

Potassium channels

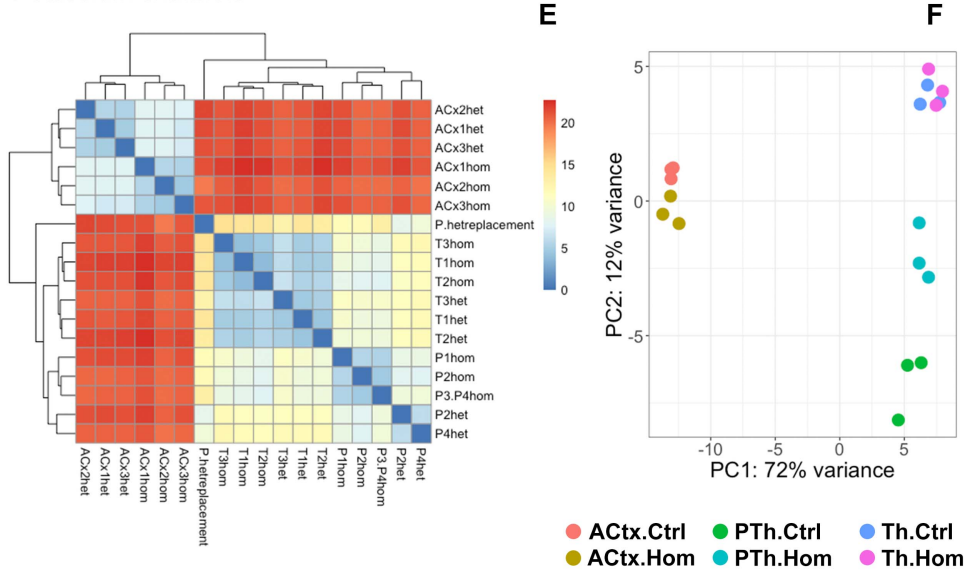

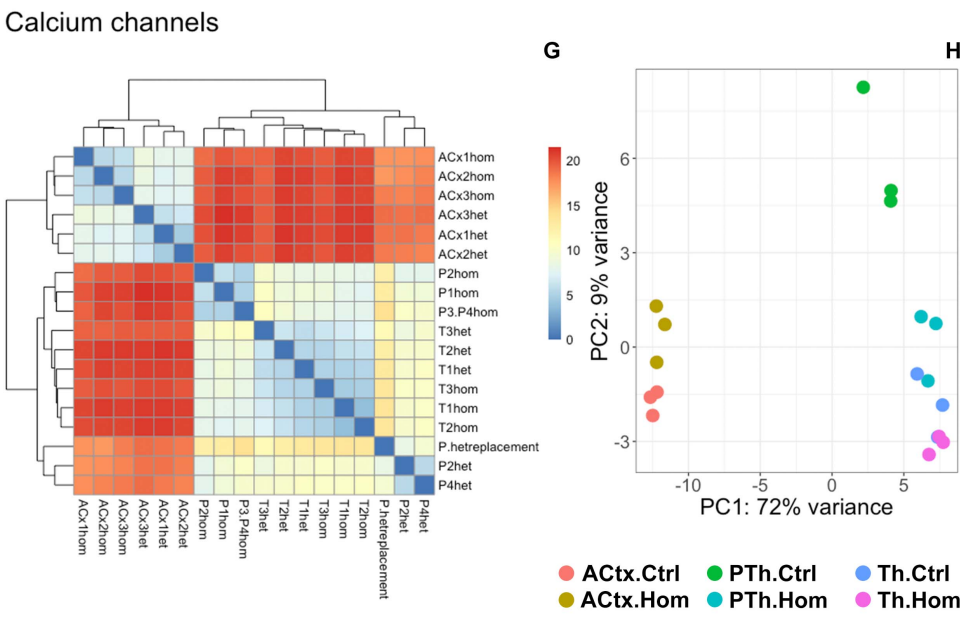

Figure 6.2 Pax6 removal from the prethalamus minimises the variance of expression profiles of AIS component genes and voltage-gated ion channels among the diencephalic tissue. Heatmap of hierarchical clustering of RNAseq data on genes annotated by the “axon initial segment” GO term (GO:0043194), **(A)**; “sodium channel activity” GO term (GO:0005272), **(C)**; “potassium channel activity” GO term (GO:0005267), **(E)**; and “calcium channel activity” GO term (GO:0005262), **(G)**. Principle component (PC) analysis on the same RNAseq data as in (A), (C), (E) and (G).

6.3.2 Increased canonical Wnt activity in the Pax6-null prethalamic cells did not produce a shift towards a thalamic profile in the expression profiles of the putative TCF/LEF-target genes

Various studies have reported the importance of the transcriptional control exerted by canonical Wnt signalling during the development of the thalamus (32,36,38,43). In Chapter 5, we found that the activity of canonical Wnt signalling was significantly upregulated in the ventricular zone of the prethalamus, which could potentially have altered the expression profiles of the prethalamic cells and made them thalamus-like.

To test this possibility, I utilised a data set that specified the 428 putative TCF/LEF target genes expressed in the adult thalamus (207). We crossed this data set with our RNAseq data, identified the overlapping genes and processed them for distance-based hierarchical clustering and PC analysis to compare how their expression changed across the three pieces of tissues in the presence and absence of Pax6.

As shown by Figure 6.3A, expression profiles of these putative TCF/LEF target genes clustered better within tissues, regardless of genotypes. PC analysis showed the same trend, as samples from the same tissues clustered better (Figure 6.3B). The variances of expression profiles of these genes between anterior cortex and the diencephalon (as observed in the axis explaining 62% of the variance) were still much higher than the variances displayed between the thalamus and prethalamus (axis of 22% variance). Although in the absence of Pax6, the expression profiles of these genes in the prethalamus showed a slight shift towards the thalamus, these results indicated that the loss of Pax6 did not alter the expression profiles of these genes to the extent that the prethalamus was becoming thalamus-like as observed before (i.e., for calcium channels or AIS GO terms).

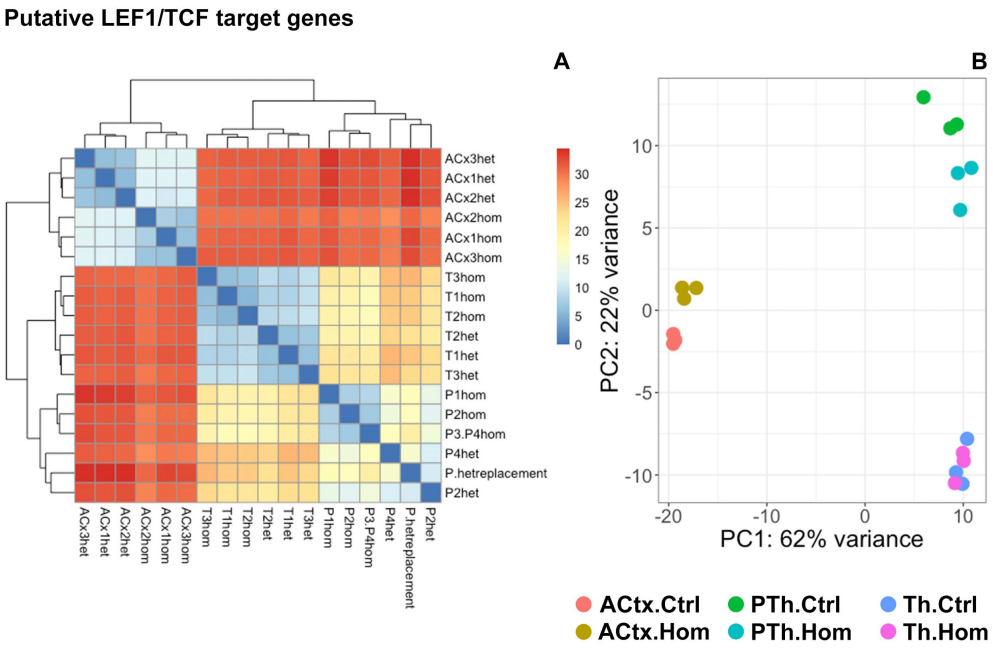

Figure 6.3 Expression profiles of putative TCF/LEF target genes did not show inter-regional changes in the absence of Pax6. (A) Heatmap of hierarchical clustering of RNAseq data on putative TCF/LEF target genes. **(B)** Principal component (PC) analysis on the same RNAseq data as in (A).

6.3.3 Loss of transcriptional control by Pax6 and upregulated canonical Wnt signally together made the Pax6-null prethalamic expression profiles of AIS component genes and voltage-gated ion channels thalamus-like

As a master regulator gene, Pax6 sits high in the hierarchy of gene regulatory networks and functions to control the transcriptions of numerous genes (128,140). To find out if the shift of expression profiles of AIS and calcium channel activity in the Pax6-null prethalamus, which had become thalamus-like, was due to the loss of direct transcriptional control of Pax6 in the prethalamic cells, we first tried to identify putative Pax6 target genes within the genes included in these GO terms.

Putative Pax6 target genes should present one or more Pax6 binding peaks in their sequences. The sequences of these Pax6 binding peaks were discovered and verified by a previous ChIP-seq study using forebrain and lens chromatin from mice (150). The association of Pax6-peaks to the selected genes was carried out using RefSeq annotation. These selected genes were the ones involved in any of the above four GO-terms, which also showed significantly dysregulated expressions in the prethalamus in our RNAseq data. The result showed that 2 of the 6 genes belonging to the axon initial segment GO term showed one or more Pax6 binding peaks. Only 1 of the 9 genes belonging to the sodium channel activity GO term was a putative Pax6 target gene, as it had one Pax6 binding peak. 11 of the 27 genes belonging to the potassium channel activity GO term showed one or more Pax6 binding peaks, whereas 11 out of 25 of the genes belonging to the calcium channel activity showed one or more Pax6 binding peaks.

As mentioned above, the prethalamic expression profile of genes in the GO term of axon initial segment had shifted to become thalamus-like in the absence of Pax6. Interestingly, AnkG, the master regulator gene of AIS formation, was found to be one of the putative Pax6 target genes as two Pax6-binding peaks (Pax6_337 and Pax6_338) were discovered within its gene sequence (Figure 6.4A). AnkG expression in the control prethalamus sample

was the lowest among the three tissues (Figure 6.4B). In the absence of Pax6, the expression level of AnkG in the prethalamus increased drastically and surpassed that in the control thalamus (Figure 6.4B).

Although the Pax6-null prethalamic expression profile of genes in the GO term of calcium channel activity had also become thalamus-like, only one calcium channel component gene, Cacna2d3, was shown to be a putative Pax6 target gene. Cacna2d3 encodes the small subunit of $\alpha 2\delta 3$ of the subfamily 2 (Cav2) of high-voltage-activated calcium channels (208). α2δ subunits are traditionally considered to be auxiliary subunits that enhance channel trafficking, increase the expression of functional calcium channels at the plasma membrane and influence the channels' biophysical properties (209). Previous studies have shown that Cacna2d3 knockout mice showed a deficiency in pain perception and sensory cross-activation, i.e. the activation of a cortical sensory region by input from another modality due to reorganisation in the brain such as after a sensory loss (208). Cacna2d3 was the only gene belonging to the calcium channel activity GO term, whose expression level was downregulated in our RNAseq data. More interestingly, the expression level of Cacna2d3 was the highest in the prethalamus among the three tissues in the control embryos. In the absence of Pax6, its expression level dropped to approach that in control thalamic tissues (Figure 6.4C).

Voltage-gated calcium channels are formed as a complex of α1 subunits, which forms the Ca2+ conducting pore, and other different subunits such as α2δ, β1-4, and γ. Based on the specific α1 subunits, the voltage-gated calcium channels can be divided into high-voltage-activated (HVA) and low-voltage-activated (LVA) calcium channels (210). The α2δ subunits as mention above associate only with HVA calcium channels (208,209). The T-type low-threshold Ca2+ channels, which mediate low-threshold calcium spikes and rebound firing, are typical representatives of the LVA calcium channels (209,210). Interestingly, the expression of the Cacna1g gene was one of the most upregulated in the Pax6-null prethalamus among the genes in the GO term of

calcium channel activity. The Cacna1g gene encodes the α1 subunit of a T-type, low-voltage activated calcium channel (209,210). As shown in Figure 6.4D, the expression levels of Cacna1g were low in control cortex and prethalamus. However, in the absence of Pax6, the expression level of Cacna1g in the prethalamus increased dramatically and was at similar levels to that in the control and Pax6-null thalamus. No Pax6 binding sites were found associated with the Cacna1g gene. However, Cacna1g is a known canonical Wnt target gene and it is highly expressed in the thalamic neurons of the mouse and rat adult brain (190,207).

These results indicated that the shift of Pax6-null prethalamic expression profiles of genes involved in axon initial segment and calcium channel activity towards thalamus-like might be due to a combined effect of loss of transcriptional control of Pax6 and activated canonical Wnt signalling.

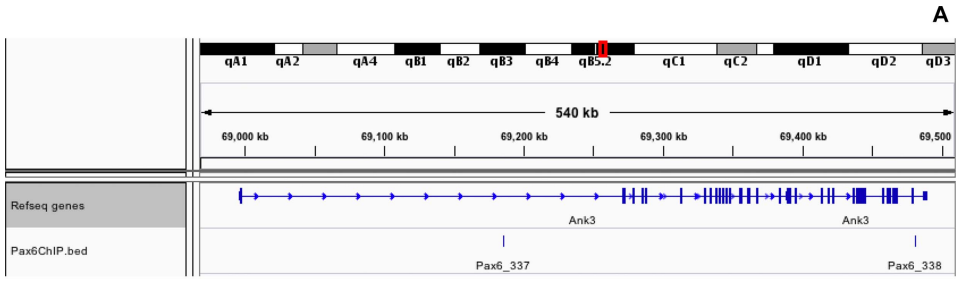
A
qA1
qA2
qA4
qB1
qB2
qB3
qB4
qB5.2
qC1
qC2
qD1
qD2
qD3
540 kb
69,000 kb
69,100 kb
69,200 kb
69,300 kb
69,400 kb
69,500
Refseq genes
Ank3
Ank3
Pax6ChIP.bed
Pax6_337
Pax6_338

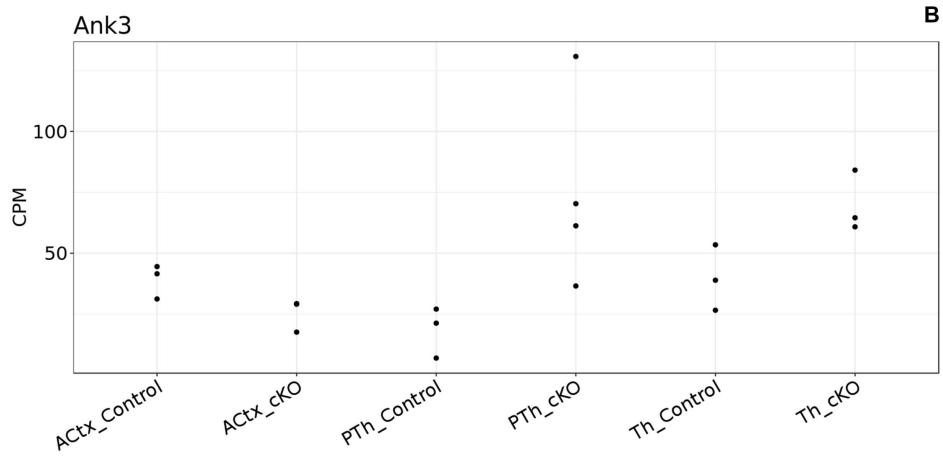
B
Ank3
CPM
100
50
ACtx_Control
ACtx_cKO
PTh_Control
PTh_cKO
Th_Control
Th_cKO

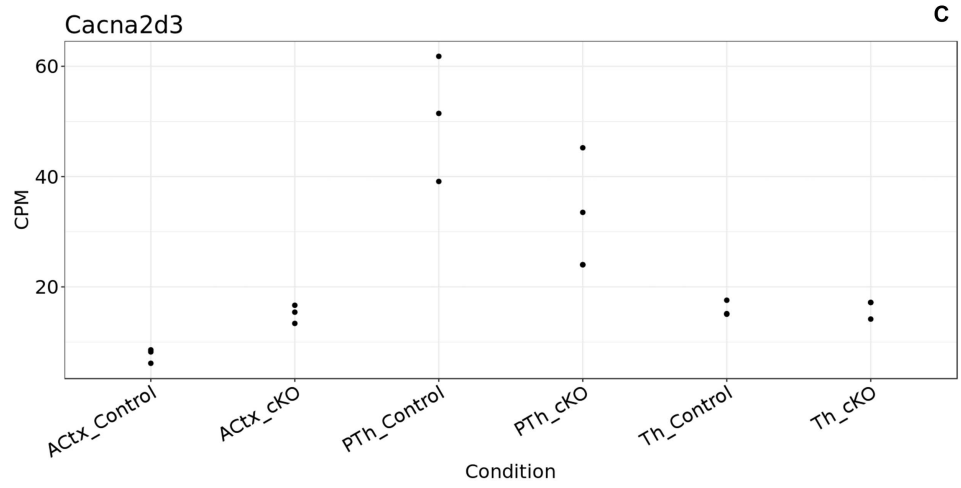
C
Cacna2d3
CPM
60
40
20
ACtx_Control
ACtx_cKO
PTh_Control
PTh_cKO
Th_Control
Th_cKO
Condition

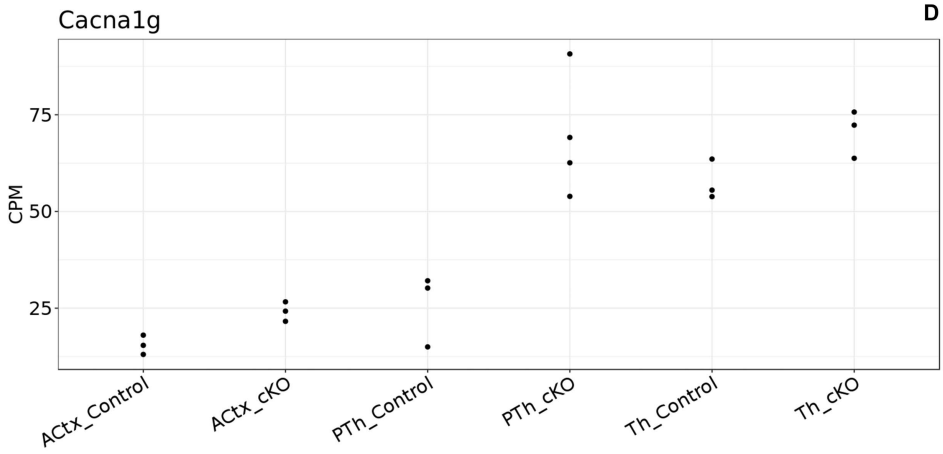
D
Cacna1g
CPM
75
50
25
ACtx_Control
ACtx_cKO
PTh_Control
PTh_cKO
Th_Control
Th_cKO

Figure 6.4 Changes of expression levels of putative Pax6 and canonical Wnt target genes in the anterior cortex, the prethalamus and thalamus in the absence of Pax6. (A) RefSeq annotation showed two Pax6-binding peaks, Pax6_337 and Pax6_338 within the AnkG (also known as Ank3) gene. Noted that neither of these binding sites are within the promotor region. **(B)** Expression levels of AnkG in the anterior cortex, the prethalamus and thalamus. The expression level of AnkG in the prethalamus under control condition was the lowest among the three pieces of tissues. In the absence of Pax6, its expression level had increased and surpassed that in the thalamic samples. **(C)** Cacna2d3 is another putative Pax6 target gene with one Pax6-binding peaks. Expression of Cacna2d3 under the control condition was the highest in the prethalamus among the three tissues. In the absence of Pax6, the expression level of Cacna2d3 had dropped to approach the expression levels in the thalamic tissues. **(D)** Cacna1g is a canonical Wnt target gene, whose expression were highest in the thalamus under control condition. In the absence of Pax6, the expression levels of Cacna1g in the prethalamus had increased to reach a similar level as that in the thalamic samples.

6.4 Discussion

In this chapter, by utilising the existing RNAseq data, we proved that the prethalamic expression profiles of genes in the GO terms of axon initial segment and calcium channel activity had become thalamus-like in the absence of Pax6. Such results supported our hypothesis that the distinct expression patterns of Pax6 in the thalamus and prethalamus helped to maintain the regional variances between these two pieces of tissues in certain ways during development. Additionally, we identified novel putative Pax6 target genes, such as AnkG, Cacna2d3 and genes encoding for subunits of the voltage-gated potassium channels. These genes are strongly associated with neuronal differentiation and function and their expression levels contribute to the characteristics of the electrophysiology profiles of the neurons. These findings revealed potential novel functions and direct transcriptional control of Pax6 in the postmitotic neurons of the prethalamus, and also mechanisms underlying regional differential development.

Another exciting finding generated by the distance-based hierarchical clustering and PC analysis was the sharp variances of expression profiles of the genes in the GO terms of axon initial segment and voltage-gated ion channels between the cortex and the diencephalon. Besides, Pax6 did probably not play a role in creating such differences as the loss of Pax6 did not change these expression profiles in the anterior cortex in any significant way. Therefore, an intriguing question to ask would be, if the differential expression of Pax6 underlies the distinct expression profiles of the axon initial segment and calcium channel activity between the thalamus and prethalamus, which transcription factors directed such different expression profiles between the cortex and diencephalon?

Another critical question to ask is why is it essential for a cortical neuron to be so different from a diencephalic neuron, and a thalamic neuron from a prethalamic neuron, in terms of the expression of genes that shape their

electrophysiological characteristics? Moreover, how does that contribute to neural circuitry formation and the functionality of the nervous system?

Take the thalamic and prethalamic neurons as examples. Previous studies have indicated that all thalamic neurons can fire in both the tonic and bursting mode, whereas prethalamus-derived neurons can fire either only in tonic mode or in both modes (67,103). However, as most of the studies analysed the electrophysiology properties of only one type of neuron, it was difficult to compare precisely how differently the neurons from the thalamus and prethalamus respond to external stimuli. From our RNAseq data, we could see that the control prethalamus at E13.5 expressed rather low levels of axon initial segment component genes and various genes encoding for voltage-gated ion channel subunits. The presence of Pax6 in the prethalamic post-mitotic cells thus seemed to restrict the expression of these genes. In the absence of Pax6, the expressions of axon initial segment component genes, subunits for voltage-gated Na+ and K+ channels and T-type low-threshold Ca2+ channels were upregulated, indicating that these Pax6-null prethalamic cells are probably more excitable and can adapt more to the burst firing mode. It would be exciting if I can verify this with in vivo electrophysiological recording.

Additionally, it will also be extremely intriguing to observe how Pax6-null mice with more excitable prethalamus-derived neurons behave. With my current experimental setup, it was not possible to generate Pax6-knockout mice postnatally. This was mainly due to the devastating effects of the loss of Pax6 in proliferating cells (E9.5). However, pilot experiments have shown that if I double the concentration of tamoxifen and apply that to the pregnant FP6CD1 females at E13.5 by oral gavage, the embryos will survive beyond P0. Mice generated this way could be optimal for us to study more about the functions of Pax6 in post-mitotic neurons, and how its absence might impact the excitability of the prethalamic neurons, the functionality of the nervous systems and the behaviour of the animals.

6.5 Summary

In this chapter, we discovered that in the absence of Pax6, the prethalamic expression profiles of genes in the GO terms of axon initial segment and calcium channel activity had become thalamus-like, due to the loss of transcriptional control of Pax6 and activated canonical Wnt signalling in the prethalamus.

Concluding remarks

The functions of Pax6 in the developing prethalamus

In this study, I was able to characterise various defects in the developing mouse prethalamus when Pax6 is lost. On the cellular level, acute deletion of Pax6 resulted in increased axon and neurite elongation of the prethalamic neurons. On the subcellular level, absence of Pax6 resulted in alteration of the structure and components of the axon initial segments of the prethalamic neurons. On the tissue level, loss of Pax6 resulted in upregulated canonical Wnt activity specifically in the ventricular zone of the prethalamus. On the transcriptome level, loss of Pax6 caused the prethalamic expression profiles of AIS components and voltage-gated Ca2+ channels to become thalamus-like.

By combining these results with the information from the RNAseq data, I propose that in normal conditions, Pax6 plays the following roles during prethalamic development. By directly or indirectly inhibiting the expression of cytoskeletal effector genes, Pax6 functions to restrict axon and neurite elongation during neuronal morphogenesis of the prethalamic neurons. By directly controlling the transcription of genes such as AnkG and Cacna2d3, and indirectly controlling the transcription of various subunits of voltage-gated Na+, K+ and Ca2+ channels, Pax6 might thus control the formation and structure of the AIS and have further impacts on the electrophysiological properties of the prethalamic neurons. In the ventricular zone of the prethalamus, by activating the expressions of Wnt antagonist genes Sfrp2 and Dkk3, Pax6 probably shields the prethalamic ventricular zone from the activity of canonical Wnt signalling. Active canonical Wnt signalling is essential for the normal development of the thalamus. In the postnatal thalamic neurons, canonical Wnt signalling also functions to control the expressions of voltage-gated ion channels, neurotransmitter receptors, synaptic vesicle proteins and so on. Many of the genes involved in these processes are exclusive to the

thalamic neurons. I have reported how the transcriptome profile of some of those genes in the prethalamus moves towards that of the thalamus in the absence of Pax6. This could be due to the combined effects of loss of transcriptional control by Pax6 and upregulated activity of the canonical Wnt signalling. In any case it indicates that Pax6 is crucial for specifying some characteristic of postmitotic prethalamic cells, especially those that make them different from thalamic neurons.

My results not only revealed novel functions of the transcription factor Pax6 in post-mitotic cells of the prethalamus, but also provided a plausible mechanism of the differential inter-regional development of the CNS.

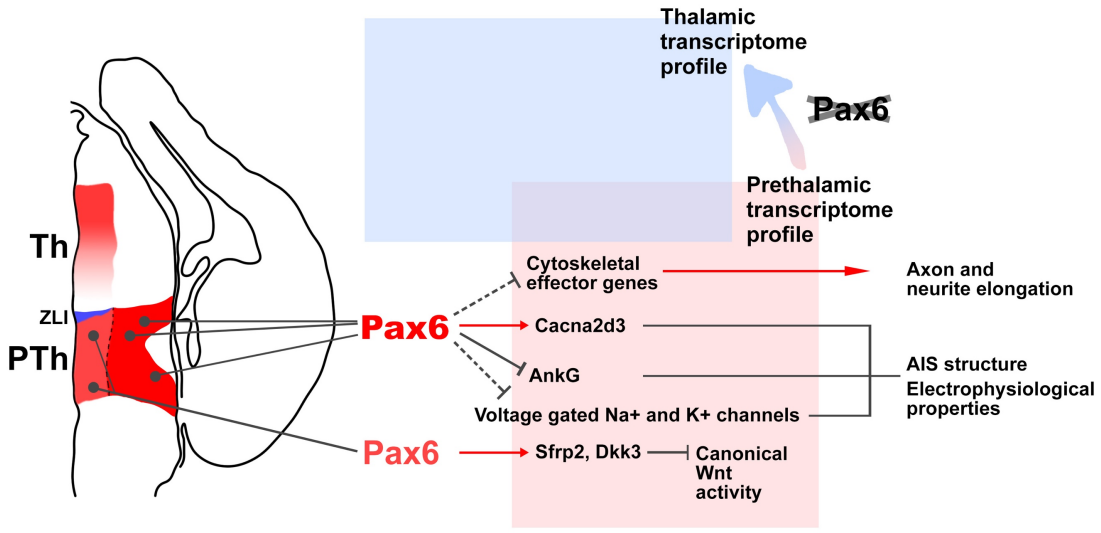

Figure 7.1 Transcriptional control of Pax6 and its various functions during prethalamic development. On the left is a schematic representation of the coronal view of half of the neural tube. The expression pattern of Pax6 is marked with regions of different colors. Pax6 expression in the thalamus is restricted to the ventricular zone, which displays a gradient that increases with distance from the ZLI. The ZLI is marked with a thin blue wedge. Pax6 expression in the prethalamus can be found in both the ventricular zone, and a subset of neurons in the mantle zone. The ventricular zone and the mantle zone are separated by a dash line. The intensity of Pax6 expression varies in the ventricular zone and the mantle zone, as the latter displays higher levels of Pax6 expression than the ventricular zone. Therefore, the presence of Pax6 in the mantle zone is presented by bolder letters than that in the ventricular zone. In the post-mitotic prethalamic cells, Pax6 can either directly or indirectly control the expressions of cytoskeletal effector genes. Many of these genes found in our RNAseq data, which show significantly dysregulated expression in the prethalamus when Pax6 is lost, can enhance axon and neurite elongation. Pax6 might also be able to directly bind to AnkG and Cacna2d3, or indirectly control the expressions of subunits of voltage-gated Na+ and K+ channels. All these genes can affect the structures of the AIS and the electrophysiological properties of the prethalamic neurons. In the prethalamic ventricular zone, where the level of Pax6 expression is slightly lower than that in the prethalamic mantle zone, Pax6 directly regulates the expressions of Sfrp2 and Dkk3, which function to antagonise the canonical Wnt activity in the prethalamus. The expressions of Pax6, together with all these direct and indirect target genes, compose the unique prethalamic transcriptome profile (represented by the pink rectangle). The thalamic transcriptome profile (represented by the light blue rectangle) overlaps with the pink rectangle as some genes are expressed by both tissues during development. In the absence of Pax6, the prethalamic transcriptome profile shifts and becomes thalamus-like, especially for genes involved in the GO terms of axon initial segment and calcium channel activities.

Future directions

With the results obtained in this thesis, I have achieved my original aim for this study, which was to shed light on the functions of Pax6 in the prethalamic post-mitotic cells. However, questions remain. Firstly, what are the mechanisms that maintain the expression and functions of Pax6 in the prethalamic post-mitotic cells? Secondly, the prethalamic post-mitotic cells express Pax6 at a higher level than the progenitor cells. How is this achieved and why is this the case? Thirdly, in a previous study, Zhang et al. found that in adult ocular tissues (cornea, lens and retina), the ratio of Pax6 transcript and Pax6(5a) transcript had decreased from 8:1, as observed in the embryonic tissues, to 1:1. Recent publication in the lab showed that the in the embryonic prethalamus, the average ratio of Pax6 against Pax6(5a) is around 9:1. Is there also a change of ratio between the Pax6 isoforms when prethalamic progenitor cells become post-mitotic? Fourthly, my previous attempts to delete Pax6 only in the post-mitotic cells had proven that the expression of Pax6 in the post-mitotic cells were much more persistent than that in the progenitor cells. For example, with the same animal model, administration of tamoxifen at E9.5 would result in Pax6 deletion in 80-90% of all the cells at around E11.5. However, Pax6 expression in the prethalamic post-mitotic cells was still present at postnatal day 0 (P0) if I administrate tamoxifen at E13.5. The underlying mechanisms for this remain elusive.

These are all questions worth pursuing, the answers to which will help us better understand the mechanisms of brain development controlled by the master regulator gene Pax6 and the genetic networks it is involved in.

References:

1. Price DJ, Jarman AP, Mason JO, Kind PC. Building brains: an introduction to neural development. John Wiley & Sons; 2017.
2. Scholpp S, Lumsden A. Building a bridal chamber: development of the thalamus. Trends Neurosci. 2010;33(8):373–80.
3. Puelles L, Harrison M, Paxinos G, Watson C. A developmental ontology for the mammalian brain based on the prosomeric model. Trends Neurosci. 2013;36(10):570–8.
4. Gezelius H, López-Bendito G. Thalamic neuronal specification and early circuit formation. Dev Neurobiol. 2017;77(7):830–43.
5. Lim Y, Golden JA. Patterning the developing diencephalon. Brain Res Rev. 2007;53(1):17–26.
6. Chen L, Guo Q, Li JYH. Transcription factor Gbx2 acts cell-nonautonomously to regulate the formation of lineage-restriction boundaries of the thalamus. Development. 2009;136(8):1317–26.
7. Crick F, Koch C. A framework for consciousness. Nat Neurosci. 2003;6(2):119.
8. Martinez-Ferre A, Martinez S. Molecular regionalization of the diencephalon. Front Neurosci. 2012;6:73.
9. Coscia DM, Narr KL, Robinson DG, Hamilton LS, Sevy S, Burdick KE, et al. Volumetric and shape analysis of the thalamus in first-episode schizophrenia. Hum Brain Mapp. 2008/06/24. 2009;30(4):1236–45.
10. Copp AJ, Greene NDE, Murdoch JN. The genetic basis of mammalian neurulation. Nat Rev Genet. 2003;4(10):784.
11. Kiecker C, Lumsden A. The role of organizers in patterning the nervous system. Annu Rev Neurosci. 2012;35:347–67.
12. Martinez-Ferre A, Martinez S. Molecular regionalization of the diencephalon. Front Neurosci. 2012/06/02. 2012;6:73.
13. Rubenstein JL, Martinez S, Shimamura K, Puelles L. The embryonic vertebrate forebrain: the prosomeric model. Science (80-). 1994/10/28. 1994;266(5185):578–80.
14. Puelles L, Rubenstein JLR. Forebrain gene expression domains and the evolving prosomeric model. Trends Neurosci. 2003;26(9):469–76.
15. Puelles L. Brain segmentation and forebrain development in amniotes. Brain Res Bull. 2001;55(6):695–710.
16. Kataoka A, Shimogori T. Fgf8 controls regional identity in the developing thalamus. Development. 2008;135(17):2873–81.
17. Kiecker C, Lumsden A. Compartments and their boundaries in vertebrate brain development. Nat Rev Neurosci. 2005;6(7):553.
18. Bell E, Ensini M, Gulisano M, Lumsden A. Dynamic domains of gene expression in the early avian forebrain. Dev Biol. 2001;236(1):76–88.
19. Larsen CW, Zeltser LM, Lumsden A. Boundary formation and compartition in the avian diencephalon. J Neurosci. 2001;21(13):4699–711.
20. Echevarría D, Vieira C, Gimeno L, Martínez S. Neuroepithelial secondary organizers and cell fate specification in the developing brain. Brain Res Rev. 2003;43(2):179–91.

21. Vieira C, Pombero A, Garcia-Lopez R, Gimeno L, Echevarria D, Martínez S. Molecular mechanisms controlling brain development: an overview of neuroepithelial secondary organizers. Int J Dev Biol. 2010;54(1):7–20.
22. Caballero IM, Manuel MN, Molinek M, Quintana-Urzainqui I, Mi D, Shimogori T, et al. Cell-autonomous repression of Shh by transcription factor Pax6 regulates diencephalic patterning by controlling the central diencephalic organizer. Cell Rep. 2014/09/02. 2014;8(5):1405–18.
23. Shimamura K, Hartigan DJ, Martinez S, Puelles L, Rubenstein JL. Longitudinal organization of the anterior neural plate and neural tube. Development. 1995;121(12):3923–33.
24. Kiecker C, Lumsden A. Hedgehog signaling from the ZLI regulates diencephalic regional identity. Nat Neurosci. 2004;7(11):1242–9.
25. Hirata T, Nakazawa M, Muraoka O, Nakayama R, Suda Y, Hibi M. Zinc-finger genes Fez and Fez-like function in the establishment of diencephalon subdivisions. Development. 2006;133(20):3993–4004.
26. Scholpp S, Foucher I, Staudt N, Peukert D, Lumsden A, Houart C. Otx1l, Otx2 and Irx1b establish and position the ZLI in the diencephalon. Development. 2007;134(17):3167–76.
27. Scholpp S, Wolf O, Brand M, Lumsden A. Hedgehog signalling from the zona limitans intrathalamica orchestrates patterning of the zebrafish diencephalon. Development. 2006;133(5):855–64.
28. Martinez-Ferre A, Navarro-Garberi M, Bueno C, Martinez S. Wnt signal specifies the intrathalamic limit and its organizer properties by regulating Shh induction in the alar plate. J Neurosci. 2013;33(9):3967–80.
29. Mattes B, Weber S, Peres J, Chen Q, Davidson G, Houart C, et al. Wnt3 and Wnt3a are required for induction of the mid-diencephalic organizer in the caudal forebrain. Neural Dev. 2012;7(1):12.
30. Chambers D, Wilson L, Maden M, Lumsden A. RALDH-independent generation of retinoic acid during vertebrate embryogenesis by CYP1B1. Development. 2007;134(7):1369–83.
31. Guinazu MF, Chambers D, Lumsden A, Kiecker C. Tissue interactions in the developing chick diencephalon. Neural Dev. 2007;2:25.
32. Hagemann AIH, Scholpp S. The tale of the three brothers–Shh, Wnt, and Fgf during development of the thalamus. Front Neurosci. 2012;6:76.
33. Vue TY, Bluske K, Alishahi A, Yang LL, Koyano-Nakagawa N, Novitch B, et al. Sonic hedgehog signaling controls thalamic progenitor identity and nuclei specification in mice. J Neurosci. 2009;29(14):4484–97.
34. Gómez-Skarmeta JL, Modolell J. < i> Iroquois</i> genes: genomic organization and function in vertebrate neural development. Curr Opin Genet Dev. 2002;12(4):403–8.
35. Vue TY, Aaker J, Taniguchi A, Kazemzadeh C, Skidmore JM, Martin DM, et al. Characterization of progenitor domains in the developing mouse thalamus. J Comp Neurol. 2007;505(1):73–91.
36. Bluske KK, Vue TY, Kawakami Y, Taketo MM, Yoshikawa K, Johnson JE, et al. β-Catenin signaling specifies progenitor cell identity in parallel

with Shh signaling in the developing mammalian thalamus. Development. 2012;dev-072314.
37. Daneman R, Agalliu D, Zhou L, Kuhnert F, Kuo CJ, Barres BA. Wnt/β-catenin signaling is required for CNS, but not non-CNS, angiogenesis. Proc Natl Acad Sci. 2009;106(2):641–6.
38. Bluske KK, Kawakami Y, Koyano-Nakagawa N, Nakagawa Y. Differential activity of Wnt/β-catenin signaling in the embryonic mouse thalamus. Dev Dyn. 2009;238(12):3297–309.
39. Braun MM, Etheridge A, Bernard A, Robertson CP, Roelink H. Wnt signaling is required at distinct stages of development for the induction of the posterior forebrain. Development. 2003;130(23):5579–87.
40. Maretto S, Cordenonsi M, Dupont S, Braghetta P, Broccoli V, Hassan AB, et al. Mapping Wnt/β-catenin signaling during mouse development and in colorectal tumors. Proc Natl Acad Sci. 2003;100(6):3299–304.
41. Quinlan R, Graf M, Mason I, Lumsden A, Kiecker C. Complex and dynamic patterns of Wnt pathway gene expression in the developing chick forebrain. Neural Dev. 2009;4(1):35.
42. Kim AS, Anderson SA, Rubenstein JL, Lowenstein DH, Pleasure SJ. Pax-6 regulates expression of SFRP-2 and Wnt-7b in the developing CNS. J Neurosci. 2001;21(5):RC132.
43. Lee M, Yoon J, Song H, Lee B, Lam DT, Yoon J, et al. Tcf7l2 plays crucial roles in forebrain development through regulation of thalamic and habenular neuron identity and connectivity. Dev Biol. 2017;424(1):62–76.
44. Suzuki-Hirano A, Shimogori T. The role of Fgf8 in telencephalic and diencephalic patterning. Semin Cell Dev Biol. 2009/07/15. 2009;20(6):719–25.
45. Mueller T, Wullimann M. Atlas of early zebrafish brain development: a tool for molecular neurogenetics. Academic Press; 2015.
46. Wang L, Bluske KK, Dickel LK, Nakagawa Y. Basal progenitor cells in the embryonic mouse thalamus-their molecular characterization and the role of neurogenins and Pax6. Neural Dev. 2011;6(1):1–19.
47. Suzuki-Hirano A, Ogawa M, Kataoka A, Yoshida AC, Itoh D, Ueno M, et al. Dynamic spatiotemporal gene expression in embryonic mouse thalamus. J Comp Neurol. 2011;519(3):528–43.
48. Ono K, Clavairoly A, Nomura T, Gotoh H, Uno A, Armant O, et al. Development of the prethalamus is crucial for thalamocortical projection formation and is regulated by Olig2. Development. 2014;141(10):2075–84.
49. Nakagawa Y, O'Leary DDM. Combinatorial expression patterns of LIM-homeodomain and other regulatory genes parcellate developing thalamus. J Neurosci. 2001;21(8):2711–25.
50. Shimogori T, Lee DA, Miranda-Angulo A, Yang Y, Wang H, Jiang L, et al. A genomic atlas of mouse hypothalamic development. Nat Neurosci. 2010;13(6):767.
51. Virolainen S-M, Achim K, Peltopuro P, Salminen M, Partanen J. Transcriptional regulatory mechanisms underlying the GABAergic neuron fate in different diencephalic prosomeres. Development.

2012;139(20):3795–805.
52. Li Z, Pratt T, Price DJ. Zic4-lineage cells increase their contribution to visual thalamic nuclei during murine embryogenesis if they are homozygous or heterozygous for loss of Pax6 function. eNeuro. 2018;5(5).
53. Horng S, Kreiman G, Ellsworth C, Page D, Blank M, Millen K, et al. Differential gene expression in the developing lateral geniculate nucleus and medial geniculate nucleus reveals novel roles for Zic4 and Foxp2 in visual and auditory pathway development. J Neurosci. 2009/10/30. 2009;29(43):13672–83.
54. Bulfone A, Puelles L, Porteus MH, Frohman MA, Martin GR, Rubenstein JL. Spatially restricted expression of Dlx-1, Dlx-2 (Tes-1), Gbx-2, and Wnt-3 in the embryonic day 12.5 mouse forebrain defines potential transverse and longitudinal segmental boundaries. J Neurosci. 1993;13(7):3155–72.
55. Mallika C, Guo Q, Li JYH. Gbx2 is essential for maintaining thalamic neuron identity and repressing habenular characters in the developing thalamus. Dev Biol. 2015;407(1):26–39.
56. Miyashita-Lin EM, Hevner R, Wassarman KM, Martinez S, Rubenstein JLR. Early neocortical regionalization in the absence of thalamic innervation. Science (80-). 1999;285(5429):906–9.
57. Sunnen CN, Simonet JC, Marsh ED, Golden JA. Arx is required for specification of the zona incerta and reticular nucleus of the thalamus. J Neuropathol Exp Neurol. 2014;73(3):253–61.
58. Quintana-Urzainqui I, Kozić Z, Mitra S, Tian T, Manuel M, Mason JO, et al. Tissue-specific actions of Pax6 on the balance of proliferation and differentiation in developing forebrain are Foxg1-dependent. iScience. 2018;
59. Clegg JM, Li Z, Molinek M, Caballero IM, Manuel MN, Price DJ. Pax6 is required intrinsically by thalamic progenitors for the normal molecular patterning of thalamic neurons but not the growth and guidance of their axons. Neural Dev. 2015;10(1):26.
60. Feng J, Xian Q, Guan T, Hu J, Wang M, Huang Y, et al. Celsr3 and Fzd3 organize a pioneer neuron scaffold to steer growing thalamocortical axons. Cereb Cortex. 2016;26(7):3323–34.
61. Achim K, Salminen M, Partanen J. Mechanisms regulating GABAergic neuron development. Cell Mol life Sci. 2014;71(8):1395–415.
62. Chattopadhyaya B, Di Cristo G, Wu CZ, Knott G, Kuhlman S, Fu Y, et al. GAD67-mediated GABA synthesis and signaling regulate inhibitory synaptic innervation in the visual cortex. Neuron. 2007;54(6):889–903.
63. Newman EA, Wu D, Taketo MM, Zhang J, Blackshaw S. Canonical Wnt signaling regulates patterning, differentiation and nucleogenesis in mouse hypothalamus and prethalamus. Dev Biol. 2018;442(2):236–48.
64. Vitalis T, Cases O, Engelkamp D, Verney C, Price DJ. Defects of tyrosine hydroxylase-immunoreactive neurons in the brains of mice lacking the transcription factor Pax6. J Neurosci. 2000;20(17):6501–16.
65. Hans J, Lammens M, Cruysberg JRM, Hori A, Shiota K, Verbist B. Development and developmental disorders of the forebrain. Clinical

Neuroembryology. Springer; 2006.
66. Inamura N, Ono K, Takebayashi H, Zalc B, Ikenaka K. Olig2 lineage cells generate GABAergic neurons in the prethalamic nuclei, including the zona incerta, ventral lateral geniculate nucleus and reticular thalamic nucleus. Dev Neurosci. 2011;33(2):118–29.
67. Pinault D. The thalamic reticular nucleus: structure, function and concept. Brain Res Rev. 2004;46(1):1–31.
68. Duan D, Fu Y, Paxinos G, Watson C. Spatiotemporal expression patterns of Pax6 in the brain of embryonic, newborn, and adult mice. Brain Struct Funct. 2013;218(2):353–72.
69. Da Silva JS, Dotti CG. Breaking the neuronal sphere: regulation of the actin cytoskeleton in neuritogenesis. Nat Rev Neurosci. 2002;3(9):694.
70. Flynn KC. The cytoskeleton and neurite initiation. Bioarchitecture. 2013;3(4):86–109.
71. Sainath R, Gallo G. Cytoskeletal and signaling mechanisms of neurite formation. Cell Tissue Res. 2015;359(1):267–78.
72. Witte H, Bradke F. The role of the cytoskeleton during neuronal polarization. Curr Opin Neurobiol. 2008;18(5):479–87.
73. Stiess M, Bradke F. Neuronal polarization: the cytoskeleton leads the way. Dev Neurobiol. 2011;71(6):430–44.
74. Noctor SC, Martínez-Cerdeño V, Ivic L, Kriegstein AR. Cortical neurons arise in symmetric and asymmetric division zones and migrate through specific phases. Nat Neurosci. 2004;7(2):136.
75. Hand R, Bortone D, Mattar P, Nguyen L, Heng JI-T, Guerrier S, et al. Phosphorylation of Neurogenin2 specifies the migration properties and the dendritic morphology of pyramidal neurons in the neocortex. Neuron. 2005;48(1):45–62.
76. Tabata H, Nakajima K. Multipolar migration: the third mode of radial neuronal migration in the developing cerebral cortex. J Neurosci. 2003;23(31):9996–10001.
77. Lowery LA, Van Vactor D. The trip of the tip: understanding the growth cone machinery. Nat Rev Mol cell Biol. 2009;10(5):332.
78. Heng JI-T, Chariot A, Nguyen L. Molecular layers underlying cytoskeletal remodelling during cortical development. Trends Neurosci. 2010;33(1):38–47.
79. Kim YT, Hur E-M, Snider WD, Zhou F-Q. Role of GSK3 signaling in neuronal morphogenesis. Front Mol Neurosci. 2011;4:48.
80. Vitriol EA, Zheng JQ. Growth cone travel in space and time: the cellular ensemble of cytoskeleton, adhesion, and membrane. Neuron. 2012;73(6):1068–81.
81. Rasband MN. The axon initial segment and the maintenance of neuronal polarity. Nat Rev Neurosci. 2010;11(8):552.
82. Leterrier C. The axon initial segment: an updated viewpoint. J Neurosci. 2018;38(9):2135–45.
83. Yogev S, Shen K. Establishing neuronal polarity with environmental and intrinsic mechanisms. Neuron. 2017;96(3):638–50.
84. Kole MHP, Ilschner SU, Kampa BM, Williams SR, Ruben PC, Stuart GJ. Action potential generation requires a high sodium channel density

in the axon initial segment. Nat Neurosci. 2008;11(2):178.
85. Lorincz A, Nusser Z. Molecular identity of dendritic voltage-gated sodium channels. Science (80-). 2010;328(5980):906–9.
86. Maarten H, Kole P, Stuart GJ. Is action potential threshold lowest in the axon. Nat Neurosci. 2008;11:1253–5.
87. Hu W, Tian C, Li T, Yang M, Hou H, Shu Y. Distinct contributions of Na v 1.6 and Na v 1.2 in action potential initiation and backpropagation. Nat Neurosci. 2009;12(8):996.
88. Palay SL, Sotelo C, Peters A, Orkand PM. The axon hillock and the initial segment. J Cell Biol. 1968;38(1):193–201.
89. Ogawa Y, Rasband MN. The functional organization and assembly of the axon initial segment. Curr Opin Neurobiol. 2008;18(3):307–13.
90. Bennett V, Baines AJ. Spectrin and ankyrin-based pathways: metazoan inventions for integrating cells into tissues. Physiol Rev. 2001;81(3):1353–92.
91. Bennett V, Lorenzo DN. Spectrin-and ankyrin-based membrane domains and the evolution of vertebrates. In: Current topics in membranes. Elsevier; 2013. p. 1–37.
92. Hedstrom KL, Ogawa Y, Rasband MN. AnkyrinG is required for maintenance of the axon initial segment and neuronal polarity. J Cell Biol. 2008;183(4):635–40.
93. Galiano MR, Jha S, Ho TS-Y, Zhang C, Ogawa Y, Chang K-J, et al. A distal axonal cytoskeleton forms an intra-axonal boundary that controls axon initial segment assembly. Cell. 2012;149(5):1125–39.
94. Zhong G, He J, Zhou R, Lorenzo D, Babcock HP, Bennett V, et al. Developmental mechanism of the periodic membrane skeleton in axons. Elife. 2014;3:e04581.
95. Xu K, Zhong G, Zhuang X. Actin, spectrin, and associated proteins form a periodic cytoskeletal structure in axons. Science (80-). 2013;339(6118):452–6.
96. Lorenzo DN, Badea A, Davis J, Hostettler J, He J, Zhong G, et al. A PIK3C3–Ankyrin-B–Dynactin pathway promotes axonal growth and multiorganelle transport. J Cell Biol. 2014;207(6):735–52.
97. Berger SL, Leo-Macias A, Yuen S, Khatri L, Pfennig S, Zhang Y, et al. Localized myosin II activity regulates assembly and plasticity of the axon initial segment. Neuron. 2018;97(3):555–70.
98. Heissler SM, Sellers JR. Myosin light chains: teaching old dogs new tricks. Bioarchitecture. 2014;4(6):169–88.
99. Tapia M, Del Puerto A, Puime A, Sánchez-Ponce D, Fronzaroli-Molinieres L, Pallas-Bazarra N, et al. GSK3 and β-catenin determines functional expression of sodium channels at the axon initial segment. Cell Mol life Sci. 2013;70(1):105–20.
100. Van Wart A, Trimmer JS, Matthews G. Polarized distribution of ion channels within microdomains of the axon initial segment. J Comp Neurol. 2007;500(2):339–52.
101. Häusser M, Stuart G, Racca C, Sakmann B. Axonal initiation and active dendritic propagation of action potentials in substantia nigra neurons. Neuron. 1995;15(3):637–47.

102. Kaphzan H, Buffington SA, Jung JI, Rasband MN, Klann E. Alterations in intrinsic membrane properties and the axon initial segment in a mouse model of Angelman syndrome. J Neurosci. 2011;31(48):17637–48.
103. Sherman SM. Tonic and burst firing: dual modes of thalamocortical relay. Trends Neurosci. 2001;24(2):122–6.
104. Willis AM, Slater BJ, Gribkova ED, Llano DA. Open-loop organization of thalamic reticular nucleus and dorsal thalamus: a computational model. J Neurophysiol. 2015;114(4):2353–67.
105. Suzuki S, Rogawski MA. T-type calcium channels mediate the transition between tonic and phasic firing in thalamic neurons. Proc Natl Acad Sci. 1989;86(18):7228–32.
106. Cain SM, Snutch TP. Contributions of T-type calcium channel isoforms to neuronal firing. Channels. 2010;4(6):475–82.
107. Destexhe A, Neubig M, Ulrich D, Huguenard J. Dendritic low-threshold calcium currents in thalamic relay cells. J Neurosci. 1998;18(10):3574–88.
108. Zhan XJ, Cox CL, Sherman SM. Dendritic depolarization efficiently attenuates low-threshold calcium spikes in thalamic relay cells. J Neurosci. 2000;20(10):3909–14.
109. Williams SR, Stuart GJ. Action potential backpropagation and somato-dendritic distribution of ion channels in thalamocortical neurons. J Neurosci. 2000;20(4):1307–17.
110. Perez-Reyes E. Molecular physiology of low-voltage-activated t-type calcium channels. Physiol Rev. 2003;83(1):117–61.
111. Cain SM, Snutch TP. T-type calcium channels in burst-firing, network synchrony, and epilepsy. Biochim Biophys Acta (BBA)-Biomembranes. 2013;1828(7):1572–8.
112. Contreras D, Curro Dossi R, Steriade M. Bursting and tonic discharges in two classes of reticular thalamic neurons. J Neurophysiol. 1992;68(3):973–7.
113. Huguenard JR, Prince DA. A novel T-type current underlies prolonged Ca (2+)-dependent burst firing in GABAergic neurons of rat thalamic reticular nucleus. J Neurosci. 1992;12(10):3804–17.
114. Hartings JA, Temereanca S, Simons DJ. High responsiveness and direction sensitivity of neurons in the rat thalamic reticular nucleus to vibrissa deflections. J Neurophysiol. 2000;83(5):2791–801.
115. Shosaku A. A comparison of receptive field properties of vibrissa neurons between the rat thalamic reticular and ventro-basal nuclei. Brain Res. 1985;347(1):36–40.
116. Landisman CE, Long MA, Beierlein M, Deans MR, Paul DL, Connors BW. Electrical synapses in the thalamic reticular nucleus. J Neurosci. 2002;22(3):1002–9.
117. RAMCHARAN EJ, GNADT JW, Sherman SM. Burst and tonic firing in thalamic cells of unanesthetized, behaving monkeys. Vis Neurosci. 2000;17(1):55–62.
118. Reinagel P, Godwin D, Sherman SM, Koch C. Encoding of visual information by LGN bursts. J Neurophysiol. 1999;81(5):2558–69.

119. Guido W, Weyand T. Burst responses in thalamic relay cells of the awake behaving cat. J Neurophysiol. 1995;74(4):1782–6.
120. Radhakrishnan V, Tsoukatos J, Davis KD, Tasker RR, Lozano AM, Dostrovsky JO. A comparison of the burst activity of lateral thalamic neurons in chronic pain and non-pain patients. Pain. 1999;80(3):567–75.
121. Kim U, Sanchez-Vives M V, McCormick DA. Functional dynamics of GABAergic inhibition in the thalamus. Science (80-). 1997;278(5335):130–4.
122. Guillery RW, Feig SL, Lozsadi DA. Paying attention to the thalamic reticular nucleus. Trends Neurosci. 1998;21(1):28–32.
123. Crabtree JW, Isaac JTR. New intrathalamic pathways allowing modality-related and cross-modality switching in the dorsal thalamus. J Neurosci. 2002;22(19):8754–61.
124. Kimura A. Diverse subthreshold cross-modal sensory interactions in the thalamic reticular nucleus: implications for new pathways of cross-modal attentional gating function. Eur J Neurosci. 2014;39(9):1405–18.
125. Ton CCT, Hirvonen H, Miwa H, Weil MM, Monaghan P, Jordan T, et al. Positional cloning and characterization of a paired box-and homeobox-containing gene from the aniridia region. Cell. 1991;67(6):1059–74.
126. Walther C, Gruss P. Pax-6, a murine paired box gene, is expressed in the developing CNS. Development. 1991;113(4):1435–49.
127. Bopp D, Burri M, Baumgartner S, Frigerio G, Noll M. Conservation of a large protein domain in the segmentation gene paired and in functionally related genes of Drosophila. Cell. 1986;47(6):1033–40.
128. Manuel MN, Mi D, Mason JO, Price DJ. Regulation of cerebral cortical neurogenesis by the Pax6 transcription factor. Front Cell Neurosci. 2015;9:70.
129. Gehring WJ, Ikeo K. Pax 6: mastering eye morphogenesis and eye evolution. Trends Genet. 1999;15(9):371–7.
130. Glaser T, Walton DS, Maas RL. Genomic structure, evolutionary conservation and aniridia mutations in the human PAX6 gene. Nat Genet. 1992;2(3):232.
131. Jun S, Desplan C. Cooperative interactions between paired domain and homeodomain. Development. 1996;122(9):2639–50.
132. Bertuccioli C, Fasano L, Jun S, Wang S, Sheng G, Desplan C. In vivo requirement for the paired domain and homeodomain of the paired segmentation gene product. Development. 1996;122(9):2673–85.
133. Hanson I, Van Heyningen V. Pax6: more than meets the eye. Trends Genet. 1995;11(7):268–72.
134. Osumi N, Shinohara H, Numayama-Tsuruta K, Maekawa M. Concise review: Pax6 transcription factor contributes to both embryonic and adult neurogenesis as a multifunctional regulator. Stem Cells. 2008;26(7):1663–72.
135. Haubst N, Berger J, Radjendirane V, Graw J, Favor J, Saunders GF, et al. Molecular dissection of Pax6 function: the specific roles of the paired domain and homeodomain in brain development. Development. 2004;131(24):6131–40.

136. Xu P-X, Zhang X, Heaney S, Yoon A, Michelson AM, Maas RL. Regulation of Pax6 expression is conserved between mice and flies. Development. 1999;126(2):383–95.
137. Kammandel B, Chowdhury K, Stoykova A, Aparicio S, Brenner S, Gruss P. Distinctcis-Essential Modules Direct the Time–Space Pattern of thePax6Gene Activity. Dev Biol. 1999;205(1):79–97.
138. Kleinjan DA, Seawright A, Childs AJ, van Heyningen V. Conserved elements in Pax6 intron 7 involved in (auto) regulation and alternative transcription. Dev Biol. 2004;265(2):462–77.
139. Morgan R. Conservation of sequence and function in the Pax6 regulatory elements. TRENDS Genet. 2004;20(7):283–7.
140. Cvekl A, Callaerts P. PAX6: 25th anniversary and more to learn. Exp Eye Res. 2017;156:10–21.
141. Kozmik Z, Czerny T, Busslinger M. Alternatively spliced insertions in the paired domain restrict the DNA sequence specificity of Pax6 and Pax8. EMBO J. 1997;16(22):6793–803.
142. Epstein J, Cai J, Glaser T, Jepeal L, Maas R. Identification of a Pax paired domain recognition sequence and evidence for DNA-dependent conformational changes. J Biol Chem. 1994;269(11):8355–61.
143. Griffin C, Kleinjan DA, Doe B, van Heyningen V. New 3′ elements control Pax6 expression in the developing pretectum, neural retina and olfactory region. Mech Dev. 2002;112(1–2):89–100.
144. Vance KW, Sansom SN, Lee S, Chalei V, Kong L, Cooper SE, et al. The long non-coding RNA Paupar regulates the expression of both local and distal genes. EMBO J. 2014;33(4):296–311.
145. Plaza S, Dozier C, Saule S. Quail Pax-6 (Pax-QNR) encodes a transcription factor able to bind and trans-activate its own promoter. Cell Growth Differ Am Assoc Cancer Res. 1993;4(12):1041–50.
146. Goudreau G, Petrou P, Reneker LW, Graw J, Löster J, Gruss P. Mutually regulated expression of Pax6 and Six3 and its implications for the Pax6 haploinsufficient lens phenotype. Proc Natl Acad Sci. 2002;99(13):8719–24.
147. Epstein JA, Glaser T, Cai J, Jepeal L, Walton DS, Maas RL. Two independent and interactive DNA-binding subdomains of the Pax6 paired domain are regulated by alternative splicing. Genes Dev. 1994;8(17):2022–34.
148. Xie Q, Cvekl A. The orchestration of mammalian tissue morphogenesis through a series of coherent feed forward loops. J Biol Chem. 2011;jbc-M111.
149. Zhang W, Cveklovam K, Oppermann B, Kantorow M, Cvekl A. Quantitation of PAX6 and PAX6 (5a) transcript levels in adult human lens, cornea, and monkey retina. Mol Vis. 2001;7:1.
150. Sun J, Rockowitz S, Xie Q, Ashery-Padan R, Zheng D, Cvekl A. Identification of in vivo DNA-binding mechanisms of Pax6 and reconstruction of Pax6-dependent gene regulatory networks during forebrain and lens development. Nucleic Acids Res. 2015;43(14):6827–46.
151. Stoykova A, Fritsch R, Walther C, Gruss P. Forebrain patterning

defects in Small eye mutant mice. Development. 1996/11/01. 1996;122(11):3453–65.
152. Mi D, Carr CB, Georgala PA, Huang Y-T, Manuel MN, Jeanes E, et al. Pax6 Exerts Regional Control of Cortical Progenitor Proliferation via Direct Repression of< i> Cdk6</i> and Hypophosphorylation of pRb. Neuron. 2013;78(2):269–84.
153. Engelkamp D, Rashbass P, Seawright A, van Heyningen V. Role of Pax6 in development of the cerebellar system. Development. 1999;126(16):3585–96.
154. Georgala PA, Carr CB, Price DJ. The role of Pax6 in forebrain development. Dev Neurobiol. 2011;71(8):690–709.
155. Hill RE, Favor J, Hogan BLM, Ton CCT, Saunders GF, Hanson IM, et al. Mouse small eye results from mutations in a paired-like homeobox-containing gene. Nature. 1991;354(6354):522.
156. Lim HT, Kim DH, Kim H. PAX6 aniridia syndrome: clinics, genetics, and therapeutics. Curr Opin Ophthalmol. 2017;28(5):436–47.
157. Hanson IM, Fletcher JM, Jordan T, Brown A, Taylor D, Adams RJ, et al. Mutations at the PAX6 locus are found in heterogeneous anterior segment malformations including Peters' anomaly. Nat Genet. 1994;6(2):168.
158. Sisodiya SM, Free SL, Williamson KA, Mitchell TN, Willis C, Stevens JM, et al. PAX6 haploinsufficiency causes cerebral malformation and olfactory dysfunction in humans. Nat Genet. 2001;28(3):214.
159. Englund C, Fink A, Lau C, Pham D, Daza RAM, Bulfone A, et al. Pax6, Tbr2, and Tbr1 are expressed sequentially by radial glia, intermediate progenitor cells, and postmitotic neurons in developing neocortex. J Neurosci. 2005;25(1):247–51.
160. Toresson H, Potter SS, Campbell K. Genetic control of dorsal-ventral identity in the telencephalon: opposing roles for Pax6 and Gsh2. Development. 2000;127(20):4361–71.
161. Stoykova A, Gotz M, Gruss P, Price J. Pax6-dependent regulation of adhesive patterning, R-cadherin expression and boundary formation in developing forebrain. Development. 1997;124(19):3765–77.
162. Pratt T, Vitalis T, Warren N, Edgar JM, Mason JO, Price DJ. A role for Pax6 in the normal development of dorsal thalamus and its cortical connections. Development. 2000;127(23):5167–78.
163. Robertshaw E, Matsumoto K, Lumsden A, Kiecker C. Irx3 and Pax6 establish differential competence for Shh-mediated induction of GABAergic and glutamatergic neurons of the thalamus. Proc Natl Acad Sci. 2013;110(41):E3919–26.
164. Manuel M, Price DJ. Role of Pax6 in forebrain regionalization. Brain Res Bull. 2005;66(4):387–93.
165. Auladell C, Pérez-Sust P, Supèr H, Soriano E. The early development of thalamocortical and corticothalamic projections in the mouse. Anat Embryol (Berl). 2000;201(3):169–79.
166. Price DJ, Clegg JM, Oliver Duocastella X, Willshaw DJ, Pratt T. The importance of combinatorial gene expression in early mammalian thalamic patterning and thalamocortical axonal guidance. Front

Neurosci. 2012;6:37.
167. Simpson TI, Pratt T, Mason JO, Price DJ. Normal ventral telencephalic expression of Pax6 is required for normal development of thalamocortical axons in embryonic mice. Neural Dev. 2009;4(1):19.
168. Sousa VH, Miyoshi G, Hjerling-Leffler J, Karayannis T, Fishell G. Characterization of Nkx6-2-derived neocortical interneuron lineages. Cereb cortex. 2009;19(suppl_1):i1–10.
169. Sebastián-Serrano A, Sandonis A, Cardozo M, Rodríguez-Tornos FM, Bovolenta P, Nieto M. Pαx6 expression in postmitotic neurons mediates the growth of axons in response to SFRP1. PLoS One. 2012;7(2):e31590.
170. Yamasaki T, Kawaji K, Ono K, Bito H, Hirano T, Osumi N, et al. Pax6 regulates granule cell polarization during parallel fiber formation in the developing cerebellum. Development. 2001;128(16):3133–44.
171. Swanson DJ, Tong Y, Goldowitz D. Disruption of cerebellar granule cell development in the Pax6 mutant, Sey mouse. Dev brain Res. 2005;160(2):176–93.
172. Li Y-H, Ghavampur S, Bondallaz P, Will L, Grenningloh G, Püschel AW. Rnd1 regulates axon extension by enhancing the microtubule destabilizing activity of SCG10. J Biol Chem. 2009;284(1):363–71.
173. Ueda S, Fujimoto S, Hiramoto K, Negishi M, Katoh H. Dock4 regulates dendritic development in hippocampal neurons. J Neurosci Res. 2008;86(14):3052–61.
174. Xiao Y, Peng Y, Wan J, Tang G, Chen Y, Tang J, et al. The atypical guanine nucleotide exchange factor Dock4 regulates neurite differentiation through modulation of Rac1 and actin dynamics. J Biol Chem. 2013;jbc-M113.
175. Kunisaki Y, Nishikimi A, Tanaka Y, Takii R, Noda M, Inayoshi A, et al. DOCK2 is a Rac activator that regulates motility and polarity during neutrophil chemotaxis. J Cell Biol. 2006;174(5):647–52.
176. Namekata K, Harada C, Taya C, Guo X, Kimura H, Parada LF, et al. Dock3 induces axonal outgrowth by stimulating membrane recruitment of the WAVE complex. Proc Natl Acad Sci. 2010;107(16):7586–91.
177. Reinhard M, Jarchau T, Walter U. Actin-based motility: stop and go with Ena/VASP proteins. Trends Biochem Sci. 2001;26(4):243–9.
178. Norris AD, Dyer JO, Lundquist EA. The Arp2/3 complex, UNC-115/abLIM, and UNC-34/Enabled regulate axon guidance and growth cone filopodia formation in Caenorhabditis elegans. Neural Dev. 2009;4(1):38.
179. Fukata Y, Itoh TJ, Kimura T, Ménager C, Nishimura T, Shiromizu T, et al. CRMP-2 binds to tubulin heterodimers to promote microtubule assembly. Nat Cell Biol. 2002;4(8):583.
180. Coutinho-Budd J, Ghukasyan V, Zylka MJ, Polleux F. The F-BAR domains from srGAP1, srGAP2, and srGAP3 differentially regulate membrane deformation. J Cell Sci. 2012;jcs-098962.
181. Quan A, Robinson PJ. Syndapin–a membrane remodelling and endocytic F-BAR protein. FEBS J. 2013;280(21):5198–212.
182. Lalli G. Regulation of neuronal polarity. Exp Cell Res.

2014;328(2):267–75.
183. Barnes AP, Polleux F. Establishment of axon-dendrite polarity in developing neurons. Annu Rev Neurosci. 2009;32.
184. Shi S-H, Cheng T, Jan LY, Jan Y-N. APC and GSK-3β are involved in mPar3 targeting to the nascent axon and establishment of neuronal polarity. Curr Biol. 2004;14(22):2025–32.
185. Nishimura T, Kato K, Yamaguchi T, Fukata Y, Ohno S, Kaibuchi K. Role of the PAR-3–KIF3 complex in the establishment of neuronal polarity. Nat Cell Biol. 2004;6(4):328.
186. Corder GW, Foreman DI. Nonparametric statistics for non-statisticians: a step-by-step approach. John Wiley & Sons; 2009.
187. Haynes LW. neuron in tissue culture. Wiley; 1999.
188. Ciani L, Salinas PC. Signalling in neural development: WNTs in the vertebrate nervous system: from patterning to neuronal connectivity. Nat Rev Neurosci. 2005;6(5):351.
189. Moon RT, Kohn AD, De Ferrari G V, Kaykas A. WNT and β-catenin signalling: diseases and therapies. Nat Rev Genet. 2004;5(9):691.
190. Wisniewska MB, Misztal K, Michowski W, Szczot M, Purta E, Lesniak W, et al. LEF1/β-catenin complex regulates transcription of the Cav3. 1 calcium channel gene (Cacna1g) in thalamic neurons of the adult brain. J Neurosci. 2010;30(14):4957–69.
191. Komiya Y, Habas R. Wnt signal transduction pathways. Organogenesis. 2008;4(2):68–75.
192. Bovolenta P, Esteve P, Ruiz JM, Cisneros E, Lopez-Rios J. Beyond Wnt inhibition: new functions of secreted Frizzled-related proteins in development and disease. J Cell Sci. 2008;121(6):737–46.
193. Filali M, Cheng N, Abbott D, Leontiev V, Engelhardt JF. Wnt-3A/beta-catenin signaling induces transcription from the LEF-1 promoter. J Biol Chem. 2002;
194. Jho E, Zhang T, Domon C, Joo C-K, Freund J-N, Costantini F. Wnt/β-catenin/Tcf signaling induces the transcription of Axin2, a negative regulator of the signaling pathway. Mol Cell Biol. 2002;22(4):1172–83.
195. Ciani L, Krylova O, Smalley MJ, Dale TC, Salinas PC. A divergent canonical WNT-signaling pathway regulates microtubule dynamics: dishevelled signals locally to stabilize microtubules. J Cell Biol. 2004;164(2):243–53.
196. Davey CF, Moens CB. Planar cell polarity in moving cells: think globally, act locally. Development. 2017;144(2):187–200.
197. Huelsken J, Birchmeier W. New aspects of Wnt signaling pathways in higher vertebrates. Curr Opin Genet Dev. 2001;11(5):547–53.
198. Kühl M, Sheldahl LC, Park M, Miller JR, Moon RT. The Wnt/Ca2+ pathway: a new vertebrate Wnt signaling pathway takes shape. Trends Genet. 2000;16(7):279–83.
199. Diep DB, Hoen N, Backman M, Machon O, Krauss S. Characterisation of the Wnt antagonists and their response to conditionally activated Wnt signalling in the developing mouse forebrain. Dev brain Res. 2004;153(2):261–70.
200. Kawano Y, Kypta R. Secreted antagonists of the Wnt signalling

pathway. J Cell Sci. 2003;116(13):2627–34.
201. Witte F, Dokas J, Neuendorf F, Mundlos S, Stricker S. Comprehensive expression analysis of all Wnt genes and their major secreted antagonists during mouse limb development and cartilage differentiation. Gene Expr Patterns. 2009;9(4):215–23.
202. Machon O, Kreslova J, Ruzickova J, Vacik T, Klimova L, Fujimura N, et al. Lens morphogenesis is dependent on Pax6-mediated inhibition of the canonical Wnt/beta-catenin signaling in the lens surface ectoderm. Genesis. 2010;48(2):86–95.
203. Ferrer-Vaquer A, Piliszek A, Tian G, Aho RJ, Dufort D, Hadjantonakis A-K. A sensitive and bright single-cell resolution live imaging reporter of Wnt/ss-catenin signaling in the mouse. BMC Dev Biol. 2010;10(1):121.
204. Oshima T, Abe M, Asano J, Hara T, Kitazoe K, Sekimoto E, et al. Myeloma cells suppress bone formation by secreting a soluble Wnt inhibitor, sFRP-2. Blood. 2005;106(9):3160–5.
205. Cha S-W, Tadjuidje E, Tao Q, Wylie C, Heasman J. Wnt5a and Wnt11 interact in a maternal Dkk1-regulated fashion to activate both canonical and non-canonical signaling in Xenopus axis formation. Development. 2008;135(22):3719–29.
206. Paiva KBS, das Graças Silva-Valenzuela M, Massironi SMG, Ko GM, Siqueira FM, Nunes FD. Differential Shh, Bmp and Wnt gene expressions during craniofacial development in mice. Acta Histochem. 2010;112(5):508–17.
207. Wisniewska MB, Nagalski A, Dabrowski M, Misztal K, Kuznicki J. Novel β-catenin target genes identified in thalamic neurons encode modulators of neuronal excitability. BMC Genomics. 2012;13(1):635.
208. Landmann J, Richter F, Oros-Peusquens A-M, Shah NJ, Classen J, Neely GG, et al. Neuroanatomy of pain-deficiency and cross-modal activation in calcium channel subunit (CACN) α2δ3 knockout mice. Brain Struct Funct. 2018;223(1):111–30.
209. Dolphin AC. Calcium channel auxiliary α 2 δ and β subunits: trafficking and one step beyond. Nat Rev Neurosci. 2012;13(8):542.
210. Dolphin AC. A short history of voltage-gated calcium channels. Br J Pharmacol. 2006;147(S1):S56–62.